

Ministry of Education and Science of the Russian Federation  
Saint Petersburg National Research University of Information  
Technologies, Mechanics, and Optics

# ***NANOSYSTEMS:***

## ***PHYSICS, CHEMISTRY, MATHEMATICS***

2016, volume 7(2)

Special Issue

INTERNATIONAL CONFERENCE  
“MATHEMATICAL CHALLENGE OF QUANTUM  
TRANSPORT IN NANOSYSTEMS – 2015.  
PIERRE DUCLOS WORKSHOP”

**Наносистемы: физика, химия, математика**

2016, том 7, № 2



# NANOSYSTEMS:

PHYSICS, CHEMISTRY, MATHEMATICS

## ADVISORY BOARD MEMBERS

**Chairman:** V.N. Vasiliev (*St. Petersburg, Russia*),  
V.M. Ievlev (*Voronezh*), P.S. Kop'ev (*St. Petersburg, Russia*), N.F. Morozov (*St. Petersburg, Russia*), V.N. Parmon (*Novosibirsk*), A.I. Rusanov (*St. Petersburg, Russia*),

## EDITORIAL BOARD

**Editor-in-Chief:** I.Yu. Popov (*St. Petersburg, Russia*)

### Section Co-Editors:

Physics – V.M. Uzdin (*St. Petersburg, Russia*),  
Chemistry, material science – V.V. Gusarov (*St. Petersburg, Russia*),  
Mathematics – I.Yu. Popov (*St. Petersburg, Russia*).

### Editorial Board Members:

V.M. Adamyan (*Odessa, Ukraine*); O.V. Al'myasheva (*St. Petersburg, Russia*);  
A.P. Alodjants (*Vladimir, Russia*); S. Bechta (*Stockholm, Sweden*); J. Behrndt (*Graz, Austria*);  
M.B. Belonenko (*Volgograd, Russia*); V.G. Bepalov (*St. Petersburg, Russia*); J. Brasche (*Clausthal, Germany*);  
A. Chatterjee (*Hyderabad, India*); S.A. Chivilikhin (*St. Petersburg, Russia*); A.V. Chizhov (*Dubna, Russia*);  
A.N. Enyashin (*Ekaterinburg, Russia*), P.P. Fedorov (*Moscow, Russia*); E.A. Gudilin (*Moscow, Russia*); V.K. Ivanov (*Moscow, Russia*),  
H. Jónsson (*Reykjavik, Iceland*); A.A. Kiselev (*Madison, USA*); Yu.S. Kivshar (*Canberra, Australia*);  
S.A. Kozlov (*St. Petersburg, Russia*); P.A. Kurasov (*Stockholm, Sweden*); A.V. Lukashin (*Moscow, Russia*);  
V.A. Margulis (*Saransk, Russia*); I.V. Melikhov (*Moscow, Russia*); G.P. Miroshnichenko (*St. Petersburg, Russia*);  
I.Ya. Mittova (*Voronezh, Russia*); H. Neidhardt (*Berlin, Germany*); K. Pankrashkin (*Orsay, France*); B.S. Pavlov (*Auckland, New Zealand*);  
A.V. Ragulya (*Kiev, Ukraine*); V. Rajendran (*Tamil Nadu, India*); A.A. Rempel (*Ekaterinburg, Russia*);  
V.Ya. Rudyak (*Novosibirsk, Russia*); D Shoikhet (*Karmiel, Israel*); P Stovicek (*Prague, Czech Republic*); V.M. Talanov (*Novocherkassk, Russia*);  
A.Ya. Vul' (*St. Petersburg, Russia*); V.A. Zagrebnov (*Marseille, France*).

### Editors:

I.V. Blinova; A.I. Popov; A.I. Trifanov; E.S. Trifanova (*St. Petersburg, Russia*),  
R. Simoneaux (*Philadelphia, Pennsylvania, USA*).

**Address:** University ITMO, Kronverkskiy pr., 49, St. Petersburg 197101, Russia.

**Phone:** +7(812)232-67-65, **Journal site:** <http://nanojournal.ifmo.ru/>,

**E-mail:** [popov1955@gmail.com](mailto:popov1955@gmail.com)

## AIM AND SCOPE

The scope of the journal includes all areas of nano-sciences. Papers devoted to basic problems of physics, chemistry, material science and mathematics inspired by nanosystems investigations are welcomed. Both theoretical and experimental works concerning the properties and behavior of nanosystems, problems of its creation and application, mathematical methods of nanosystem studies are considered.

The journal publishes scientific reviews (up to 30 journal pages), research papers (up to 15 pages) and letters (up to 5 pages). All manuscripts are peer-reviewed. Authors are informed about the referee opinion and the Editorial decision.

# Content

## FROM THE EDITORIAL BOARD

<b>International Conference “Mathematical Challenge of Quantum Transport in Nanosystems - 2015. Pierre Duclos Workshop”</b>	<b>267</b>
---	------------

## INVITED SPEAKERS

S. Albeverio, S. Fassari, F. Rinaldi <b>Spectral properties of a symmetric three-dimensional quantum dot with a pair of identical attractive <math>\delta</math>-impurities symmetrically situated around the origin</b>	<b>268</b>
J. Behrndt, M. Langer, V. Lotoreichik <b>Boundary triples for Schrödinger operators with singular interactions on hypersurfaces</b>	<b>290</b>
C. Cacciapuoti, A. Mantile, A. Posilicano <b>Time dependent delta-prime interactions in dimension one</b>	<b>303</b>
A. Mantile, A. Posilicano <b>Laplacians with singular perturbations supported on hypersurfaces</b>	<b>315</b>

## CONTRIBUTED TALKS

I.V. Makeev, I.Yu. Popov <b>Steady Stokes flow between confocal semi-ellipses</b>	<b>324</b>
A.A. Boitsev, H. Neidhardt, I.Yu. Popov <b>Dirac operator coupled to bosons</b>	<b>332</b>
A.V. Siklitskaya, S.G. Yastrebov, R. Smith <b>An interpretation of the strongest X-ray diffraction peak for various carbon nanoclusters</b>	<b>340</b>
A.D. Kiselev, D.O. Plutenko <b>Light scattering of Laguerre – Gaussian beams: near-field structures and symmetries</b>	<b>349</b>

V.D. Dubrovskaya, S.A. Chivilikhin <b>Temperature dependence of the optical fiber cable parameters in subcarrier wave quantum communication systems</b>	<b>371</b>
A.E. Ivanova, S.A. Chivilikhin, A.V. Gleim <b>The use of beam- and fiber splitters in quantum random number generators based on vacuum fluctuations</b>	<b>378</b>
A.G. Petrashen, N.V. Sytenko <b>Laser generation without inversion on the fine levels of the helium atom</b>	<b>384</b>
<b>Information for authors</b>	<b>394</b>

## **FROM THE EDITORIAL BOARD**

In this issue we publish the Proceedings of the International Conference **Mathematical Challenge of Quantum Transport in Nanosystems**. “**Pierre Duclos Workshop**” organized by Saint Petersburg National Research University of Information Technologies, Mechanics, and Optics in September 2015. This workshop was the ninth of a series which has the aim to bring together specialists in nanosystem modeling, mathematicians and condensed matter physicists.

### **PROGRAM COMMITTEE**

Igor Yu. Popov (ITMO University, Russia) – Chairman  
Sergey N. Naboko (St. Petersburg State University, Russia)  
Boris S. Pavlov (NZIAS, New Zealand)  
George P. Miroshnichenko (ITMO University, Russia)

### **LOCAL ORGANIZING COMMITTEE**

Vladimir N. Vasilyev – Chairman  
Igor Yu. Popov – Vice-Chairman  
Ekaterina S. Trifanova  
Irina V. Blinova  
Alexander I. Trifanov  
Anton I. Popov  
Anton A. Boitsev

### **INVITED SPEAKERS**

Jussi Behrndt (Graz, Austria)  
Boris Pavlov (Auckland, New Zealand)  
Pavel Stovicek (Prague, Czech Republic)  
Andrea Posilicano (Como, Italy)  
Silvestro Fassari (Locarno, Switzerland)  
Claudio Cacciapuoti (Como, Italy)  
Andrea Mantile (Reims, France)  
Jaroslav Dittrich (Rez, Czech Republic)

### **THE MAIN TOPICS OF THE CONFERENCE**

Spectral theory  
Scattering  
Quantum transport  
Quantum communications and computations

# Spectral properties of a symmetric three-dimensional quantum dot with a pair of identical attractive $\delta$ -impurities symmetrically situated around the origin

S. Albeverio<sup>1,2,3,4</sup>, S. Fassari<sup>2,5,6</sup> and F. Rinaldi<sup>2,6,7</sup>

<sup>1</sup>Institut für Angewandte Mathematik, HCM, IZKS, BiBoS, Universität Bonn, Endenicheralee 60, D-53115 Bonn, Germany

<sup>2</sup>CERFIM, PO Box 1132, CH-6601 Locarno, Switzerland

<sup>3</sup>Centre Interfacultaire Bernoulli, EPFL, CH-1015 Lausanne, Switzerland

<sup>4</sup>Chair Professorship, Department of Mathematics and Statistics, King Fahd University of Petroleum and Minerals, Dhahran, KSA

<sup>5</sup>ISR, Aeulistr.10, CH-9470 Buchs, Switzerland

<sup>6</sup>Università degli Studi Guglielmo Marconi, Via Plinio 44, I-00193 Rome, Italy

<sup>7</sup>BIS Group of Institutions, Gagra-Moga, Punjab under Punjab Technical University, Punjab, India

silvestro.fassari@isr.ch

**PACS 02.30.Gp, 02.30.Hq, 02.30.Hq, 02.30.Lt, 02.30.Sa, 02.30.Tb, 03.65.Db, 03.65.Ge, 68.65.Hb**

**DOI 10.17586/2220-8054-2016-7-2-268-289**

In this presentation, we wish to provide an overview of the spectral features for the self-adjoint Hamiltonian of the three-dimensional isotropic harmonic oscillator perturbed by either a single attractive  $\delta$ -interaction centered at the origin or by a pair of identical attractive  $\delta$ -interactions symmetrically situated with respect to the origin. Given that such Hamiltonians represent the mathematical model for quantum dots with sharply localized impurities, we cannot help having the renowned article by Brüning, Geyler and Lobanov [1] as our key reference. We shall also compare the spectral features of the aforementioned three-dimensional models with those of the self-adjoint Hamiltonian of the harmonic oscillator perturbed by an attractive  $\delta'$ -interaction in one dimension, fully investigated in [2, 3], given the existence in both models of the remarkable spectral phenomenon called "level crossing". The rigorous definition of the self-adjoint Hamiltonian for the singular double well model will be provided through the explicit formula for its resolvent (Green's function). Furthermore, by studying in detail the equation determining the ground state energy for the double well model, it will be shown that the concept of "positional disorder", introduced in [1] in the case of a quantum dot with a single  $\delta$ -impurity, can also be extended to the model with the twin impurities in the sense that the greater the distance between the two impurities is, the less localized the ground state will be. Another noteworthy spectral phenomenon will also be determined; for each value of the distance between the two centers below a certain threshold value, there exists a range of values of the strength of the twin point interactions for which the first excited symmetric bound state is more tightly bound than the lowest antisymmetric bound state. Furthermore, it will be shown that, as the distance between the two impurities shrinks to zero, the 3D-Hamiltonian with the singular double well (requiring renormalization to be defined) does not converge to the one with a single  $\delta$ -interaction centered at the origin having twice the strength, in contrast to its one-dimensional analog for which no renormalization is required. It is worth stressing that this phenomenon has also been recently observed in the case of another model requiring the renormalization of the coupling constant, namely the one-dimensional Salpeter Hamiltonian perturbed by two twin attractive  $\delta$ -interactions symmetrically situated at the same distance from the origin.

**Keywords:** level crossing, degeneracy, point interactions, renormalisation, Schrödinger operators, quantum dots, perturbed quantum oscillators.

*Received:* 7 November 2015

## 1. Introduction

In this work, we wish to further extend our previous research on various types of point perturbations of Schrödinger Hamiltonians with or without harmonic confinement (see, e.g., [2–11]) to the physical models utilized to describe three-dimensional quantum dots.

This presentation will try to be an expansion of the detailed spectral analysis carried out in [1], in the sense that, after briefly reviewing in Section 2 the findings of [1,9] for the case of a three-dimensional quantum dot with a single impurity consisting of a point interaction centered at the origin, we are going to investigate in Section 3 the model with two twin attractive point impurities symmetrically situated with respect to the bottom of the harmonic confining potential. In Section 2, by analyzing the behavior of the new energy levels created by a point perturbation as functions of the parameter labeling the self-adjoint extensions, physically characterized by being proportional to the inverse scattering length (see [1,4]), we are going to stress the analogy of the presence of the so-called “level crossings” between the newly created eigenenergies of bound states with a given symmetry and those of the unperturbed harmonic oscillator unaffected by the singular perturbation pertaining to bound states having the opposite symmetry. We will also underline the difference between this three-dimensional model and the one-dimensional one, studied in [2,3], in which the harmonic oscillator is perturbed by a so-called  $\delta'$ -interaction, whose quadratic form is given by the expression  $|\delta'\rangle \langle \delta'|$ .

The first step in the investigation outlined in Section 3 will necessarily be the rigorous definition of the self-adjoint Hamiltonian representing the energy operator for our model. This will be achieved by first introducing the usual ultraviolet energy cut-off and then making the coupling constant dependent on the cut-off itself in such a way that the typical cancellation of divergences will take place in the norm-resolvent limit once the cut-off is removed.

Once the explicit expression of the resolvent (Green’s function) is obtained, its poles will provide us with the eigenvalues (energy levels) for the three-dimensional harmonic oscillator perturbed by singular interactions (3D quantum dot with point impurities). The noticeable difference between the bound state equation pertaining to the model with a single impurity centered at the origin (described in Section 2) and the one for the singular double well is the inevitable absence of the simple expression containing the ratio of Gamma functions enabling us to study all the eigenvalues on an equal footing. Although it is still possible, at least conceptually, to carry out the analysis of the entire discrete spectrum, the operational task is made quite challenging by the fact that the equation for an eigenvalue pertaining to a bound state with a given symmetry may not be used for the eigenvalue pertaining to the next upper bound state with the same symmetry without the modifications needed to cancel the inevitable appearance of divergences, a procedure outlined in [2,8–11] in the case of the other aforementioned models.

As a consequence, we have necessarily restricted our task to a rather detailed description of the behavior of the lowest lying eigenvalues (energy levels) of the spectrum with respect to the variations of the two key parameters of the model, one labelling the self-adjoint extensions of the operator (or its reciprocal) and the other one given by the distance between either impurity and the origin.

Given that the findings of our analysis in Section 3 are unavoidably linked to some possible avenues of future research, we refrain from anticipating them in an abbreviated fashion at this stage, as they will be summarized in detail in Section 4, the final section in which

the most important conclusions will be drawn and some perspectives for future work will be sketched.

**2. The three-dimensional isotropic harmonic oscillator perturbed by a single attractive point perturbation centered at the origin**

We wish to start our analysis by revisiting the model used in [1] to describe a 3D-quantum dot, namely the three-dimensional isotropic harmonic oscillator perturbed by an attractive point perturbation. The spectroscopy of such a Schrödinger Hamiltonian was also fully investigated in [9] under the restriction of having the impurity, that is to say the point perturbation, situated at the origin. Hence, the Hamiltonian was given by the self-adjoint operator making sense of the heuristic expression (see [9]):

$$H_\beta = H_0 - \beta\delta(\vec{x}), \quad H_0 = \frac{1}{2} \sum_{i=1}^3 \left( -\frac{d^2}{dx_i^2} + x_i^2 \right) = \sum_{i=1}^3 a_i^+ a_i + \frac{3}{2} \tag{2.1}$$

( $a_i$  and its adjoint being the usual annihilation and creation operators associated with  $H_0$ ).

The eigenfunctions of  $H_0$ , the Hamiltonian of the three-dimensional harmonic oscillator, can clearly be expressed in terms of those of their one-dimensional counterparts, namely:

$$\Psi_{\vec{n}}(\vec{x}) = \psi_{n_1}(x)\psi_{n_2}(y)\psi_{n_3}(z).$$

Although, in this case, the radial symmetry of the model could obviously be exploited, as was done in [1], we adhere to the Cartesian framework used in [9] in view of our prospective investigation of the model in which  $H_0$  is perturbed by two attractive deltas. Before moving forward, it is crucial to notice that the function:

$$(H_0 - E)^{-1}(0, \vec{x}) = \sum_{|\vec{n}|=0}^{\infty} \frac{\Psi_{2\vec{n}}(0)}{(|2\vec{n}| + \frac{3}{2} - E)} \Psi_{2\vec{n}}(\vec{x}) \tag{2.2}$$

is square integrable. In fact, by considering without loss of generality only negative values of  $E$ , by means of Parseval's identity, we obtain the following estimate:

$$\sum_{|\vec{n}|=0}^{\infty} \frac{\Psi_{2\vec{n}}^2(0)}{(|2\vec{n}| + \frac{3}{2} - E)^2} \leq \sum_{|\vec{n}|=0}^{\infty} \frac{\Psi_{2\vec{n}}^2(0)}{(2n_1 + \frac{1}{2})^{2/3} (2n_2 + \frac{1}{2})^{2/3} (2n_3 + \frac{1}{2})^{2/3}} = \left[ \sum_{n=0}^{\infty} \frac{\psi_{2n}^2(0)}{(2n + 1/2)^{2/3}} \right]^3 < \infty, \tag{2.3}$$

taking into account the well-known pointwise decay of the harmonic oscillator eigenfunctions (see, e.g., [12, 13]), precisely that  $\lim_{n \rightarrow \infty} n^{1/4} \psi_n(x) < \infty$ , for any fixed  $x$ .

As was shown in [9], using the coupling constant renormalization procedure,  $H_\beta$  is rigorously defined (for any  $\beta$  different from zero) by means of its resolvent, namely:

$$(H_\beta - E)^{-1} = (H_0 - E)^{-1} + \frac{|(H_0 - E)^{-1}(\cdot, 0)\rangle \langle (H_0 - E)^{-1}(0, \cdot)|}{\beta^{-1} - E \left[ \sum_{|\vec{n}|=0}^{\infty} \frac{\Psi_{2\vec{n}}^2(0)}{(|2\vec{n}| + \frac{3}{2})(|2\vec{n}| + \frac{3}{2} - E)} \right]}, \tag{2.4}$$

for any negative  $E$  below  $E_0(\beta)$ , the ground state energy (lowest eigenvalue) of  $H_\beta$ , that is to say the first root of the equation:

$$\beta^{-1} = E \left[ \sum_{|\vec{n}|=0}^{\infty} \frac{\Psi_{2\vec{n}}^2(0)}{(|2\vec{n}| + \frac{3}{2})(|2\vec{n}| + \frac{3}{2} - E)} \right] \quad (2.5)$$

as was done in [9] (and in similar contexts in [2, 8, 10, 11]), the series on the right hand side of (2.5) can be recast as an integral. This can be achieved by taking advantage of two crucial properties that will be exploited throughout this work: the well-known integral relationship between the resolvent and the semigroup of any semibounded operator for any  $E$  below the lowest point in the spectrum (see, e.g., [14] page 204), as well as the fact that the integral kernel of the semigroup of the three-dimensional harmonic oscillator is perfectly separable (see [1] page 1278), such that (2.5) reads for any  $E < 3/2$ :

$$\beta^{-1} = \frac{1}{\sqrt{\pi^3}} \int_0^{\infty} \frac{e^{\frac{3}{2}t} (e^{Et} - 1)}{(e^{2t} - 1)^{\frac{3}{2}}} dt, \quad (2.5a)$$

or equivalently,

$$\beta^{-1} = \frac{1}{\sqrt{\pi^3}} \int_0^{\infty} \frac{e^{-\frac{3}{2}t} (e^{Et} - 1)}{(1 - e^{-2t})^{\frac{3}{2}}} dt. \quad (2.5b)$$

By means of a simple change of variable inside the latter integral, (2.5b) can be rewritten as an integral over a bounded interval (involving Mehler's kernel):

$$\beta^{-1} = \frac{1}{\sqrt{\pi^3}} \int_0^1 \frac{\xi^{\frac{1}{2}} (\xi^{-E} - 1)}{(1 - \xi^2)^{\frac{3}{2}}} d\xi. \quad (2.5c)$$

By setting  $\alpha = 1/\beta$  and

$$\alpha_0 = \beta_0^{-1} = \frac{1}{\sqrt{\pi^3}} \int_0^1 \frac{1 - \xi^{\frac{1}{2}}}{(1 - \xi^2)^{\frac{3}{2}}} d\xi = \frac{\Gamma(3/4)}{\pi \cdot \Gamma(1/4)} \cong 0.107585,$$

(2.5c) can be further transformed into:

$$\alpha - \alpha_0 = \frac{1}{\sqrt{\pi^3}} \int_0^1 \frac{\xi^{\frac{1}{2}-E} - 1}{(1 - \xi^2)^{3/2}} d\xi. \quad (2.5d)$$

In perfect analogy with what was done in the aforementioned articles, the integral on the right hand side can be converted into a ratio of Gamma functions as follows:

$$\alpha_0 - \alpha = \frac{\Gamma(\frac{3}{4} - \frac{E}{2})}{\pi \Gamma(\frac{1}{4} - \frac{E}{2})}. \quad (2.5e)$$

It is crucial to realize that (2.5e) holds also to the right of  $E = 3/2$ , enabling us to determine all the eigenvalues and not only the ground state energy. Of course, our analysis in this work is entirely consistent with what was observed in [9] (see the final remark in [2] as well). The graph of the ground state energy as a function of the extension parameter  $\alpha = 1/\beta$  is shown below (Fig. 1). As is evident,  $E_0(\alpha) \rightarrow 3/2$  as  $\alpha \rightarrow +\infty$ .

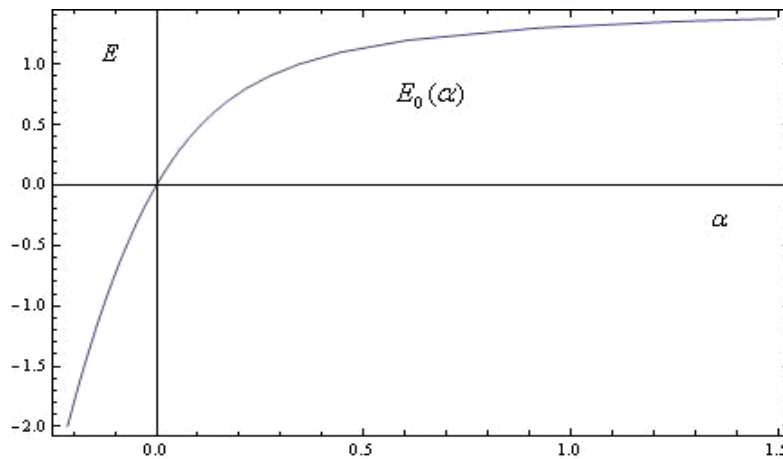


FIG. 1. The ground state energy of the 3D-isotropic harmonic oscillator perturbed by an attractive point interaction situated at the origin as a function of the extension parameter  $\alpha = 1/\beta$

At this stage, it might be worth recalling that the corresponding bound state equation for the one-dimensional Hamiltonian:

$$h(\alpha) = h_{1/\alpha} = \frac{1}{2} \left( -\frac{d^2}{dx^2} + x^2 \right) - \frac{1}{\alpha} |\delta'(x)\rangle\langle\delta'(x)|,$$

defined rigorously by means of its resolvent in two different ways in [2,3], is instead:

$$\alpha_0^{1D} - \alpha = 2 \frac{\Gamma\left(\frac{3}{4} - \frac{E}{2}\right)}{\Gamma\left(\frac{1}{4} - \frac{E}{2}\right)}, \quad \alpha_0^{1D} = 2 \frac{\Gamma(3/4)}{\Gamma(1/4)} \cong 0.675978. \tag{2.6}$$

Conversely, the corresponding bound state equation for the one-dimensional Hamiltonian is:

$$h(\lambda) = \frac{1}{2} \left( -\frac{d^2}{dx^2} + x^2 \right) - \lambda \delta(x) = \frac{1}{2} \left( -\frac{d^2}{dx^2} + x^2 \right) - \lambda |\delta(x)\rangle\langle\delta(x)|,$$

taking account of the obvious identity in the sense of quadratic forms between the  $\delta$ -interaction, namely the quadratic form  $|\delta\rangle\langle\delta|$ , and the so-called  $\delta$ -potential (whose quadratic form is instead  $(\cdot, \delta \cdot)$ ), reads:

$$\lambda = 2 \frac{\Gamma\left(\frac{3}{4} - \frac{E}{2}\right)}{\Gamma\left(\frac{1}{4} - \frac{E}{2}\right)}, \tag{2.7}$$

(see [2, 8, 15]).

The fact that (2.7), unlike (2.5e) and (2.6), involves only the coupling constant is a clear manifestation of the fact that  $h(\lambda)$  can be easily defined by means of the KLMN theorem (see [16]) without the renormalization required for the other two models.

The higher energy levels are even more interesting, as they exhibit the phenomenon called “level crossing”. As was pointed out in [2] (see also a similar remark in [9]): “as a consequence of the presence of the point perturbation acting only on states with zero angular momentum, the  $\frac{(2l+1)(2l+2)}{2}$ -degeneracy of the eigenvalue  $E_{2l} = 2l + \frac{3}{2}$  gets lowered by one due to the emergence of the simple eigenvalue generated by the perturbation. Such a simple eigenvalue, regarded as a function of the extension parameter  $\alpha$ , does cross the next lower unperturbed eigenvalue  $E_{2l-1} = (2l-1) + \frac{3}{2}$ ”.

As can be seen in Fig. 2, it is quite noteworthy that all these level crossings take place exactly at  $\alpha = \alpha_0$  (approximately equal to 0.107585), adopting the renormalization used in [9]. As was stressed in [2]:

*“by using instead the alternative renormalization (3.6), the location of all the level crossings would be exactly  $\tilde{\alpha}^{(3)}=0$ , leading to the graph shown in Fig. 4(a) of the aforementioned paper by Brüning, Geyley and Lobanov”.*

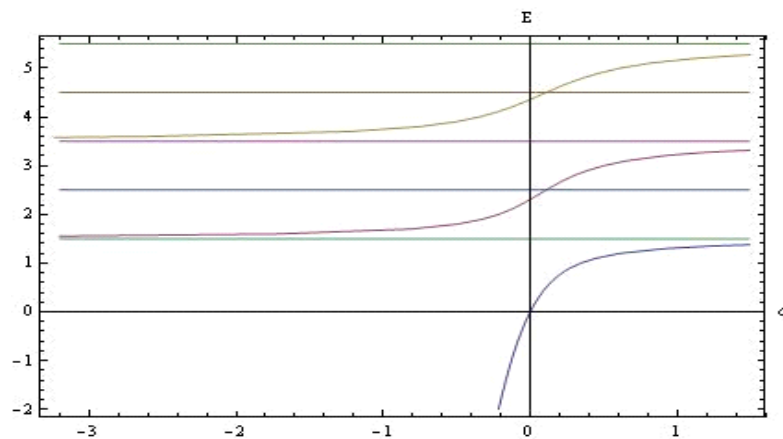


FIG. 2. The ground state energy and the next two symmetric eigenenergies of the 3D-isotropic harmonic oscillator with an attractive  $\delta$ -perturbation situated at the origin as functions of the extension parameter  $\alpha = 1/\beta$

The very same phenomenon observed in [2] for the one-dimensional Hamiltonian  $h(\alpha)$ , for which all the level crossings take place exactly at  $\alpha = \alpha_0^{(1D)}$  (approximately equal to 0.675978) using the renormalization (2.4a) of that paper, is to be regarded as being even more remarkable. Citing again our considerations in [2], it can be stated that:

*“from the point of view of the structure of the spectral curves representing the eigenvalues (energy levels) as functions of the extension parameter and neglecting the degeneracy of the three-dimensional eigenvalues, the harmonic oscillator perturbed by the point interaction considered here ( $|\delta'(x)\rangle\langle\delta'(x)|$ ) seems to be a more legitimate one-dimensional counterpart than the delta distribution as the latter bears no resemblance of the 3D-level crossing involving eigenstates of different symmetry. Having stated that analogy, an important difference must also be pointed out: whilst in the case of the perturbed isotropic oscillator the eigenenergy of the simple eigenvalue created by the point interaction (emerging out of a degenerate level with an even value of the total angular momentum) can cross the next lower unperturbed level (having an odd value of the total angular momentum) beyond a certain threshold of the key parameter of that model, something of an opposite nature occurs in the one-dimensional model being studied here: each perturbed odd eigenvalue can fall below the next lower unperturbed even eigenvalue beyond a certain threshold. As a consequence, the symmetry of the ground state wave function can change in the case of a sufficiently strong  $\delta'$ -interaction (the ground state wave function being given by an odd function discontinuous at the origin)”.*

The spectral features of the Hamiltonian for our perturbed isotropic oscillator described in the previous remarks can be visualized in the above graph (Fig. 2) displaying the new ground state energy  $E_0(\alpha)$  and those of the two symmetric bound states  $E_2(\alpha)$  and  $E_4(\alpha)$  which emerge from the 7/2 and 11/2 levels as a result of the perturbation and are confined inside the intervals  $(3/2, 7/2)$  and  $(7/2, 11/2)$ , as functions of the extension parameter, as well as their level crossings with the unperturbed antisymmetric states  $E = 5/2$  and  $E = 9/2$ . Both of these

occur, as anticipated above, at  $\alpha = \alpha_0$  (approximately equal to 0.107585). It is worth reminding the reader that the degeneracy of  $E = 7/2$  has been lowered to five and that of  $E = 11/2$  to fourteen.

**3. The three-dimensional isotropic harmonic oscillator perturbed by two twin attractive point perturbations symmetrically situated with respect to the origin**

We wish to continue our analysis of the three-dimensional model by considering the heuristic Hamiltonian:

$$H_{\{\beta, \vec{x}_0\}} = H_0 - \beta [\delta(\vec{x} - \vec{x}_0) + \delta(\vec{x} + \vec{x}_0)], \quad \vec{x}_0 = (x_0, 0, 0), \quad x_0 > 0. \quad (3.1)$$

As pointed out in the final remarks in [17] (see also the references therein), the model with a singular double well has been increasingly utilized in the recent condensed matter theory literature “since, in combination with a cubic nonlinearity, it leads to a particular type of the nonlinear Schrödinger equation for Bose-Einstein condensates (Gross-Pitaevskii equation)”.

By essentially mimicking what was done in [2, 9], we can start by performing the standard ultraviolet cut-off and making the coupling  $\mu = \mu(\ell, \beta) > 0$  dependent upon the related upper limit  $0 < \ell < +\infty$  for the energy, which leads to the introduction of a perfectly defined self-adjoint Hamiltonian:

$$H_{\{\ell, \beta, \vec{x}_0\}} = H_0 - \mu(\ell, \beta) \sum_{|\vec{l}|=0, |\vec{m}|=0}^{\ell} |\Psi_{\vec{l}}\rangle [\Psi_{\vec{l}}(\vec{x}_0) \Psi_{\vec{m}}(\vec{x}_0) + \Psi_{\vec{l}}(-\vec{x}_0) \Psi_{\vec{m}}(-\vec{x}_0)] \langle \Psi_{\vec{m}}|, \quad (3.2)$$

which implies that for any sufficiently negative  $E$  we can write:

$$H_{\{\ell, \beta, \vec{x}_0\}} - E = (H_0 - E)^{1/2} \left\{ I - \mu(\ell, \beta) \left[ |(H_0^\ell - E)^{-1/2}(\cdot, -\vec{x}_0)\rangle \langle (H_0^\ell - E)^{-1/2}(-\vec{x}_0, \cdot)| + |(H_0^\ell - E)^{-1/2}(\cdot, \vec{x}_0)\rangle \langle (H_0^\ell - E)^{-1/2}(\vec{x}_0, \cdot)| \right] \right\} (H_0 - E)^{1/2}. \quad (3.3)$$

Therefore, in order to explicitly write the resolvent of the left hand side of (3.2), it is crucial to determine the inverse of the operator inside the curly brackets on the right hand side of (3.3). We wish to remind the reader that the expression of the resolvent given by the inverse of (3.3) is known as Tiktopoulos’ formula, commonly used in dealing with perturbations of semibounded operators (see, e.g., Theor. VIII.25 in [18]). It is worth noting that in the latter expansion of the resolvent the crucial role is played by an operator of the type:

$$(A + I)^{-1/2} (A_n - A) (A + I)^{-1/2}, \quad A \geq 0,$$

which is isospectral to the more widely investigated Birman-Schwinger operator (see, e.g., [19, 20] in the case of perturbations of the negative Laplacian in one dimension). In perfect analogy with what was done in [7, 11, 17], it is possible to rewrite the operator of rank two inside the square brackets on the right hand side of (3.3) as follows:

$$\begin{aligned} & |(H_0^\ell - E)^{-1/2}(\cdot, -\vec{x}_0)\rangle \langle (H_0^\ell - E)^{-1/2}(-\vec{x}_0, \cdot)| + |(H_0^\ell - E)^{-1/2}(\cdot, \vec{x}_0)\rangle \langle (H_0^\ell - E)^{-1/2}(\vec{x}_0, \cdot)| \\ & 2 \left[ |(H_0^\ell - E)^{-1/2}(\cdot, \vec{x}_0)\rangle \langle (H_0^\ell - E)^{-1/2}(\vec{x}_0, \cdot)| + |(H_0^\ell - E)^{-1/2}(\cdot, \vec{x}_0)\rangle \langle (H_0^\ell - E)^{-1/2}(\vec{x}_0, \cdot)| \right], \end{aligned} \quad (3.4)$$

where

$$\begin{aligned} (H_0^\ell - E)^{-1/2}(\vec{x}_0, \vec{x}) & := \sum_{|\vec{n}|=0}^{\ell} \frac{\Psi_{2\vec{n}}(\vec{x}_0)}{(|2\vec{n}| + \frac{3}{2} - E)^{1/2}} \Psi_{2\vec{n}}(\vec{x}), \\ (H_0^\ell - E)^{-1/2}(\vec{x}_0, \vec{x}) & := \end{aligned}$$

$$\sum_{|\vec{n}|=0}^{\ell} \frac{\psi_{2n_1+1}(x_0)\psi_{2n_2}(0)\psi_{2n_3}(0)}{(2n_1 + 2n_2 + 2n_3 + \frac{5}{2} - E)^{1/2}} \psi_{2n_1+1}(x)\psi_{2n_2}(y)\psi_{2n_3}(z),$$

which implies their mutual orthogonality.

By essentially mimicking what was done in the aforementioned papers, it is rather straightforward to obtain the algebra for the powers of the rank-two operator on the right hand side of (3.4):

$$\begin{aligned} & \left\{ 2 \left[ |(H_0^\ell - E)_s^{-1/2}(\cdot, \vec{x}_0)\rangle \langle (H_0^\ell - E)_s^{-1/2}(\vec{x}_0, \cdot)| + \right. \right. \\ & \quad \left. \left. |(H_0^\ell - E)_{as}^{-1/2}(\cdot, \vec{x}_0)\rangle \langle (H_0^\ell - E)_{as}^{-1/2}(\vec{x}_0, \cdot)| \right] \right\}^{m+1} = \\ & 2^{m+1} \left\{ [(H_0^\ell - E)_s^{-1}(\vec{x}_0, \vec{x}_0)]^m |(H_0^\ell - E)_s^{-1/2}(\cdot, \vec{x}_0)\rangle \langle (H_0^\ell - E)_s^{-1/2}(\vec{x}_0, \cdot)| + \right. \\ & \quad \left. [(H_0^\ell - E)_{as}^{-1}(\vec{x}_0, \vec{x}_0)]^m |(H_0^\ell - E)_{as}^{-1/2}(\cdot, \vec{x}_0)\rangle \langle (H_0^\ell - E)_{as}^{-1/2}(\vec{x}_0, \cdot)| \right\}, \quad (3.5) \end{aligned}$$

given that:

$$\left\| (H_0^\ell - E)_s^{-1/2}(\vec{x}_0, \cdot) \right\|_2^2 = \sum_{|\vec{n}|=0}^{\ell} \frac{\Psi_{2\vec{n}}^2(\vec{x}_0)}{|2\vec{n}| + \frac{3}{2} - E} = (H_0^\ell - E)_s^{-1}(\vec{x}_0, \vec{x}_0),$$

and similarly for the square of the norm of  $(H_0^\ell - E)_{as}^{-1/2}(\vec{x}_0, \cdot)$ . Hence, the inverse of the operator inside the curly brackets of (3.3) can be written as a new rank-two operator:

$$\begin{aligned} & \frac{1}{\frac{1}{2\mu(\ell, \beta)} - (H_0^\ell - E)_s^{-1}(\vec{x}_0, \vec{x}_0)} \left| (H_0^\ell - E)_s^{-1/2}(\cdot, \vec{x}_0)\rangle \langle (H_0^\ell - E)_s^{-1/2}(\vec{x}_0, \cdot) \right| + \\ & \frac{1}{\frac{1}{2\mu(\ell, \beta)} - (H_0^\ell - E)_{as}^{-1}(\vec{x}_0, \vec{x}_0)} \left| (H_0^\ell - E)_{as}^{-1/2}(\cdot, \vec{x}_0)\rangle \langle (H_0^\ell - E)_{as}^{-1/2}(\vec{x}_0, \cdot) \right|. \quad (3.6) \end{aligned}$$

Therefore, the inverse of the operator on the left hand side of (3.3) is:

$$\begin{aligned} (H_{\{\ell, \beta, \vec{x}_0\}} - E)^{-1} &= (H_0 - E)^{-1} + \\ & \frac{1}{\frac{1}{2\mu(\ell, \beta)} - (H_0^\ell - E)_s^{-1}(\vec{x}_0, \vec{x}_0)} \left| (H_0^\ell - E)_s^{-1}(\cdot, \vec{x}_0)\rangle \langle (H_0^\ell - E)_s^{-1}(\vec{x}_0, \cdot) \right| + \\ & \frac{1}{\frac{1}{2\mu(\ell, \beta)} - (H_0^\ell - E)_{as}^{-1}(\vec{x}_0, \vec{x}_0)} \left| (H_0^\ell - E)_{as}^{-1}(\cdot, \vec{x}_0)\rangle \langle (H_0^\ell - E)_{as}^{-1}(\vec{x}_0, \cdot) \right|. \quad (3.7) \end{aligned}$$

At this stage, we need to thoroughly investigate what occurs when the ultraviolet cut-off gets removed, that is to say the behavior of (3.7) as  $\ell \rightarrow +\infty$ .

As a consequence of the simple estimate:

$$\begin{aligned} \sum_{|\vec{n}|=0}^{\ell} \frac{\Psi_{2\vec{n}}^2(\vec{x}_0)}{(|2\vec{n}| + \frac{3}{2} - E)^2} &\leq \sum_{|\vec{n}|=0}^{\infty} \frac{\Psi_{2\vec{n}}^2(\vec{x}_0)}{(|2\vec{n}| + \frac{3}{2} - E)^2} \leq \\ & \left[ \sum_{n=0}^{\infty} \frac{\psi_{2n}^2(x_0)}{(2n + 1/2)^{2/3}} \right] \left[ \sum_{n=0}^{\infty} \frac{\psi_{2n}^2(0)}{(2n + 1/2)^{2/3}} \right]^2 < \infty, \quad (3.8) \end{aligned}$$

it is immediate to realize that  $(H_0^\ell - E)_s^{-1}(\vec{x}_0, \cdot)$  will converge in the Hilbert space norm to the following:

$$(H_0 - E)_s^{-1}(\vec{x}_0, \vec{x}) := \sum_{|\vec{n}|=0}^{\infty} \frac{\Psi_{2\vec{n}}(\vec{x}_0)}{|2\vec{n}| + \frac{3}{2} - E} \Psi_{2\vec{n}}(\vec{x}). \tag{3.9}$$

The latter convergence implies in a straightforward manner that the rank-one operator:

$$\left| (H_0^\ell - E)_s^{-1}(\cdot, \vec{x}_0) \right\rangle \left\langle (H_0^\ell - E)_s^{-1}(\vec{x}_0, \cdot) \right|,$$

will converge in the trace class norm to the following:

$$\left| (H_0 - E)_s^{-1}(\cdot, \vec{x}_0) \right\rangle \left\langle (H_0 - E)_s^{-1}(\vec{x}_0, \cdot) \right|.$$

Similarly, it follows that:

$$\left| (H_0^\ell - E)_{as}^{-1}(\cdot, \vec{x}_0) \right\rangle \left\langle (H_0^\ell - E)_{as}^{-1}(\vec{x}_0, \cdot) \right| \rightarrow \left| (H_0 - E)_{as}^{-1}(\cdot, \vec{x}_0) \right\rangle \left\langle (H_0 - E)_{as}^{-1}(\vec{x}_0, \cdot) \right|,$$

with

$$(H_0 - E)_{as}^{-1}(\vec{x}_0, \vec{x}) := \sum_{|\vec{n}|=0}^{\infty} \frac{\psi_{2n_1+1}(x_0)\psi_{2n_2}(0)\psi_{2n_3}(0)}{(2n_1 + 2n_2 + 2n_3 + \frac{5}{2} - E)^{1/2}} \psi_{2n_1+1}(x)\psi_{2n_2}(y)\psi_{2n_3}(z). \tag{3.10}$$

Therefore, the only problem caused by the removal of the ultraviolet cut-off is the divergence of the series inside each denominator in the second and third term on the right hand side of (3.7). However, we still have the freedom of choosing the  $\ell$ -dependence of  $\mu(\ell, \beta)$  in such a way that the typical ‘‘cancellation of infinities’’ may take place. Let us set:

$$\frac{1}{\mu(\ell, \beta)} = \frac{1}{\beta} + \sum_{|\vec{n}|=0}^{\ell} \frac{\Psi_{2\vec{n}}^2(0)}{|2\vec{n}| + \frac{3}{2}}, \tag{3.11}$$

or equivalently:

$$\mu(\ell, \beta) = \beta \left[ 1 + \beta \sum_{|\vec{n}|=0}^{\ell} \frac{\Psi_{2\vec{n}}^2(0)}{|2\vec{n}| + \frac{3}{2}} \right]^{-1}. \tag{3.11b}$$

In perfect accordance with the use of the term ‘‘attractive’’ in [2, 3, 9, 17], it is clear that  $\mu(\ell, \beta) > 0$  for the large values of  $\ell$  involved in the limit, regardless of the sign of  $\beta$ . This makes the singular interaction attractive because of the presence of the negative sign in the second term in (3.2). Hence, for any  $E < 3/2$ :

$$\frac{1}{2\mu(\ell, \beta)} - (H_0^\ell - E)_s^{-1}(\vec{x}_0, \vec{x}_0) = \frac{1}{2\beta} + \frac{1}{2} \sum_{|\vec{n}|=0}^{\ell} \frac{\Psi_{2\vec{n}}^2(0)}{|2\vec{n}| + \frac{3}{2}} - \sum_{|\vec{n}|=0}^{\ell} \frac{\Psi_{2\vec{n}}^2(\vec{x}_0)}{|2\vec{n}| + \frac{3}{2} - E}, \tag{3.12}$$

and

$$\begin{aligned} \frac{1}{2\mu(\ell, \beta)} - (H_0^\ell - E)_{as}^{-1}(\vec{x}_0, \vec{x}_0) = \\ \frac{1}{2\beta} + \frac{1}{2} \sum_{|\vec{n}|=0}^{\ell} \frac{\Psi_{2\vec{n}}^2(0)}{|2\vec{n}| + \frac{3}{2}} - \sum_{|\vec{n}|=0}^{\ell} \frac{\psi(x_0)_{2n_1+1}^2 \psi_{2n_2}^2(0) \psi_{2n_3}^2(0)}{2n_1 + 2n_2 + 2n_3 + \frac{5}{2} - E}, \end{aligned} \tag{3.12a}$$

(as will be seen shortly, considered separately, the latter expression is well defined for any  $E < 5/2$ ).

By taking advantage of the integral representation for the resolvent of the three-dimensional harmonic oscillator for any  $E < 3/2$ , that is to say the aforementioned Mehler’s kernel, as well

as of the explicit expressions of the symmetric and antisymmetric components of the integral kernel of the semigroup for the one-dimensional harmonic oscillator established in [11], the limit of the right hand side of (3.12), as  $\ell \rightarrow +\infty$  can be written as:

$$\begin{aligned} \frac{1}{2\beta} + \frac{1}{2\pi^{3/2}} \left[ \int_0^1 \frac{\xi^{1/2}}{(1-\xi^2)^{3/2}} d\xi - \int_0^1 \frac{\xi^{1/2-E} \left[ e^{-x_0^2 \frac{1-\xi}{1+\xi}} + e^{-x_0^2 \frac{1+\xi}{1-\xi}} \right]}{(1-\xi^2)^{3/2}} d\xi \right] = \\ \frac{1}{2\beta} + \frac{1}{2\pi^{3/2}} \int_0^1 \frac{\xi^{1/2} \left[ 1 - \xi^{-E} \left( e^{-x_0^2 \frac{1-\xi}{1+\xi}} + e^{-x_0^2 \frac{1+\xi}{1-\xi}} \right) \right]}{(1-\xi^2)^{3/2}} d\xi < \infty. \end{aligned} \quad (3.13)$$

Similarly, for any  $E < 5/2$ , the limit of the other denominator is given by:

$$\frac{1}{2\beta} + \frac{1}{2\pi^{3/2}} \int_0^1 \frac{\xi^{1/2} \left[ 1 - \xi^{-E} \left( e^{-x_0^2 \frac{1-\xi}{1+\xi}} - e^{-x_0^2 \frac{1+\xi}{1-\xi}} \right) \right]}{(1-\xi^2)^{3/2}} d\xi < \infty, \quad (3.13a)$$

taking into account that, as pointed out in [11], we have:

$$\xi^{-1} \left( e^{-x_0^2 \frac{1-\xi}{1+\xi}} - e^{-x_0^2 \frac{1+\xi}{1-\xi}} \right) \rightarrow 4x_0^2,$$

as  $\xi \rightarrow 0_+$ , which implies that  $\xi^{1/2-E} \left( e^{-x_0^2 \frac{1-\xi}{1+\xi}} - e^{-x_0^2 \frac{1+\xi}{1-\xi}} \right)$  has an integrable singularity at  $0_+$  as long as  $E < 5/2$ .

Hence, for any  $x_0 > 0$  and any  $E < 3/2$  (resp.  $E < 5/2$ ), the difference of the two divergent series on the right hand side of (3.12) (resp. (3.12a)) yields a finite limit. Then, it is not difficult to prove that, as a consequence of the first resolvent identity, the same holds at any other point away from  $\sigma(H_0)$ .

Therefore, the norm resolvent limit of (3.7) after removing the ultraviolet cut-off is given by:

$$\begin{aligned} (H_0 - E)^{-1} + \frac{|(H_0 - E)_s^{-1}(\cdot, \vec{x}_0)\rangle \langle (H_0 - E)_s^{-1}(\vec{x}_0, \cdot)|}{\frac{1}{2\beta} + \lim_{\ell \rightarrow +\infty} \left[ \frac{1}{2} \sum_{|\vec{n}|=0}^{\ell} \frac{\Psi_{2\vec{n}}^2(0)}{|2\vec{n}| + \frac{3}{2}} - \sum_{|\vec{n}|=0}^{\ell} \frac{\Psi_{2\vec{n}}^2(\vec{x}_0)}{|2\vec{n}| + \frac{3}{2} - E} \right]} \\ \frac{|(H_0 - E)_{as}^{-1}(\cdot, \vec{x}_0)\rangle \langle (H_0 - E)_{as}^{-1}(\vec{x}_0, \cdot)|}{\frac{1}{2\beta} + \lim_{\ell \rightarrow +\infty} \left[ \frac{1}{2} \sum_{|\vec{n}|=0}^{\ell} \frac{\Psi_{2\vec{n}}^2(0)}{|2\vec{n}| + \frac{3}{2}} - \sum_{|\vec{n}|=0}^{\ell} \frac{\psi_{2n_1+1}^2(x_0) \psi_{2n_2}^2(0) \psi_{2n_3}^2(0)}{2n_1 + 2n_2 + 2n_3 + \frac{5}{2} - E} \right]}. \end{aligned} \quad (3.14)$$

In particular, for any  $E < 3/2$ , we have the following integral representation:

$$(H_0 - E)^{-1} + \frac{|(H_0 - E)_s^{-1}(\cdot, \vec{x}_0)\rangle\langle(H_0 - E)_s^{-1}(\vec{x}_0, \cdot)|}{\frac{1}{2\beta} + \frac{1}{2\pi^{3/2}} \int_0^1 \frac{\xi^{1/2} \left[1 - \xi^{-E} \left(e^{-x_0^2 \frac{1-\xi}{1+\xi}} + e^{-x_0^2 \frac{1+\xi}{1-\xi}}\right)\right]}{(1 - \xi^2)^{3/2}} d\xi} + \frac{|(H_0 - E)_{as}^{-1}(\cdot, \vec{x}_0)\rangle\langle(H_0 - E)_{as}^{-1}(\vec{x}_0, \cdot)|}{\frac{1}{2\beta} + \frac{1}{2\pi^{3/2}} \int_0^1 \frac{\xi^{1/2} \left[1 - \xi^{-E} \left(e^{-x_0^2 \frac{1-\xi}{1+\xi}} - e^{-x_0^2 \frac{1+\xi}{1-\xi}}\right)\right]}{(1 - \xi^2)^{3/2}} d\xi}. \quad (3.14a)$$

By essentially mimicking the proofs used in some of the above-mentioned papers [2, 9, 17], it can be rigorously shown that the latter operator is indeed the resolvent of a semibounded self-adjoint operator for any  $E$  below  $E_0(\beta)$ , the lowest zero of the denominator in the second term in (3.14) and (3.14a). Furthermore, the explicit form of the resolvent clearly implies its analyticity in norm in close proximity to 0 (since we have an analytic family in the sense of Kato, see [14, 21]) as a function of  $\beta$ .

The results obtained so far can thus be summarized in the following theorem.

**Theorem 3.1.** *The rigorous Hamiltonian of the three-dimensional isotropic oscillator, perturbed by two identical attractive point interactions situated symmetrically with respect to the origin at the points  $\pm\vec{x}_0 = (\pm x_0, 0, 0)$ ,  $x_0 > 0$ , making sense of the merely formal expression (3.1), is the self-adjoint operator  $H_{\{\beta, \vec{x}_0\}}$  whose resolvent is given by the bounded operator (3.14). The latter is the limit of the resolvents (3.7) (of the Hamiltonians with the energy cut-off defined by (3.2)) in the norm topology of bounded operators on  $L_2(\mathbb{R}^3)$  once the energy cut-off is removed. Furthermore,  $H_{\{\beta, \vec{x}_0\}}$ , regarded as a function of  $\beta$ , is an analytic family in the sense of Kato.*

Of course, unlike the Hamiltonian analyzed in Section 2, we can no longer hope to have the bound state equation expressed in terms of a ratio of Gamma functions.

Nevertheless, since the limit of the difference of the divergent series appearing in the first (resp. second) denominator of (3.14) gives rise to a smooth multibranch function of the energy parameter, with its vertical asymptotes given by the symmetric (resp. antisymmetric) eigenvalues of the unperturbed Hamiltonian, we can rely on the findings of [8–11] to have it expressed in terms of an integral that will have to be suitably modified for each single level in order to avoid the unpleasant appearance of divergences.

**Remark.** *In perfect accordance with what was observed in [10] for the analogous one-dimensional model with a single point impurity centered away from the origin, and in [11] for the model having a pair of twin impurities symmetrically situated with respect to the origin, it is worth pointing out that whenever the location of the impurities coincides with a node of an eigenfunction for the one-dimensional harmonic oscillator (here we are obviously excluding the trivial case  $x_0 = 0$ ), then the corresponding eigenvalue will not be affected at all by the singular perturbation. In other words, if*

$$\psi_{2m_1}(x_0) = 0, \quad x_0 > 0 \quad (\text{respectively } \psi_{2m_1+1}(x_0) = 0),$$

then

$$\Psi_{2\vec{m}}(\vec{x}), \quad \vec{m} = (m_1, m_2, m_3) \quad (\text{resp. } \psi_{2m_1+1}(x)\psi_{2m_2}(y)\psi_{2m_3}(z)t)$$

belongs to the kernel of the first (resp. second) rank-one operator in (3.14) and the corresponding eigenvalue

$$|2\vec{m}| + \frac{3}{2} \quad \left( \text{resp. } 2m_1 + 2m_2 + 2m_3 + \frac{5}{2} \right)$$

will stay in the spectrum with its original multiplicity.

Hence, for any  $E < 3/2$ , the equation determining the ground state energy is given by:

$$\frac{1}{\beta} = \frac{1}{\pi^{3/2}} \int_0^1 \frac{\xi^{1/2} \left[ \xi^{-E} \left( e^{-x_0^2 \frac{1-\xi}{1+\xi}} + e^{-x_0^2 \frac{1+\xi}{1-\xi}} \right) - 1 \right]}{(1-\xi^2)^{3/2}} d\xi. \quad (3.15)$$

By setting  $\alpha = 1/\beta$  and

$$\alpha_0^+(x_0) = \frac{1}{\pi^{3/2}} \int_0^1 \frac{\left( e^{-x_0^2 \frac{1-\xi}{1+\xi}} + e^{-x_0^2 \frac{1+\xi}{1-\xi}} \right) - \xi^{1/2}}{(1-\xi^2)^{3/2}} d\xi < \infty, \quad (3.15a)$$

the equation can be exactly recast in a manner that is completely analogous to (2.5d), that is to say:

$$\alpha - \alpha_0^+(x_0) = \frac{1}{\pi^{3/2}} \int_0^1 \frac{(\xi^{1/2-E} - 1) \left( e^{-x_0^2 \frac{1-\xi}{1+\xi}} + e^{-x_0^2 \frac{1+\xi}{1-\xi}} \right)}{(1-\xi^2)^{3/2}} d\xi. \quad (3.15b)$$

The graph for the solution of the above equation, i.e. the ground state energy as a function of the extension parameter, is shown below in Fig. 3 for  $x_0 = 0.2$ .

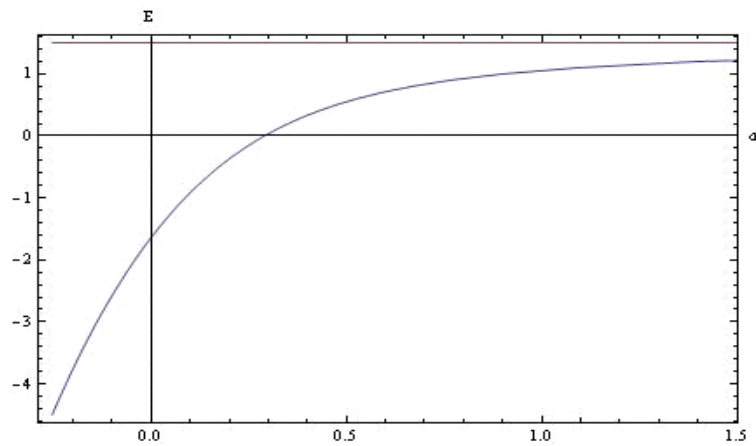


FIG. 3. The ground state energy for the 3D-isotropic harmonic oscillator perturbed by a pair of identical attractive point interactions symmetrically situated at a distance  $x_0 = 0.2$  from the origin as a function of the extension parameter  $\alpha = 1/\beta$

Similarly, the equation determining the energy of the lowest antisymmetric bound state for any  $E < 5/2$ , namely:

$$\frac{1}{\beta} = \frac{1}{\pi^{3/2}} \int_0^1 \frac{\xi^{1/2} \left[ \xi^{-E} \left( e^{-x_0^2 \frac{1-\xi}{1+\xi}} - e^{-x_0^2 \frac{1+\xi}{1-\xi}} \right) - 1 \right]}{(1-\xi^2)^{3/2}} d\xi, \quad (3.16)$$

after setting

$$\alpha_0^-(x_0) = \frac{1}{\pi^{3/2}} \int_0^1 \frac{\left( e^{-x_0^2 \frac{1-\xi}{1+\xi}} - e^{-x_0^2 \frac{1+\xi}{1-\xi}} \right) - \xi^{1/2}}{(1-\xi^2)^{3/2}} d\xi < \infty, \quad (3.16a)$$

can be recast as:

$$\alpha - \alpha_0^-(x_0) = \frac{1}{\pi^{3/2}} \int_0^1 \frac{(\xi^{1/2-E} - 1) \left( e^{-x_0^2 \frac{1-\xi}{1+\xi}} - e^{-x_0^2 \frac{1+\xi}{1-\xi}} \right)}{(1-\xi^2)^{3/2}} d\xi. \quad (3.16b)$$

The graph for the solution of the above equation, representing the energy of the lowest anti-symmetric bound state as a function of the extension parameter, is shown below in Fig. 4 for  $x_0 = 0.2$ .

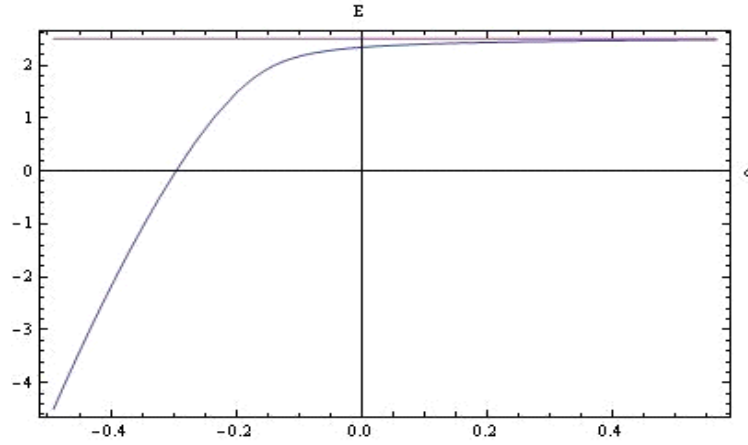


FIG. 4. The energy for the lowest antisymmetric bound state of the 3D-isotropic harmonic oscillator perturbed by a pair of identical attractive point interactions symmetrically situated at a distance  $x_0 = 0.2$  from the origin as a function of the extension parameter  $\alpha = 1/\beta$

By further exploiting the technique developed in the aforementioned papers [8–11] to obtain cancellation of the divergences as we move to the right of  $E = 3/2$ , we can also study the equation determining the second symmetric bound state energy.

Given that:

$$\lim_{\ell \rightarrow +\infty} \left[ \frac{1}{2} \sum_{|\vec{n}|=0}^{\ell} \frac{\Psi_{2\vec{n}}^2(0)}{2|\vec{n}| + \frac{3}{2}} - \sum_{|\vec{n}|=0}^{\ell} \frac{\Psi_{2\vec{n}}^2(\vec{x}_0)}{2|\vec{n}| + \frac{3}{2} - E} \right] = \frac{1}{2} \frac{\Psi_0^2(0)}{3/2} - \frac{\Psi_0^2(\vec{x}_0)}{3/2 - E} + \lim_{\ell \rightarrow +\infty} \left[ \frac{1}{2} \sum_{|\vec{n}|=1}^{\ell} \frac{\Psi_{2\vec{n}}^2(0)}{2|\vec{n}| + \frac{3}{2}} - \sum_{|\vec{n}|=1}^{\ell} \frac{\Psi_{2\vec{n}}^2(\vec{x}_0)}{2|\vec{n}| + \frac{3}{2} - E} \right], \quad (3.17)$$

and

$$\frac{\Psi_0^2(0)}{3/2} = \frac{1}{\pi^{3/2}} \int_0^1 \xi^{1/2} d\xi, \quad \frac{\Psi_0^2(x_0)}{3/2 - E} = \frac{e^{-x_0^2}}{\pi^{3/2}} \int_0^1 \xi^{1/2-E} d\xi,$$

the equation determining the second symmetric bound state energy is given by:

$$\frac{1}{\beta} = \frac{2e^{-x_0^2}}{(3/2 - E)\pi^{3/2}} - \frac{2}{3\pi^{3/2}} + \frac{1}{\pi^{3/2}} \int_0^1 \frac{\xi^{1/2} [(1 - \xi^2)^{3/2} - 1]}{(1 - \xi^2)^{3/2}} d\xi + \frac{1}{\pi^{3/2}} \int_0^1 \frac{\xi^{1/2-E} \left[ e^{-x_0^2(1-\xi)/(1+\xi)} + e^{-x_0^2(1+\xi)/(1-\xi)} - 2e^{-x_0^2}(1 - \xi^2)^{3/2} \right]}{(1 - \xi^2)^{3/2}} d\xi. \quad (3.18)$$

Since the quantity

$$e^{-x_0^2(1-\xi)/(1+\xi)} + e^{-x_0^2(1+\xi)/(1-\xi)} - 2e^{-x_0^2}(1 - \xi^2)^{3/2}$$

behaves like  $c\xi^2 + O(\xi^4)$  in the region to the right of the origin, it is quite evident that the numerator inside the second integral on the right hand side of (3.18) has an integrable singularity at the lower limit of integration for any  $E < 7/2$ , that is to say the third eigenvalue of the unperturbed 3D-isotropic harmonic oscillator. One can immediately notice that both integrals on the right hand side of (3.18) diverge as  $\xi \rightarrow 1_-$ . However, by rewriting their sum as:

$$\frac{1}{\pi^{3/2}} \int_0^1 \frac{\xi^{1/2} \left\{ (1 - \xi^2)^{3/2} - 1 - \xi^{-E} \left[ 2e^{-x_0^2}(1 - \xi^2)^{3/2} - e^{-x_0^2(1-\xi)/(1+\xi)} - e^{-x_0^2(1+\xi)/(1-\xi)} \right] \right\}}{(1 - \xi^2)^{3/2}} d\xi,$$

it is a bit tedious but straightforward to check that:

$$\frac{\xi^{1/2} \left\{ (1 - \xi^2)^{3/2} - 1 - \xi^{-E} \left[ 2e^{-x_0^2}(1 - \xi^2)^{3/2} - e^{-x_0^2(1-\xi)/(1+\xi)} - e^{-x_0^2(1+\xi)/(1-\xi)} \right] \right\}}{1 - \xi^2} \rightarrow L_E < \infty,$$

as  $\xi \rightarrow 1_-$ , which implies the integrable nature of the singularity at the upper limit of integration and, therefore, the cancellation of the two divergent quantities on the right hand side of (3.18). Hence, for any  $3/2 < E < 7/2$ , the equation determining the second symmetric bound state energy can be recast as:

$$\frac{1}{\beta} = \frac{2e^{-x_0^2}}{(3/2 - E)\pi^{3/2}} - \frac{2}{3\pi^{3/2}} + \frac{1}{\pi^{3/2}} \times \int_0^1 \frac{\xi^{1/2} \left\{ (1 - \xi^2)^{3/2} - \xi^{-E} \left[ 2e^{-x_0^2}(1 - \xi^2)^{3/2} - e^{-x_0^2(1-\xi)/(1+\xi)} - e^{-x_0^2(1+\xi)/(1-\xi)} \right] \right\}}{(1 - \xi^2)^{3/2}} d\xi. \quad (3.18a)$$

The latter equation can be further transformed into:

$$\alpha - \alpha_0^+(x_0) = \frac{2e^{-x_0^2}}{(3/2 - E)\pi^{3/2}} - \frac{2}{3\pi^{3/2}} + \frac{1}{\pi^{3/2}} \times \left[ \int_0^1 \frac{\xi^{1/2} \left\{ (1 - \xi^2)^{3/2} - \xi^{-E} \left[ 2e^{-x_0^2}(1 - \xi^2)^{3/2} - e^{-x_0^2(1-\xi)/(1+\xi)} - e^{-x_0^2(1+\xi)/(1-\xi)} \right] \right\}}{(1 - \xi^2)^{3/2}} d\xi + \int_0^1 \frac{-e^{-x_0^2(1-\xi)/(1+\xi)} - e^{-x_0^2(1+\xi)/(1-\xi)}}{(1 - \xi^2)^{3/2}} d\xi \right]. \quad (3.18b)$$

Figure 5 shows the plot for the counterpart of Fig. 2 for  $x_0 = 0.2$  with the five lowest eigenvalues, namely  $E_0(\alpha)$ ,  $E_1(\alpha)$ ,  $E_2(\alpha)$  (clearly omitting their dependence on  $x_0$  to make the

notation less cumbersome), the new eigenenergies created by the pair of twin point interactions, in addition to  $5/2$  and  $7/2$ , whose degeneracy has now been lowered to two and five respectively.

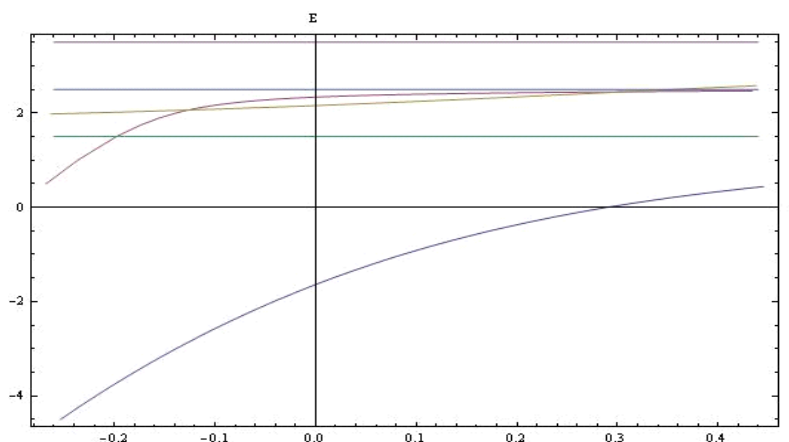


FIG. 5. The ground state energy and the next two eigenenergies created by two identical attractive  $\delta$ -perturbations situated symmetrically at the same distance from the origin,  $x_0 = 0.2$ , as functions of the extension parameter  $\alpha = 1/\beta$

It is worth stressing that, in addition to level crossings of the same type as those encountered in the aforementioned articles [1,9], which occur in the case of a single  $\delta$ -impurity, involving the new eigenvalues created by the point perturbations and the eigenvalues of the unperturbed harmonic oscillator preserved under the perturbation due to their degeneracy, two further level crossings of a new type involving  $E_1(\alpha)$  and  $E_2(\alpha)$  (the two new energy levels created by the singular double-well perturbation above the ground state one), can be observed at the values  $\alpha_2$  (approximately equal to  $-0.126478$ ) and  $\alpha_3$  (approximately equal to  $0.309201$ ). It seems rather remarkable to us that, for such a small value of the distance  $x_0$ , there is a range of values for the extension parameter  $\alpha$ , namely the interval  $(\alpha_2, \alpha_3)$ , inside which  $E_2(\alpha) < E_1(\alpha)$ . In other words, when the coupling is sufficiently strong (taking account of the fact that  $\alpha = 1/\beta$ ) and the distance between the two centers is sufficiently small (this point will be made more precise shortly), the second symmetric bound state created by the singular perturbation can become more tightly bound than the lowest antisymmetric bound state. Furthermore, the energy level created by the perturbation at  $\alpha_2$  (resp.  $\alpha_3$ ) is doubly degenerate, since  $E_1(\alpha_2) = E_2(\alpha_2)$  (resp.  $E_1(\alpha_3) = E_2(\alpha_3)$ ).

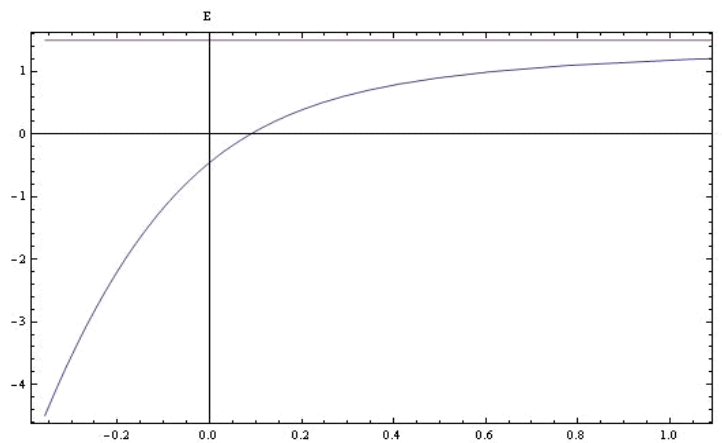
In addition to the value  $\alpha_4$  (approximately equal to  $0.356236$ ), where  $E_2(\alpha) = 5/2$ , it is also worth including the value  $\alpha_1$  (approximately equal to  $-0.198151$ ) where  $E_1(\alpha) = 3/2$ , even though  $E = 3/2$  is no longer an eigenvalue. Then, the spectral features displayed in Fig. 5 can be summarized in Table 1.

Next, we will show how an increase in  $x_0$  affects the energy levels considered before. As clearly shown by the comparison between the graph of the ground state energy as a function of  $\alpha$  in Fig. 6 for  $x_0 = 0.4$  and its analogue in Fig. 3 for  $x_0 = 0.2$ , we have  $E_0(\alpha; 0.2) < E_0(\alpha; 0.4)$  for any  $\alpha$ .

Although we cannot strictly use the definition of “positional disorder” given in [1] for the 3D-isotropic quantum dot with a single impurity because of the presence of the vector  $-\vec{x}_0$  in our model, we, nevertheless, believe that the concept is still valid in the sense that the greater the distance between the two impurities is, the less localized the ground state will be. It might be worth noting that this is in full agreement with our findings in some of the aforementioned papers [7, 11, 17] on one-dimensional singular double wells (see also [10]).

TABLE 1. The ordering of the five lowest eigenvalues over the corresponding five intervals of the extension parameter for  $x_0 = 0.2$ 

$\alpha < \alpha_1$	$E_0(\alpha) < E_1(\alpha) < 3/2 < E_2(\alpha) < 5/2$
$\alpha_1 \leq \alpha < \alpha_2$	$E_0(\alpha) < 3/2 \leq E_1(\alpha) < E_2(\alpha) < 5/2$
$\alpha_2 \leq \alpha < \alpha_3$	$E_0(\alpha) < 3/2 < E_2(\alpha) \leq E_1(\alpha) < 5/2$
$\alpha_3 \leq \alpha < \alpha_4$	$E_0(\alpha) < 3/2 < E_1(\alpha) \leq E_2(\alpha) < 5/2$
$\alpha_4 \leq \alpha$	$E_0(\alpha) < 3/2 < E_1(\alpha) < 5/2 \leq E_2(\alpha) < 7/2$

FIG. 6. The ground state energy of the 3D-isotropic harmonic oscillator perturbed by a pair of identical attractive point interactions symmetrically situated at a distance  $x_0 = 0.4$  from the origin as a function of the extension parameter  $\alpha = 1/\beta$ 

The graph of the lowest antisymmetric eigenvalue created by the singular double well when the separation distance becomes  $x_0 = 0.4$  is also provided below (Fig.7).

We now wish to provide the analog of Fig. 5 for  $x_0 = 0.3$  (Fig. 8).

As can be clearly seen in the plot, a remarkable change in the energy spectrum has now occurred: *for any value of the extension parameter we have  $E_1(\alpha) < E_2(\alpha)$ , that is to say, the new energy levels created by the double well perturbation completely avoid each other*, borrowing the terminology used in articles such as [22] on the spectral phenomenon called “level repulsion” or “avoided level crossing”. Of course, we still have the level crossing between  $E_2(\alpha)$  and  $5/2$ , the antisymmetric eigenvalue of the 3D-isotropic harmonic oscillator whose degeneracy has now been lowered to two by the perturbation.

The threshold value of  $x_0$ , denoted by  $X_t$  in the following, can be determined by observing that for that particular value, the two spectral curves  $E_1(\alpha, X_t)$  and  $E_2(\alpha, X_t)$  must have the same value as well as the same partial derivative with respect to the extension parameter  $\alpha$ . Hence,  $X_t$  is the second coordinate of the point representing the solution of the following

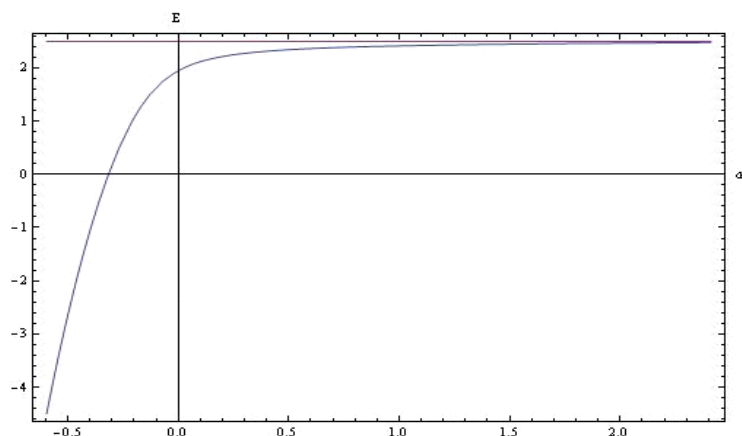


FIG. 7. The energy for the lowest antisymmetric bound state of the 3D-isotropic harmonic oscillator perturbed by a pair of identical attractive point interactions symmetrically situated at a distance  $x_0 = 0.4$  from the origin as a function of the extension parameter  $\alpha = 1/\beta$

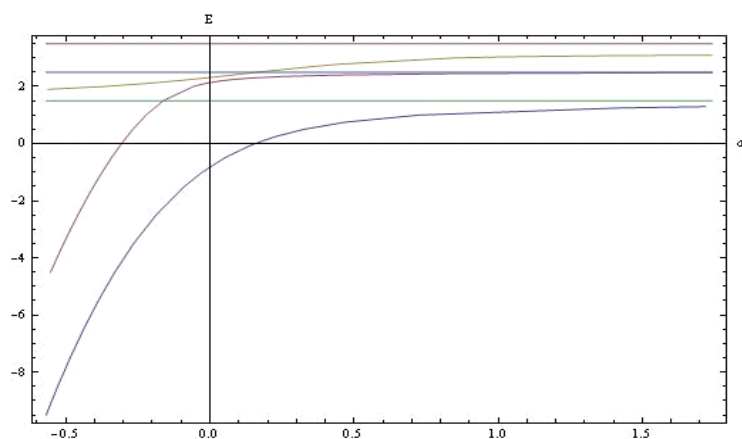


FIG. 8. The ground state energy and the next two eigenenergies created by two attractive  $\delta$ -perturbations situated symmetrically at the same distance from the origin,  $x_0 = 0.3$ , as functions of the extension parameter  $\alpha = 1/\beta$

system:

$$\begin{cases} E_1(\alpha, x_0) = E_2(\alpha, x_0); \\ \frac{\partial}{\partial \alpha} E_1(\alpha, x_0) = \frac{\partial}{\partial \alpha} E_2(\alpha, x_0). \end{cases} \quad (3.19)$$

For any fixed value of the distance  $x_0$ , the function  $E_1(\alpha, x_0)$  with domain given by the entire real axis and range  $(-\infty, 5/2)$  has its inverse given by  $\alpha_1(E, x_0)$  with domain  $(-\infty, 5/2)$  and range equal to the entire real axis.

Similarly, if we restrict  $E_2(\alpha, x_0)$  to the domain  $(-\infty, \alpha^*]$  and range  $(-\infty, 5/2]$ , with  $E_2(\alpha^*, x_0) = 5/2$ , its inverse function is  $\alpha_2(E, x_0)$  with domain  $(-\infty, 5/2]$  and range  $(-\infty, \alpha^*]$ . Both functions can actually be written in terms of explicit integrals and functions:

$$\alpha_1(E, x_0) = \frac{1}{\pi^{3/2}} \int_0^1 \frac{\xi^{1/2} \left[ \xi^{-E} \left( e^{-x_0^2 \frac{1-\xi}{1+\xi}} - e^{-x_0^2 \frac{1+\xi}{1-\xi}} \right) - 1 \right]}{(1-\xi^2)^{3/2}} d\xi,$$

$$\alpha_2(E, x_0) = \frac{2e^{-x_0^2}}{(3/2 - E)\pi^{3/2}} - \frac{2}{3\pi^{3/2}} + \frac{1}{\pi^{3/2}} \times \int_0^1 \frac{\xi^{1/2} \left\{ (1 - \xi^2)^{3/2} - 1 - \xi^{-E} \left[ 2e^{-x_0^2} (1 - \xi^2)^{3/2} - e^{-x_0^2(1-\xi)/(1+\xi)} - e^{-x_0^2(1+\xi)/(1-\xi)} \right] \right\}}{(1 - \xi^2)^{3/2}} d\xi$$

(of course, we could alternatively use (3.16b) and (3.18b)).

Consequently, also taking into account the well-known theorem on the derivative of the inverse function, instead of obtaining  $X_t$  by solving the system (3.19), it is easier from a computational point of view to derive its value by solving the system:

$$\begin{cases} \alpha_1(E, x_0) = \alpha_2(E, x_0); \\ \frac{\partial}{\partial E} \alpha_1(E, x_0) = \frac{\partial}{\partial E} \alpha_2(E, x_0). \end{cases} \quad (3.19a)$$

The numerical solution of (3.19a) is the point with coordinates  $E = E_t$  (approximately equal to 2.29949),  $x_0 = X_t$  (approximately equal to 0.2339644), where both functions  $\alpha_1$  and  $\alpha_2$  attain the value  $\alpha_t$  (approximately equal to 0.0829). The plot of the tangential contact between the two spectral curves for  $x_0 = X_t$  is provided below in Fig. 9.

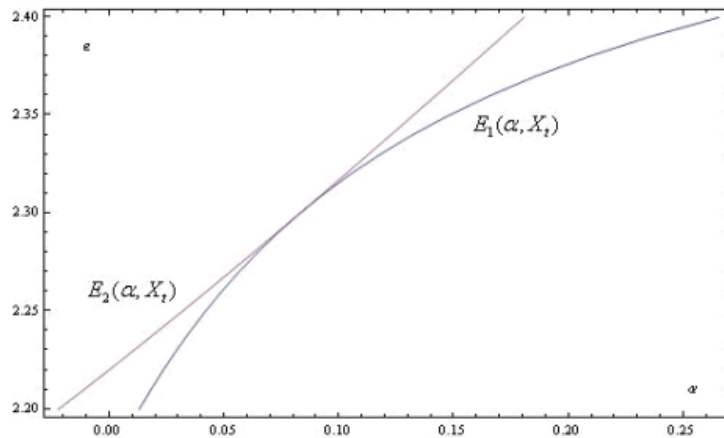


FIG. 9. The curves of the two eigenenergies  $E_1(\alpha, X_t)$  and  $E_2(\alpha, X_t)$  ( $X_t$  being approximately equal to 0.2339644) intersecting each other tangentially at  $\alpha = \alpha_t$  (approximately equal to 0.0829)

Hence, what has been seen regarding the three different spectral configurations for the two energy levels  $E_1(\alpha, x_0)$  and  $E_2(\alpha, x_0)$  can be summarized by means of the following Table 2, which clearly shows the role played by the threshold value  $x_0 = X_t$ .

The table thus makes our earlier statement written below Fig. 5 more precise: *for any  $x_0 < X_t$ , there exists an interval  $(\alpha_2(x_0), \alpha_3(x_0))$  (using the same indices used above) of values for the extension parameter  $\alpha$  (or equivalently of its reciprocal  $\beta$ ) for which  $E_2(\alpha, x_0) < E_1(\alpha, x_0)$ . In other words, as the values of  $|\alpha|$  in that range are rather small ( $\alpha_2(0.2)$  approximately equal to  $-0.126478$  and  $\alpha_3(0.2)$  approximately equal to  $0.309201$  in our previous example) and the corresponding values of  $|\beta|$  are large, such a singular configuration of those two eigenvalues (energy levels), characterized by having the second excited symmetric*

TABLE 2. The three possible configurations involving the two energy levels  $E_1(\alpha, x_0)$  and  $E_2(\alpha, x_0)$  as the distance parameter  $x_0$  varies

$x_0 < X_t \cong 0.2339644$	two distinct intersections between $E_1(\alpha, x_0)$ and $E_2(\alpha, x_0)$
$x_0 = X_t \cong 0.2339644,$ $\alpha_t \cong 0.0829$	one tangential intersection between $E_1(\alpha, x_0)$ and $E_2(\alpha, x_0)$
$x_0 > X_t \cong 0.2339644$	no intersection since $E_1(\alpha, x_0) < E_2(\alpha, x_0)$

bound state more tightly bound than the lowest antisymmetric one, can only occur by shrinking the distance between the two impurities below the threshold and raising their strength. Moreover, it can be seen that the interval expands as  $x_0$  shrinks to zero.

Therefore, it might be fair to say that a wider separation of the two zero-range impurities makes the structure of the spectrum more similar to that of the unperturbed isotropic harmonic oscillator. As a matter of fact, it is not difficult to convince oneself that, for any fixed value of the coupling  $\beta$  (or, equivalently, of the extension parameter  $\alpha$ ), the denominators of both rank-one operators in (3.14) or (3.14a) are bound to diverge as  $x_0 \rightarrow +\infty$ . Hence, the resolvent of our Hamiltonian will approach that of the 3D-isotropic harmonic oscillator in the limit  $x_0 \rightarrow +\infty$ . As a result, that is in perfect agreement with its one-dimensional counterpart established in Theorem 2.2(a) in [11].

However, a sharp contrast with the one-dimensional model occurs for the opposite limit analyzed in Theorem 2.2(b) in [11]. In fact, by noting that the right hand sides of both (3.15) and (3.16) become divergent as  $x_0 \rightarrow 0_+$ , it is clear that the lowest eigenvalue of our Hamiltonian will decrease without any lower bound as the distance shrinks to zero. Therefore, in sharp contrast with the one-dimensional case, we cannot expect in the limit  $x_0 \rightarrow 0_+$  to obtain the operator studied in Section 2 with the strength of the point interaction doubled. It might also be worth reminding the reader that, as is well known to Quantum Chemistry students, three-dimensional interactions with a nonzero range do not manifest this singular behavior as the distance between the two centers shrinks to zero, as the classical textbook example of  $H_2^+$  smoothly approaching  $He^+$  in the limit  $R \rightarrow 0_+$  clearly shows (see [23–25]).

The same singular spectral phenomenon has been recently observed in [17] where another model requiring a renormalization procedure, that is to say the one-dimensional Salpeter Hamiltonian with a double well of identical attractive point interactions, was investigated. Our spectral finding in this work confirms the general conjecture formulated in the above-mentioned paper that, when we deal with point interactions requiring the renormalization of the coupling constant (either because of the higher dimension or because of the different kinetic term), we must inevitably give up “the intuitive idea that in the limit ( $x_0 \rightarrow 0_+$ ) the eigenvalue should approach the ground state energy pertaining to a single delta with double strength”.

In analogy with what was proved in [17], it will be shown in a forthcoming paper that the only possible way of obtaining the expected behavior in the limit also in the case of the operator investigated in this work is to make the coupling constant  $\mu(\ell, \beta)$  used in the renormalization procedure suitably dependent on the separation distance  $x_0$ .

#### 4. Conclusions and perspectives

After reviewing the spectral features of a three-dimensional isotropic quantum dot with an attractive point impurity situated at the origin (the bottom of the confining harmonic potential), a model investigated in papers such as [1, 9, 26], the model in which a pair of twin attractive point impurities gets inserted into the 3D-isotropic quantum dot has been studied by first defining in a rigorous manner the self-adjoint Hamiltonian representing the energy operator for such a model. Since the energy eigenvalues are given by the poles of the resolvent, its explicit expression has enabled us to start the spectral analysis of the model. Although the bound state equation no longer has the simple expression involving a ratio of Gamma functions, as was the case in the presence of a single impurity centered at the origin, it is still possible to carry out, at least conceptually, the required spectral analysis.

Here, we have restricted our task to a rather detailed description of the behavior of the lowest lying spectrum eigenvalues (energy levels) with respect to variations of the two key parameters of the model, one labeling the self-adjoint extensions of the operator (or its reciprocal) and the other one given by the distance between either impurity and the origin.

The important spectral phenomenon called "positional disorder" singled out in [1] (see also the references cited therein as well as [10]) in the case of a single point impurity located away from the origin retains its validity in the sense that the more separated the twin impurities are the less localized the ground state is.

In addition to the level crossings involving the spectral curve of each new singular perturbation-created eigenenergy and the next lower eigenvalue of the unperturbed harmonic oscillator (still present in the spectrum because of its degeneracy), another seemingly more noteworthy spectral phenomenon occurs. There exists a threshold for the separation distance between the twin impurities, above which, the spectral curve  $E_2(\alpha, x_0)$ , representing the energy of the second symmetric bound state, lies entirely above  $E_1(\alpha, x_0)$ , the curve pertaining to the energy for the lowest antisymmetric bound state. Below that threshold, there exists a range of values of the extension parameter, which is physically characterized by being proportional to the inverse scattering length, over which  $E_2(\alpha, x_0) \leq E_1(\alpha, x_0)$ , implying the existence of two new types of level crossings. From the point of view of what could be called "spectral engineering", the latter implies that the second symmetric bound state can become more tightly bound than the lowest antisymmetric bound state provided the separation distance is below the threshold and the extension parameter is sufficiently small. At the threshold value we have shown the existence of a single tangential intersection between the two spectral curves. As a consequence, the narrower the separation between the impurities is, the wider the aforementioned range is.

The current analysis could be further extended to the next higher eigenvalues to explore the existence of other distance thresholds leading to level crossings of the new type.

It has also been pointed out that, in full accordance with the findings of [17] for another singular double well model requiring renormalization of the coupling constant, and in total contrast to those of [11] for the one-dimensional counterpart of the model studied in this note, not requiring the renormalization procedure, the limit of our Hamiltonian as the separation distance shrinks to zero is not given by the Hamiltonian of the 3D-isotropic quantum dot with a single point impurity centered at the origin having twice the strength. It is our intention to prove in a forthcoming paper that the expected behavior in the limit can be achieved by making the coupling constant used in the renormalization procedure also dependent on the separation distance.

Finally, we also intend to extend our investigation to the two-dimensional counterpart of the model given the growing relevance of that dimension in Nanophysics, as attested by some

contributions to the relevant literature, such as [27–30]. Of course, as can be seen in the case of the 2D-isotropic quantum dot with a single impurity, fully studied in [31], some logarithmic divergences, which are typical of two-dimensional Quantum Mechanics, are inevitably bound to arise.

### Acknowledgments

Silvestro Fassari and Fabio Rinaldi wish to express their heartfelt gratitude to Prof. I. Popov and Prof. I. Lobanov for their kind invitation to present the main contents of this note during one of the sessions of the conference “Mathematical Challenge of Quantum Transport in Nanosystems”, held at ITMO University, St. Petersburg, Russian Federation (9 – 11 September 2015).

Sergio Albeverio is very grateful to Prof. Nicolas Monod, Director of “Centre Interfacultaire Bernoulli – EPFL”, Lausanne, for the warm hospitality during his stay there as organiser jointly with Prof. A. B. Cruzeiro and Prof. D. Holm of the semester programme “Geometric Mechanics, Variational and Stochastic Methods” (January – June 2015).

S. Fassari and F. Rinaldi also wish to thank Prof. A. B. Cruzeiro and Prof. J. C. Zambrini for their warm hospitality on the occasion of their visit to CIB – EPFL.

### References

- [1] Brüning J., Geyler V., Lobanov I. Spectral properties of a short-range impurity in a quantum dot. *Journal of Mathematical Physics*, 2004, **45**, P. 1267–1290.
- [2] Albeverio S., Fassari S., Rinaldi F. A remarkable spectral feature of the Schrödinger Hamiltonian of the harmonic oscillator perturbed by an attractive  $\delta'$ -interaction centred at the origin: double degeneracy and level crossing. *Journal of Physics A: Mathematical and Theoretical*, 2013, **46**(38), 385305.
- [3] Albeverio S., Fassari S., Rinaldi F. The Hamiltonian of the harmonic oscillator with an attractive  $\delta'$ -interaction centred at the origin as approximated by the one with a triple of attractive  $\delta$ -interactions. *Journal of Physics A: Mathematical and Theoretical*, 2016, **49**(2), 025302.
- [4] Albeverio S., Gesztesy F., Høegh-Krohn R., Holden H. *Solvable models in Quantum Mechanics*. AMS (Chelsea Series) second edition (with an appendix by P. Exner), 2004.
- [5] Albeverio S., Kurasov P. *Singular Perturbations of Differential Operators: Solvable Type Operators*. Cambridge University Press, 2000.
- [6] Albeverio S., Dabrowski L., Kurasov P. Symmetries of Schrödinger operators with point interactions. *Letters in Mathematical Physics*, 1998, **45**, P. 33–47.
- [7] Fassari S., Rinaldi F. On the spectrum of the Schrödinger Hamiltonian with a particular configuration of three point interactions. *Reports on Mathematical Physics*, 2009, **64**(3), P. 367–393.
- [8] Fassari S., Inglese G. On the spectrum of the harmonic oscillator with a  $\delta$ -type perturbation. *Helvetica Physica Acta*, 1994, **67**, P. 650–659.
- [9] Fassari S., Inglese G. Spectroscopy of a three-dimensional isotropic harmonic oscillator with a  $\delta$ -type perturbation. *Helvetica Physica Acta*, 1996, **69**, P. 130–140.
- [10] Fassari S., Inglese G. On the spectrum of the harmonic oscillator with a  $\delta$ -type perturbation II. *Helvetica Physica Acta*, 1997, **70**, P. 858–865.
- [11] Fassari S., Rinaldi F. On the spectrum of the Schrödinger Hamiltonian of the one-dimensional harmonic oscillator perturbed by two identical attractive point interactions. *Reports on Mathematical Physics*, 2012, **69**(3), P. 353–370.
- [12] Plancherel M., Rotach W. Sur les valeurs asymptotiques des polynomes d’Hermite. *Commentarii Mathematici Helvetici*, 1929, **1**(1), P. 227–254.
- [13] Mityagin B., Siegl P. Root system of singular perturbations of the harmonic oscillator type operators. *ArXiv*: 1307.6245, 2013.
- [14] Reed M., Simon B. *Analysis of Operators – Methods of Modern Mathematical Physics IV*, Academic Press NY, 1978.
- [15] Avakian M.P., Pogosyan G.S., Sissakian A.N., Ter-Antonyan V.M. Spectroscopy of a singular linear oscillator. *Physics Letters A*, 1987, **124**( 4–5), P. 233–236.

- [16] Reed M., Simon B. *Fourier Analysis, Self-adjointness – Methods of Modern Mathematical Physics II*, Academic Press NY, 1975.
- [17] Albeverio S., Fassari S., Rinaldi F. The discrete spectrum of the spinless Salpeter Hamiltonian perturbed by  $\delta$ -interactions. *Journal of Physics A: Mathematical and Theoretical*, 2015, **48**(18), 185301.
- [18] Reed M., Simon B. *Functional Analysis – Methods of Modern Mathematical Physics I*, Academic Press NY, 1972.
- [19] Klaus M. A remark about weakly coupled one-dimensional Schrödinger operators. *Helvetica Physica Acta*, 1979, **52**, P. 223–229.
- [20] Fassari S. An estimate regarding one-dimensional point interactions. *Helvetica Physica Acta*, 1995, **68**, P. 121–125.
- [21] Kato T. *Perturbation Theory for Linear Operators*, Springer Verlag Heidelberg–NY, 1995.
- [22] Demkov Yu.N., Kurasov P.B. Von Neumann-Wigner Theorem: level repulsion and degenerate eigenvalues. *Theoretical and Mathematical Physics*, 2007, **153**(1), P. 1407–1422.
- [23] Schmidtke H.-H. *Quantenchemie* Weinheim: VCH, 1987 (in German).
- [24] Byers Brown W., Steiner E. On the electronic energy of a one-electron diatomic molecule near the united atom. *Journal of Chemical Physics*, 1966, **44**, P. 3934.
- [25] Klaus M. On  $H_2^+$  for small internuclear separation. *Journal of Physics A: Mathematical and General*, 1983, **16**, P. 2709–2720.
- [26] Gonzalez-Santander C., Dominguez-Adame F. Non-local separable solutions of two interacting particles in a harmonic trap. *Physics Letters A*, 2011, **375**, P. 314–317.
- [27] Gonzalez-Santander C., Dominguez-Adame F. Exciton states and optical absorption in quantum wires under laser radiation. *Physics Letters A*, 2010, **374**, P. 2259–2261.
- [28] Gonzalez-Santander C., Dominguez-Adame F. Modelling of Coulomb interaction in parabolic quantum wires. *Physica E*, 2009, **41**, P. 1645–1647.
- [29] Lima R.P.A., Amado M., Dominguez-Adame F. A solvable model of hydrogenic impurities in quantum dots. *Nanotechnology*, 2008, **19**, P. 135402–5406.
- [30] Lopez S., Dominguez-Adame F. Non-local potential approach to the ground state of confined excitons in quantum dots. *Semiconductor Science Technology*, 2002, **17**, P. 227–229.
- [31] Tusek M. *Analysis of Two-dimensional Quantum Models with Singular Potentials*. Diploma Thesis Czech Technical University in Prague, Faculty of Nuclear Sciences and Physical Engineering, 2006.

# Boundary triples for Schrödinger operators with singular interactions on hypersurfaces

J. Behrndt<sup>1</sup>, M. Langer<sup>2</sup> and V. Lotoreichik<sup>3</sup>

<sup>1</sup>Institut für Numerische Mathematik, Technische Universität Graz,  
Steyrergasse 30, 8010 Graz, Austria

<sup>2</sup>Department of Mathematics and Statistics, University of Strathclyde,  
26 Richmond Street, Glasgow G1 1XH, United Kingdom

<sup>3</sup>Department of Theoretical Physics, Nuclear Physics Institute CAS,  
250 68 Řež near Prague, Czech Republic

behrndt@tugraz.at, m.langer@strath.ac.uk, lotoreichik@ujf.cas.cz

**PACS 02.30.Tb, 03.65.Db**

**DOI 10.17586/2220-8054-2016-7-2-290-302**

The self-adjoint Schrödinger operator  $A_{\delta,\alpha}$  with a  $\delta$ -interaction of constant strength  $\alpha$  supported on a compact smooth hypersurface  $\mathcal{C}$  is viewed as a self-adjoint extension of a natural underlying symmetric operator  $S$  in  $L^2(\mathbb{R}^n)$ . The aim of this note is to construct a boundary triple for  $S^*$  and a self-adjoint parameter  $\Theta_{\delta,\alpha}$  in the boundary space  $L^2(\mathcal{C})$  such that  $A_{\delta,\alpha}$  corresponds to the boundary condition induced by  $\Theta_{\delta,\alpha}$ . As a consequence, the well-developed theory of boundary triples and their Weyl functions can be applied. This leads, in particular, to a Krein-type resolvent formula and a description of the spectrum of  $A_{\delta,\alpha}$  in terms of the Weyl function and  $\Theta_{\delta,\alpha}$ .

**Keywords:** Boundary triple, Weyl function, Schrödinger operator, singular potential,  $\delta$ -interaction, hypersurface.

*Received: 22 January 2016*

## 1. Introduction

Boundary triples and their Weyl functions are efficient and frequently used tools in the extension theory of symmetric operators and the spectral analysis of their self-adjoint extensions. Roughly speaking, a boundary triple consists of two boundary mappings that satisfy an abstract second Green's identity and a maximality condition. With the help of a boundary triple, all self-adjoint extensions of a symmetric operator can be parameterized via abstract boundary conditions that involve a self-adjoint parameter in a boundary space. In addition, the spectral properties of these self-adjoint extensions can be described with the help of the Weyl function and the corresponding boundary parameters. We refer the reader to [1–5] and Section 2 for more details on boundary triples and their Weyl functions.

The main objective of this note is to provide and discuss boundary triples and their Weyl functions for self-adjoint Schrödinger operators in  $L^2(\mathbb{R}^n)$  with  $\delta$ -interactions of strength  $\alpha \in \mathbb{R}$  supported on a compact smooth hypersurface  $\mathcal{C}$  that separates  $\mathbb{R}^n$  into a smooth bounded domain  $\Omega_i$  and an unbounded smooth exterior domain  $\Omega_e$ . In an informal way, such an operator is often written in the form

$$A_{\delta,\alpha} = -\Delta - \alpha\delta_{\mathcal{C}}, \quad (1)$$

where  $\delta_{\mathcal{C}}$  denotes the  $\delta$ -distribution supported on  $\mathcal{C}$ . A precise definition of the self-adjoint operator  $A_{\delta,\alpha}$  in terms of boundary or interface conditions is given at the beginning of Section 3 below; see also [6, 7] for an equivalent definition via quadratic forms. Schrödinger operators with  $\delta$ -interactions are frequently used in mathematical physics to model interactions of quantum particles; we refer to the monographs [8] and [9], to the review article [10] and to [6, 11–25] for a small selection of related papers on spectral analysis of such operators.

Let  $A_{\text{free}}$  be the usual self-adjoint realization of  $-\Delta$  in  $L^2(\mathbb{R}^n)$  and let  $A_{\delta,\alpha}$  be the self-adjoint operator with  $\delta$ -interaction on  $\mathcal{C}$  in (1). We consider the densely defined, closed symmetric operator  $S = A_{\text{free}} \cap A_{\delta,\alpha}$  in  $L^2(\mathbb{R}^n)$  and its adjoint  $S^*$ , and we construct a boundary triple  $\{L^2(\mathcal{C}), \Gamma_0, \Gamma_1\}$  for  $S^*$  and a self-adjoint parameter  $\Theta_{\delta,\alpha}$  in  $L^2(\mathcal{C})$  such that

$$A_{\text{free}} = S^* \upharpoonright \ker \Gamma_0 \quad \text{and} \quad A_{\delta,\alpha} = S^* \upharpoonright \ker(\Gamma_1 - \Theta_{\delta,\alpha}\Gamma_0).$$

Although it is clear from the general theory that such a boundary triple and a self-adjoint parameter  $\Theta_{\delta,\alpha}$  exist, its construction is not trivial. Our idea here is based on a coupling of two boundary triples for elliptic PDEs which involve the Dirichlet-to-Neumann map as a regularization (see [26–28]), the restriction of this coupling to a suitable intermediate extension, and certain transforms of boundary triples and corresponding parameters. These efforts and technical considerations are worthwhile for various reasons. In particular, if  $\gamma$  and  $M$  denote the  $\gamma$ -field and Weyl function corresponding to the boundary triple  $\{L^2(\mathcal{C}), \Gamma_0, \Gamma_1\}$  (see Section 2 for more details), then it follows immediately from the general theory in [3,4] that the resolvent difference of  $A_{\text{free}}$  and  $A_{\delta,\alpha}$  admits the representation

$$(A_{\delta,\alpha} - \lambda)^{-1} - (A_{\text{free}} - \lambda)^{-1} = \gamma(\lambda)(\Theta_{\delta,\alpha} - M(\lambda))^{-1}\gamma(\bar{\lambda})^*$$

for all  $\lambda \in \rho(A_{\delta,\alpha})$  and belongs to some operator ideal in  $L^2(\mathbb{R}^n)$  if and only if the resolvent of  $\Theta_{\delta,\alpha}$  belongs to the analogous operator ideal in  $L^2(\mathcal{C})$ ; see Theorem 3.5. As a special case, the Schatten–von Neumann properties of the resolvent difference of  $A_{\text{free}}$  and  $A_{\delta,\alpha}$  carry over to the resolvent of  $\Theta_{\delta,\alpha}$ , and vice versa. Moreover, the spectral properties of  $A_{\delta,\alpha}$  can be described with the help of the perturbation term  $(\Theta_{\delta,\alpha} - M(\lambda))^{-1}$ . We mention that in the context of the more general notion of quasi boundary triples and their Weyl functions from [29,30] a similar approach as in this note and closely related results can be found in [6,31]; we also refer to [27,28,32–37] for other methods in extension theory of elliptic differential operators.

## 2. Boundary triples and Weyl functions

In this preparatory section, we recall the notion of boundary triples, associated  $\gamma$ -fields and Weyl functions, and discuss some of their properties. For a more detailed exposition, we refer the reader to [1–5,38].

In the following, let  $\mathfrak{H}$  be a Hilbert space, let  $S$  be a densely defined, closed symmetric operator in  $\mathfrak{H}$ , and let  $S^*$  be the adjoint operator.

**Definition 2.1.** *A triple  $\{\mathcal{G}, \Gamma_0, \Gamma_1\}$  is called a boundary triple for  $S^*$  if  $\mathcal{G}$  is a Hilbert space and  $\Gamma_0, \Gamma_1 : \text{dom } S^* \rightarrow \mathcal{G}$  are linear mappings that satisfy the abstract second Green’s identity*

$$(S^*f, g)_{\mathfrak{H}} - (f, S^*g)_{\mathfrak{H}} = (\Gamma_1f, \Gamma_0g)_{\mathcal{G}} - (\Gamma_0f, \Gamma_1g)_{\mathcal{G}}$$

for all  $f, g \in \text{dom } S^*$ , and the mapping  $\Gamma := (\Gamma_0, \Gamma_1)^{\top} : \text{dom } S^* \rightarrow \mathcal{G} \times \mathcal{G}$  is surjective.

Recall that a boundary triple  $\{\mathcal{G}, \Gamma_0, \Gamma_1\}$  for  $S^*$  exists if and only if the defect numbers of  $S$  coincide or, equivalently,  $S$  admits self-adjoint extensions in  $\mathfrak{H}$ . Moreover, a boundary triple is not unique (except in the trivial case  $S = S^*$ ). The following special observation will be used in Section 3: suppose that  $\{\mathcal{G}, \Gamma_0, \Gamma_1\}$  is a boundary triple for  $S^*$  and let  $G$  be a bounded self-adjoint operator in  $\mathcal{G}$ ; then  $\{\mathcal{G}, \Gamma'_0, \Gamma'_1\}$ , where

$$\begin{pmatrix} \Gamma'_0 \\ \Gamma'_1 \end{pmatrix} = \begin{pmatrix} I & G \\ 0 & I \end{pmatrix} \begin{pmatrix} \Gamma_0 \\ \Gamma_1 \end{pmatrix}, \tag{2}$$

is also a boundary triple for  $S^*$ . Recall also that  $\text{dom } S = \ker \Gamma_0 \cap \ker \Gamma_1$  and that the mapping

$$\Theta \mapsto A_{\Theta} := S^* \upharpoonright \{f \in \text{dom } S^* : \Gamma f = (\Gamma_0f, \Gamma_1f)^{\top} \in \Theta\} \tag{3}$$

establishes a bijective correspondence between the closed linear subspaces (relations) in  $\mathcal{G} \times \mathcal{G}$  and the closed linear extensions  $A_\Theta \subset S^*$  of  $S$ . In the case when  $\Theta$  is (the graph of) an operator, the closed extension  $A_\Theta$  in (3) is given by

$$A_\Theta = S^* \upharpoonright \ker(\Gamma_1 - \Theta\Gamma_0). \tag{4}$$

It is important to note that the identity  $(A_\Theta)^* = A_{\Theta^*}$  holds and hence  $A_\Theta$  in (3)–(4) is self-adjoint in  $\mathfrak{H}$  if and only if  $\Theta$  is self-adjoint in  $\mathcal{G}$ . It follows, in particular, that the extension

$$A_0 = S^* \upharpoonright \ker \Gamma_0 \tag{5}$$

is self-adjoint. This extension often plays the role of a fixed extension within the family of self-adjoint extensions of  $S$ . We also mention that  $\Theta$  in (3) is an unbounded operator if and only if the extensions  $A_0$  and  $A_\Theta$  are disjoint but not transversal, that is,

$$S = A_\Theta \cap A_0 \quad \text{and} \quad A_\Theta \hat{+} A_0 \subsetneq S^*, \tag{6}$$

where  $\hat{+}$  denotes the sum of subspaces. Note that this appears only in the case when  $\mathcal{G}$  is infinite-dimensional, that is, the defect numbers of  $S$  are both infinite.

The next theorem can be found in [39]. Very roughly speaking, it can be regarded as converse to the above considerations. Here, the idea is to start with boundary mappings defined on the domain of some operator  $T$  that satisfy the abstract second Green’s identity and some additional conditions, and to conclude that  $T$  coincides with the adjoint of the restriction of  $T$  to the intersection of the kernels of the boundary mappings. Theorem 2.2 will be used in the proof of Lemma 3.1.

**Theorem 2.2.** *Let  $T$  be a linear operator in  $\mathfrak{H}$ , let  $\mathcal{G}$  be a Hilbert space and assume that  $\Gamma_0, \Gamma_1 : \text{dom } T \rightarrow \mathcal{G}$  are linear mappings that satisfy the following conditions:*

- (i) *there exists a self-adjoint restriction  $A_0$  of  $T$  in  $\mathfrak{H}$  such that  $\text{dom } A_0 \subset \ker \Gamma_0$ ;*
- (ii)  $\text{ran}(\Gamma_0, \Gamma_1)^\top = \mathcal{G} \times \mathcal{G}$ ;
- (iii) *for all  $f, g \in \text{dom } T$  the abstract Green’s identity*

$$(Tf, g)_\mathfrak{H} - (f, Tg)_\mathfrak{H} = (\Gamma_1 f, \Gamma_0 g)_\mathcal{G} - (\Gamma_0 f, \Gamma_1 g)_\mathcal{G}$$

*holds.*

*Then  $S := T \upharpoonright (\ker \Gamma_0 \cap \ker \Gamma_1)$  is a densely defined, closed, symmetric operator in  $\mathfrak{H}$  such that  $S^* = T$  and  $\{\mathcal{G}, \Gamma_0, \Gamma_1\}$  is a boundary triple for  $S^*$  with the property  $A_0 = S^* \upharpoonright \ker \Gamma_0$ .*

In the following, we assume that  $S$  is a densely defined, closed, symmetric operator in  $\mathfrak{H}$  and that  $\{\mathcal{G}, \Gamma_0, \Gamma_1\}$  is a boundary triple for  $S^*$ . Let  $A_0 = S^* \upharpoonright \ker \Gamma_0$  be as in (5) and observe that the following direct sum decomposition of  $\text{dom } S^*$  is valid:

$$\text{dom } S^* = \text{dom } A_0 \dot{+} \ker(S^* - \lambda) = \ker \Gamma_0 \dot{+} \ker(S^* - \lambda), \quad \lambda \in \rho(A_0).$$

It follows, in particular, that  $\Gamma_0 \upharpoonright \ker(S^* - \lambda)$  is a bijective operator from  $\ker(S^* - \lambda)$  onto  $\mathcal{G}$ . The inverse is denoted by

$$\gamma(\lambda) = (\Gamma_0 \upharpoonright \ker(S^* - \lambda))^{-1}, \quad \lambda \in \rho(A_0);$$

when viewed as a function  $\lambda \mapsto \gamma(\lambda)$  on  $\rho(A_0)$ , we call  $\gamma$  the  $\gamma$ -field corresponding to the boundary triple  $\{\mathcal{G}, \Gamma_0, \Gamma_1\}$ . The Weyl function  $M$  associated with  $\{\mathcal{G}, \Gamma_0, \Gamma_1\}$  is defined by

$$M(\lambda) = \Gamma_1 \gamma(\lambda) = \Gamma_1 (\Gamma_0 \upharpoonright \ker(S^* - \lambda))^{-1}, \quad \lambda \in \rho(A_0).$$

It can be shown that the values  $M(\lambda)$  of the Weyl function  $M$  are bounded, everywhere defined operators in  $\mathcal{G}$ , that  $M$  is a holomorphic function on  $\rho(A_0)$  with the properties  $M(\lambda) = M(\bar{\lambda})^*$  and that  $\text{Im } M(\lambda)$  is uniformly positive for  $\lambda \in \mathbb{C}^+$ , i.e.  $M$  is an operator-valued Nevanlinna or Riesz–Herglotz function that is uniformly strict; see [2].

### 3. Schrödinger operators with $\delta$ -interactions on hypersurfaces

Let  $\Omega_i \subset \mathbb{R}^n$ ,  $n \geq 2$ , be a bounded domain with  $C^\infty$ -smooth boundary  $\mathcal{C} = \partial\Omega_i$  and let  $\Omega_e = \mathbb{R}^n \setminus \overline{\Omega}_i$  be the corresponding exterior domain with the same  $C^\infty$ -smooth boundary  $\partial\Omega_e = \mathcal{C}$ . In the following,  $f_i|_{\mathcal{C}}$  and  $f_e|_{\mathcal{C}}$  denote the traces of functions in  $\Omega_i$  and  $\Omega_e$ , respectively; if  $f_i|_{\mathcal{C}} = f_e|_{\mathcal{C}}$ , we also set  $f|_{\mathcal{C}} := f_i|_{\mathcal{C}} = f_e|_{\mathcal{C}}$ . Moreover,  $\partial_{\nu_i} f_i|_{\mathcal{C}}$  and  $\partial_{\nu_e} f_e|_{\mathcal{C}}$  denote the traces of their normal derivatives; here we agree that the normal vectors  $\nu_i$  and  $\nu_e$  point outwards of the domains, so that,  $\nu_i = -\nu_e$ .

In the following, let  $\alpha \neq 0$  be a real constant and consider the Schrödinger operator with a  $\delta$ -interaction of strength  $\alpha$  supported on  $\mathcal{C}$  defined by

$$A_{\delta,\alpha} f = -\Delta f, \quad \text{dom } A_{\delta,\alpha} = \left\{ f = \begin{pmatrix} f_i \\ f_e \end{pmatrix} \in H^2(\Omega_i) \times H^2(\Omega_e), \begin{matrix} f_i|_{\mathcal{C}} = f_e|_{\mathcal{C}}, \\ \alpha f|_{\mathcal{C}} = \partial_{\nu_i} f_i|_{\mathcal{C}} + \partial_{\nu_e} f_e|_{\mathcal{C}} \end{matrix} \right\}. \quad (7)$$

According to [6, Theorem 3.5 and Theorem 3.6] the operator  $A_{\delta,\alpha}$  is self-adjoint in  $L^2(\mathbb{R}^n)$  and corresponds to the densely defined, closed sesquilinear form

$$\begin{aligned} \mathfrak{a}_{\delta,\alpha}[f, g] &= (\nabla f, \nabla g)_{(L^2(\mathbb{R}^n))^n} - \alpha(f|_{\mathcal{C}}, g|_{\mathcal{C}})_{L^2(\mathcal{C})}, \\ \text{dom } \mathfrak{a}_{\delta,\alpha} &= H^1(\mathbb{R}^n). \end{aligned}$$

Observe that the normal derivatives of the functions in  $\text{dom } A_{\delta,\alpha}$  may have a jump at the interface  $\mathcal{C}$  or, more precisely, that  $f \in \text{dom } A_{\delta,\alpha}$  is contained in  $H^2(\mathbb{R}^n)$  if and only if  $\partial_{\nu_i} f_i|_{\mathcal{C}} = -\partial_{\nu_e} f_e|_{\mathcal{C}}$ . We also recall that the essential spectrum of the operator  $A_{\delta,\alpha}$  is  $[0, \infty)$  and that the negative spectrum consists of a finite number of eigenvalues of finite multiplicity; see [6, 7]. In the following, we fix some point  $\eta$  such that

$$\eta \in \rho(A_{\delta,\alpha}) \cap (-\infty, 0). \quad (8)$$

In Proposition 3.3 below, we specify a boundary triple  $\{L^2(\mathcal{C}), \Gamma_0, \Gamma_1\}$  for the adjoint of the densely defined, closed, symmetric operator

$$Sf = -\Delta f, \quad \text{dom } S = \{f \in H^2(\mathbb{R}^n) : f|_{\mathcal{C}} = 0\}, \quad (9)$$

such that the free or unperturbed Schrödinger operator

$$A_{\text{free}} f = -\Delta f, \quad \text{dom } A_{\text{free}} = H^2(\mathbb{R}^n),$$

corresponds to the kernel of the first boundary mapping  $\Gamma_0$ . Note that the operator  $A_{\delta,\alpha}$  in (7) is a self-adjoint extension of  $S$  and that the defect numbers  $\dim(\text{ran}(S \mp i)^\perp)$  are infinite. Hence, the abstract considerations in Section 2 ensure that there exists a self-adjoint operator or relation  $\Theta_{\delta,\alpha}$  such that

$$A_{\delta,\alpha} = S^* \upharpoonright \ker(\Gamma_1 - \Theta_{\delta,\alpha} \Gamma_0). \quad (10)$$

The parameter  $\Theta_{\delta,\alpha}$  and further properties of the operator  $A_{\delta,\alpha}$  will be discussed in Lemma 3.4 and Theorem 3.5 below.

Some further notations and preparatory results are required before Proposition 3.3 can be stated and proved. Consider the densely defined, closed, symmetric operators

$$S_i f_i = -\Delta f_i, \quad \text{dom } S_i = H_0^2(\Omega_i),$$

and

$$S_e f_e = -\Delta f_e, \quad \text{dom } S_e = H_0^2(\Omega_e),$$

in  $L^2(\Omega_i)$  and  $L^2(\Omega_e)$ , respectively. Their adjoints are given by the maximal operators

$$S_i^* f_i = -\Delta f_i, \quad \text{dom } S_i^* = \{f_i \in L^2(\Omega_i) : -\Delta f_i \in L^2(\Omega_i)\},$$

and

$$S_e^* f_e = -\Delta f_e, \quad \text{dom } S_e^* = \{f_e \in L^2(\Omega_e) : -\Delta f_e \in L^2(\Omega_e)\},$$

where the expressions  $-\Delta f_i$  and  $-\Delta f_e$  are understood in the sense of distributions. It is important to note that  $H^2(\Omega_i)$  and  $H^2(\Omega_e)$  are proper subsets of the maximal domains  $\text{dom } S_i^*$  and  $\text{dom } S_e^*$ , respectively, and that the symmetric operator  $S$  in (9) is an infinite-dimensional extension of the orthogonal sum  $S_i \oplus S_e$ , which is also a symmetric operator in  $L^2(\mathbb{R}^n) = L^2(\Omega_i) \oplus L^2(\Omega_e)$ . Recall from [27, 40] that the trace maps admit continuous extensions to the maximal domains (equipped with the graph norms):

$$\text{dom } S_i^* \ni f_i \mapsto f_i|_{\mathcal{C}} \in H^{-1/2}(\mathcal{C}), \quad \text{dom } S_i^* \ni f_i \mapsto \partial_{\nu_i} f_i|_{\mathcal{C}} \in H^{-3/2}(\mathcal{C}),$$

and

$$\text{dom } S_e^* \ni f_e \mapsto f_e|_{\mathcal{C}} \in H^{-1/2}(\mathcal{C}), \quad \text{dom } S_e^* \ni f_e \mapsto \partial_{\nu_e} f_e|_{\mathcal{C}} \in H^{-3/2}(\mathcal{C}).$$

Furthermore, consider the self-adjoint extensions  $A_i^D$  and  $A_e^D$  of  $S_i$  and  $S_e$ , respectively, corresponding to Dirichlet boundary conditions on  $\mathcal{C}$ :

$$A_i^D f_i = -\Delta f_i, \quad \text{dom } A_i^D = H_0^1(\Omega_i) \cap H^2(\Omega_i),$$

and

$$A_e^D f_e = -\Delta f_e, \quad \text{dom } A_e^D = H_0^1(\Omega_e) \cap H^2(\Omega_e).$$

Since  $A_i^D$  and  $A_e^D$  are both non-negative, it is clear that  $\eta$  in (8) belongs to  $\rho(A_i^D) \cap \rho(A_e^D)$ , and hence, we have the direct sum decompositions

$$\text{dom } S_i^* = \text{dom } A_i^D \dot{+} \ker(S_i^* - \eta) = (H_0^1(\Omega_i) \cap H^2(\Omega_i)) \dot{+} \ker(S_i^* - \eta) \quad (11)$$

and

$$\text{dom } S_e^* = \text{dom } A_e^D \dot{+} \ker(S_e^* - \eta) = (H_0^1(\Omega_e) \cap H^2(\Omega_e)) \dot{+} \ker(S_e^* - \eta). \quad (12)$$

We agree to decompose functions  $f_i \in \text{dom } S_i^*$  and  $f_e \in \text{dom } S_e^*$  in the form

$$f_i = f_i^D + f_i^\eta \quad \text{and} \quad f_e = f_e^D + f_e^\eta, \quad (13)$$

where  $f_i^D \in \text{dom } A_i^D$ ,  $f_i^\eta \in \ker(S_i^* - \eta)$ , and  $f_e^D \in \text{dom } A_e^D$ ,  $f_e^\eta \in \ker(S_e^* - \eta)$ .

In the following, we often make use of the operators

$$\iota = (-\Delta_{\mathcal{C}} + I)^{\frac{1}{4}} \quad \text{and} \quad \iota^{-1} = (-\Delta_{\mathcal{C}} + I)^{-\frac{1}{4}},$$

where  $\Delta_{\mathcal{C}}$  denotes the Laplace–Beltrami operator on  $\mathcal{C}$ . Both mappings  $\iota$  and  $\iota^{-1}$  are regarded as isomorphisms

$$\iota : H^s(\mathcal{C}) \rightarrow H^{s-\frac{1}{2}}(\mathcal{C}) \quad \text{and} \quad \iota^{-1} : H^t(\mathcal{C}) \rightarrow H^{t+\frac{1}{2}}(\mathcal{C})$$

for  $s, t \in \mathbb{R}$ , and also as operators that establish the duality

$$(\iota\varphi, \iota^{-1}\psi)_{L^2(\mathcal{C})} = \langle \varphi, \psi \rangle_{H^{1/2}(\mathcal{C}) \times H^{-1/2}(\mathcal{C})}$$

for  $\varphi \in H^{1/2}(\mathcal{C})$  and  $\psi \in H^{-1/2}(\mathcal{C})$ , when the spaces  $H^{1/2}(\mathcal{C})$  and  $H^{-1/2}(\mathcal{C})$  are equipped with the corresponding norms. Note also that  $\iota^{-1}$  can be viewed as a bounded self-adjoint operator in  $L^2(\mathcal{C})$  with  $\text{ran } \iota^{-1} = H^{1/2}(\mathcal{C})$  and that  $\iota$  with domain  $\text{dom } \iota = H^{1/2}(\mathcal{C})$  is an unbounded self-adjoint operator in  $L^2(\mathcal{C})$  with  $0 \in \rho(\iota)$ .

Now we have finally collected all necessary notation to state the first lemma.

**Lemma 3.1.** *Let  $S$  be the densely defined, closed, symmetric operator in (9). Then the adjoint  $S^*$  of  $S$  is given by*

$$S^*f = -\Delta f, \quad \text{dom } S^* = \left\{ f = \begin{pmatrix} f_i \\ f_e \end{pmatrix} \in \text{dom } S_i^* \times \text{dom } S_e^*, f_i|_C = f_e|_C \right\}. \quad (14)$$

Further, let

$$\Upsilon_0 f = \iota^{-1} f|_C \quad \text{and} \quad \Upsilon_1 f = -\iota(\partial_{\nu_i} f_i^D|_C + \partial_{\nu_e} f_e^D|_C) \quad (15)$$

for  $f = (f_i, f_e)^\top \in \text{dom } S^*$  and with  $f_i^D, f_e^D$  as in (13). Then  $\{L^2(C), \Upsilon_0, \Upsilon_1\}$  is a boundary triple for  $S^*$  with the property  $A_i^D \oplus A_e^D = S^* \upharpoonright \ker \Upsilon_0$ .

*Proof.* The assertions in Lemma 3.1 will be proved with the help of Theorem 2.2. To this end, we set

$$Tf = -\Delta f, \quad \text{dom } T = \left\{ f = \begin{pmatrix} f_i \\ f_e \end{pmatrix} \in \text{dom } S_i^* \times \text{dom } S_e^*, f_i|_C = f_e|_C \right\},$$

and consider the boundary mappings  $\Upsilon_0, \Upsilon_1 : \text{dom } T \rightarrow L^2(C)$  in (15). First of all, we note that item (i) in Theorem 2.2 is satisfied with the self-adjoint operator  $A_0 = A_i^D \oplus A_e^D$  since for any function  $f = (f_i, f_e)^\top \in \text{dom}(A_i^D \oplus A_e^D) \subset H^2(\Omega_i) \times H^2(\Omega_e)$  one has  $f_i \in \text{dom } S_i^*$ ,  $f_e \in \text{dom } S_e^*$ , and  $f_i|_C = f_e|_C$ . In order to see that the mapping

$$\begin{pmatrix} \Upsilon_0 \\ \Upsilon_1 \end{pmatrix} : \text{dom } T \rightarrow L^2(C) \times L^2(C) \quad (16)$$

is surjective, let  $\varphi, \psi \in L^2(C)$ . Since the Neumann trace map is surjective from  $H^2(\Omega_i) \cap H_0^1(\Omega_i)$  onto  $H^{1/2}(C)$  and from  $H^2(\Omega_e) \cap H_0^1(\Omega_e)$  onto  $H^{1/2}(C)$ , there exist  $f_i^D \in \text{dom } A_i^D$  and  $f_e^D \in \text{dom } A_e^D$  such that  $\partial_{\nu_i} f_i^D|_C = \partial_{\nu_e} f_e^D|_C = -\frac{1}{2}\iota^{-1}\psi \in H^{1/2}(C)$ . Next, we choose  $f_i^\eta \in \ker(S_i^* - \eta)$  and  $f_e^\eta \in \ker(S_e^* - \eta)$  such that  $f_i^\eta|_C = f_e^\eta|_C = \iota\varphi \in H^{-1/2}(C)$ , which is possible by the surjectivity of the trace map from the maximal domain onto  $H^{-1/2}(C)$ ; cf. [27, 40, 41]. Now, it is easy to see that  $f = (f_i^D + f_i^\eta, f_e^D + f_e^\eta)^\top \in \text{dom } T$  satisfies

$$\Upsilon_0 f = \iota^{-1} f|_C = \varphi \quad \text{and} \quad \Upsilon_1 f = -\iota(\partial_{\nu_i} f_i^D|_C + \partial_{\nu_e} f_e^D|_C) = \psi,$$

and hence the map (16) is onto. Next, we verify that the abstract second Green's identity

$$(Tf, g)_{L^2(\mathbb{R}^n)} - (f, Tg)_{L^2(\mathbb{R}^n)} = (\Upsilon_1 f, \Upsilon_0 g)_{L^2(C)} - (\Upsilon_0 f, \Upsilon_1 g)_{L^2(C)}, \quad f, g \in \text{dom } T, \quad (17)$$

holds. For this, it is useful to recall that Green's identity for  $f_i = f_i^D + f_i^\eta$  and  $g_i = g_i^D + g_i^\eta$  yields

$$\begin{aligned} (S_i^* f_i, g_i)_{L^2(\Omega_i)} - (f_i, S_i^* g_i)_{L^2(\Omega_i)} \\ = \langle f_i|_C, \partial_{\nu_i} g_i^D|_C \rangle_{H^{-1/2}(C) \times H^{1/2}(C)} - \langle \partial_{\nu_i} f_i^D|_C, g_i|_C \rangle_{H^{1/2}(C) \times H^{-1/2}(C)}, \end{aligned} \quad (18)$$

and for  $f_e = f_e^D + f_e^\eta$  and  $g_e = g_e^D + g_e^\eta$  in the analogous form

$$\begin{aligned} (S_e^* f_e, g_e)_{L^2(\Omega_e)} - (f_e, S_e^* g_e)_{L^2(\Omega_e)} \\ = \langle f_e|_C, \partial_{\nu_e} g_e^D|_C \rangle_{H^{-1/2}(C) \times H^{1/2}(C)} - \langle \partial_{\nu_e} f_e^D|_C, g_e|_C \rangle_{H^{1/2}(C) \times H^{-1/2}(C)}. \end{aligned} \quad (19)$$

Since  $T$  is a restriction of the orthogonal sum  $S_i^* \oplus S_e^*$  and  $f_i|_C = f_e|_C$ ,  $g_i|_C = g_e|_C$  for  $f, g \in \text{dom } T$ , we conclude from (18) and (19) that

$$\begin{aligned}
& (Tf, g)_{L^2(\mathbb{R}^n)} - (f, Tg)_{L^2(\mathbb{R}^n)} \\
&= (S_i^* f_i, g_i)_{L^2(\Omega_i)} - (f_i, S_i^* g_i)_{L^2(\Omega_i)} + (S_e^* f_e, g_e)_{L^2(\Omega_e)} - (f_e, S_e^* g_e)_{L^2(\Omega_e)} \\
&= \langle f_i|_C, \partial_{\nu_i} g_i^D|_C \rangle_{H^{-1/2}(C) \times H^{1/2}(C)} - \langle \partial_{\nu_i} f_i^D|_C, g_i|_C \rangle_{H^{1/2}(C) \times H^{-1/2}(C)} \\
&\quad + \langle f_e|_C, \partial_{\nu_e} g_e^D|_C \rangle_{H^{-1/2}(C) \times H^{1/2}(C)} - \langle \partial_{\nu_e} f_e^D|_C, g_e|_C \rangle_{H^{1/2}(C) \times H^{-1/2}(C)} \\
&= \langle f|_C, \partial_{\nu_i} g_i^D|_C + \partial_{\nu_e} g_e^D|_C \rangle_{H^{-1/2}(C) \times H^{1/2}(C)} - \langle \partial_{\nu_i} f_i^D|_C + \partial_{\nu_e} f_e^D|_C, g|_C \rangle_{H^{1/2}(C) \times H^{-1/2}(C)} \\
&= (\iota^{-1} f|_C, \iota(\partial_{\nu_i} g_i^D|_C + \partial_{\nu_e} g_e^D|_C))_{L^2(C)} - (\iota(\partial_{\nu_i} f_i^D|_C + \partial_{\nu_e} f_e^D|_C), \iota^{-1} g|_C)_{L^2(C)} \\
&= (-\iota(\partial_{\nu_i} f_i^D|_C + \partial_{\nu_e} f_e^D|_C), \iota^{-1} g|_C)_{L^2(C)} - (\iota^{-1} f|_C, -\iota(\partial_{\nu_i} g_i^D|_C + \partial_{\nu_e} g_e^D|_C))_{L^2(C)} \\
&= (\Upsilon_1 f, \Upsilon_0 g)_{L^2(C)} - (\Upsilon_0 f, \Upsilon_1 g)_{L^2(C)}
\end{aligned}$$

holds. Thus, (17) is shown and item (iii) in Theorem 2.2 is satisfied. Hence, Theorem 2.2 implies that the symmetric operator

$$\widehat{S} := T \upharpoonright (\ker \Upsilon_0 \cap \ker \Upsilon_1) \quad (20)$$

is densely defined, closed and its adjoint coincides with  $T$ . We show that  $\widehat{S}$  coincides with the symmetric operator  $S$  in (9). Note first that Theorem 2.2 also implies that

$$A_i^D \oplus A_e^D = T \upharpoonright \ker \Upsilon_0. \quad (21)$$

Both operators,  $S$  and  $\widehat{S}$ , are restrictions of the operator in (21). We now let  $f = (f_i, f_e)^\top \in \text{dom}(A_i^D \oplus A_e^D) = \ker \Upsilon_0$ . For such  $f$ , we have

$$f \in \ker \Upsilon_1 \iff \partial_{\nu_i} f_i|_C + \partial_{\nu_e} f_e|_C = 0 \iff f \in H^2(\mathbb{R}^n) \iff f \in \text{dom } S.$$

Thus,  $\widehat{S} = S$ . Now, the remaining statements in Lemma 3.1 follow immediately from Theorem 2.2.  $\square$

Next, we specify the Weyl function  $N$  and the  $\gamma$ -field  $\zeta$  corresponding to the boundary triple  $\{L^2(C), \Upsilon_0, \Upsilon_1\}$  in Lemma 3.1. It is clear from the definition of  $\Upsilon_0$  that the  $\gamma$ -field acts as follows:

$$\zeta(\lambda) : L^2(C) \rightarrow L^2(\mathbb{R}^n), \quad \varphi \mapsto f_\lambda, \quad \lambda \in \rho(A_i^D) \cap \rho(A_e^D) = \mathbb{C} \setminus [0, \infty),$$

where  $f_\lambda = (f_{i,\lambda}, f_{e,\lambda})^\top \in H^2(\Omega_i) \times H^2(\Omega_e)$  satisfies  $-\Delta f_{i,\lambda} = \lambda f_{i,\lambda}$ ,  $-\Delta f_{e,\lambda} = \lambda f_{e,\lambda}$  and

$$f_{i,\lambda}|_C = f_{e,\lambda}|_C = \iota\varphi.$$

In order to specify the Weyl function  $N$ , we recall the definition of the Dirichlet-to-Neumann maps  $\mathcal{D}_i(\lambda)$  and  $\mathcal{D}_e(\lambda)$  associated with the Laplacians on  $\Omega_i$  and  $\Omega_e$ , respectively. Note first that for  $\varphi, \psi \in H^{-1/2}(C)$  and  $\lambda \in \rho(A_i^D)$  and  $\mu \in \rho(A_e^D)$  the boundary value problems

$$-\Delta f_i = \lambda f_i, \quad f_i|_C = \varphi \quad \text{and} \quad -\Delta f_e = \mu f_e, \quad f_e|_C = \psi$$

admit unique solutions  $f_{i,\lambda} \in \text{dom } S_i^*$  and  $f_{e,\mu} \in \text{dom } S_e^*$ . Hence, the operators

$$\mathcal{D}_{i,-1/2}(\lambda) f_{i,\lambda}|_C = \partial_{\nu_i} f_{i,\lambda}|_C, \quad \text{dom } \mathcal{D}_{i,-1/2}(\lambda) = H^{-1/2}(C), \quad (22)$$

and

$$\mathcal{D}_{e,-1/2}(\mu) f_{e,\mu}|_C = \partial_{\nu_e} f_{e,\mu}|_C, \quad \text{dom } \mathcal{D}_{e,-1/2}(\mu) = H^{-1/2}(C), \quad (23)$$

are well defined, and map  $H^{-1/2}(\mathcal{C})$  into  $H^{-3/2}(\mathcal{C})$ . We have used the index  $-1/2$  in the definition of the Dirichlet-to-Neumann maps in (22) and (23) to indicate that their domain is  $H^{-1/2}(\mathcal{C})$ . For the following, it is important that the restrictions

$$\mathcal{D}_i(\lambda)f_{i,\lambda}|_{\mathcal{C}} = \partial_{\nu_i}f_{i,\lambda}|_{\mathcal{C}}, \quad \text{dom } \mathcal{D}_i(\lambda) = H^1(\mathcal{C}),$$

and

$$\mathcal{D}_e(\mu)f_{e,\mu}|_{\mathcal{C}} = \partial_{\nu_e}f_{e,\mu}|_{\mathcal{C}}, \quad \text{dom } \mathcal{D}_e(\mu) = H^1(\mathcal{C}),$$

of  $\mathcal{D}_{i,-1/2}(\lambda)$  and  $\mathcal{D}_{e,-1/2}(\mu)$  to  $H^1(\mathcal{C})$  are densely defined, closed, unbounded operators in  $L^2(\mathcal{C})$  that satisfy

$$\mathcal{D}_i(\lambda)^* = \mathcal{D}_i(\bar{\lambda}) \quad \text{and} \quad \mathcal{D}_e(\mu)^* = \mathcal{D}_e(\bar{\mu})$$

for all  $\lambda \in \rho(A_i^D)$  and for all  $\mu \in \rho(A_e^D)$ , respectively. For  $\lambda \in \rho(A_i^D) \cap \rho(A_e^D) = \mathbb{C} \setminus [0, \infty)$ , it is convenient to introduce the operators

$$\mathcal{E}_{-1/2}(\lambda) := \mathcal{D}_{i,-1/2}(\lambda) + \mathcal{D}_{e,-1/2}(\lambda) \quad \text{and} \quad \mathcal{E}(\lambda) := \mathcal{D}_i(\lambda) + \mathcal{D}_e(\lambda). \quad (24)$$

Furthermore, the restrictions of  $\mathcal{D}_{i,-1/2}(\lambda)$  and  $\mathcal{D}_{e,-1/2}(\mu)$  to  $H^{3/2}(\mathcal{C})$  will be used. These restrictions are denoted by  $\mathcal{D}_{i,3/2}(\lambda)$  and  $\mathcal{D}_{e,3/2}(\mu)$ , respectively; they map  $H^{3/2}(\mathcal{C})$  into  $H^{1/2}(\mathcal{C})$ , and as above the index  $3/2$  is used to indicate that their domain is  $H^{3/2}(\mathcal{C})$ .

**Lemma 3.2.** *Let  $S$  be the symmetric operator in (9), let  $\{L^2(\mathcal{C}), \Upsilon_0, \Upsilon_1\}$  be the boundary triple for  $S^*$  in Lemma 3.1 and fix  $\eta$  as in (8). For  $\lambda \in \rho(A_i^D) \cap \rho(A_e^D) = \mathbb{C} \setminus [0, \infty)$  the operators  $\mathcal{E}_{-1/2}(\lambda)$  in (24) have the property*

$$\text{ran}(\mathcal{E}_{-1/2}(\lambda) - \mathcal{E}_{-1/2}(\eta)) \subset H^{1/2}(\mathcal{C}) \quad (25)$$

and the Weyl function corresponding to the boundary triple  $\{L^2(\mathcal{C}), \Upsilon_0, \Upsilon_1\}$  is given by

$$N(\lambda) = -\iota(\mathcal{E}_{-1/2}(\lambda) - \mathcal{E}_{-1/2}(\eta))\iota, \quad \lambda \in \mathbb{C} \setminus [0, \infty).$$

*Proof.* Let  $\lambda \in \rho(A_i^D) \cap \rho(A_e^D)$  and let  $f_\lambda = (f_{i,\lambda}, f_{e,\lambda}) \in \ker(S^* - \lambda)$ . Then  $f_{i,\lambda}|_{\mathcal{C}} = f_{e,\lambda}|_{\mathcal{C}}$  and according to (11)–(13) we have

$$f_{i,\lambda} = f_{i,\lambda}^D + f_{i,\lambda}^\eta \quad \text{and} \quad f_{e,\lambda} = f_{e,\lambda}^D + f_{e,\lambda}^\eta,$$

where  $f_{i,\lambda}^D \in \text{dom } A_i^D$ ,  $f_{i,\lambda}^\eta \in \ker(S_i^* - \eta)$ ,  $f_{e,\lambda}^D \in \text{dom } A_e^D$  and  $f_{e,\lambda}^\eta \in \ker(S_e^* - \eta)$ . Hence, it follows with the help of  $f_{i,\lambda}|_{\mathcal{C}} = f_{i,\lambda}^\eta|_{\mathcal{C}}$  and  $f_{e,\lambda}|_{\mathcal{C}} = f_{e,\lambda}^\eta|_{\mathcal{C}}$ , and the definition of the Dirichlet-to-Neumann maps that

$$\begin{aligned} & (\mathcal{E}_{-1/2}(\lambda) - \mathcal{E}_{-1/2}(\eta))\iota\Upsilon_0f_\lambda \\ &= (\mathcal{D}_{i,-1/2}(\lambda) - \mathcal{D}_{i,-1/2}(\eta) + \mathcal{D}_{e,-1/2}(\lambda) - \mathcal{D}_{e,-1/2}(\eta))f_\lambda|_{\mathcal{C}} \\ &= \mathcal{D}_{i,-1/2}(\lambda)f_{i,\lambda}|_{\mathcal{C}} - \mathcal{D}_{i,-1/2}(\eta)f_{i,\lambda}^\eta|_{\mathcal{C}} + \mathcal{D}_{e,-1/2}(\lambda)f_{e,\lambda}|_{\mathcal{C}} - \mathcal{D}_{e,-1/2}(\eta)f_{e,\lambda}^\eta|_{\mathcal{C}} \\ &= \partial_{\nu_i}f_{i,\lambda}|_{\mathcal{C}} - \partial_{\nu_i}f_{i,\lambda}^\eta|_{\mathcal{C}} + \partial_{\nu_e}f_{e,\lambda}|_{\mathcal{C}} - \partial_{\nu_e}f_{e,\lambda}^\eta|_{\mathcal{C}} \\ &= \partial_{\nu_i}(f_{i,\lambda} - f_{i,\lambda}^\eta)|_{\mathcal{C}} + \partial_{\nu_e}(f_{e,\lambda} - f_{e,\lambda}^\eta)|_{\mathcal{C}} \\ &= \partial_{\nu_i}f_{i,\lambda}^D|_{\mathcal{C}} + \partial_{\nu_e}f_{e,\lambda}^D|_{\mathcal{C}} \end{aligned} \quad (26)$$

and hence

$$-\iota(\mathcal{E}_{-1/2}(\lambda) - \mathcal{E}_{-1/2}(\eta))\iota\Upsilon_0f_\lambda = -\iota(\partial_{\nu_i}f_{i,\lambda}^D|_{\mathcal{C}} + \partial_{\nu_e}f_{e,\lambda}^D|_{\mathcal{C}}) = \Upsilon_1f_\lambda.$$

Also, the inclusion (25) follows from (26) since  $f_{i,\lambda}^D \in H^2(\Omega_i)$  and  $f_{e,\lambda}^D \in H^2(\Omega_e)$ , and hence,  $\partial_{\nu_i}f_{i,\lambda}^D|_{\mathcal{C}} + \partial_{\nu_e}f_{e,\lambda}^D|_{\mathcal{C}} \in H^{1/2}(\mathcal{C})$  in (26), and for any

$$\varphi \in \text{dom } \mathcal{E}_{-1/2}(\lambda) = \text{dom } \mathcal{E}_{-1/2}(\eta) = H^{-1/2}(\mathcal{C}),$$

there exists  $f_\lambda = (f_{i,\lambda}, f_{e,\lambda})^\top \in \ker(S^* - \lambda)$  and  $f_\eta = (f_{i,\eta}, f_{e,\eta}) \in \ker(S^* - \eta)$  such that

$$f_{i,\lambda}|_C = f_{e,\lambda}|_C = \varphi = f_{i,\eta}|_C = f_{e,\eta}|_C.$$

□

In the following proposition, we provide a boundary triple for  $S^*$  such that the operator  $A_{\text{free}}$  corresponds to the first boundary mapping. For this, we modify the boundary triple in Lemma 3.1 in a suitable manner.

**Proposition 3.3.** *Let  $S$  be the densely defined, closed, symmetric operator in (9) with adjoint  $S^*$  in (14), and let  $\mathfrak{E}(\eta) = \iota\mathcal{E}(\eta)\iota$ . Then,  $\mathfrak{E}(\eta)^{-1}$  is a bounded self-adjoint operator in  $L^2(\mathcal{C})$  and  $\{L^2(\mathcal{C}), \Gamma_0, \Gamma_1\}$ , where*

$$\Gamma_0 f = \iota^{-1} f|_C + \mathfrak{E}(\eta)^{-1} \iota (\partial_{\nu_i} f_i^D|_C + \partial_{\nu_e} f_e^D|_C) \quad \text{and} \quad \Gamma_1 f = -\iota (\partial_{\nu_i} f_i^D|_C + \partial_{\nu_e} f_e^D|_C), \quad (27)$$

is a boundary triple for  $S^*$  with the property  $A_{\text{free}} = S^* \upharpoonright \ker \Gamma_0$ . For  $\lambda \in \mathbb{C} \setminus [0, \infty)$  the Weyl function corresponding to  $\{L^2(\mathcal{C}), \Gamma_0, \Gamma_1\}$  is given by

$$M(\lambda) = -\iota (\mathcal{E}_{-1/2}(\lambda) - \mathcal{E}_{-1/2}(\eta)) \iota (I + \mathfrak{E}(\eta)^{-1} \iota (\mathcal{E}_{-1/2}(\lambda) - \mathcal{E}_{-1/2}(\eta)) \iota).$$

*Proof.* First, we show that  $\mathfrak{E}(\eta)^{-1} = \iota^{-1} \mathcal{E}(\eta)^{-1} \iota^{-1}$  is a bounded self-adjoint operator in  $L^2(\mathcal{C})$ . Observe that  $\mathcal{E}(\eta) = \mathcal{D}_i(\eta) + \mathcal{D}_e(\eta)$  is injective. In fact, we assume that  $\mathcal{E}(\eta)\varphi = 0$  for some  $\varphi \in H^1(\mathcal{C})$ ,  $\varphi \neq 0$ . Then, there exists  $f_\eta = (f_i^\eta, f_e^\eta)^\top \in \ker(S^* - \eta)$  such that  $f_\eta|_C = \varphi$  and hence

$$0 = \mathcal{E}(\eta)\varphi = \mathcal{E}(\eta)f_\eta|_C = \mathcal{D}_i(\eta)f_i^\eta|_C + \mathcal{D}_e(\eta)f_e^\eta|_C = \partial_{\nu_i} f_i^\eta|_C + \partial_{\nu_e} f_e^\eta|_C. \quad (28)$$

Together with  $f_i^\eta|_C = f_e^\eta|_C$ , this implies that  $f_\eta \in \text{dom } A_{\text{free}}$  and hence  $\ker(A_{\text{free}} - \eta) \neq \{0\}$ . This is impossible, as  $\eta < 0$ . Thus  $\mathcal{E}(\eta)$  is injective. It follows from [6, Proposition 3.2 (iii)] that  $\mathcal{E}(\eta)$  is surjective. Hence,  $\mathcal{E}(\eta)^{-1}$  is a bounded self-adjoint operator in  $L^2(\mathcal{C})$ . Since  $\iota^{-1}$  is also a bounded self-adjoint operator in  $L^2(\mathcal{C})$ , it is clear that  $\mathfrak{E}(\eta)^{-1} = \iota^{-1} \mathcal{E}(\eta)^{-1} \iota^{-1}$  is a bounded self-adjoint operator in  $L^2(\mathcal{C})$ .

Now, let  $\{L^2(\mathcal{C}), \Upsilon_0, \Upsilon_1\}$  be the boundary triple in Lemma 3.1. Note that the boundary mappings  $\Gamma_0$  and  $\Gamma_1$  in (27) satisfy:

$$\begin{pmatrix} \Gamma_0 \\ \Gamma_1 \end{pmatrix} = \begin{pmatrix} I & -\mathfrak{E}(\eta)^{-1} \\ 0 & I \end{pmatrix} \begin{pmatrix} \Upsilon_0 \\ \Upsilon_1 \end{pmatrix}.$$

Hence, it follows that  $\{L^2(\mathcal{C}), \Gamma_0, \Gamma_1\}$  is a boundary triple for  $S^*$ ; see (2) in Section 2. Again, we let  $N$  denote the Weyl function corresponding to the boundary triple  $\{L^2(\mathcal{C}), \Upsilon_0, \Upsilon_1\}$ . It is not difficult to see that the Weyl function corresponding to  $\{L^2(\mathcal{C}), \Gamma_0, \Gamma_1\}$  is given by

$$M(\lambda) = N(\lambda)(I - \mathfrak{E}(\eta)^{-1}N(\lambda))^{-1}, \quad \lambda \in \mathbb{C} \setminus [0, \infty).$$

Hence, the form of the Weyl function  $M$  follows from Lemma 3.2.

It remains to be shown that  $A_{\text{free}} = S^* \upharpoonright \ker \Gamma_0$  holds. Assume that for some  $f \in \text{dom } S^*$  we have

$$\iota^{-1} f|_C + \mathfrak{E}(\eta)^{-1} \iota (\partial_{\nu_i} f_i^D|_C + \partial_{\nu_e} f_e^D|_C) = 0. \quad (29)$$

As  $\ker \mathcal{E}_{-1/2}(\eta) = \{0\}$  (this can be seen as in (28)), this is equivalent to

$$\mathcal{E}_{-1/2}(\eta)f|_C + (\partial_{\nu_i} f_i^D|_C + \partial_{\nu_e} f_e^D|_C) = 0.$$

Furthermore, since

$$\mathcal{E}_{-1/2}(\eta)f|_C = \mathcal{D}_{i,-1/2}(\eta)f_i^\eta|_C + \mathcal{D}_{e,-1/2}(\eta)f_e^\eta|_C = \partial_{\nu_i} f_i^\eta|_C + \partial_{\nu_e} f_e^\eta|_C$$

holds for  $f$  decomposed as in (13), we conclude that (29) is equivalent to

$$\partial_{\nu_i} f_i^\eta|_C + \partial_{\nu_e} f_e^\eta|_C + \partial_{\nu_i} f_i^D|_C + \partial_{\nu_e} f_e^D|_C = 0,$$

which in turn is equivalent to

$$\partial_{\nu_i} f_i|_C + \partial_{\nu_e} f_e|_C = 0.$$

Therefore,  $f \in \ker \Gamma_0$  if and only if  $f \in \text{dom } A_{\text{free}}$ . □

Our next goal is to identify the self-adjoint parameter  $\Theta_{\delta,\alpha}$  such that (10) holds with the boundary triple in Proposition 3.3.

**Lemma 3.4.** *Let  $S$  be the densely defined, closed, symmetric operator in (9) with adjoint  $S^*$  in (14), and let  $\{L^2(\mathcal{C}), \Gamma_0, \Gamma_1\}$  be the boundary triple in Proposition 3.3. Then*

$$\Theta_{\delta,\alpha} = \iota(\mathcal{D}_{i,3/2}(\eta) + \mathcal{D}_{e,3/2}(\eta) - \alpha)\iota\left(I - \mathfrak{E}(\eta)^{-1}\iota(\mathcal{D}_{i,3/2}(\eta) + \mathcal{D}_{e,3/2}(\eta) - \alpha)\iota\right)^{-1}$$

is an unbounded self-adjoint operator in  $L^2(\mathcal{C})$  such that the Schrödinger operator  $A_{\delta,\alpha}$  in (7) corresponds to  $\Theta_{\delta,\alpha}$ , that is,

$$A_{\delta,\alpha} = S^* \upharpoonright \ker(\Gamma_1 - \Theta_{\delta,\alpha}\Gamma_0). \tag{30}$$

*Proof.* We make use of the fact that the boundary triple  $\{L^2(\mathcal{C}), \Upsilon_0, \Upsilon_1\}$  in Lemma 3.1 and the boundary triple  $\{L^2(\mathcal{C}), \Gamma_0, \Gamma_1\}$  in Proposition 3.3 are related via

$$\Gamma_0 = \Upsilon_0 - \mathfrak{E}(\eta)^{-1}\Upsilon_1 \quad \text{and} \quad \Gamma_1 = \Upsilon_1, \tag{31}$$

and we also make use of the operator

$$\Lambda_{\delta,\alpha} = \iota(\mathcal{D}_{i,3/2}(\eta) + \mathcal{D}_{e,3/2}(\eta) - \alpha)\iota, \quad \text{dom } \Lambda_{\delta,\alpha} = H^2(\mathcal{C}). \tag{32}$$

Our first task is to show that

$$A_{\delta,\alpha} = S^* \upharpoonright \ker(\Upsilon_1 - \Lambda_{\delta,\alpha}\Upsilon_0) \tag{33}$$

holds. In fact,  $f \in \ker(\Upsilon_1 - \Lambda_{\delta,\alpha}\Upsilon_0)$  if and only if  $f \in \text{dom } S^*$  and

$$\iota(\mathcal{D}_{i,3/2}(\eta) + \mathcal{D}_{e,3/2}(\eta) - \alpha)f|_C = -\iota(\partial_{\nu_i} f_i^D|_C + \partial_{\nu_e} f_e^D|_C),$$

where  $f|_C \in \text{dom } \mathcal{D}_{i,3/2}(\eta) = \text{dom } \mathcal{D}_{e,3/2}(\eta) = H^{3/2}(\mathcal{C})$ , together with elliptic regularity, also implies that  $f = (f_i, f_e)^\top$  with  $f_i \in H^2(\Omega_i)$  and  $f_e \in H^2(\Omega_e)$ . With  $f$  decomposed as in (13) we have

$$(\mathcal{D}_{i,3/2}(\eta) + \mathcal{D}_{e,3/2}(\eta) - \alpha)f|_C = \partial_{\nu_i} f_i^\eta|_C + \partial_{\nu_e} f_e^\eta|_C - \alpha f|_C.$$

Therefore,  $f \in \ker(\Upsilon_1 - \Lambda_{\delta,\alpha}\Upsilon_0)$  if and only if  $f = (f_i, f_e)^\top \in \text{dom } S^*$  with  $f_i \in H^2(\Omega_i)$  and  $f_e \in H^2(\Omega_e)$  and

$$\partial_{\nu_i} f_i^\eta|_C + \partial_{\nu_e} f_e^\eta|_C - \alpha f|_C = -(\partial_{\nu_i} f_i^D|_C + \partial_{\nu_e} f_e^D|_C),$$

and the latter can be rewritten in the form

$$\partial_{\nu_i} f_i|_C + \partial_{\nu_e} f_e|_C = \alpha f|_C.$$

We have shown (33), and as  $A_{\delta,\alpha}$  is a self-adjoint operator in  $L^2(\mathbb{R}^n)$ , it follows that  $\Lambda_{\delta,\alpha}$  in (32) is an unbounded self-adjoint operator in  $L^2(\mathcal{C})$ .

Next, we consider the operator

$$\Theta_{\delta,\alpha} = \Lambda_{\delta,\alpha}(I - \mathfrak{E}(\eta)^{-1}\Lambda_{\delta,\alpha})^{-1} \tag{34}$$

on its natural domain; note that  $\ker(I - \mathfrak{E}(\eta)^{-1}\Lambda_{\delta,\alpha}) = \{0\}$  as otherwise  $\mathfrak{E}(\eta)\varphi = \Lambda_{\delta,\alpha}\varphi$  for some non-trivial  $\varphi \in H^2(\mathcal{C})$ , which is a contradiction to  $\alpha \neq 0$ . Now, we assume that

$f \in \ker(\Gamma_1 - \Theta_{\delta,\alpha}\Gamma_0)$ . Then, (31) and (34) yield

$$\begin{aligned}
\Upsilon_1 f - \Lambda_{\delta,\alpha}\Upsilon_0 f &= \Gamma_1 f - \Lambda_{\delta,\alpha}(\Gamma_0 + \mathfrak{E}(\eta)^{-1}\Upsilon_1) f \\
&= \Gamma_1 f - \Lambda_{\delta,\alpha}(\Gamma_0 + \mathfrak{E}(\eta)^{-1}\Gamma_1) f \\
&= \Gamma_1 f - \Lambda_{\delta,\alpha}(\Gamma_0 + \mathfrak{E}(\eta)^{-1}\Theta_{\delta,\alpha}\Gamma_0) f \\
&= \Gamma_1 f - \Lambda_{\delta,\alpha}(I + \mathfrak{E}(\eta)^{-1}\Lambda_{\delta,\alpha}(I - \mathfrak{E}(\eta)^{-1}\Lambda_{\delta,\alpha})^{-1})\Gamma_0 f \\
&= \Gamma_1 f - \Lambda_{\delta,\alpha}(I - \mathfrak{E}(\eta)^{-1}\Lambda_{\delta,\alpha})^{-1}\Gamma_0 f \\
&= \Gamma_1 f - \Theta_{\delta,\alpha}\Gamma_0 f \\
&= 0,
\end{aligned}$$

and hence  $f \in \ker(\Upsilon_1 - \Lambda_{\delta,\alpha}\Upsilon_0)$ . The converse inclusion is shown in the same way and therefore

$$\ker(\Gamma_1 - \Theta_{\delta,\alpha}\Gamma_0) = \ker(\Upsilon_1 - \Lambda_{\delta,\alpha}\Upsilon_0)$$

and thus the extensions

$$S^* \upharpoonright \ker(\Gamma_1 - \Theta_{\delta,\alpha}\Gamma_0) \quad \text{and} \quad S^* \upharpoonright \ker(\Upsilon_1 - \Lambda_{\delta,\alpha}\Upsilon_0),$$

coincide. Therefore, (33) implies (30). Since  $A_{\delta,\alpha}$  is self-adjoint in  $L^2(\mathbb{R}^n)$ , it also follows from (30) that  $\Theta_{\delta,\alpha}$  is self-adjoint in  $L^2(\mathcal{C})$ . Moreover, as  $S$  in (9) coincides with the intersection of  $A_{\text{free}}$  and  $A_{\delta,\alpha}$ , that is,  $A_{\text{free}}$  and  $A_{\delta,\alpha}$  are disjoint, and since  $A_{\text{free}}$  and  $A_{\delta,\alpha}$  are not transversal, one concludes that  $\Theta_{\delta,\alpha}$  is an unbounded operator in  $L^2(\mathcal{C})$ ; cf. (6).  $\square$

We are now able to obtain some immediate and important consequences from the previous considerations, well-known results for boundary triples and Weyl functions [3, 4] and the resolvent estimates in [6, 42].

**Theorem 3.5.** *Let  $S$  be the densely defined, closed, symmetric operator in (9) with adjoint  $S^*$  in (14), let  $\{L^2(\mathcal{C}), \Gamma_0, \Gamma_1\}$  be the boundary triple in Proposition 3.3 with*

$$A_{\text{free}} = S^* \upharpoonright \ker \Gamma_0,$$

*and let  $\gamma$  and  $M$  be the  $\gamma$ -field and Weyl function corresponding to  $\{L^2(\mathcal{C}), \Gamma_0, \Gamma_1\}$ . Furthermore, let  $\Theta_{\delta,\alpha}$  be as in Lemma 3.4 so that*

$$A_{\delta,\alpha} = S^* \upharpoonright \ker(\Gamma_1 - \Theta_{\delta,\alpha}\Gamma_0).$$

*Then, the following assertions hold for all  $\lambda \notin [0, \infty)$ :*

- (i)  $\lambda \in \sigma_p(A_{\delta,\alpha})$  if and only if  $0 \in \sigma_p(\Theta_{\delta,\alpha} - M(\lambda))$ ;
- (ii)  $\lambda \in \rho(A_{\delta,\alpha})$  if and only if  $0 \in \rho(\Theta_{\delta,\alpha} - M(\lambda))$ ;
- (iii) for all  $\lambda \in \rho(A_{\delta,\alpha})$  the resolvent formula

$$(A_{\delta,\alpha} - \lambda)^{-1} - (A_{\text{free}} - \lambda)^{-1} = \gamma(\lambda)(\Theta_{\delta,\alpha} - M(\lambda))^{-1}\gamma(\bar{\lambda})^*$$

*is valid, and the resolvent difference of  $A_{\delta,\alpha}$  and  $A_{\text{free}}$  belongs to the Schatten-von Neumann ideal  $\mathfrak{S}_p(L^2(\mathbb{R}^n))$  for all  $p > \frac{n-1}{3}$ ;*

- (iv) for all  $\xi \in \rho(\Theta_{\delta,\alpha})$  the operator  $(\Theta_{\delta,\alpha} - \xi)^{-1}$  belongs to the Schatten-von Neumann ideal  $\mathfrak{S}_p(L^2(\mathcal{C}))$  for all  $p > \frac{n-1}{3}$ .

## Acknowledgements

J. Behrndt and V. Lotoreichik gratefully acknowledge financial support by the Austrian Science Fund (FWF): Project P 25162-N26. J. Behrndt also wishes to thank Professor Igor Popov for the pleasant and fruitful research stay at the ITMO University in St. Petersburg in September 2015. V. Lotoreichik was also supported by the Czech Science Foundation (GAČR) under the project 14-06818S.

## References

- [1] Brüning J., Geyley V., Pankrashkin K. Spectra of self-adjoint extensions and applications to solvable Schrödinger operators. *Rev. Math. Phys.*, 2008, **20**, P. 1–70.
- [2] Derkach V.A., Hassi S., Malamud M.M., de Snoo H. Boundary relations and their Weyl families. *Trans. Amer. Math. Soc.*, 2006, **358**, P. 5351–5400.
- [3] Derkach V.A., Malamud M.M. Generalized resolvents and the boundary value problems for Hermitian operators with gaps. *J. Funct. Anal.*, 1991, **95**, P. 1–95.
- [4] Derkach V.A., Malamud M.M. The extension theory of Hermitian operators and the moment problem. *J. Math. Sci.*, 1995, **73**, P. 141–242.
- [5] Gorbachuk V.I., Gorbachuk M.L. *Boundary Value Problems for Operator Differential Equations*, Kluwer Academic Publ., Dordrecht, 1991.
- [6] Behrndt J., Langer M., Lotoreichik V. Schrödinger operators with  $\delta$  and  $\delta'$ -potentials supported on hypersurfaces. *Ann. Henri Poincaré*, 2013, **14**, P. 385–423.
- [7] Brasche J.F., Exner P., Kuperin Yu.A., Šeba P. Schrödinger operators with singular interactions. *J. Math. Anal. Appl.*, 1994, **184**, P. 112–139.
- [8] Albeverio S., Gesztesy F., Hoegh-Krohn R., Holden H. *Solvable Models in Quantum Mechanics*. With an appendix by Pavel Exner. AMS Chelsea Publishing, 2005.
- [9] Exner P., Kovařík H. *Quantum Waveguides*, Theoretical and Mathematical Physics, Springer, 2015.
- [10] Exner P. Leaky quantum graphs: a review. *Proc. Symp. Pure Math.*, 2008, **77**, P. 523–564.
- [11] Albeverio S., Kostenko A., Malamud M., Neidhardt H. Spherical Schrödinger operators with  $\delta$ -type interactions. *J. Math. Phys.*, 2013, **54**, 052103, 24 pp.
- [12] Behrndt J., Exner P., Lotoreichik V. Schrödinger operators with  $\delta$  and  $\delta'$  interactions on Lipschitz surfaces and chromatic numbers of associated partitions. *Rev. Math. Phys.*, 2014, **26**, 1450015, 43 pp.
- [13] Duchêne V., Raymond N. Spectral asymptotics of a broken delta interaction. *J. Phys. A*, 2014, **47**, 155203, 19 pp.
- [14] Exner P. An isoperimetric problem for leaky loops and related mean-chord inequalities. *J. Math. Phys.*, 2005, **46**, 062105, 10 pp.
- [15] Exner P., Fraas M. On geometric perturbations of critical Schrödinger operators with a surface interaction. *J. Math. Phys.*, 2009, **50**, 112101, 12 pp.
- [16] Exner P., Ichinose T. Geometrically induced spectrum in curved leaky wires. *J. Phys. A*, 2001, **34**, P. 1439–1450.
- [17] Exner P., Kondej S. Bound states due to a strong  $\delta$  interaction supported by a curved surface. *J. Phys. A*, 2003, **36**, P. 443–457.
- [18] Exner P., Kondej S. Scattering by local deformations of a straight leaky wire. *J. Phys. A*, 2005, **38**, P. 4865–4874.
- [19] Exner P., Pankrashkin K. Strong coupling asymptotics for a singular Schrödinger operator with an interaction supported by an open arc. *Comm. Partial Differential Equations*, 2014, **39**, P. 193–212.
- [20] Exner P., Yoshitomi K. Asymptotics of eigenvalues of the Schrödinger operator with a strong  $\delta$ -interaction on a loop. *J. Geom. Phys.*, 2002, **41**, P. 344–358.
- [21] Kondej S., Lotoreichik V. Weakly coupled bound state of 2-D Schrödinger operator with potential-measure. *J. Math. Anal. Appl.*, 2014, **420**, P. 1416–1438.
- [22] Kondej S., Veselič I. Lower bounds on the lowest spectral gap of singular potential Hamiltonians. *Ann. Henri Poincaré*, 2007, **8**, P. 109–134.
- [23] Mantile A., Posilicano A., Sini M. Self-adjoint elliptic operators with boundary conditions on not closed hypersurfaces. ArXiv:1505.07236, 2015.
- [24] Popov I. Yu. The operator extension theory, semitransparent surface and short range potential. *Math. Proc. Camb. Phil. Soc.*, 1995, **118**, P. 555–563.

- [25] Stollmann P., Voigt J. Perturbation of Dirichlet forms by measures. *Potential Anal.*, 1996, **5**, P. 109–138.
- [26] Brown B.M., Grubb G., Wood I.G.  $M$ -functions for closed extensions of adjoint pairs of operators with applications to elliptic boundary problems. *Math. Nachr.*, 2009, **282**, P. 314–347.
- [27] Grubb G. A characterization of the non-local boundary value problems associated with an elliptic operator. *Ann. Scuola Norm. Sup. Pisa (3)*, 1968, **22**, P. 425–513.
- [28] Malamud M.M. Spectral theory of elliptic operators in exterior domains. *Russ. J. Math. Phys.*, 2010, **17**, P. 96–125.
- [29] Behrndt J., Langer M. Boundary value problems for elliptic partial differential operators on bounded domains. *J. Funct. Anal.*, 2007, **243**, P. 536–565.
- [30] Behrndt J., Langer M. Elliptic operators, Dirichlet-to-Neumann maps and quasi boundary triples, in: *Operator Methods for Boundary Value Problems*, London Math. Soc. Lecture Note Series, 2012, **404**, P. 121–160.
- [31] Behrndt J., Langer M., Lotoreichik V. Spectral estimates for resolvent differences of self-adjoint elliptic operators. *Integral Equations Operator Theory*, 2013, **77**, P. 1–37.
- [32] Gesztesy F., Mitrea M. Generalized Robin boundary conditions, Robin-to-Dirichlet maps, and Krein-type resolvent formulas for Schrödinger operators on bounded Lipschitz domains. *Proc. Sympos. Pure Math.*, Amer. Math. Soc., Providence, RI, 2008, **79**, P. 105–173.
- [33] Gesztesy F., Mitrea M. A description of all self-adjoint extensions of the Laplacian and Krein-type resolvent formulas on non-smooth domains. *J. Anal. Math.*, 2011, **113**, P. 53–172.
- [34] Grubb G. Extension theory for elliptic partial differential operators with pseudodifferential methods. *London Math. Soc. Lecture Note Series*, 2012, **404**, P. 221–258.
- [35] Posilicano A. Self-adjoint extensions of restrictions. *Oper. Matrices*, 2008, **2**, P. 1–24.
- [36] Posilicano A., Raimondi L. Krein’s resolvent formula for self-adjoint extensions of symmetric second-order elliptic differential operators. *J. Phys. A*, 2009, **42**, 015204, 11 pp.
- [37] Post O. Boundary pairs associated with quadratic forms. *Math. Nachr.*, 2015, doi: 10.1002/mana.201500048.
- [38] Schmüdgen K. *Unbounded Self-Adjoint Operators on Hilbert Space*, Springer, Dordrecht, 2012.
- [39] Behrndt J., Langer M. On the adjoint of a symmetric operator. *J. Lond. Math. Soc. (2)*, 2010, **82**, P. 563–580.
- [40] Lions J., Magenes E. *Non-Homogeneous Boundary Value Problems and Applications I*. Springer-Verlag, Berlin–Heidelberg–New York, 1972.
- [41] Grubb G. *Distributions and Operators*. Graduate Texts in Mathematics, vol. 252, Springer, New York, 2009.
- [42] Behrndt J., Grubb G., Langer M., Lotoreichik V. Spectral asymptotics for resolvent differences of elliptic operators with  $\delta$  and  $\delta'$ -interactions on hypersurfaces. *J. Spectral Theory*, 2015, **5**, P. 697–729.

## Time dependent delta-prime interactions in dimension one

C. Cacciapuoti<sup>1</sup>, A. Mantile<sup>2</sup>, A. Posilicano<sup>1</sup>

<sup>1</sup> DiSAT, Sezione di Matematica, Università dell’Insubria,  
via Valleggio 11, 22100 Como, Italy

<sup>2</sup> Laboratoire de Mathématiques, Université de Reims - FR3399 CNRS,  
Moulin de la Housse BP 1039, 51687 Reims, France

claudio.cacciapuoti@uninsubria.it, andrea.mantile@univ-reims.fr,  
andrea.posilicano@uninsubria.it

PACS 02.30.Jr, 03.65.Db, 02.30.Rz

DOI 10.17586/2220-8054-2016-7-2-303-314

We solve the Cauchy problem for the Schrödinger equation corresponding to the family of Hamiltonians  $H_{\gamma(t)}$  in  $L^2(\mathbb{R})$  which describes a  $\delta'$ -interaction with time-dependent strength  $1/\gamma(t)$ . We prove that the strong solution of such a Cauchy problem exists whenever the map  $t \mapsto \gamma(t)$  belongs to the fractional Sobolev space  $H^{3/4}(\mathbb{R})$ , thus weakening the hypotheses which would be required by the known general abstract results. The solution is expressed in terms of the free evolution and the solution of a Volterra integral equation.

**Keywords:** time dependent point interactions, delta-prime interaction, non-autonomous Hamiltonians.

*Received: 10 February 2016*

### 1. Introduction

In this paper, we address the generation problem for the family of time-dependent Hamiltonians  $H_{\gamma(t)}$ , where  $H_{\gamma(t)}$ , for any fixed real  $t$ , denotes the self-adjoint operator in  $L^2(\mathbb{R})$  describing a  $\delta'$ -interaction of strength  $1/\gamma(t)$  (see [1, 2], [3, Chapter I.4] and references therein).

Most of the literature on time dependent point interactions focuses on perturbations of the free dynamics of the form of a Dirac’s delta time dependent potential. In three dimensions time dependent  $\delta$ -interactions were studied in [4, 5] and in [6] in relation with the problem of ionization under periodic perturbations, see also [7]. In two dimensions, very recently, the problem of the well-posedness was studied in [8]. In one dimension, this kind of non-autonomous Hamiltonians was analyzed in [9], see also [10].

It is well known that in one dimension, the family of point perturbations of the Laplacian is richer than in two and three dimensions, and includes  $\delta$  and  $\delta'$  perturbations, as well as their combinations. In this paper, we focus attention on the topical case of a time dependent  $\delta'$ -interaction.

We remark that time-dependent  $\delta$ -interactions have a non-linear counterpart, see, e.g., [11–13] in three dimensions, and [14, 15]. More recently, a systematic study of the blow-up in the one dimensional case was started in [16]. In one dimension, in particular, such models find applications to the propagation of optical waves in Kerr media, or one-dimensional many body systems, see, e.g., [17–20] and references therein. The problem of the derivation of non-linear  $\delta$ -interactions from scaled regular dynamics was recently studied in one- and three-dimensions [21–23].

Several results discussed in the present paper set the groundworks for defining the non-linear point interactions of  $\delta'$ -type and for the study of the problem of their derivation from scaled regular dynamics.

We recall that the definition of  $H_\gamma$  is given by the theory of self-adjoint extensions of the symmetric operator:

$$H^\circ = -\Delta \equiv -\frac{d^2}{dx^2}, \quad D(H^\circ) = C_0^\infty(\mathbb{R} \setminus \{0\}),$$

and, for any real  $\gamma$ , reads as follows:

$$H_\gamma \psi(x) = -\frac{d^2 \psi}{dx^2}(x), \quad x \neq 0, \tag{1}$$

$$D(H_\gamma) = \{\psi \in L^2(\mathbb{R}) : \psi = \phi + q\eta, \phi \in X^\nu, q \in \mathbb{C}, \phi'(0) = \gamma q\}, \tag{2}$$

where  $\eta(x) := \frac{1}{2} \operatorname{sgn}(x)$  and for any  $\nu \geq 0$  we defined  $X^\nu$  as the space of tempered distributions with Fourier transform in  $L^2(\mathbb{R}, |k|^{2\nu} dk)$ .

We remark that if  $f \in X^\nu$ , then its Fourier transform might be a distribution as well. Moreover, for  $\nu = m + \sigma$ , with  $m$  integer and  $1/2 < \sigma \leq 1$ , if  $f \in X^\nu$  then  $f \in C^m(\mathbb{R})$ , see Prop. 2.1 below. Hence,  $\phi$  in  $D(H_\gamma)$  is a  $C^1(\mathbb{R})$  function and  $\phi'(0)$  in the boundary condition is well defined.

The action of the operator  $H_\gamma$  can be understood also by exploiting the decomposition  $\psi = \phi + q\eta$ : this leads to

$$H_\gamma \psi(x) = -\phi''(x), \quad x \in \mathbb{R}. \tag{3}$$

When  $\gamma(t)$  is assigned as a real valued function of time, the domain  $D(H_{\gamma(t)})$  changes in time with the boundary condition  $\phi'(0) = \gamma(t)q$ . In contrast, the quadratic form corresponding to  $H_\gamma$  is given by

$$Q_\gamma(\psi) = \|\phi'\|^2 + \gamma|q|^2, \\ D(Q_\gamma) = \{\psi \in L^2(\mathbb{R}) : \psi = \phi + q\eta, \phi \in X^1, q \in \mathbb{C}\},$$

and so  $Q_{\gamma(t)}$  has a time-independent domain. Thus, by the abstract results in [24] and [10], assuming that the map  $t \mapsto \gamma(t)$  is differentiable, there exists an unitary propagator  $U_{t,s}$  in  $L^2(\mathbb{R})$ , continuously mapping  $D(H_{\gamma(s)})$  onto  $D(H_{\gamma(t)})$ , such that  $\psi(t) := U_{t,0}\psi_0$  is the (strong) solution of the Cauchy problem:

$$\begin{cases} i \frac{d}{dt} \psi(t) = H_{\gamma(t)} \psi(t) \\ \psi(0) = \psi_0 \in D(H_{\gamma(0)}) \end{cases} \tag{4}$$

However, as the case of time-dependent self-adjoint extensions  $H_{\alpha(t)}$  (corresponding to a  $\delta$ -interaction) studied in [9] suggests, the quite explicit knowledge of the action and operator domain of  $H_\gamma$  should allow one to solve the Cauchy problem (4) under weaker regularity conditions on  $\gamma(t)$ . Indeed, as we show in this paper, this is the case and problem (4) has a strong, unique solution whenever the map  $t \mapsto \gamma(t)$  is in the fractional Sobolev space  $H^{3/4}(\mathbb{R})$ , a condition weaker than the differentiability hypotheses required in [24] and [10]. Such a  $H^{3/4}$  hypothesis is the same required in the paper [9] in order to guarantee that the Cauchy problem for the family  $H_{\alpha(t)}$  has a strong solution. However, in contrast to [9], here we make use neither of sophisticated analytic tools (paraproducts) nor of abstract generation theorems (as the ones provided in [24] and [25]); instead, following the same strategy as in the paper [26], we apply a more direct approach which exploits definitions (1) and (2), providing a relatively explicit expression for the solution of (4) with initial datum  $\psi_0 = \phi_0 + q_0\eta$  in  $D(H_{\gamma(0)})$ :

$$\psi(t) = \phi(t) + q(t)\eta, \tag{5}$$

with

$$\phi(t) = e^{it\Delta}\phi_0 - \int_0^t ds \dot{q}(s)e^{i(t-s)\Delta}\eta, \tag{6}$$

where  $t \mapsto q(t)$  solves the Volterra-type integral equation

$$q(t) = f_0(t) - \sqrt{\frac{4i}{\pi}} \int_0^t ds \frac{\gamma(s)q(s)}{\sqrt{t-s}} \tag{7}$$

and the source term  $f_0$  is defined as:

$$f_0(t) := q_0 + \sqrt{\frac{4i}{\pi}} \int_0^t ds \frac{(e^{is\Delta}\phi_0)'(0)}{\sqrt{t-s}}. \tag{8}$$

We shall prove the following well-posedness result:

**Theorem 1.** *Let  $T > 0$ ,  $\gamma \in H^{3/4}(0, T)$ , and set  $\gamma_0 = \gamma(0)$ . Let  $\psi_0 = \phi_0 + q_0\eta \in D(H_{\gamma_0})$ . Then, for any  $t \in [0, T]$ , there exists a unique strong solution for the Cauchy problem (4) given by  $\psi(t) = \phi(t) + q(t)\eta$  as in Eqs. (6) – (8). Moreover, the map  $t \mapsto H_{\gamma(t)}\psi(t)$  belongs to  $C([0, T], L^2(\mathbb{R}))$ .*

We briefly discuss the heuristic derivation of the solution. The solution of the Schrödinger equation with  $H_\gamma$  as Hamiltonian satisfies the distributional equation:

$$i \frac{\partial}{\partial t} \psi(t) = -\psi''(t) + q(t)\delta'_0, \tag{9}$$

where  $\delta'_0$  is the first derivative of the Dirac delta-distribution. Let us assume, in the first part of this discussion, that the source term  $q(t)$  is an assigned function. Since  $\eta'' = \delta'_0$ , it is natural to seek for solutions of the form (5). Setting  $\psi(t) = \phi(t) + q(t)\eta$  in Eq. (9) gives the following equation for  $\phi(t)$ :

$$i \frac{\partial}{\partial t} \phi(t) = -\phi''(t) - i\dot{q}(t)\eta.$$

Eq. (6) follows directly from the Duhamel’s formula. Indeed by integration by parts, see Section 2.3 (in particular Eqs. (15) and (17)), one obtains the following equation for  $\psi(t)$ :

$$\psi(t) = e^{it\Delta}\psi_0 - i \int_0^t ds q(s)e^{i(t-s)\Delta}\delta'_0. \tag{9a}$$

This can be understood as Duhamel’s formula applied to Eq. (9).

The equation for  $q(t)$  is obtained by imposing the boundary condition  $\phi'(0) = \gamma q$ , using Eq. (6) to compute the l.h.s. in the boundary condition. We postpone the details of the calculation to Section 2.3. Here we note that the boundary condition turns the flow associated to Eq. (9) into a unitary flow. In fact, one can show that:

$$\frac{d}{dt} \|\psi(t)\|^2 = 2 \operatorname{Im} \bar{q}(t)\phi'(0, t).$$

Hence, if the boundary condition is satisfied, one has  $\frac{d}{dt} \|\psi(t)\| = 0$ .

We remark that a function  $\psi \in D(H_\gamma)$  can be written as the sum of a regular and singular part with both functions in  $L^2$  by introducing a regularization parameter  $\lambda$ . More precisely, define:

$$G_\lambda(x) := -\frac{e^{-\sqrt{\lambda}|x|}}{2\sqrt{\lambda}} \quad \lambda > 0.$$

The function  $G_\lambda$  is the solution of the distributional equation  $G''_\lambda = \delta_0 + \lambda G_\lambda$ . The domain  $D(H_\gamma)$  can be rewritten as

$$D(H_\gamma) = \left\{ \psi \in L^2(\mathbb{R}) : \psi = \phi_\lambda + qG'_\lambda, \phi_\lambda \in H^2(\mathbb{R}), q \in \mathbb{C}, \phi'_\lambda(0) = \left(\gamma + \frac{\sqrt{\lambda}}{2}\right)q \right\},$$

and the action of  $H_\gamma$  can be understood by the identity:

$$(H_\gamma + \lambda)\psi(x) = -\phi''_\lambda(x) + \lambda\phi_\lambda(x), \quad x \in \mathbb{R},$$

see, e.g., [3]. Eq. (3) is obtained by taking  $\lambda \rightarrow 0$ .

We note that the charge equation (7) does not depend on  $\lambda$ , it is easy to see that:

$$f_0(t) = \sqrt{\frac{4i}{\pi}} \int_0^t ds \frac{(e^{is\Delta}\psi_0)'(0)}{\sqrt{t-s}},$$

see Eqs. (18) and (19) below. The equation for the regular part  $\phi_\lambda$ , instead, does involve the regularization parameter, precisely

$$\phi_\lambda(t) = e^{it\Delta}\phi_{\lambda,0} - \int_0^t ds (\dot{q}(s) + \lambda q(s))e^{i(t-s)\Delta}G'_\lambda.$$

We note that, even if the regularization would avoid few issues with convolutions and Fourier transforms, which must otherwise be interpreted in distributional sense, it makes formulae more involved and introduces an unnecessary parameter. For those reasons, we decided to avoid it.

The paper consists of one additional section in which we prove Theorem 1.

## 2. Proof of Theorem 1

### 2.1. Notation and preliminaries

In what follows,  $C$  denotes a generic positive constant whose value may change from line to line.

We denote by  $\hat{\psi}$  the spatial Fourier transform of  $\psi$ :

$$\hat{\psi}(k) = \int_{\mathbb{R}} dx e^{-ikx} \psi(x).$$

The time-Fourier transform of  $f$  is denoted by  $\mathcal{F}f$  and defined as:

$$\mathcal{F}f(\omega) = \int_{\mathbb{R}} dt e^{-i\omega t} f(t) .$$

With these definitions, the Fourier transform of the convolution is:

$$(\widehat{\psi * \phi})(k) = \hat{\psi}(k)\hat{\phi}(k),$$

and similarly for the time-Fourier transform.

In the following, we denote by  $U(t)$  the free unitary group  $e^{i\Delta t}$ , we recall that its explicit expression is given by:

$$U(t)\psi(x) = \int_{\mathbb{R}} dy \frac{e^{\frac{i(x-y)^2}{4t}}}{\sqrt{4\pi it}} \psi(y),$$

which in Fourier transform reads:

$$\widehat{U(t)\psi}(k) = e^{-ik^2 t} \hat{\psi}(k).$$

**Proposition 2.1.** For  $\nu = m + \sigma$ , with  $m$  integer and  $1/2 < \sigma \leq 1$ , it results  $X^\nu \subset C^m(\mathbb{R})$ .

*Proof.* In Fourier transform:

$$f^{(m)}(x) - f^{(m)}(y) = \frac{1}{2\pi} \int_{\mathbb{R}} dk (ik)^m (e^{ikx} - e^{iky}) \hat{f}(k).$$

We note that:

$$\begin{aligned} \left| \int_{|k|<1} dk (ik)^m (e^{ikx} - e^{iky}) \hat{f}(k) \right| &\leq C|x-y|^\sigma \int_{|k|<1} dk |k|^{m+\sigma} |\hat{f}(k)| \\ &\leq C|x-y|^\sigma \|\hat{f}\|_{L^2(\mathbb{R}, |k|^{2\nu} dk)}. \end{aligned} \quad (10)$$

Moreover:

$$\begin{aligned} \left| \int_{|k|>1} dk (ik)^m (e^{ikx} - e^{iky}) \hat{f}(k) \right| &\leq C \int_{|k|>1} dk |k|^m |\hat{f}(k)| \\ &\leq C \left( \int_{|k|>1} \frac{dk}{|k|^{2\sigma}} \right)^{\frac{1}{2}} \|\hat{f}\|_{L^2(\mathbb{R}, |k|^{2\nu} dk)}. \end{aligned} \quad (11)$$

Then, the continuity of  $f^{(m)}$  follows from the bounds (10) and (11), and the dominated convergence theorem.  $\square$

We will make use of fractional Sobolev spaces; for this reason we recall few definitions. For any  $-\infty \leq a < b \leq +\infty$  and  $\nu \in (0, 1)$ , we set:

$$[f]_{H^\nu(a,b)} := \left( \int_{[a,b]^2} ds ds' \frac{|f(s) - f(s')|^2}{|s - s'|^{1+2\nu}} \right)^{1/2},$$

which is sometimes referred to as Gagliardo (semi)norm of  $f$ . The space  $H^\nu(a, b)$ , for  $-\infty \leq a < b \leq +\infty$  and  $\nu \in (0, 1)$ , is the space of functions for which the norm

$$\|f\|_{H^\nu(a,b)} = \|f\|_{L^2(a,b)} + [f]_{H^\nu(a,b)}$$

is finite. To define the space  $H^\nu(a, b)$  for  $\nu > 1$  not integer, one sets  $\nu = m + \sigma$ , where  $m$  is an integer and  $\sigma \in (0, 1)$ . Then  $H^\nu(a, b)$  is the space of functions such that  $f \in H^m(a, b)$  and  $f^{(m)} \in H^\sigma(a, b)$ .

**Remark 2.2.** Note that, for  $\nu \in (0, 1)$  there exists a constant  $C_\nu$  such that:

$$[f]_{H^\nu(\mathbb{R})} = C_\nu \|\mathcal{F}f\|_{L^2(\mathbb{R}, |\omega|^{2\nu} d\omega)},$$

for any  $f \in X^\nu$ , this is a direct consequence of Plancherel's theorem (see [27], Proposition 1.37). This identity, together with Prop. 2.1 implies that, for all  $\nu > 1/2$ , and  $a$  and  $b$  finite, if  $f \in X^\nu$  then  $f \in H^\nu(a, b)$ , and, consequently, it belongs to  $H^\mu(a, b)$  for all  $0 \leq \mu \leq \nu$ . Also, if  $f \in L^2(a, b)$  and  $f \in X^\nu$ , then  $f \in H^\nu(a, b)$ , and, consequently, in  $H^\mu(a, b)$  for all  $0 \leq \mu \leq \nu$ .

We recall that, for  $-\infty \leq a < b \leq +\infty$ , the space  $L^2(a, b)$  can be identified with  $H^0(a, b)$ , and  $L^2(\mathbb{R})$  can be identified with  $X^0$ .

For the norms, we shall use the notation  $\|\cdot\| = \|\cdot\|_{L^2(\mathbb{R})}$ .

We denote by  $I$  the operator:

$$If(t) = \frac{1}{\sqrt{\pi}} \int_0^t ds \frac{f(s)}{\sqrt{t-s}}. \tag{12}$$

We shall use the following results which establish the regularization properties of the operator  $I$ .

**Lemma 2.3.** *Let  $\nu \geq 0$  and  $T > 0$ . Assume that  $f \in X^\nu$  and has support in  $[0, T]$ , then  $If \in X^{\nu+1/2}$ .*

*Proof.* The integral kernel:

$$A(t) = \frac{1}{\sqrt{\pi}} \frac{\Theta(t)}{\sqrt{t}},$$

where  $\Theta$  is the Heaviside function, is a tempered distribution and

$$\mathcal{F}A(\omega) = \frac{1}{\sqrt{|\omega|}} \left( \frac{\sqrt{i}}{2} \Theta(\omega) + \frac{1}{\sqrt{2}} (\Theta(-\omega) + i\Theta(\omega)) \right).$$

Let  $f \in X^\nu$ . The convolution of  $A$  and  $f$ ,  $If = A * f$ , is a tempered distributions and  $\mathcal{F}If = \mathcal{F}A\mathcal{F}f$ , see, e.g., [28, Th. 14.25]. Then,

$$\| |\cdot|^{\nu+1/2} \mathcal{F}If \| \leq C \| |\cdot|^\nu \mathcal{F}f \|.$$

□

We recall the following technical lemma:

**Lemma 2.4.** *Let  $-\infty < a < b < \infty$  and let  $f \in H^\nu(a, b)$  with  $\nu \geq 0$ . Define*

$$\tilde{f}(s) = \begin{cases} f(s) & \text{if } s \in [a, b]; \\ 0 & \text{otherwise.} \end{cases}$$

*i) If  $0 \leq \nu < 1/2$ , then  $\tilde{f} \in H^\nu(\mathbb{R})$ .*

ii) If  $1/2 < \nu < 3/2$  and  $f(a) = f(b) = 0$ , then  $\tilde{f} \in H^\nu(\mathbb{R})$ .

For the proof, see for example [29, Th. 11.4], see also [30, Th. III.3.2].  
We shall also use the following:

**Proposition 2.5.** *Let  $\mu > 1/2$  and  $0 \leq \nu \leq \mu$ . If  $g \in H^\mu(a, b)$  and  $f \in H^\nu(a, b)$  then  $fg \in H^\nu(a, b)$ .*

For the proof we refer to [30].

### 2.2. Well-posedness of the charge equation

In this section, we study the well-posedness of the charge equation (7).

We start with the following lemma, which gives the regularity properties of the inhomogeneous term in Eq. (7):

**Lemma 2.6.** *Let  $\phi_0 \in X^2$ , then  $(U(\cdot)\phi_0)'(0) \in X^{3/4}$ .*

*Proof.* Since  $\phi_0' \in L^2(\mathbb{R})$ , one has that the distributional identity:

$$(U(t)\phi_0)'(x) = \int_{\mathbb{R}} dy \frac{e^{\frac{i(x-y)^2}{4t}}}{\sqrt{4\pi it}} \phi_0'(y)$$

shows that  $(U(t)\phi_0)' \in L^2(\mathbb{R})$ . By using the Fourier transform, one has that:

$$(U(t)\phi_0)'(0) = \frac{1}{2\pi} \int_{\mathbb{R}} dk e^{-ik^2 t} \widehat{\phi_0}'(k).$$

By splitting the integral in  $dk$  for  $k > 0$  and  $k < 0$ , and by using the change of variables  $k = \sqrt{\omega}$  for  $k > 0$  and  $k = -\sqrt{\omega}$  for  $k < 0$ , it follows that:

$$(U(t)\phi_0)'(0) = \frac{i}{4\pi} \int_0^\infty \frac{d\omega}{\sqrt{\omega}} e^{-i\omega t} \left( \widehat{\phi_0}'(\sqrt{\omega}) + \widehat{\phi_0}'(-\sqrt{\omega}) \right).$$

Hence:

$$\mathcal{F}((U(\cdot)\phi_0)'(0))(\omega) = \frac{i}{2\sqrt{\omega}} \Theta(-\omega) \left( \widehat{\phi_0}'(\sqrt{-\omega}) + \widehat{\phi_0}'(-\sqrt{-\omega}) \right),$$

where  $\Theta$  denotes the Heaviside function. To prove that  $\mathcal{F}((U(\cdot)\phi_0)'(0)) \in L^2(\mathbb{R}, |\omega|^{\frac{3}{2}} d\omega)$ , it is enough to note that

$$\| |\cdot|^{\frac{3}{4}} \mathcal{F}((U(\cdot)\phi_0)'(0)) \| \leq C \| |\cdot| \widehat{\phi_0}' \| = C \| |\cdot|^2 \widehat{\phi_0}' \|,$$

where we used the change of variables  $k^2 = \omega$ . □

We are now ready to prove the main result of this section.

**Lemma 2.7.** *Let  $T > 0$ ,  $\gamma \in H^{3/4}(0, T)$ , and set  $\gamma_0 = \gamma(0)$ . Let  $\psi_0 = \phi_0 + q_0 \eta \in D(H_{\gamma_0})$ . Then, Eq. (7) admits a unique solution  $q \in H^{5/4}(0, T)$ .*

*Proof.* We split the proof in two steps: first, we prove that there exists a unique solution  $q \in L^2(0, T)$ , then, by a bootstrap argument, we show that such solution belongs to  $H^{5/4}(0, T)$ .

We start by step 1. We use several results from the monograph [31]. We set:

$$k(t, s) = \sqrt{\frac{4i}{\pi}} \frac{\gamma(s)}{\sqrt{t-s}}$$

and rewrite the equation as:

$$q(t) = f_0(t) - \int_0^t ds k(t, s)q(s). \tag{13}$$

This is a linear nonconvolution Volterra equation to which we can apply the results in [31, Ch. 9]. We start by noticing that for any finite interval  $J \subset \mathbb{R}^+$ ,  $k(t, s)$  is a Volterra kernel of type  $L^2$ , more precisely:

$$\| \|k\| \|_{L^2(J)} := \sup_{\substack{\|h\|_{L^2(J)} \leq 1 \\ \|g\|_{L^2(J)} \leq 1}} \int_J \int_J ds dt |h(t)k(t, s)g(s)| \leq C|J|^{1/2} \|\gamma\|_{L^\infty(J)}.$$

Hence, the interval  $[0, T]$  can be divided into finitely many subintervals  $J_i$  such that  $\| \|k\| \|_{L^2(J_i)} < 1$  on each  $J_i$ , and, as a consequence of Cor. 9.3.14 in [31], one has that  $k$  has a resolvent of type  $L^2$  on  $[0, T]$ . By applying Th. 9.3.6 of [31], we conclude that Eq. (13) has a unique solution in  $L^2(0, T)$ .

We can now proceed to the second step of the proof, which consists in showing that such a solution belongs to  $H^{5/4}(0, T)$ . By Lemma 2.6 and Rem. 2.2, one has  $(U(\cdot)\phi_0)'(0) \in H^\nu(0, T)$  for all  $0 \leq \nu \leq 3/4$ . We set:

$$Q(t) = q(t) - q_0 \quad \text{and} \quad F(t) = \sqrt{4i}((U(t)\phi_0)'(0) - \gamma(t)q(t)) \quad t \in [0, T].$$

We denote by  $\tilde{Q}$  the function obtained by prolonging  $Q$  to zero outside  $[0, T]$  and remark that the claim  $\tilde{Q} \in X^\nu$  implies  $Q \in H^\mu(0, T)$  for all  $0 \leq \mu \leq \nu$ , see Rem. 2.2, therefore  $q \in H^\mu(0, T)$ .

By the charge equation (7), the identity  $Q = IF$  holds true for a.a.  $t \in [0, T]$ , here  $I$  is the operator defined in (12). Since, by Prop. 2.5,  $F \in L^2(0, T)$  we can define  $\tilde{F} \in L^2(\mathbb{R})$  by extending it to zero. Then, by Lemma 2.3,  $\tilde{Q} = I\tilde{F} \in X^{1/2}$ , hence,  $Q \in H^{1/4}(0, T)$  and  $q \in H^{1/4}(0, T)$ .

We can repeat the argument. We start with the observation that now we know that  $F \in H^{1/4}(0, T)$  and conclude that  $q \in H^{3/4}(0, T)$ . Here, we use Lemma 2.4-i) to claim that  $\tilde{F} \in H^{1/4}(\mathbb{R})$  which in turn implies  $\tilde{F} \in X^{1/4}$ .

To conclude the proof, we must slightly adjust the argument above. So far, we have proved that  $F \in H^{3/4}(0, T)$ , moreover we know that  $F(0) = 0$ , because the boundary condition  $\phi_0'(0) = \gamma_0 q_0$  holds true by assumption. Define  $F^s : [0, 2T] \rightarrow \mathbb{C}$  by reflection of  $F$  about  $t = T$ . We have that  $F^s(0) = F^s(2T) = 0$ . We define  $\tilde{F}^s : \mathbb{R} \rightarrow \mathbb{C}$  by extending  $F^s$  to zero and use Lemma 2.4-ii) to claim that  $\tilde{F}^s \in H^{3/4}(\mathbb{R})$ , and, consequently,  $\tilde{F} \in X^{3/4}$ . Reapplying Lemma 2.3, we conclude that  $q \in H^{5/4}(0, T)$ .  $\square$

### 2.3. Proof of Theorem 1

The function  $\phi(t)$  defined by Eq. (6) exists and is unique for all  $t \in [0, T]$ . Next we prove that  $\phi(t) \in X^2$ . Let us rewrite Eq. (6) as:

$$\phi(t) = U(t)\phi_0 + \tilde{\phi}(t),$$

where we set:

$$\tilde{\phi}(t) = - \int_0^t ds \dot{q}(s) U(t-s) \eta. \quad (14)$$

One has that  $U(t)\phi_0 \in X^2$ , because  $\|\widehat{U(t)\phi_0}\|_{L^2(\mathbb{R}, |k|^4 dk)} = \|\hat{\phi}_0\|_{L^2(\mathbb{R}, |k|^4 dk)}$ .

We are left to prove that  $\tilde{\phi} \in X^2$ . We recall that the Fourier transform of  $\eta$  is the distribution  $-i \text{PV} \frac{1}{k}$  (where PV stands for principal value). We have that:

$$\begin{aligned} \|\hat{\tilde{\phi}}(t)\|_{L^2(\mathbb{R}, |k|^4 dk)}^2 &= \frac{1}{2\pi} \int_{\mathbb{R}} dk k^2 \left| \int_0^t ds e^{-ik^2(t-s)} \dot{q}(s) \right|^2 \\ &= \frac{1}{2\pi} \int_0^\infty d\omega \omega^{\frac{1}{2}} \left| \int_0^t ds e^{i\omega s} \dot{q}(s) \right|^2 \leq C \|\dot{q}\|_{H^{1/4}(0,T)}. \end{aligned} \quad (14a)$$

Here, the inequality follows from the same argument used in the proof of Prop. 3.3 in [23].

Next, we prove that  $\psi(t) = \phi(t) + q(t)\eta \in L^2(\mathbb{R})$ . Since  $\phi(t) \in C^1(\mathbb{R})$ , see Prop. 2.1, and  $\eta$  is bounded,  $\psi(t) \in L^2_{loc}(\mathbb{R})$ . Hence, it is enough to prove that  $(1-\chi)\psi(t) \in L^2(\mathbb{R})$ , where  $\chi$  is the characteristic function of the interval  $[-1, 1]$ . In the definition of  $\phi(t)$ , see Eq. (6), we use the identity:

$$\int_0^t ds \dot{q}(s) U(t-s) \eta = q(t)\eta - q_0 U(t)\eta - \int_0^t ds q(s) \frac{\partial}{\partial s} U(t-s) \eta,$$

which gives:

$$\psi(t) = U(t)\psi_0 + \int_0^t ds q(s) \frac{\partial}{\partial s} U(t-s) \eta. \quad (15)$$

Since  $U(t)\psi_0 \in L^2(\mathbb{R})$ , we are left to prove that the second term at the r.h.s., times the function  $(1-\chi)$ , is also in  $L^2(\mathbb{R})$ . We note that:

$$\begin{aligned} (U(t)\eta)(x) &= \int_{\mathbb{R}} dy \frac{e^{i\frac{(x-y)^2}{4t}}}{\sqrt{4\pi it}} \eta(y) \\ &= \frac{1}{2} \frac{1}{\sqrt{4\pi it}} \left( \int_{-\infty}^x dy e^{i\frac{y^2}{4t}} - \int_x^\infty dy e^{i\frac{y^2}{4t}} \right). \end{aligned} \quad (16)$$

From which, we get:

$$\frac{\partial}{\partial t} (U(t)\eta)(x) = -\frac{1}{2} \frac{1}{\sqrt{4\pi i}} \frac{x}{t^{3/2}} e^{i\frac{x^2}{4t}} = -\sqrt{\frac{i}{\pi}} \frac{\sqrt{t}}{x} \frac{d}{dt} e^{i\frac{x^2}{4t}}.$$

We remark that the first equality can be understood in distributional sense as:

$$\frac{\partial}{\partial t} (U(t)\eta) = i(U(t)\eta)'' = i(U(t)\eta'') = i(U(t)\delta'_0), \quad (17)$$

from which, one deduces that Eq. (15) is equivalent to Eq. (5).

This then gives:

$$\begin{aligned} \int_0^t ds q(s) \frac{\partial}{\partial t} (U(t-s)\eta)(x) &= \sqrt{\frac{i}{\pi}} \frac{1}{x} \int_0^t ds q(s) \sqrt{t-s} \frac{d}{ds} e^{i\frac{x^2}{4(t-s)}} \\ &= \sqrt{\frac{i}{\pi}} \frac{1}{x} \left( -q_0 \sqrt{t} e^{i\frac{x^2}{4t}} - \int_0^t ds \dot{q}(s) \sqrt{t-s} e^{i\frac{x^2}{4(t-s)}} + \frac{1}{2} \int_0^t ds \frac{q(s)}{\sqrt{t-s}} e^{i\frac{x^2}{4(t-s)}} \right). \end{aligned}$$

We gained a factor  $1/x$  which gives the bound:

$$\left\| (1-\chi) \int_0^t ds q(s) \frac{\partial}{\partial t} U(t-s)\eta \right\| \leq C (\|q\|_{L^\infty(0,T)} + \|\dot{q}\|_{L^1(0,T)}) \leq C \quad t \in [0, T].$$

Next, we prove that the boundary condition  $\phi'(0) = \gamma(t)q$  holds true for all  $t \in [0, T]$ . From Eq. (16), we obtain:

$$(U(t)\eta)'(0) = \frac{1}{\sqrt{4\pi i t}}, \tag{18}$$

hence

$$\phi'(0, t) = (U(t)\phi_0)'(0) - \int_0^t ds \frac{1}{\sqrt{4\pi i(t-s)}} \dot{q}(s).$$

We apply the operator  $I$ , defined in (12), and use the charge equation (7) to obtain

$$(I\phi'(0, \cdot))(t) = (I(U(\cdot)\phi_0)'(0))(t) - \frac{1}{\sqrt{4i}}(q(t) - q_0) = (I\gamma q)(t),$$

which implies the boundary condition. Here, we used the identities:

$$I(\pi(\cdot))^{-1/2}(t) = \frac{1}{\sqrt{\pi}} \int_0^t ds \frac{1}{\sqrt{t-s}} \frac{1}{\sqrt{\pi s}} = 1 \quad \text{and} \quad I^2 f(t) = \int_0^t ds f(s). \tag{19}$$

By Eq. (3), to prove the continuity of the map  $t \mapsto H_{\gamma(t)}\psi(t)$  in  $L^2(\mathbb{R})$ , it is enough to show the continuity of  $\|\phi''(t)\|$ . As the continuity of  $U(t)\phi_0$  is obvious, we just need to show that:

$$\lim_{\delta \rightarrow 0} \left\| \hat{\phi}(t+\delta) - \hat{\phi}(t) \right\|_{L^2(\mathbb{R}, |k^4| dk)}^2 = 0.$$

By Eqs. (14) and (14a), this is reduced to show that:

$$\lim_{\delta \rightarrow 0} \int_{\mathbb{R}} dk k^2 \left| \int_t^{t+\delta} ds e^{-ik^2 s} \dot{q}(s) \right|^2 = 0.$$

For the proof of this statement, we refer to the proof of Prop. 3.3 in [23]. □

## Acknowledgements

The authors acknowledge the support of the FIR 2013 project “Condensed Matter in Mathematical Physics”, Ministry of University and Research of Italian Republic (code RBFR13WAET).

## References

- [1] Gesztesy F. and Holden H. A new class of solvable models in quantum mechanics describing point interactions on the line, *J. Phys. A*, 1987, **20**(15), P. 5157–5177.
- [2] Šeba P. Some remarks on the  $\delta'$ -interaction in one dimension, *Rep. Math. Phys.*, 1986, **24**(1), P. 111–120.
- [3] Albeverio S., Gesztesy F., Hoegh-Krohn R., and Holden H. Solvable Models in Quantum Mechanics, *AMS*, 2005. With an appendix of P. Exner.
- [4] Sayapova M. R. and Yafaev D. R. The evolution operator for time-dependent potentials of zero radius, *Boundary value problems of mathematical physics*, vol. 159, Part 12, Work collection, Trudy Mat. Inst. Steklov., 1983, P. 167–174.
- [5] Yafaev D. R. Scattering theory for time-dependent zero-range potentials, *Annales de l'IHP Physique théorique*, 1984, **40**(4), P. 343–359.
- [6] Correggi M., Dell'Antonio G., Figari R., and Mantile A. Ionization for Three Dimensional Time-Dependent Point Interactions, *Comm. Math. Phys.*, 2005, **257**(1), P. 169–192.
- [7] Correggi M. and Dell'Antonio G. Decay of a bound state under a time-periodic perturbation: a toy case, *J. Phys. A*, 2005, **38**(22), P. 4769–4781.
- [8] Carlone R., Correggi M., and Figari R. Two-dimensional time-dependent point interactions, arXiv:1601.02390 [math-ph], 2016, 17 pp.
- [9] Hmidi T., Mantile A., and Nier F. Time-dependent Delta-interactions for 1D Schrödinger Hamiltonians, *Math. Phys. Anal. Geom.*, 2009, **13**(1), P. 83–103.
- [10] Neidhardt H. and Zagrebnov V. A. Linear non-autonomous Cauchy problems and evolution semigroups, *Adv. Differential Equations*, 2009, **14**(3/4), P. 289–340.
- [11] Adami R., Dell'Antonio G., Figari R., and Teta A. The Cauchy problem for the Schrödinger equation in dimension three with concentrated nonlinearity, *Ann. Inst. H. Poincaré Anal. Non Linéaire*, 2003, **20**(3), P. 477–500.
- [12] Adami R., Dell'Antonio G., Figari R., and Teta A. Blow-up solutions for the Schrödinger equation in dimension three with a concentrated nonlinearity, *Ann. Inst. H. Poincaré Anal. Non Linéaire*, 2004, **21**(1), P. 121–137.
- [13] Adami R., Noja D., and Ortoleva C. Orbital and asymptotic stability for standing waves of a nonlinear Schrödinger equation with concentrated nonlinearity in dimension three, *J. Math. Phys.*, 2013, **54**(1), P. 013501.
- [14] Adami R. and Teta A. A Simple Model of Concentrated Nonlinearity, *Mathematical Results in Quantum Mechanics* (Dittrich J., Exner P., and Tater M., eds.), Operator Theory Advances and Applications, Birkhäuser Basel, January 1999, P. 183–189.
- [15] Adami R. and Teta A. A class of nonlinear Schrödinger equations with concentrated nonlinearity, *J. Funct. Anal.*, 2001, **180**(1), P. 148–175.
- [16] Holmer J. and Liu C., Blow-up for the 1D nonlinear Schrödinger equation with point nonlinearity I: Basic theory, arXiv:1510.03491 [math.AP], 2015, 22 pp.
- [17] Dror N. and Malomed B. A. Solitons supported by localized nonlinearities in periodic media, *Phys. Rev. A*, 2011, **83**(3), P. 033828.
- [18] Hennig D., Tsironis G., Molina M., and Gabriel H. A nonlinear quasiperiodic Kronig-Penney model, *Phys. Lett. A*, 1994, **190**(3-4), P. 259–263.
- [19] Malomed B. A. and Azbel M. Y. Modulational instability of a wave scattered by a nonlinear center, *Phys. Rev. B*, 1993, **47**(16), P. 10402–10406.
- [20] Molina M. and Bustamante C. The attractive nonlinear delta-function potential, *Am. J. Phys.*, 2002, **70**, P. 67–70.
- [21] Cacciapuoti C. On the derivation of the Schrödinger equation with point-like nonlinearity, *Nanonsystems: Phys., Chem., Math*, 2015, **6**, P. 79–94.
- [22] Cacciapuoti C., Finco D., Noja D., and Teta A. The NLS Equation in Dimension One with Spatially Concentrated Nonlinearities: the Pointlike Limit, *Lett. Math. Phys.*, 2014, **104**(12), P. 1557–1570.

- [23] Cacciapuoti C., Finco D., Noja D., and Teta A. The point-like limit for a NLS equation with concentrated nonlinearity in dimension three, arXiv:1511.06731 [math-ph], 2015, 35 pp.
- [24] Kisyński J. Sur les opérateurs de Green des problèmes de Cauchy abstraits, *Studia Mathematica*, 1964, **3**(23), P. 285–328.
- [25] Kato T. Linear evolution equations of “hyperbolic” type, *J. Fac. Sci. Univ. Tokyo Sect. I*, 1970, **17**(6), P. 241–258.
- [26] Dell’Antonio G. F., Figari R., and Teta A., A limit evolution problem for time-dependent point interactions, *J. Funct. Anal.*, 1996, **142**(1), P. 249–274.
- [27] Bahouri H., Chemin J.-Y., and Danchin R. *Fourier analysis and nonlinear partial differential equations*, vol. 343, Springer Science & Business Media, 2011.
- [28] Duistermaat J. J. and Kolk J. A. *Distributions: Theory and Applications*, Springer, 2010.
- [29] Lions J. L. and Magenes E. *Non-homogeneous boundary value problems and applications*, vol. 1, Springer, Berlin, 1972.
- [30] Strichartz R. S. Multipliers on fractional Sobolev spaces, *J. Math. Mech*, 1967, **16**(9), P. 1031–1060.
- [31] Gripenberg G., Londen S. O., and Staffans O., *Volterra integral and functional equations*, vol. 34, Cambridge University Press, 1990.

# Laplacians with singular perturbations supported on hypersurfaces

A. Mantile<sup>1</sup>, A. Posilicano<sup>2</sup>

<sup>1</sup>Laboratoire de Mathématiques de Reims, EA4535 URCA,  
Fédération de Recherche ARC Mathématiques, FR 3399 CNRS, France  
<sup>2</sup>DiSAT, Sezione di Matematica, Università dell’Insubria, via Valleggio 11,  
I-22100 Como, Italy

andrea.mantile@univ-reims.fr, andrea.posilicano@uninsubria.it

**PACS 02.30.Tb, 02.30.Jr**

**DOI 10.17586/2220-8054-2016-7-2-315-323**

We review the main results of our recent work on singular perturbations supported on bounded hypersurfaces. Our approach consists in using the theory of self-adjoint extensions of restrictions to build self-adjoint realizations of the  $n$ -dimensional Laplacian with linear boundary conditions on (a relatively open part of) a compact hypersurface. This allows one to obtain Kreĭn-like resolvent formulae where the reference operator coincides with the free selfadjoint Laplacian in  $\mathbb{R}^n$ , providing in this way with an useful tool for the scattering problem from a hypersurface. As examples of this construction, we consider the cases of Dirichlet and Neumann boundary conditions assigned on an unclosed hypersurface.

**Keywords:** Kreĭn’s resolvent formula, boundary conditions, self-adjoint extensions.

*Received: 02 March 2016*

## 1. Introduction

In a recent paper [1], the complete family of self-adjoint elliptic operators with interface conditions assigned on a hypersurface in  $\mathbb{R}^n$  was realized. Derived from the abstract theory of selfadjoint extensions of restrictions developed in [2–5], our approach leads to Kreĭn type formulae for the resolvent difference between the perturbed operator and the corresponding free selfadjoint model with domain  $H^2(\mathbb{R}^n)$ . This is a relevant point for the interface perspective of studying the scattering problem. Moreover, while some sub-families of extensions (mainly those concerned with the  $\delta$  or  $\delta'$  interface conditions) have been largely investigated by using quadratic form or quasi-boundary triple techniques (see [6–25]), for others models presented in [1], and in particular those concerned with local interface conditions of Dirichlet and Neumann type, a rigorous analysis was not previously given.

The aim of this report is to provide a shortened introduction to this analysis, giving the essential information about the construction of our models in the case of singular perturbations of the  $n$ -dimensional Laplacian with interface conditions. In this framework, we recall the basic results needed to construct the whole family of singular perturbations and then focus on the explicit examples of ”global” and ”local” Dirichlet- and Neumann-type boundary conditions. For the detailed proofs, we refer to [1].

After recalling in Section 1 the main properties of the trace maps and the layer operators related to the surface  $\Gamma$ , we introduce our model in Section 2 through the symmetric operator:

$$\Delta^\circ = \Delta \upharpoonright \{u \in H^2(\mathbb{R}^n) : u|_\Gamma = (\nu \cdot \nabla) u|_\Gamma = 0\}, \quad (1)$$

where  $\nu$  denotes the exterior unit normal on  $\Gamma$ . The self-adjoint realizations of the Laplacian with boundary conditions involving linear relations between lateral traces on  $\Gamma$ , or on a relatively open

part  $\Sigma \subset \Gamma$ , are defined as selfadjoint extensions of  $\Delta^\circ$ . The general construction provided in [2–5] allows us to define these extensions as singular perturbations of the free Laplacian operator defined by  $\text{dom}(\Delta) = H^2(\mathbb{R}^n)$ . In this framework, the perturbed operators are parametrized through couples  $(\Pi, \Theta)$ , where  $\Pi$  is an orthogonal projector on the Hilbert trace space  $H^{3/2}(\Gamma) \oplus H^{1/2}(\Gamma)$  and  $\Theta$  is a self-adjoint operator in the Hilbert space given by the range of  $\Pi$ . In Theorem 3.1 and Corollary 3.5, we define this family of extensions in terms  $(\Pi, \Theta)$  and give the corresponding Kreĭn-like resolvent formulae, while their spectral properties and the conditions for the wave operators existence and completeness are given in Theorem 3.3. The connection between this abstract parametrization and explicit boundary (or interface) conditions is the main issue concerned with this approach. In Section 3 we consider this point in the particular cases of the Dirichlet and Neumann conditions on  $\Gamma$  and on  $\Sigma \subset \Gamma$ .

## 2. Preliminaries

Let  $\Omega \subset \mathbb{R}^n$  be open and suppose its boundary  $\Gamma = \partial\Omega$  is a smooth  $(n-1)$ -dimensional compact manifold. In this case,  $H^s(\Omega)$ ,  $s \in \mathbb{R}$ , is defined by  $H^s(\Omega) := \{u|_\Omega : u \in H^s(\mathbb{R}^n)\}$ ,  $u|_\Omega$  denoting the restriction of  $u$  to  $\Omega$  and  $H^s(\mathbb{R}^n)$  denoting the usual scale of Hilbert-Sobolev spaces on  $\mathbb{R}^n$  defined by Fourier transform. The Sobolev spaces of  $L^2$ -functions on  $\Gamma$ , next denoted with  $H^s(\Gamma)$ , are defined by using an atlas of  $\Gamma$  and the Sobolev space on flat, open, bounded,  $(n-1)$ -dimensional domains (see e.g. [26, Chapter 1], [27, Chapter 3]);  $H^{-s}(\Gamma)$  identifies with the dual space of  $H^s(\Gamma)$ ;  $\langle \cdot, \cdot \rangle_{-s,s}$  denotes the  $H^{-s}$ - $H^s$  duality. Considering the Riemannian structure inherited from  $\mathbb{R}^n$ , the space  $H^s(\Gamma)$  identifies with  $\text{dom}((-\Delta_\Gamma)^{s/2})$  with respect to the scalar product:

$$\langle \phi, \varphi \rangle_{H^s(\Gamma)} := \langle \Lambda^s \phi, \Lambda^s \varphi \rangle_{L^2(\Gamma)}, \quad \Lambda := (-\Delta_\Gamma + 1)^{1/2}, \quad (2)$$

being  $\Delta_\Gamma$  the self-adjoint operator in  $L^2(\Gamma)$  corresponding to the Laplace-Beltrami operator on the complete Riemannian manifold  $\Gamma$  (see e.g. [26, Remark 7.6, Chapter 1]). According to this definition,  $\Lambda^r$  is self-adjoint in  $H^s(\Gamma)$  with domain  $H^{s+r}(\Gamma)$  and acts as a unitary map  $\Lambda^r : H^s(\Gamma) \rightarrow H^{s-r}(\Gamma)$ .

For a bounded open domain  $\Omega$ , we set:  $\Omega_- = \Omega$  and  $\Omega_+ = \mathbb{R}^n \setminus \Omega$ , while  $\nu$  denotes the outward normal vector on  $\Gamma = \partial\Omega$ . The domain of the maximal Laplacian in  $L^2(\Omega_\pm)$  is next denoted by:

$$L^2_\Delta(\Omega_\pm) := \{u \in L^2(\Omega) : \Delta u \in L^2(\Omega_\pm)\} \quad (3)$$

and we define:

$$L^2_\Delta(\mathbb{R}^n \setminus \Gamma) := L^2_\Delta(\Omega_-) \oplus L^2_\Delta(\Omega_+). \quad (4)$$

We also pose:

$$H^s(\mathbb{R}^n \setminus \Gamma) := H^s(\Omega_-) \oplus H^s(\Omega_+). \quad (5)$$

The one-sided, zero-order, trace operators  $\gamma_0^\pm$  act on a smooth function  $u \in C^\infty(\overline{\Omega_\pm})$  as  $\gamma_0^\pm u = u|_\Gamma$ , where  $\varphi|_\Gamma$  is the restriction to  $\Gamma$ . These maps uniquely extend to bounded linear operators (see e.g. [27, Theorem 3.37]):

$$\gamma_0^\pm \in \mathcal{B}(H^s(\Omega_\pm), H^{s-1/2}(\Gamma)), \quad s > \frac{1}{2}. \quad (6)$$

The one-sided first-order trace operators are given by  $\gamma_1^\pm u := \nu \cdot \gamma_0^\pm(\nabla u)$ ; from (6) there follows:

$$\gamma_1^\pm \in \mathcal{B}(H^s(\Omega_\pm), H^{s-\frac{3}{2}}(\Gamma)), \quad s > \frac{3}{2}. \quad (7)$$

Using these maps, the two-sided bounded trace operators are defined according to:

$$\gamma_0 : H^s(\mathbb{R}^n \setminus \Gamma) \rightarrow H^{s-\frac{1}{2}}(\Gamma), \quad \gamma_0(u_- \oplus u_+) := \frac{1}{2}(\gamma_0^+ u_+ + \gamma_0^- u_-), \quad (8)$$

$$\gamma_1 : H^s(\mathbb{R}^n \setminus \Gamma) \rightarrow H^{s-\frac{3}{2}}(\Gamma), \quad \gamma_1(u_- \oplus u_+) := \frac{1}{2}(\gamma_1^+ u_+ + \gamma_1^- u_-), \quad (9)$$

while the corresponding jumps are:

$$[\gamma_0] : H^s(\mathbb{R}^n \setminus \Gamma) \rightarrow H^{s-\frac{1}{2}}(\Gamma), \quad [\gamma_0](u_- \oplus u_+) := \gamma_0^+ u_+ - \gamma_0^- u_-, \quad (10)$$

$$[\gamma_1] : H^s(\mathbb{R}^n \setminus \Gamma) \rightarrow H^{s-\frac{3}{2}}(\Gamma), \quad [\gamma_1](u_- \oplus u_+) := \gamma_1^+ u_+ - \gamma_1^- u_-. \quad (11)$$

By [26, Theorem 6.5, Section 6, Chapter 2], the maps  $\gamma_0^\pm$  and  $\gamma_1^\pm$  can be further extended to:

$$\hat{\gamma}_0^\pm \in \mathcal{B}(L_\Delta^2(\Omega_\pm), H^{-1/2}(\Gamma)), \quad (12)$$

and

$$\hat{\gamma}_1^\pm \in \mathcal{B}(L_\Delta^2(\Omega_\pm), H^{-3/2}(\Gamma)), \quad (13)$$

thus producing the extended jumps maps:

$$[\hat{\gamma}_0] : L_\Delta^2(\mathbb{R}^n \setminus \Gamma) \rightarrow H^{-\frac{1}{2}}(\Gamma), \quad [\hat{\gamma}_0](u_- \oplus u_+) := \hat{\gamma}_0^+ u_+ - \hat{\gamma}_0^- u_-, \quad (14)$$

$$[\hat{\gamma}_1] : L_\Delta^2(\mathbb{R}^n \setminus \Gamma) \rightarrow H^{-\frac{3}{2}}(\Gamma), \quad [\hat{\gamma}_1](u_- \oplus u_+) := \hat{\gamma}_1^+ u_+ - \hat{\gamma}_1^- u_-. \quad (15)$$

In what follows, the  $n$ -dimensional free Laplacian is defined by  $\text{dom}(\Delta) = H^2(\mathbb{R}^n)$ . This is a selfadjoint and negatively-defined operator with:  $\sigma(\Delta) = \sigma_{ac}(\Delta) = (-\infty, 0]$ , and for all  $z \in \mathbb{C} \setminus \mathbb{R}_-$  it follows that:

$$(-\Delta + z)^{-1} \in \mathcal{B}(H^s(\mathbb{R}^n), H^{s+2}(\mathbb{R}^n)) \quad (16)$$

Given an open and bounded smooth domain  $\Omega$ , the single and double-layer operators related to  $(-\Delta + z)^{-1}$  and to the surface  $\Gamma = \partial\Omega$  are defined for any  $z \in \mathbb{C} \setminus \mathbb{R}_-$  by:

$$\langle SL_z \phi, u \rangle_{L^2(\mathbb{R}^n)} := \langle \phi, \gamma_0(-\Delta + \bar{z})^{-1} u \rangle_{-3/2, 3/2}, \quad (17)$$

$$\langle DL_z \varphi, u \rangle_{L^2(\mathbb{R}^n)} := \langle \varphi, \gamma_1(-\Delta + \bar{z})^{-1} u \rangle_{-1/2, 1/2}. \quad (18)$$

Due to the mapping properties (6) – (7) and (16), these relation define bounded maps on  $H^{-3/2}(\Gamma)$  and  $H^{-1/2}(\Gamma)$ , provided that  $z \in \mathbb{C} \setminus \mathbb{R}_-$ ; we have:

$$SL_z \in \mathcal{B}(H^{-3/2}(\Gamma), L^2(\mathbb{R}^n)), \quad DL_z \in \mathcal{B}(H^{-1/2}(\Gamma), L^2(\mathbb{R}^n)). \quad (19)$$

The integral kernel of  $(-\Delta + z)^{-1}$ ,  $z \in \mathbb{C} \setminus \mathbb{R}_-$ , is given by:

$$\mathcal{K}_z(x - y) = \frac{1}{2\pi} \left( \frac{\sqrt{z}}{2\pi \|x - y\|} \right)^{n/2-1} K_{n/2-1}(\sqrt{z} \|x - y\|), \quad \text{Re } \sqrt{z} > 0,$$

where  $K_\alpha$  denotes the modified Bessel functions of second kind of order  $\alpha$ . This is a smooth function for  $x \neq y$  and the relations (17) and (18) give:

$$SL_z \phi(x) = \int_\Gamma \mathcal{K}_z(x - y) \phi(y) d\sigma_\Gamma(y), \quad x \notin \Gamma \text{ and } \phi \in L^2(\Gamma), \quad (20)$$

and

$$DL_z \varphi(x) = \int_\Gamma \nu(y) \cdot \nabla \mathcal{K}_z(x - y) \varphi(y) d\sigma_\Gamma(y), \quad x \notin \Gamma \text{ and } \varphi \in L^2(\Gamma), \quad (21)$$

where  $\sigma_\Gamma$  denotes the surface measure. In particular, one has (see [27, eqs. (6.18) and (6.19)]):

$$\forall x \notin \Gamma, \quad \Delta SL_z \phi(x) = z SL_z \phi(x), \quad \Delta DL_z \varphi(x) = z DL_z \varphi(x), \quad (22)$$

from which, we obtain

$$SL_z \in \mathcal{B}(H^{-3/2}(\Gamma), L^2_\Delta(\mathbb{R}^n \setminus \Gamma)), \quad DL_z \in \mathcal{B}(H^{-1/2}(\mathbb{R}^n \setminus \Gamma), L^2_\Delta(\mathbb{R}^n \setminus \Gamma)); \quad (23)$$

in particular, the representation:

$$L^2_\Delta(\mathbb{R}^n \setminus \Gamma) = \{u = u_0 + SL_z\phi + DL_z\varphi, u_0 \in H^2(\mathbb{R}^n), \phi \oplus \varphi \in H^{-3/2}(\Gamma) \oplus H^{-1/2}(\Gamma)\}, \quad (24)$$

holds for any  $z \in \mathbb{C} \setminus \mathbb{R}_-$  (see [1, Lemma 4.2]). In the following, we choose  $z = 1$  and set

$$SL := SL_1, \quad DL := DL_1. \quad (25)$$

### 3. Singular perturbations supported on hypersurfaces.

Let  $\Omega \subset \mathbb{R}^n$ , be open and bounded with smooth boundary  $\Gamma$  and denote:

$$\gamma : H^2(\mathbb{R}^n) \rightarrow H^{3/2}(\Gamma) \oplus H^{1/2}(\Gamma), \quad \gamma u := \gamma_0 u \oplus \gamma_1 u. \quad (26)$$

The singular perturbations of the free Laplacian supported on  $\Gamma$  are next defined as the selfadjoint extensions of the closed symmetric operator:

$$\Delta^\circ := \Delta \upharpoonright \ker(\gamma), \quad (27)$$

where

$$\ker(\gamma) = H_0^2(\Omega_+) \oplus H_0^2(\Omega_-), \quad H_0^2(\Omega_\pm) := \{u_\pm \in H^2(\Omega_\pm) : \gamma_0^\pm u_\pm = \gamma_1^\pm u_\pm = 0\}. \quad (28)$$

The corresponding adjoint coincides with the maximal Laplacian in  $\mathbb{R}^n \setminus \Gamma$ , i.e.

$$(\Delta^\circ)^* = \Delta \upharpoonright L^2_\Delta(\Omega_+) \oplus L^2_\Delta(\Omega_-). \quad (29)$$

Using the alternative representation given in (24), we have:

$$(\Delta^\circ)^* u = \Delta u_0 + z(SL_z\phi + DL_z\varphi). \quad (30)$$

Moreover,  $(\Delta^\circ)^*$  and the distributional Laplacian are related by the identity (see e.g. in [28, Theorem 3.1]):

$$(\Delta^\circ)^* u = \Delta u - [\hat{\gamma}_1]u \delta_\Gamma - [\hat{\gamma}_0]u \partial_\nu \delta_\Gamma. \quad (31)$$

Here, for  $f \in H^{-s}(\Gamma)$ ,  $f\delta_\Gamma$  and  $f\partial_\nu\delta_\Gamma$  are the distributions supported on  $\Gamma$  defined by:

$$(f\delta_\Gamma, \chi) = \langle \bar{f}, \gamma_0 \chi \rangle_{-s,s}, \quad \text{and} \quad (f\partial_\nu\delta_\Gamma, \chi) = -\langle \bar{f}, \gamma_1 \chi \rangle_{-s,s}. \quad (32)$$

In particular, taking  $f = 1$ , for any  $\chi \in \mathcal{C}_0^\infty(\Omega)$  one has:

$$(\delta_\Gamma, \chi) = \int_\Gamma \chi(x) d\sigma_\Gamma(x), \quad (33)$$

and

$$(\partial_\nu\delta_\Gamma, \chi) = -\int_\Gamma \partial_\nu \chi(x) d\sigma_\Gamma(x). \quad (34)$$

Let us recall that  $\gamma$  belongs to  $\mathcal{B}(H^2(\mathbb{R}^n), H^{3/2}(\Gamma) \oplus H^{1/2}(\Gamma))$ , is surjective and has a kernel dense in  $L^2(\mathbb{R}^n)$  [1, Lemma 4.1]. Hence, the approach developed in [2–5] applies to our framework and allows us to construct all self-adjoint extensions of  $\Delta^\circ$ . For generic elliptic selfadjoint operators with smooth coefficients, this strategy has been implemented in [1] to which we refer for the detailed proofs. The auxiliary operators  $G_z$  are next defined by the duality:

$$\langle G_z \xi, u \rangle_{L^2(\mathbb{R}^n)} = \langle \xi, \gamma(-\Delta + z)^{-1} u \rangle_\Gamma, \quad \xi \in H^{-3/2}(\Gamma) \oplus H^{-1/2}(\Gamma), u \in L^2(\mathbb{R}^n). \quad (35)$$

for all  $z \in \mathbb{C} \setminus \mathbb{R}_-$ . From (17) – (18) it easily follows that:

$$G_z \in \mathcal{B}(H^{-3/2}(\Gamma) \oplus H^{-1/2}(\Gamma), L^2(\mathbb{R}^n)), \quad G_z(\phi \oplus \varphi) = SL_z\phi + DL_z\varphi. \quad (36)$$

In what follows, we set:

$$G := G_1, \quad G(\phi \oplus \varphi) = SL\phi + DL\varphi. \quad (37)$$

With this notation, the adjoint  $(\Delta^\circ)^*$  is rephrased as:

$$\text{dom}((\Delta^\circ)^*) = \{u = u_0 + G(\phi \oplus \varphi), u_0 \in H^2(\mathbb{R}^n), \phi \oplus \varphi \in H^{-3/2}(\Gamma) \oplus H^{-1/2}(\Gamma)\}, \quad (38)$$

$$(\Delta_0)^* = \Delta u_0 + G(\phi \oplus \varphi). \quad (39)$$

We introduce the map:  $M_z = \gamma(G - G_z)$  whose action on  $H^{-3/2}(\Gamma) \oplus H^{-1/2}(\Gamma)$  is explicitly given by:

$$M_z := \begin{pmatrix} \gamma_0(SL - SL_z) & \gamma_0(DL - DL_z) \\ \gamma_1(SL - SL_z) & \gamma_1(DL - DL_z) \end{pmatrix}. \quad (40)$$

From [1, eq. (2.6)], it results that:

$$M_z \in \mathcal{B}(H^{-3/2}(\Gamma) \oplus H^{-1/2}(\Gamma), H^{3/2}(\Gamma) \oplus H^{1/2}(\Gamma)). \quad (41)$$

In what follows,

$$\Pi : H^{3/2}(\Gamma) \oplus H^{1/2}(\Gamma) \rightarrow H^{3/2}(\Gamma) \oplus H^{1/2}(\Gamma), \quad (42)$$

denotes an orthogonal projector on the Hilbert space  $H^{3/2}(\Gamma) \oplus H^{1/2}(\Gamma)$ ,

$$\Pi' : H^{-3/2}(\Gamma) \oplus H^{-1/2}(\Gamma) \rightarrow H^{-3/2}(\Gamma) \oplus H^{-1/2}(\Gamma), \quad (43)$$

is the corresponding dual projector and

$$\Theta : \text{dom}(\Theta) \subseteq \text{ran}(\Pi)' \rightarrow \text{ran}(\Pi), \quad (44)$$

is selfadjoint in the sense of the duality, i.e.:  $\Theta = \Theta'$ . In this framework, the selfadjoint extensions of  $\Delta^\circ$  are parametrized by the couples  $(\Pi, \Theta)$ . In particular, adapting [1, Theorem 2.1 and Lemma 4.9] to the present framework, there follows:

**Theorem 3.1.** *Let  $\Pi : H^{3/2}(\Gamma) \oplus H^{1/2}(\Gamma) \rightarrow H^{3/2}(\Gamma) \oplus H^{1/2}(\Gamma)$  be an orthogonal projector and  $\Theta : \text{dom}(\Theta) \subseteq \text{ran}(\Pi)' \rightarrow \text{ran}(\Pi)$  selfadjoint. Any self-adjoint extension of  $\Delta_0$  is of the kind  $\Delta_{\Pi, \Theta}$ ,*

$$\Delta_{\Pi, \Theta} := \quad (45)$$

$$(\Delta^\circ)^* \upharpoonright \{u = u_0 + SL\phi + DL\varphi, u_0 \in H^2(\mathbb{R}^n), \phi \oplus \varphi \in \text{dom}(\Theta) : \Pi\gamma u_0 = \Theta(\phi \oplus \varphi)\}.$$

The set:

$$Z_{\Pi, \Theta} := \{z \in \mathbb{C} \setminus \mathbb{R}_- : \Theta + \Pi M_z \Pi' \text{ has a bounded inverse}\}, \quad (46)$$

is not void; in particular,  $\mathbb{C} \setminus \mathbb{R} \subseteq Z_{\Pi, \Theta} \subseteq \text{res}(\Delta_{\Pi, \Theta})$  and for any  $z \in Z_{\Pi, \Theta}$  the resolvent of  $\Delta_{\Pi, \Theta}$  is given by the Krěin type formula:

$$(-\Delta_{\Pi, \Theta} + z)^{-1} u = (-\Delta + z)^{-1} u + G_z \Pi' (\Theta + \Pi M_z \Pi')^{-1} \Pi \gamma (-\Delta + z)^{-1} u, \quad (47)$$

where  $G_z$  and  $M_z$  are defined in (36) and (40) respectively.

**Remark 3.2.** Let us notice that the  $\Pi'$  appearing in (47) act as the inclusion map  $\Pi' : \text{ran}(\Pi)' \rightarrow H^{-3/2}(\Gamma) \oplus H^{-1/2}(\Gamma)$ . This means that one does not need to know  $\Pi'$  explicitly: it suffices to know the subspace  $\text{ran}(\Pi') = \text{ran}(\Pi)'$ .

The next result gives information on the spectrum and scattering of  $\Delta_{\Pi, \Theta}$ . For the proof of such results, we refer to [1, Lemma 4.9, Corollary 4.12 and Remark 4.14]. Let us remark that hypothesis (49) below typically holds in the case of global boundary conditions, i.e. assigned on whole boundary  $\Gamma$ , while hypothesis (50) typically holds in the case of local ones, i.e. assigned on an open part  $\Sigma \subset \Gamma$ .

**Theorem 3.3.** 1) *Suppose:*

$$\text{dom}(\Theta) \subseteq H^{s_1}(\Gamma) \oplus H^{s_2}(\Gamma), \quad s_1 > -\frac{3}{2}, \quad s_2 > -\frac{1}{2}. \quad (48)$$

*Then,*

$$\sigma_{\text{ess}}(\Delta_{\Pi, \Theta}) = (-\infty, 0].$$

2) *Suppose either:*

$$\text{dom}(\Theta) \subseteq H^{\frac{1}{2}}(\Gamma) \oplus H^{\frac{3}{2}}(\Gamma), \quad (49)$$

*or*

$$\text{dom}(f_{\tilde{\Theta}}) \subseteq H^{5/2}(\Gamma) \oplus H^{\frac{3}{2}}(\Gamma), \quad (50)$$

*holds, where  $f_{\tilde{\Theta}}$  is sesquilinear form associated to the self-adjoint operator in  $\text{ran}(\Pi)$  defined by  $\tilde{\Theta} := \Theta(\Lambda^3 \oplus \Lambda)$ . Then:*

$$\sigma_{\text{ac}}(\Delta_{\Pi, \Theta}) = (-\infty, 0], \quad (51)$$

*and the wave operators:*

$$W_{\pm} := s\text{-}\lim_{t \rightarrow \pm\infty} e^{-it\Delta_{\Pi, \Theta}} e^{it\Delta}, \quad W_{\pm} := s\text{-}\lim_{t \rightarrow \pm\infty} e^{-it\Delta} e^{it\Delta_{\Pi, \Theta}} P_{\text{ac}}$$

*exist and are complete, i.e. the limits exists everywhere w.r.t. strong convergence,  $\text{ran}(W_{\pm}) = L^2(\mathbb{R}^n)_{\text{ac}}$ ,  $\text{ran}(W_{\pm}) = L^2(\mathbb{R}^n)$  and  $W_{\pm}^* = W_{\pm}$ , where  $L^2(\mathbb{R}^n)_{\text{ac}}$  denotes the absolutely continuous subspace of  $L^2(\mathbb{R}^n)$  with respect to  $\Delta_{\Pi, \Theta}$  and  $P_{\text{ac}}$  is the corresponding orthogonal projector.*

**Remark 3.4.** Let us notice that the apparent discrepancy between the indices in the two conditions (49) and (50) is due to the fact that the first one applies to operators acting between the dual pair  $(\text{ran}(\Pi)', \text{ran}(\Pi))$ , whereas the second one regards sesquilinear forms in the space  $\text{ran}(\Pi)$ . When written in terms of  $\tilde{\Theta}$ , condition (49) reads as  $\text{dom}(\tilde{\Theta}) \subseteq H^{\frac{7}{2}}(\Gamma) \oplus H^{\frac{5}{2}}(\Gamma)$ .

Under hypothesis (49), it is possible to introduce an alternative description of  $\Delta_{\Pi, \Theta}$  (see [1, Corollary 4.8]):

**Corollary 3.5.** *Let  $\Delta_{\Pi, \Theta}$  be defined according to Theorem 3.1 with  $\Theta$  fulfilling (49). Define*

$$B_{\Theta} := \Theta + \Pi\gamma G\Pi' : \text{dom}(\Theta) \subseteq \text{ran}(\Pi') \rightarrow \text{ran}(\Pi). \quad (52)$$

*Then:*

$$\text{dom}(\Delta_{\Pi, \Theta}) = \{u \in H^2(\mathbb{R}^n \setminus \Gamma) : [\gamma]u \in \text{dom}(\Theta), \Pi\gamma u = B_{\Theta}[\gamma]u\}, \quad (53)$$

*where  $[\gamma]u := (-[\gamma_1]u) \oplus ([\gamma_0]u)$ , and*

$$(-\Delta_{\Pi, \Theta} + z)^{-1} - (-\Delta + z)^{-1} = G_z\Pi'(B_{\Theta} - \Pi\gamma G_z\Pi')^{-1}\Pi\gamma(-\Delta + z)^{-1}, \quad z \in Z_{\Pi, \Theta}. \quad (54)$$

#### 4. Dirichlet and Neumann boundary conditions on $\Sigma \subseteq \Gamma$

In this section, we apply our results to self-adjoint adjoint realizations of the Laplacian with Dirichlet and Neumann type boundary conditions on  $\Sigma \subseteq \Gamma$ . For proofs and more details on such realizations, we refer to [1, Sections 5 – 6]. In particular, by the results given there, hypothesis (49) or (50) hold for the models considered here, namely: (49) is satisfied in the case of "global" boundary conditions (i.e. assigned on the whole  $\Gamma$ ), while (50) holds in the case of "local" boundary conditions (i.e. assigned on  $\Sigma \subset \Gamma$ ).

In the following, given  $X \subset \Gamma$  closed, we use the definition:

$$H_X^s(\Gamma) := \{\phi \in H^s(\Gamma) : \text{supp}(\phi) \subseteq X\}. \quad (55)$$

Given  $\Sigma \subset \Gamma$  relatively open with a Lipschitz boundary, we denote by  $\Pi_{\Sigma}$  the orthogonal projector in the Hilbert space  $H^s(\Gamma)$ ,  $s > 0$ , such that  $\text{ran}(\Pi_{\Sigma}) = H_{\Sigma^c}^s(\Gamma)^{\perp}$ . One has  $\text{ran}(\Pi_{\Sigma}^{\perp}) =$

$H_{\Sigma}^{-s}(\Gamma)$ . Moreover, we use the identifications  $H_{\Sigma^c}^s(\Gamma)^\perp \simeq H^s(\Sigma)$  and  $H_{\Sigma}^{-s}(\Gamma) \simeq H^s(\Sigma)'$ . In particular, by the former, the orthogonal projection  $\Pi_\Sigma$  can be identified with the restriction map  $R_\Sigma : H^s(\Gamma) \rightarrow H^s(\Sigma)$ ,  $R_\Sigma \phi := \phi|_\Sigma$ .

#### 4.1. Dirichlet boundary conditions

The self-adjoint extension  $\Delta_D$  corresponding to Dirichlet boundary conditions on the whole  $\Gamma$  is given by the direct sum  $\Delta_D = \Delta_{\Omega_+^D} \oplus \Delta_{\Omega_-^D}$ , where

$$\Delta_{\Omega_\pm^D} := \Delta \upharpoonright \{u \in H^2(\Omega_\pm) : \gamma_0^\pm u = 0\}. \quad (56)$$

Since:

$$\text{dom}(\Delta_{\Omega_+^D}) \oplus \text{dom}(\Delta_{\Omega_-^D}) = \{u \in H^2(\mathbb{R}^n \setminus \Gamma) : [\gamma_0]u = 0, \gamma_0 u = 0\}, \quad (57)$$

with the parametrization introduced in Corollary 3.5, this corresponds to the choice  $\Pi(\phi \oplus \varphi) := \phi \oplus 0$ , and  $B_\Theta = 0$ . Hence, from (31) we get:

$$\Delta_D u = \Delta u - [\gamma_1]u \delta_\Gamma.$$

Moreover, using the identity:  $(\gamma_0 SL_z)^{-1} = P_z^- - P_z^+$ , where  $P_z^\pm$  denote the Dirichlet-to-Neumann operators for  $\Omega_\pm$  respectively (see e.g. [1, equation (5.4)]), one has, for any  $z \in \mathbb{C} \setminus \mathbb{R}_-$ ,

$$(-\Delta_D + z)^{-1} = (-\Delta + z)^{-1} + SL_z(P_z^+ - P_z^-)\gamma_0(-\Delta + z)^{-1}. \quad (58)$$

Now, we turn to Dirichlet boundary conditions supported on a relatively open part  $\Sigma \subset \Gamma$  with Lipschitz boundary. We denote by  $\Delta_{D,\Sigma}$  the self-adjoint extension corresponding to the orthogonal projector defined by  $\Pi(\phi \oplus \varphi) := (\Pi_\Sigma \phi) \oplus 0 \equiv (\phi|_\Sigma) \oplus 0$  and to the self-adjoint operator  $\Theta(\phi \oplus \varphi) := (-\Theta_{D,\Sigma} \phi) \oplus 0$ :

$$\Theta_{D,\Sigma} : \text{dom}(\Theta_{D,\Sigma}) \subseteq H_{\Sigma}^{-3/2}(\Gamma) \rightarrow H^{3/2}(\Sigma), \quad \Theta_{D,\Sigma} \phi := (\gamma_0 SL \phi)|_\Sigma, \quad (59)$$

$$\text{dom}(\Theta_{D,\Sigma}) := \{\phi \in H_{\Sigma}^{-1/2}(\Gamma) : (\gamma_0 SL \phi)|_\Sigma \in H^{3/2}(\Sigma)\}. \quad (60)$$

By Theorem 3.1 and (31), one has:

$$\Delta_{D,\Sigma} u = \Delta u - [\hat{\gamma}_1]u \delta_{\Sigma}, \quad (61)$$

$$\text{dom}(\Delta_{D,\Sigma}) = \{u \in H^1(\mathbb{R}^n) \cap L_\Delta^2(\mathbb{R}^n \setminus \Gamma) : [\hat{\gamma}_1]u \in \text{dom}(\Theta_{D,\Sigma}), (\gamma_0 u)|_\Sigma = 0\}, \quad (62)$$

$$\subseteq \{u \in H^1(\mathbb{R}^n) \cap L_\Delta^2(\mathbb{R}^n \setminus \Gamma) : (\gamma_0^- u)|_\Sigma = (\gamma_0^+ u)|_\Sigma = 0, ([\hat{\gamma}_1]u)|_{\Sigma^c} = 0\} \quad (63)$$

and

$$(-\Delta_{D,\Sigma} + z)^{-1} = (-\Delta + z)^{-1} - SL_z \Pi'_\Sigma (R_\Sigma \gamma_0 SL_z \Pi'_\Sigma)^{-1} R_\Sigma \gamma_0 (-\Delta + z)^{-1}. \quad (64)$$

#### 4.2. Neumann boundary conditions

Let us consider the self-adjoint extension corresponding to Neumann boundary conditions on the whole  $\Gamma$ ; this is given by the direct sum  $\Delta_N = \Delta_{\Omega_+^N} \oplus \Delta_{\Omega_-^N}$ , where:

$$\Delta_{\Omega_\pm^N} := \Delta \upharpoonright \{u \in H^2(\Omega_\pm) : \gamma_1^\pm u = 0\}. \quad (65)$$

Since:

$$\text{dom}(\Delta_{\Omega_+^N}) \oplus \text{dom}(\Delta_{\Omega_-^N}) = \{u \in H^2(\mathbb{R}^n \setminus \Gamma) : [\gamma_1]u = \gamma_1 u = 0\}, \quad (66)$$

with the parametrization introduced in Corollary 3.5, this corresponds to the choice  $\Pi(\phi \oplus \varphi) := 0 \oplus \varphi$ , and  $B_\Theta = 0$ . From (31), it follows that:

$$\Delta_N u = \Delta u - [\gamma_0]u \nu \cdot \nabla \delta_\Gamma,$$

and, denoting with  $Q_z^\pm$  the Neumann-to-Dirichlet operators for  $\Omega_\pm$  respectively, the relation  $(\gamma_1 DL_z)^{-1} = Q_z^+ - Q_z^-$ , (see e.g. [1, equation (5.7)]) yields, for  $z \in \mathbb{C} \setminus \mathbb{R}_-$ ,

$$(-\Delta_N + z)^{-1} = (-\Delta + z)^{-1} + DL_z(Q_z^+ - Q_z^-)\gamma_1(-\Delta + z)^{-1}. \quad (67)$$

Next, we turn to Neumann boundary conditions supported on a relatively open part  $\Sigma \subset \Gamma$  with Lipschitz boundary. We denote by  $\Delta_{N,\Sigma}$  the self-adjoint extension corresponding to the orthogonal projector defined by  $\Pi(\phi \oplus \varphi) := 0 \oplus (\Pi_\Sigma \varphi) \equiv 0 \oplus (\varphi|_\Sigma)$  and to the self-adjoint operator  $\Theta(\phi \oplus \varphi) := 0 \oplus (-\Theta_{N,\Sigma} \varphi)$ :

$$\Theta_{N,\Sigma} : \text{dom}(\Theta_{N,\Sigma}) \subseteq H_{\bar{\Sigma}}^{-1/2}(\Gamma) \rightarrow H^{1/2}(\Sigma), \quad \Theta_{N,\Sigma} \varphi = (\hat{\gamma}_1 DL\varphi)|_\Sigma, \quad (68)$$

$$\text{dom}(\Theta_{N,\Sigma}) := \{\varphi \in H_{\bar{\Sigma}}^{-1/2}(\Gamma) : (\hat{\gamma}_1 DL\varphi)|_\Sigma \in H^{1/2}(\Sigma)\}. \quad (69)$$

By Theorem 3.1 and (31), we have:

$$\Delta_{N,\Sigma} u = \Delta u - [\hat{\gamma}_0] u \nu \cdot \nabla \delta_{\bar{\Sigma}}, \quad (70)$$

$$\text{dom}(\Delta_{N,\Sigma}) = \{u \in H^1(\mathbb{R}^n \setminus \bar{\Sigma}) \cap L_\Delta^2(\mathbb{R}^n \setminus \Gamma) : [\hat{\gamma}_0] u \in \text{dom}(\Theta_{N,\Sigma}), [\hat{\gamma}_1] u = 0, (\hat{\gamma}_1 u)|_\Sigma = 0\} \quad (71)$$

$$\subseteq \{u \in H^1(\mathbb{R}^n \setminus \bar{\Sigma}) \cap L_\Delta^2(\mathbb{R}^n \setminus \Gamma) : (\hat{\gamma}_1^- u)|_\Sigma = (\hat{\gamma}_1^+ u)|_\Sigma = 0, ([\hat{\gamma}_1] u)|_{\bar{\Sigma}^c} = 0\} \quad (72)$$

and

$$(-\Delta_{N,\Sigma} + z)^{-1} = (-\Delta + z)^{-1} - DL_z \Pi'_\Sigma (R_\Sigma \hat{\gamma}_1 DL_z \Pi'_\Sigma)^{-1} R_\Sigma \hat{\gamma}_1 (-\Delta + z)^{-1}. \quad (73)$$

## References

- [1] Mantile A., Posilicano A., Sini M. Self-adjoint elliptic operators with boundary conditions on not closed hypersurfaces. Preprint [arXiv:1505.07236](https://arxiv.org/abs/1505.07236), 2015.
- [2] Posilicano A. A Kr em-like formula for singular perturbations of self-adjoint operators and applications. *J. Funct. Anal.*, 2001, **183**, P. 109–147.
- [3] Posilicano A. Self-adjoint extensions by additive perturbations. *Ann. Sc. Norm. Super. Pisa Cl. Sci.*, 2003, **2(5)**, P. 1–20.
- [4] Posilicano A. Boundary triples and Weyl functions for singular perturbations of self-adjoint operators. *Methods Funct. Anal. Topology*, 2004, **10**, P. 57–63.
- [5] Posilicano A. Self-adjoint extensions of restrictions. *Oper. Matrices*, 2008, **2**, P. 483–506.
- [6] Albeverio S., Brasche J., R ockner M. Dirichlet forms and generalized Schr odinger operators. In: *Schr odinger operators*, Lecture Notes in Phys., **345**, P. 1–42, Springer, Berlin, 1989.
- [7] Albeverio S., Fenstad J.E., et al. Perturbations of the Laplacian supported by null sets, with applications to polymer measures and quantum fields. *Phys. Lett. A*, 1984, **104**, P. 396–400.
- [8] Albeverio S., Fenstad J.E., et al. Schr odinger operators with potentials supported by null sets, in *Ideas and Methods in Mathematical Analysis* (Albeverio S., Fenstad J.R., Holden H., and Lindstr om T. m, Eds.), Vol. II, Cambridge Univ. Press, New York/Cambridge, MA, 1991.
- [9] Antoine J.-P., Gesztesy F., Shabani J. Exactly solvable models of sphere interactions in quantum mechanics. *J. Phys. A*, 1987, **20**, P. 3687–3712.
- [10] Behrndt J., Exner P., Lotoreichik V. Schr odinger operators with  $\delta$ -interactions supported on conical surfaces. *J. Phys. A*, 2014, **47(35)**, 355202, 16 pp.
- [11] Behrndt J., Exner P., Lotoreichik V. Schr odinger operators with  $\delta$ - and  $\delta'$ -interactions on Lipschitz surfaces and chromatic numbers of associated partitions. *Rev. Math. Phys.*, 2014, **26**, 1450015, 43 pp.
- [12] Behrndt J., Grubb G., Langer M., Lotoreichik V. Spectral asymptotics for resolvent differences of elliptic operators with  $\delta$  and  $\delta'$ -interactions on hypersurfaces. *J. Spectr. Theory*, 2015, **5**, P. 697–729.
- [13] Behrndt J., Langer M., Lotoreichik V. Spectral Estimates for Resolvent Differences of Self-Adjoint Elliptic Operators. *Integr. Equ. Oper. Theory*, 2013, **77**, P. 1–37.
- [14] Behrndt J., Langer M., Lotoreichik V. Schr odinger operators with  $\delta$ - and  $\delta'$ -potentials supported on hypersurfaces. *Ann. Henri Poincar e*, 2013, **14**, P. 385–423.
- [15] Exner P. Spectral properties of Schr odinger operators with a strongly attractive  $\delta$  interaction supported by a surface. In: *Proc. NSF Summer Research Conference (Mt. Holyoke 2002)*, Contemp. Math., Amer. Math. Providence, R.I., 2003.
- [16] Exner P. Leaky quantum graphs: a review. *Proc. Symp. Pure Math.*, 2008, **77**, P. 523–564.
- [17] Exner P., Praas M. On geometric perturbations of critical Schr odinger operators with a surface interaction. *J. Math. Phys.*, 2009, **50**, 112101.

- [18] Exner P., Ichinose I. Geometrically induced spectrum in curved leaky wires. *J. Phys. A*, 2001, **34**, P. 1439–1450.
- [19] Exner P., Kondej S. Curvature-induced bound states for a  $\delta$  interaction supported by a curve in  $\mathbb{R}^3$ . *Ann. Henri Poincaré*, 2002, **3**, P. 967–981.
- [20] Exner P., Kondej S. Bound states due to a strong  $\delta$  interaction supported by a curved surface. *J. Phys. A*, 2003, **36**, P. 443–457.
- [21] Exner P., Kondej S. Scattering by local deformations of a straight leaky wire. *J. Phys. A*, 2005, **38**, P. 4865–4874.
- [22] Exner P., Pankrashkin K. Strong coupling asymptotics for a singular Schrödinger operator with an interaction supported by an open arc. *Comm. Partial Diff. Eq.*, 2014, **39**, P. 193–212.
- [23] Exner P., Yoshitomi K. Band gap of the Schrödinger operator with a strong  $\delta$ -interaction on a periodic curve. *Ann. Henri Poincaré*, 2001, **2**, P. 1139–1158.
- [24] Figari R., Teta A. Effective potential and fluctuations for a boundary value problem on a randomly perforated domain. *Lett. Math. Phys.*, 1992, **26**, P. 295–305.
- [25] Figari R., Teta A. A boundary value problem of mixed type on perforated domains. *Asymptotic Anal.*, 1993, **6**, P. 271–284.
- [26] Lions J.-L., Magenes E. *Non-homogeneous Boundary Value Problems and Applications*. Springer, New-York, 1972.
- [27] McLean W. *Strongly elliptic systems and boundary integral equations*. Cambridge University Press, Cambridge, 2000.
- [28] Dias N.C., Posilicano A., Prata J.N. Self-adjoint, globally defined Hamiltonian operators for systems with boundaries. *Commun. Pure Appl. Anal.*, 2011, **10**, P. 1687–1706.

## Steady Stokes flow between confocal semi-ellipses

I. V. Makeev, I. Yu. Popov

ITMO University, Kronverkskiy, 49, St. Petersburg, 197101, Russia

popov1955@gmail.com

**PACS** 68.90.+g, 05.60.-k, 62.10.+s

**DOI** 10.17586/2220-8054-2016-7-2-324-331

Analytical solutions for the Stokes equations in a cavity bounded by two confocal semi-ellipses and two line segments are derived here. The exact solution for the stream function, in the form of a Fourier series, is obtained. Eddy structure is described for different boundary conditions.

**Keywords:** Stokes flow, biharmonic equation.

*Received:* 22 January 2016

### 1. Introduction

Micro- and nanoflows are new fields of nanotechnology. Flow through nanostructures is known to have many interesting unusual peculiarities [1]. Particularly, one observes a phenomenon analogous to superfluidity [2], the dependence of viscosity on the nanotube's diameter [3] and other such effects. The theory of nanoflow is not well-developed. There are only a few works suggesting theoretical explanations for these phenomena (see, e.g., [4–6]). It has been shown that hydrodynamic equations should be modified for nanoflows [7], but the Stokes approximation is appropriate due to the smallness of the Reynolds number [8].

The most interesting question is about the eddy structure for nanoflow. The information about it can be used for several nanophysical and nanochemical applications. Particularly, it was shown experimentally that there is a separation of a fluid's components in nanochannels [9]. Among other reasons, it is related with the existence of eddies. One observes component separation within an eddy due to differences in the components' densities. As a result, this property opens the way for the creation of a chemical nanoreactor. Namely, due to component separation, the reagents needed for some chemical reaction are collected within some local domain inside the eddy. Correspondingly, one has strong localization of the chemical reaction in this domain only. We have the opportunity to use this phenomenon, only if we can predict the eddy structure for different system parameters. Particularly, if the flow is induced by the boundary condition, we require information about the dependence of the eddy structure on the boundary conditions.

One can mention that similar processes take place in non-autonomous phases [10]. It is interesting to note that the analogous mathematical problem also present in geophysics [11].

Stokes flows in various domains were studied by analytical methods in many papers. There are a number of works describing the flow over a rectangular cavity [12–18]. The solutions for the Stokes equations for the annular cavities were investigated in [19–25]. Stokes flow in regions partially bounded by segments of ellipses was considered in [26,27]. Corner eddies in the Stokes flow problems were studied in [28–30].

In the present paper, we describe the Stokes flow in a horseshoe domain formed by two semi-ellipses and two segments (Fig. 1). The flow is induced by inhomogeneous boundary conditions. We investigate the eddy structure for different boundary conditions. Although the

investigation was inspired by the nanoflows problem, the result concerns the classical Stokes flow problem.

### 2. Problem formulation and solution

Let us consider Stokes flow in a cavity bounded by two confocal semi-ellipses,  $S_1$  and  $S_2$  and two line segments,  $AB$  and  $CD$  (Fig. 1). Flow in the cavity is induced by the velocities  $V_{top}$  and  $V_{bot}$  at  $S_1$  and  $S_2$  respectively. On segments  $AB$  and  $CD$ , we assume free-slip conditions.

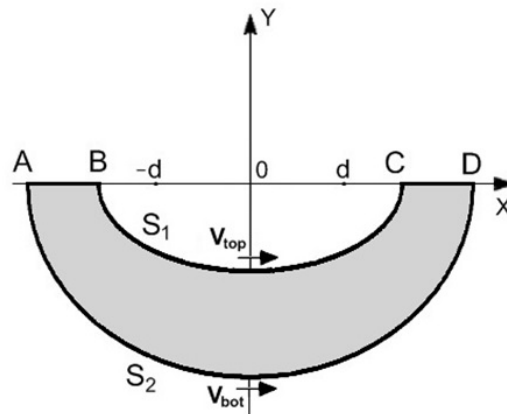


FIG. 1. The domain in the Cartesian coordinates.  $(-d, 0), (d, 0)$  are the ellipse foci

In the 2D case, the Stokes equations can be reduced to the biharmonic equation for the stream function  $\Psi$ :

$$\Delta^2 \Psi = 0. \tag{1}$$

We make the transformation of the cavity to the elliptic coordinates system:

$$x = d \cos(\xi_2) \cosh(\xi_1), \quad y = d \sin(\xi_2) \sinh(\xi_1).$$

The Laplace operator takes the form:

$$\Delta = \frac{1}{d^2 (\cosh^2(\xi_1) - \cos^2(\xi_2))} \left( \frac{\partial^2}{\partial \xi_1^2} + \frac{\partial^2}{\partial \xi_2^2} \right).$$

Our domain transforms to a rectangle on Fig. 2. Semi-ellipses  $S_1, S_2$  in elliptic coordinate system will convert to segments  $\xi_1 = \xi_{01}, \xi_1 = \xi_{02}, \pi \leq \xi_2 \leq 2\pi$ .

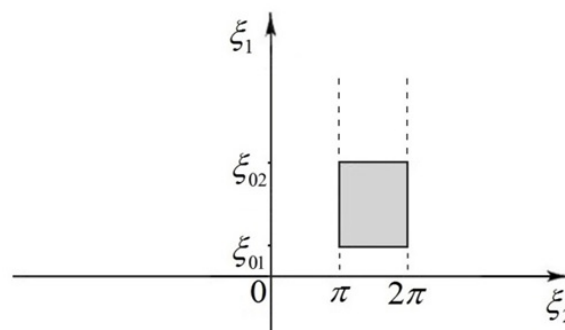


FIG. 2. The domain in elliptic coordinates

Let us consider the following chain of equations:

$$\Delta\Psi = \Psi_1, \quad (2)$$

$$\Delta\Psi_1 = 0. \quad (3)$$

The boundary conditions for stream function are:

$$\Psi(\xi_1, 0) = 0, \quad \Psi(\xi_1, \pi) = 0, \quad \xi_{01} \leq \xi_1 \leq \xi_{02}; \quad (4)$$

$$\Psi(\xi_{01}, \xi_2) = 0, \quad \Psi(\xi_{02}, \xi_2) = 0, \quad \pi \leq \xi_2 \leq 2\pi; \quad (5)$$

$$\frac{\partial^2\Psi}{\partial\xi_2^2}\Big|_{\xi_2=\pi} = 0, \quad \frac{\partial^2\Psi}{\partial\xi_2^2}\Big|_{\xi_2=2\pi} = 0, \quad \xi_{01} \leq \xi_1 \leq \xi_{02}; \quad (6)$$

$$\frac{1}{h}\frac{\partial\Psi}{\partial\xi_1}(\xi_{01}, \xi_2) = V_{S_1}(\xi_2), \quad \frac{1}{h}\frac{\partial\Psi}{\partial\xi_1}(\xi_{02}, \xi_2) = V_{S_2}(\xi_2), \quad \pi \leq \xi_2 \leq 2\pi. \quad (7)$$

Lame coefficients are:  $h_{\xi_1} = h_{\xi_2} = h = d\sqrt{\cosh^2(\xi_1) - \cos^2(\xi_2)}$ .

The function  $\Psi_1(\xi_1, \xi_2)$  in (3) can be found by standard separation of variables (for calculations we take  $m$  terms):

$$\Psi_1 = \sum_{k=1}^m (c_{1k}e^{k\xi_1} + c_{2k}e^{-k\xi_1}) \sin(k\xi_2). \quad (8)$$

We derive a solution of Eq. (2) in the form of the Fourier series:

$$\Psi(\xi_1, \xi_2) = \sum_{k=1}^n \Psi_{1k}(\xi_1) \sin(k\xi_2), \quad \pi \leq \xi_2 \leq 2\pi \quad (9)$$

$$\begin{aligned} \Psi_{11}(\xi_1) = & a_{31}e^{\xi_1} + a_{41}e^{-\xi_1} + \frac{1}{8}(a_{11} + a_{21})\xi_1 e^{\xi_1} - \frac{1}{8}(a_{11} + a_{21})\xi_1 e^{-\xi_1} \\ & + \frac{1}{32}(a_{11} - a_{13})e^{3\xi_1} + \frac{1}{32}(a_{21} - a_{23})e^{-3\xi_1} \end{aligned}$$

$$\begin{aligned} \Psi_{1k}(\xi_1) = & a_{3k}e^{k\xi_1} + a_{4k}e^{-k\xi_1} + \frac{1}{16(1-k)}(a_{1,k} - a_{1,k-2})e^{(k-2)\xi_1} + \frac{1}{16(1+k)}(a_{1,k} - a_{1,k+2})e^{(k+2)\xi_1} \\ & + \frac{1}{16(1-k)}(a_{2,k} - a_{2,k-2})e^{-(k-2)\xi_1} + \frac{1}{16(1+k)}(a_{2,k} - a_{2,k+2})e^{-(k+2)\xi_1}, \quad k \geq 2. \end{aligned}$$

Formula (9) is a general solution of equation (1). Each function  $\Psi_{1k}(\xi_1)$  depends on the coefficients from sets  $a_1, a_2, a_3, a_4$ . Here,  $a_1 = a_{11} \dots a_{1(n-2)}$ ,  $a_2 = a_{21} \dots a_{2(n-2)}$ ,  $a_3 = a_{31} \dots a_{3n}$ ,  $a_4 = a_{41} \dots a_{4n}$ . We then need to find coefficients  $a_1, a_2, a_3, a_4$  to satisfy the boundary conditions for the stream function. Conditions (4),(6) are satisfied for arbitrary values of the coefficients  $a_1, a_2, a_3, a_4$ .

We now denote  $\Psi_{1k}(a_1, a_2, a_3, a_4)$  by  $\Psi_{1k}(\xi_1)$ . Condition (5) leads to the algebraic relations between coefficients:

$$\begin{aligned} \Psi_{1k}(a_1, a_2, a_3, a_4)\Big|_{\xi_1=\xi_{01}} &= 0, \\ \Psi_{1k}(a_1, a_2, a_3, a_4)\Big|_{\xi_1=\xi_{02}} &= 0, \quad k = 1 \dots n. \end{aligned} \quad (10)$$

The first condition in (7) takes the form:

$$\sum_{k=1}^n \frac{\partial}{\partial\xi_1} \Psi_{1k} \sin(k\xi_2)\Big|_{\xi_1=\xi_{01}} = V_{top}(\xi_2) d\sqrt{\cosh^2(\xi_{01}) - \cos^2(\xi_2)}.$$

Let us consider the function in the right hand side as a Fourier series:

$$\sum_{k=1}^n \frac{\partial}{\partial \xi_1} \Psi_{1k} \sin(k\xi_2) |_{\xi_1=\xi_{01}} = \sum_{k=1}^n C_{k1} \sin(k\xi_2), \tag{11}$$

where

$$C_{k1} = e^{-k\xi_{01}} \frac{-1}{k\pi} d \int_0^\pi V_{top}(\xi_2) \sqrt{\cosh^2(\xi_{01}) - \cos^2(\xi_2)} \sin(k\xi_2) d\xi_2.$$

The coefficients  $C_{k1}$  can easily be found numerically. The means of calculating  $C_{k2}$  for the second condition in (7) is analogous. Thus, condition (7) can be represented as an algebraic relation between coefficients:

$$\frac{\partial}{\partial \xi_1} \Psi_{1k}(a_{1k}, a_{2k}, a_{3k}, a_{4k}) |_{\xi_1=\xi_{01}} = C_{k1}, \quad k = 1 \dots n; \tag{12}$$

$$\frac{\partial}{\partial \xi_1} \Psi_{1k}(a_{1k}, a_{2k}, a_{3k}, a_{4k}) |_{\xi_1=\xi_{02}} = C_{k2}, \quad k = 1 \dots n. \tag{13}$$

As a result, coefficients  $a_1, a_2, a_3, a_4$  are the solutions for a system of linear equations. This system includes the sets of equations (10) and some equations from the sets (12), (13).

### 3. Discussion

The expression for stream function (9) has been completely defined above. If we fix ellipse half axes and vary the velocity of the moving part of the boundary, we can obtain different pictures of the flow. The following figures shows fluid streamlines for different velocity functions at  $S_1$  and  $S_2$ .

For all the examples described below, the ellipse half axes are  $a = 0.4; b = 0.12$  for  $S_1$  and  $a = 0.86; b = 0.76$  for  $S_2$ .

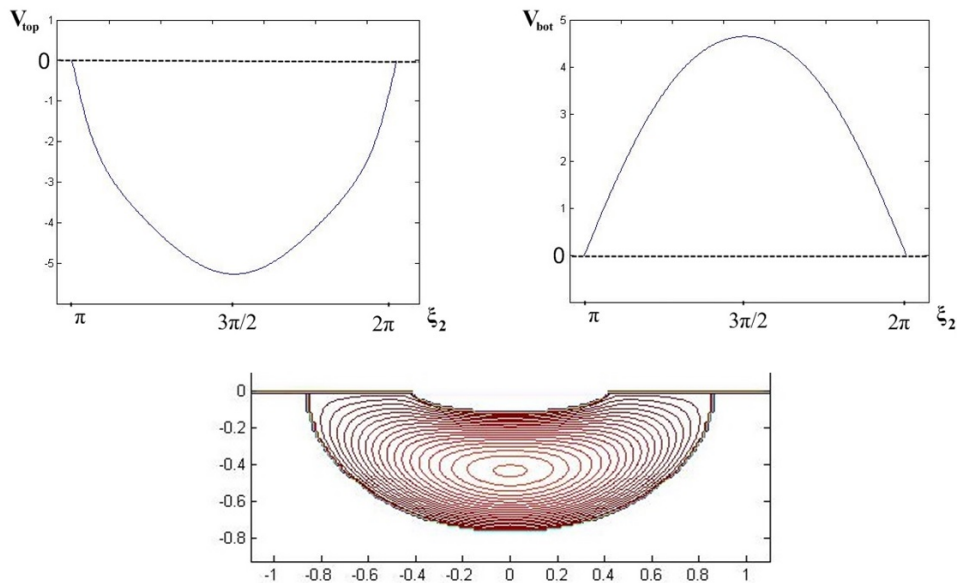


FIG. 3. Velocities on  $S_1$  and  $S_2$  have opposite directions. Functions  $V_{top}(\xi_2)$  and  $V_{bot}(\xi_2)$  do not change sign. We have no separation points at the boundary. The whole domain is a single vortex region

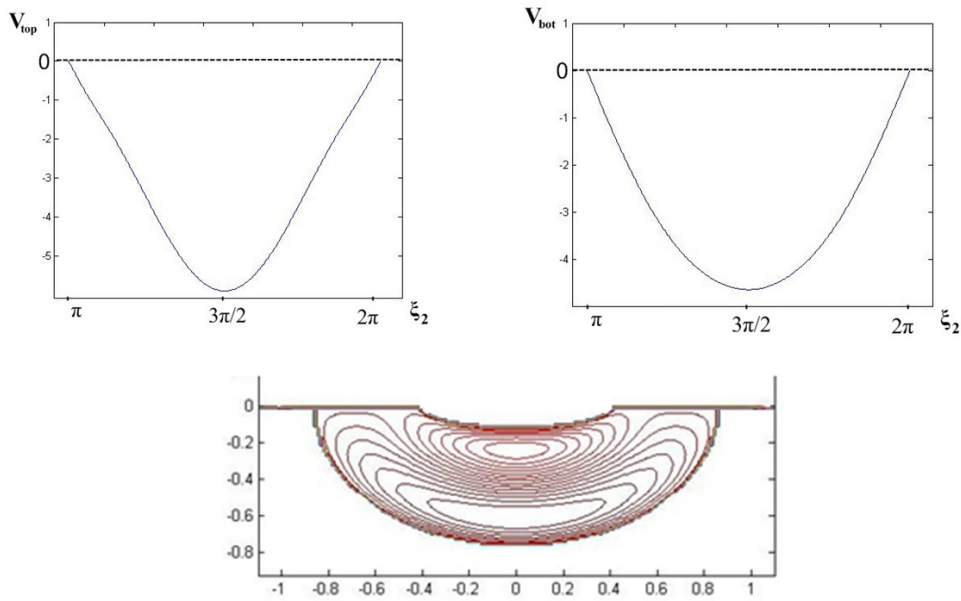


FIG. 4. Functions  $V_{S_1}(\xi_2)$  and  $V_{S_2}(\xi_2)$  do not change sign. We have no separation points at  $S_1$  and  $S_2$ . Velocities on  $S_1$  and  $S_2$  are in the same direction. We obtain separation points at segments  $AB$  and  $CD$ . The domain is divided into two subdomains. On the centerline ( $x = 0$ ), we obtain two stagnation points (at these points the fluid is totally stationary), we compare that with [20]

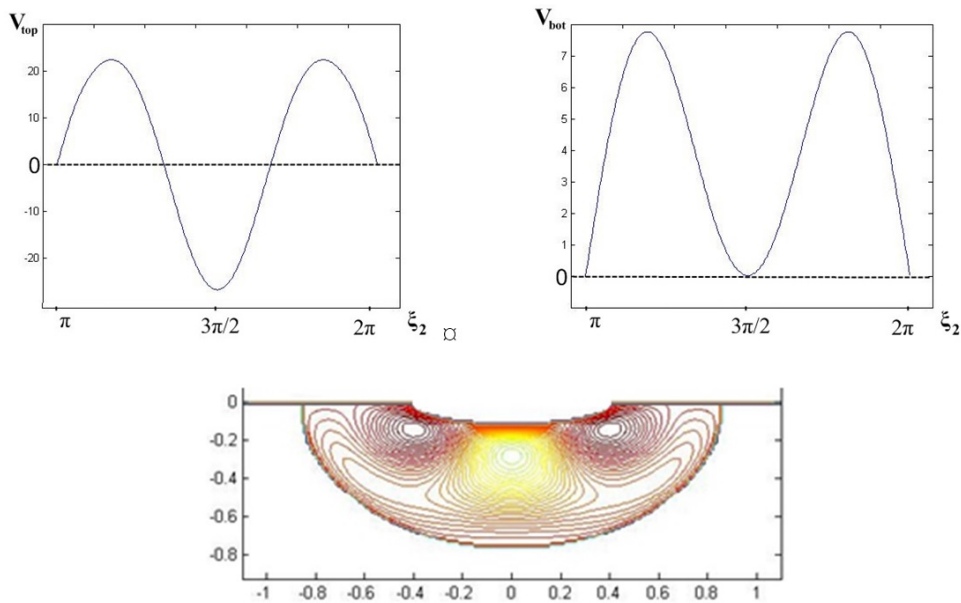


FIG. 5. Function  $V_{S_1}(\xi_2)$  changes its sign. We obtain two separation points at  $S_1$ . Function  $V_{S_2}(\xi_2)$  doesn't change its sign. We have no separation points at  $S_2$ . The velocities at the corners of  $S_1$  and  $S_2$  are in the same direction. We obtain a single separation point for each segment,  $AB$  and  $CD$

**4. Numerical analysis**

We construct the solution of Eq.(1) by a finite-difference method. The discrete expression for the biharmonic equation, using forward finite difference method, has the form:

$$20\Psi_0 - 8(\Psi_1 + \Psi_2 + \Psi_3 + \Psi_4) + \Psi_5 + \Psi_7 + \Psi_9 + \Psi_{11} + 2(\Psi_6 + \Psi_8 + \Psi_{10} + \Psi_{12}) = 0.$$

The stencil for the finite difference scheme is shown in Fig. 6. The node with number 0 corresponds to a stream function node for which the biharmonic equation is formulated.

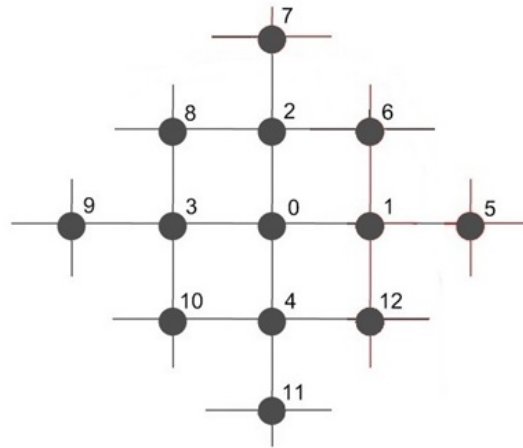


FIG. 6. Stencil nodes numbering

We calculate the relative errors with  $L_1$  norm and estimate the quality of numerical solution. The dependence of the relative error  $E$  via the grid step  $d$  for Fig. 4 is shown in Fig. 7. The positive slope confirms the convergence of the algorithm.

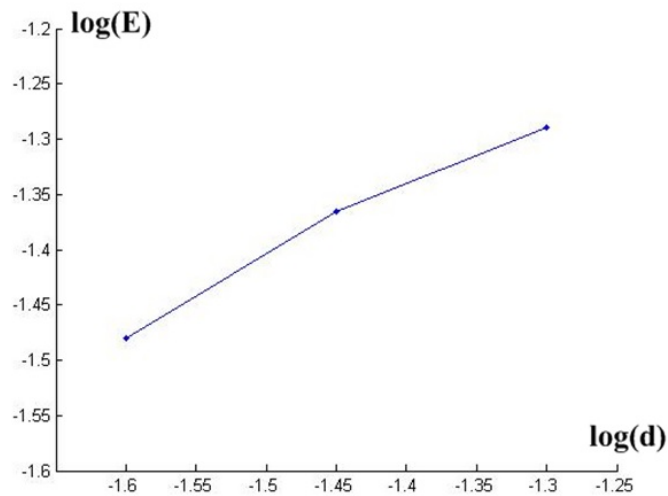


FIG. 7. Error norm via the grid resolution (logarithmic scale)

## 5. Conclusion

We obtained exact solutions for the biharmonic equation for the stream function of the Stokes flow. We fixed the geometrical parameters of the domain and varied the boundary conditions. Doing so allowed us to change the flow structure drastically. This could open up opportunities for controlling flow structure by external actions.

## Acknowledgements

This work was partially financially supported by the Government of the Russian Federation (grant 074-U01), by Ministry of Science and Education of the Russian Federation (GOSZADANIE 2014/190, Projects No 14.Z50.31.0031 and No. 1.754.2014/K), by grant MK-5001.2015.1 of the President of the Russian Federation, by grant 16-11-10330 of Russian Science Foundation.

## References

- [1] Li D. *Encyclopedia of Microfluidics and Nanofluidics*, 2008 Springer, New York.
- [2] Rivera J. L. and Starr F. W., Rapid transport of water via carbon nanotube. *J. Phys. Chem. C*, 2010, **114**, P. 3737–3742.
- [3] Kang W. and Landman U., Universality crossover of the pinch-off shape profiles of collapsing liquid nanobridges. *Phys. Rev. Lett.*, 2007, **98**, P. 064504/1–4.
- [4] Chivilikhin S.A., Popov I.Yu., Gusarov V.V., and Svitenkov A.I., Model of fluid flow in a nano-channel. *Russian J. Math. Phys.*, 2007, **15**, P. 410–412.
- [5] Maslov V.P. Superfluidity of classical liquid in a nanotube for even and odd numbers of neutrons in a molecule. *Theor. Math. Phys.*, 2007, **153**, P. 1677–1696.
- [6] Belonenko M.B., Chivilikhin S.A., Gusarov V.V., Popov I.Yu., and Rodygina O.A. Soliton-induced flow in carbon nanotube. *Europhys. Lett.*, 2013, **101**, P. 66001/1–3.
- [7] Popov I.Yu. Statistical derivation of modified hydrodynamic equations for nanotube flows. 2011, *Physica Scripta*, **83**, P. 045601/1–3.
- [8] Chivilikhin S.A., Gusarov V.V., Popov I.Yu. Flows in nanostructures: hybrid classical-quantum models. *Nanosystems: Phys. Chem. Math.*, 2012, **3**(1), P. 7–26.
- [9] Kononova S.V., Korytkova E.N., Romashkova K.A., Kuznetsov Yu.P., Gofman I.V., Svetlichnyi V.M., Gusarov V.V. Nanocomposite on the basis of amide imide resin with hydrosilycate nanoparticles of different morphology. *J. Appl. Chem.*, 2007, **80**(12), P. 2064–2070.
- [10] Gusarov V.V. and Popov I.Yu. Flows in two-dimensional non-autonomous phases in polycrystalline system. *Nuovo Cimento D*, 1996, **18**(7), P. 799–805.
- [11] Ismail-Zadeh A. and Tackley P., *Computational Methods for Geodynamics*, 2010, Cambridge University Press, Cambridge.
- [12] Gürçan F. Streamline Topologies in Stokes Flow Within Lid-Driven Cavities. *Theoretical and Computational Fluid Dynamics*, 2003, **17**(1), P. 19–30.
- [13] Gürçan F., Gaskell P.H., Savage M.D., and Wilson M.C.T. Eddy genesis and transformation of Stokes flow in a double-lid driven cavity. *J. of Mechanical Engineering Science*, 2003, **217**, P. 353–363.
- [14] Shankar P.N. The eddy structure in Stokes flow in a cavity. *J. Fluid Mechanics*, 1993, **250**, P. 371–383.
- [15] Meleshko V.V. Steady Stokes flow in a rectangular cavity. *Proc. R. Soc. Lond*, 1996, **A. 452**, P. 1999–2022.
- [16] van der Woude D., Clercx H.J.H., van Heijst G.J.F., and Meleshko V.V. Stokes flow in a rectangular cavity by rotlet forcing. *Phys. Fluids*, 2007, **19**(8), P. 083602.
- [17] Popov I.Yu. Operator extensions theory and eddies in creeping flow. *Phys. Scr.*, 1993, **47**, P. 682–686.
- [18] Popov I.Yu. Stokeslet and the operator extensions theory. *Rev. Mat. Univ., Compl. Madrid*, 1996, **9**(1), P. 235–258.
- [19] Sturges L. D. Stokes flow in a two-dimensional cavity with moving end walls. *Phys. Fluids*, 1986, **29**(5), P. 1731–1734.
- [20] Krasnopolskaya N.S., Meleshko V.V., Peters G.W.M., Meijer H.E.Y., Steady Stokes flow in an annular cavity, *Q. J. Mech. Appl. Math.*, 1996, **49**(4), P. 593–619.
- [21] Hackborn W. W. An analysis of a Stokes flow in an annular region. *Canadian Applied Mathematics Quarterly*, 2000, **8**, P. 171–183.

- [22] Murad A, Sen. Stokes Flow between Two Cylinders. *Journal of Bangladesh Academy of Sciences*, 2012, **36**(1), P. 123–135.
- [23] Gaskell P.H., Savage M.D., and Wilson M. Stokes flow in a half-filled annulus between rotating coaxial cylinders. *J. Fluid Mechanics*, 1997, **337**, P. 263–282.
- [24] Blinova I.V. Model of non-axisymmetric flow in nanotube. *Nanosystems: Phys. Chem. Math.*, 2013, **4**(3), P. 320–323.
- [25] Gugel Yu.V., Popov I.Yu., and Popova S.L. Hydrotron: creep and slip. *Fluid Dyn. Res.*, 1996, **18**, P. 199–210.
- [26] Saadjan E., Midoux N., and André. On the solution of Stokes' equations between confocal ellipses. *Phys. Fluids*, 1994, **6**, P. 3833.
- [27] Popov I.Yu., and Makeev I.V. A benchmark solution for 2-D Stokes flow over cavity. *Z. Angew. Math. Phys.*, 2014, **65**, P. 339–348.
- [28] Moffatt H.K. Viscous and resistive eddies near a sharp corner, *J. Fluid Mech.*, 1964, **18**, P. 1–18.
- [29] Moffatt H.K. Viscous eddies near a sharp corner. *Arch. Mech. Stosowanej*, 1964, **16**, P. 365–372.
- [30] Blinova I.V., Kyz'yurova K.N., and Popov I.Yu. Stokes flow driven by a Stokeslet in a cone. *Acta Mechanica*, 2014, **225**, P. 3115–3121.
- [31] Gerya T. *Introduction to Numerical Geodynamic Modelling*, 2010, Cambridge University Press, Cambridge.

## Dirac operator coupled to bosons

A. A. Boitsev<sup>1</sup>, H. Neidhardt<sup>2</sup>, I. Y. Popov<sup>1</sup>

<sup>1</sup>ITMO University, Kronverkskiy, 49, St. Petersburg, 197101, Russia

<sup>2</sup>Weierstrass Institute for Applied Analysis and Stochastics,  
Mohrenstr. 39, D-10117, Berlin, Germany

boitsevanton@gmail.com, hagen.neidhardt@wias-berlin.de, popov1955@gmail.com

**PACS 02.30.Tb**

**DOI 10.17586/2220-8054-2016-7-2-332-339**

We consider a model of point-like interaction between electrons and bosons in a cavity. The electrons are relativistic and are described by a Dirac operator on a bounded interval while the bosons are treated by second quantization. The model fits into the extension theory of symmetric operators. Our main technical tool to handle the model is the so-called boundary triplet approach to extensions of symmetric operators. The approach allows explicit computation of the Weyl function.

**Keywords:** Dirac operator, bosons, operator extension, boundary triplet, second quantization.

*Received: 13 January 2016*

### 1. Introduction

The problem of electro-magnetic field's influence on an electron's spectral and transport properties has attracted great interest from physicists due to its importance both from fundamental and engineering viewpoints (see, e.g., [1] and references therein). It is important to find solvable models to describe this phenomenon. We present a simple model in the framework of extension theory of symmetric operators. The electro-magnetic field can be described classically or it can be quantized. Using a classical description, such a model was proposed in [2]. The case of quantized electro-magnetic field is more complicated. As an example of this type of model, we can mention [3], [4]. In the present paper, we suggest a model of point-like interaction between a relativistic fermion (the Dirac operator) and bosons (infinite matrix operator in the Fock space). We use the boundary triplet approach to describe extensions of symmetric operators (see, e.g., [8–13, 15]).

In the following, we consider a particular example of point interaction for a quantum system  $\{\mathfrak{D}, D_0\}$  with a quantum reservoir  $\{\mathfrak{T}, T\}$ , where  $D_0$  denotes the self-adjoint Dirac operator defined in the Hilbert space  $\mathfrak{D} = L^2(\Delta, \mathbb{C}^2)$ , where  $\Delta = (a; b)$ , and  $T$  is the so-called boson operator defined in the Hilbert space  $\mathfrak{T} = l_2(\mathbb{N}_0)$ . Before introducing the operators, let us slightly specify the approach.

At first, we consider a system consisting of a quantum system  $\{\mathfrak{D}, D_0\}$  and a quantum reservoir  $\{\mathfrak{T}, T\}$ . This system's composed Hamiltonian is given by the self-adjoint operator:

$$L_0 := D_0 \otimes I_{\mathfrak{T}} + I_{\mathfrak{D}} \otimes T,$$

which acts in  $\mathfrak{L} := \mathfrak{D} \otimes \mathfrak{T}$ . In order to describe the interaction, we restrict the operator  $D_0$  to a densely defined closed symmetric operator  $D$  and consider the densely defined symmetric operator:

$$L := D \otimes I_{\mathfrak{T}} + I_{\mathfrak{D}} \otimes T, \tag{1.1}$$

with  $\text{dom}(L) = \text{dom}(D) \otimes \text{dom}(T)$ , where:

$$(Df)(x) := -ic \frac{d}{dx} \otimes \sigma_1 f(x) + \frac{c^2}{2} \otimes \sigma_3 f(x), \quad x \in \Delta, \quad (1.2)$$

$$f \in \text{dom}(D) := W_0^{1,2}(\Delta, \mathbb{C}^2) := \{f \in W^{1,2}(\Delta, \mathbb{C}^2) : f(a) = f(b) = 0\}.$$

Here,

$$\sigma_1 := \begin{pmatrix} 0 & 1 \\ 1 & 0 \end{pmatrix} \quad \text{and} \quad \sigma_3 := \begin{pmatrix} 1 & 0 \\ 0 & -1 \end{pmatrix}.$$

$T$  denotes a boson operator in the Hilbert space  $\mathfrak{H} = l_2(\mathbb{N}_0)$  such that:

$$T\vec{\xi} = T\{\xi_k\}_{k \in \mathbb{N}_0} = \{k\xi_k\}_{k \in \mathbb{N}_0}, \quad (1.3)$$

$$\vec{\xi} = \{\xi_k\}_{k \in \mathbb{N}_0} \in \text{dom}(T) := \{\{\xi_k\}_{k \in \mathbb{N}_0} \in l_2(\mathbb{N}_0) : \{k\xi_k\}_{k \in \mathbb{N}_0} \in l_2(\mathbb{N}_0)\}.$$

To construct self-adjoint extensions we use the boundary triplet approach. Notice that there are extensions which do not correspond to any interaction between both subsystems. From the physical point of view it is very important to obtain those extensions which realistically describe point interactions.

## 2. Preliminaries

### 2.1. Linear relations

A linear relation  $\Theta$  in  $\mathcal{H}$  is a closed linear subspace of  $\mathcal{H} \oplus \mathcal{H}$ . The set of all linear relations in  $\mathcal{H}$  is denoted by  $\tilde{\mathcal{C}}(\mathcal{H})$ . We also denote by  $\mathcal{C}(\mathcal{H})$  the set of all closed linear (not necessarily densely defined) operators in  $\mathcal{H}$ . Identifying each operator  $T \in \mathcal{C}(\mathcal{H})$  with its graph  $\text{gr}(T)$ , we regard  $\mathcal{C}(\mathcal{H})$  as a subset of  $\tilde{\mathcal{C}}(\mathcal{H})$ .

The role of the set  $\tilde{\mathcal{C}}(\mathcal{H})$  in extension theory becomes apparent from Proposition 2.3. However, its role in the operator theory is substantially motivated by the following circumstances: in contrast to  $\mathcal{C}(\mathcal{H})$ , the set  $\tilde{\mathcal{C}}(\mathcal{H})$  is closed with respect to taking inverse and adjoint relations  $\Theta^{-1}$  and  $\Theta^*$ , respectively. The latter is given by:  $\Theta^{-1} = \{\{g, f\} : \{f, g\} \in \Theta\}$  and

$$\Theta^* = \left\{ \begin{pmatrix} k \\ k' \end{pmatrix} : (h', k) = (h, k') \text{ for all } \begin{pmatrix} h \\ h' \end{pmatrix} \in \Theta \right\}.$$

A linear relation  $\Theta$  is called symmetric if  $\Theta \subset \Theta^*$  and self-adjoint if  $\Theta = \Theta^*$ .

### 2.2. Boundary triplets and proper extensions

Let us briefly recall some basic facts regarding boundary triplets. Let  $A$  be a densely defined closed symmetric operator with equal deficiency indices  $n_{\pm}(A) := \dim(\mathfrak{N}_{\pm i})$ ,  $\mathfrak{N}_z := \ker(A^* - z)$ ,  $z \in \mathbb{C}_{\pm}$ , acting on some separable Hilbert space  $\mathfrak{H}$ .

#### Definition 2.1.

- (i)  $A$  closed extension  $\tilde{A}$  of  $A$  is called proper if  $\text{dom}(A) \subset \text{dom}(\tilde{A}) \subset \text{dom}(A^*)$ .
- (ii) Two proper extensions  $\tilde{A}'$ ,  $\tilde{A}$  are called disjoint if  $\text{dom}(\tilde{A}') \cap \text{dom}(\tilde{A}) = \text{dom}(A)$  and transversal if in addition  $\text{dom}(\tilde{A}') + \text{dom}(\tilde{A}) = \text{dom}(A^*)$ .

We denote by  $\text{Ext}_A$  the set of all proper extensions of  $A$  completed by the non-proper extensions  $A$  and  $A^*$ . For instance, any self-adjoint or maximally dissipative (accumulative) extension is proper.

**Definition 2.2** ([11]). A triplet  $\Pi = \{\mathcal{H}, \Gamma_0, \Gamma_1\}$ , where  $\mathcal{H}$  is an auxiliary Hilbert space and  $\Gamma_0, \Gamma_1 : \text{dom}(A^*) \rightarrow \mathcal{H}$  are linear mappings, is called a boundary triplet for  $A^*$  if the “abstract Green’s identity”,

$$(A^*f, g) - (f, A^*g) = (\Gamma_1f, \Gamma_0g) - (\Gamma_0f, \Gamma_1g), \quad f, g \in \text{dom}(S^*), \tag{2.1}$$

is satisfied and the mapping  $\Gamma := (\Gamma_0, \Gamma_1)^\top : \text{dom}(A^*) \rightarrow \mathcal{H} \oplus \mathcal{H}$  is surjective, i.e.  $\text{ran}(\Gamma) = \mathcal{H} \oplus \mathcal{H}$ . ◊

A boundary triplet  $\Pi = \{\mathcal{H}, \Gamma_0, \Gamma_1\}$  for  $A^*$  always exists whenever  $n_+(A) = n_-(A)$ . Note also that  $n_\pm(A) = \dim(\mathcal{H})$  and  $\ker(\Gamma_0) \cap \ker(\Gamma_1) = \text{dom}(A)$ .

With any boundary triplet  $\Pi$  one associates two canonical self-adjoint extensions  $A_j := S^* \upharpoonright \ker(\Gamma_j)$ ,  $j \in \{0, 1\}$ . Conversely, for any self-adjoint extension  $A_0 = S_0^* \in \text{Ext}_S$  there exists a (non-unique) boundary triplet  $\Pi = \{\mathcal{H}, \Gamma_0, \Gamma_1\}$  for  $A^*$  such that  $A_0 := A^* \upharpoonright \ker(\Gamma_0)$ .

Using the concept of boundary triplets, one can parametrize all proper extensions of  $A$  in the following way.

**Proposition 2.3** ([9,13]). *Let  $\Pi = \{\mathcal{H}, \Gamma_0, \Gamma_1\}$  be a boundary triplet for  $A^*$ . Then the mapping:*

$$\text{Ext}_A \ni \tilde{A} \rightarrow \Gamma \text{dom}(\tilde{A}) = \{(\Gamma_0f, \Gamma_1f)^\top : f \in \text{dom}(\tilde{A})\} =: \Theta \in \tilde{\mathcal{C}}(\mathcal{H}), \tag{2.2}$$

establishes a bijective correspondence between the sets  $\text{Ext}_A$  and  $\tilde{\mathcal{C}}(\mathcal{H})$ . We write  $\tilde{A} = A_\Theta$  if  $\tilde{A}$  corresponds to  $\Theta$  by (2.2). Moreover, the following holds:

- (i)  $A_\Theta^* = A_{\Theta^*}$ , in particular,  $A_\Theta^* = A_\Theta$  if and only if  $\Theta^* = \Theta$ .
- (ii)  $A_\Theta$  is symmetric (self-adjoint) if and only if  $\Theta$  is symmetric (self-adjoint).
- (iii) The extensions  $A_\Theta$  and  $A_0$  are disjoint (transversal) if and only if there is a closed (bounded) operator  $B$  such that  $\Theta = \text{gr}(B)$ . In this case (2.2) takes the form:

$$A_\Theta := A_{\text{gr}(B)} = A^* \upharpoonright \ker(\Gamma_1 - B\Gamma_0). \tag{2.3}$$

In particular,  $A_j := A^* \upharpoonright \ker(\Gamma_j) = A_{\Theta_j}$ ,  $j \in \{0, 1\}$ , where  $\Theta_0 := \begin{pmatrix} \{0\} \\ \mathcal{H} \end{pmatrix}$  and  $\Theta_1 := \begin{pmatrix} \mathcal{H} \\ \{0\} \end{pmatrix} = \text{gr}(\mathbb{O})$  where  $\mathbb{O}$  denotes the zero operator in  $\mathcal{H}$ . Note also that  $\tilde{\mathcal{C}}(\mathcal{H})$  contains the trivial linear relations  $\{0\} \times \{0\}$  and  $\mathcal{H} \times \mathcal{H}$  corresponding to  $A$  and  $A^*$ , respectively, for any boundary triplet  $\Pi$ .

### 2.3. Gamma field and Weyl function

It is well known that the Weyl function is an important tool in the direct and inverse spectral theory of Sturm-Liouville operators. In [8, 9], the concept of Weyl function was generalized to the case of an arbitrary symmetric operator  $A$  with  $n_+(A) = n_-(A) \leq \infty$ . Following [9] we briefly recall basic facts on Weyl functions and Gamma fields associated with a boundary triplet  $\Pi$ .

**Definition 2.4** ([8, 9]). Let  $\Pi = \{\mathcal{H}, \Gamma_0, \Gamma_1\}$  be a boundary triplet for  $A^*$  and  $A_0 = A^* \upharpoonright \ker(\Gamma_0)$ . The operator valued functions  $\gamma(\cdot) : \rho(A_0) \rightarrow [\mathcal{H}, \mathcal{H}]$  and  $M(\cdot) : \rho(A_0) \rightarrow [\mathcal{H}]$  defined by the following:

$$\gamma(z) := (\Gamma_0 \upharpoonright \mathfrak{N}_z)^{-1}, \quad \mathfrak{N}_z = \ker(A^* - z) \quad \text{and} \quad M(z) := \Gamma_1 \gamma(z), \quad z \in \rho(A_0), \tag{2.4}$$

are called the Gamma field and the Weyl function, respectively, corresponding to the boundary triplet  $\Pi$ .

Clearly, the Weyl function can equivalently be defined by:

$$M(z)\Gamma_0 f_z = \Gamma_1 f_z, \quad f_z \in \mathfrak{N}_z, \quad z \in \rho(A_0).$$

The Gamma field  $\gamma(\cdot)$  and the Weyl function  $M(\cdot)$  in (2.4) are well defined. Moreover, both  $\gamma(\cdot)$  and  $M(\cdot)$  are holomorphic on  $\rho(A_0)$  and the following relations:

$$\gamma(z) = (I + (z - \zeta)(A_0 - z)^{-1})\gamma(\zeta), \quad z, \zeta \in \rho(A_0), \tag{2.5}$$

and

$$M(z) - M(\zeta)^* = (z - \bar{\zeta})\gamma(\zeta)^*\gamma(z), \quad z, \zeta \in \rho(A_0), \tag{2.6}$$

hold. Identity (2.6) yields that  $M(\cdot)$  is  $[\mathcal{H}]$ -valued Nevanlinna function ( $M(\cdot) \in R[\mathcal{H}]$ ), i.e.  $M(\cdot)$  is  $[\mathcal{H}]$ -valued holomorphic function on  $\mathbb{C}_\pm$  satisfying:

$$M(z) = M(\bar{z})^* \quad \text{and} \quad \frac{\text{Im}(M(z))}{\text{Im}(z)} \geq 0, \quad z \in \mathbb{C}_+ \cup \mathbb{C}_-.$$

It also follows also from (2.6) that  $0 \in \rho(\text{Im}(M(z)))$  for all  $z \in \mathbb{C}_\pm$ .

A Weyl function  $M(\cdot)$  is said to be of a scalar type if there exists a scalar Nevanlinna function  $m(\cdot)$  such that the the representation:

$$M(z) = m(z)I_{\mathcal{H}}, \quad z \in \mathbb{C}_+, \tag{2.7}$$

holds where  $I_{\mathcal{H}}$  is the identity operator in  $\mathcal{H}$ , see [5]. Obviously,  $M(\cdot)$  is of a scalar type if  $n_\pm(A) = 1$ .

### 2.4. Krein-type formula for resolvents

Let  $\Pi = \{\mathcal{H}, \Gamma_0, \Gamma_1\}$  be a boundary triplet for  $A^*$ ,  $M(\cdot)$  and  $\gamma(\cdot)$  the corresponding Weyl function and Gamma field, respectively. For any proper (not necessarily self-adjoint) extension  $\tilde{A}_\Theta \in \text{Ext}_A$  with non-empty resolvent set  $\rho(\tilde{A}_\Theta)$ , the following Krein-type formula holds (cf. [8–10]):

$$(A_\Theta - z)^{-1} - (A_0 - z)^{-1} = \gamma(z)(\Theta - M(z))^{-1}\gamma^*(\bar{z}), \quad z \in \rho(A_0) \cap \rho(A_\Theta). \tag{2.8}$$

Formula (2.8) extends the known Krein formula for canonical resolvents to the case of any  $A_\Theta \in \text{Ext}_A$  with  $\rho(S_\Theta) \neq \emptyset$ . Moreover, due to relations (2.2), (2.3) and (2.4) formula (2.8) is connected with the boundary triplet  $\Pi$ . We emphasize that this connection makes it possible to apply the Krein-type formula (2.8) to boundary value problems.

### 2.5. Direct sum of operators

Let  $S_n$  be a densely defined closed symmetric operator in a Hilbert space  $\mathfrak{H}_n$  with  $n_+(S_n) = n_-(S_n) \leq \infty$ ,  $n \in \mathbb{N}$ . Consider the operator  $S := \bigoplus_{n=1}^\infty S_n$  acting in  $\mathfrak{H} := \bigoplus_{n=1}^\infty \mathfrak{H}_n$ , the Hilbert direct sum of Hilbert spaces  $\mathfrak{H}_n$ . By definition,  $\mathfrak{H} = \{f = \bigoplus_{n=1}^\infty f_n : f_n \in \mathfrak{H}_n, \sum_{n=1}^\infty \|f_n\|^2 < \infty\}$ . From this, it is apparent that:

$$S^* = \bigoplus_{n=1}^\infty S_n^*, \quad \text{dom}(S^*) = \{f = \bigoplus_{n=1}^\infty f_n \in \mathfrak{H} : f_n \in \text{dom}(S_n^*), \sum_{n=1}^\infty \|S_n^* f_n\|^2 < \infty\}.$$

**Theorem 2.5** (Theorem 2.10 of [7]). *Let  $\Pi_n = \{\mathcal{H}_n, \Gamma_0^n, \Gamma_1^n\}$  be a boundary triplet for  $S_n^*$  and  $M_n(\cdot)$  the corresponding Weyl function,  $n \in \mathbb{N}$ . A direct sum  $\Pi = \bigoplus_{n=1}^{\infty} \Pi_n$  forms an ordinary boundary triplet for the operator  $S^* = \bigoplus_{n=1}^{\infty} S_n^*$  if and only if*

$$\sup_n \|M_n(i)\|_{\mathcal{H}_n} < \infty, \quad \sup_n \|(\operatorname{Im}(M_n(i)))^{-1}\|_{\mathcal{H}_n}. \tag{2.9}$$

### 3. Weyl function computation

Let us describe the procedure to obtain all extension of the operator (1.1). Firstly, let us consider symmetric Dirac operator, defined by (1.2). The adjoint operator  $D^*$  appears as:

$$\begin{aligned} (D^*f)(x) &= -ic \frac{d}{dx} \otimes \sigma_1 f(x) + \frac{c^2}{2} \otimes \sigma_3 f(x), \quad x \in \Delta, \\ f \in \operatorname{dom}(D^*) &= W^{1,2}(\Delta, \mathbb{C}^2). \end{aligned} \tag{3.1}$$

The triplet  $\Pi_D = \{\mathcal{H}^D, \Gamma_0^D, \Gamma_1^D\}$ ,  $\mathcal{H}^D := \mathbb{C}^2$ ,

$$\begin{aligned} \Gamma_0^D \begin{pmatrix} f_1 \\ f_2 \end{pmatrix} &:= \frac{1}{\sqrt{2}} \begin{pmatrix} f_1(a) + f_1(b) \\ f_1(a) - f_1(b) \end{pmatrix}, \\ \Gamma_1^D \begin{pmatrix} f_1 \\ f_2 \end{pmatrix} &:= \frac{ic}{\sqrt{2}} \begin{pmatrix} f_2(a) - f_2(b) \\ f_2(a) + f_2(b) \end{pmatrix}, \end{aligned} \tag{3.2}$$

$f \in \operatorname{dom}(D^*)$ , forms a boundary triplet for  $D^*$ . The Gamma field and the Weyl function are given by:

$$\gamma^D(z) \begin{pmatrix} \xi_1 \\ \xi_2 \end{pmatrix} = \frac{1}{\sqrt{2}} \begin{pmatrix} \frac{\cos(k(z)(x-\nu))}{\cos(k(z)d)} & \frac{\sin(k(z)(x-\nu))}{\sin(k(z)d)} \\ ik_1(z) \frac{\sin(k(z)(x-\nu))}{\cos(k(z)d)} & ik_1(z) \frac{\cos(k(z)(x-\nu))}{\sin(k(z)d)} \end{pmatrix} \begin{pmatrix} \xi_1 \\ \xi_2 \end{pmatrix}, \tag{3.3}$$

$z \in \mathbb{C}_{\pm}$ . Here,

$$k(z) := \frac{1}{c} \sqrt{z^2 - \frac{c^4}{4}}, \quad z \in \mathbb{C}, \tag{3.4}$$

where the branch of the multifunction  $k(\cdot)$  is fixed by the condition  $k(x) > 0$  for  $x > \frac{c^2}{2}$ .

Notice that  $k(\cdot)$  is holomorphic in  $\mathbb{C} \setminus \left[-\frac{c^2}{2}, \frac{c^2}{2}\right]$ . Furthermore,

$$k_1(z) := \frac{ck(z)}{z + \frac{c^2}{2}}, \quad z \in \mathbb{C}. \tag{3.5}$$

which is also holomorphic in  $\mathbb{C} \setminus \left[-\frac{c^2}{2}, \frac{c^2}{2}\right]$ . The function  $k_1(\cdot)$  admits the representation:

$$k_1(z) = \sqrt{\frac{z - \frac{c^2}{2}}{z + \frac{c^2}{2}}}, \quad z \in \mathbb{C}, \tag{3.6}$$

where the branch of  $\sqrt{\frac{z - \frac{c^2}{2}}{z + \frac{c^2}{2}}}$  is fixed by the condition  $\sqrt{\frac{x - \frac{c^2}{2}}{x + \frac{c^2}{2}}} > 0$  for  $x > \frac{c^2}{2}$ . We obtain the following:

$$M^D(z) = \begin{pmatrix} m_1^D(z) & 0 \\ 0 & m_2^D(z) \end{pmatrix}, \quad z \in \mathbb{C}_\pm, \tag{3.7}$$

where

$$\begin{aligned} m_1^D(z) &:= ck_1(z) \tan(k(z)d) \\ m_2^D(z) &:= -ck_1(z) \cot(k(z)d), \end{aligned} \quad z \in \mathbb{C}_\pm, \tag{3.8}$$

and  $d := \frac{b-a}{2}$ ,  $\nu := \frac{b+a}{2}$ . The self-adjoint extension  $D^{(1)} := D^* \upharpoonright \ker(\Gamma_0^D)$  has the domain:

$$\text{dom}(D^{(1)}) = \{f \in W^{1,2}(\Delta, \mathbb{C}^2) : f_1(a) = f_1(b) = 0\}, \tag{3.9}$$

while the extension  $D^{(2)} := D^* \upharpoonright \ker(\Gamma_1^D)$  has the domain:

$$\text{dom}(D^{(2)}) = \{f \in W^{1,2}(\Delta, \mathbb{C}^2) : f_2(a) = f_2(b) = 0\}. \tag{3.10}$$

In the following, we denote elements of  $\mathfrak{L}$  by  $\vec{f}$ . In particular, we use the notation:

$$\vec{f} = \begin{pmatrix} \vec{f}_1 \\ \vec{f}_2 \end{pmatrix}, \quad \vec{f}_j \in L^2(\Delta_c, \mathfrak{X}), \quad j = 1, 2. \tag{3.11}$$

Let us construct the boundary triplet  $\Pi_L = \{\mathcal{H}^L, \Gamma_0^L, \tilde{\Gamma}_1^L\}$  for  $L^*$ .

Operator  $T$  gives us spectral decomposition  $T = \bigoplus_{n=0}^\infty T_n$ , where  $T_n$  – bounded self-adjoint operator defined on  $\mathfrak{X}_n$ ,  $\mathfrak{X} = \bigoplus_{n=0}^\infty \mathfrak{X}_n$ . Thus, operator  $L$  admits the representation:

$$L = \bigoplus_{n=0}^\infty L_n = \bigoplus_{n=0}^\infty D \otimes I_{\mathfrak{X}_n} + I_{\mathfrak{D}} \otimes T_n.$$

For each  $L_n$  boundary triplet, the Gamma field and the Weyl function can be obtained easily, as  $T_n$  is bounded, see [6]. The problem is that the direct sum of boundary triplets, in general, is not a boundary triplet. The typical approach to such a problem is a regularization procedure, see [14]. However, in our case, the regularization is not necessary.

**Theorem 3.1.** *The Weyl function  $M^L(\cdot)$  is given by:*

$$M^L(z) = \begin{pmatrix} m_1^D(z - T) & 0 \\ 0 & m_2^D(z - T) \end{pmatrix}, \quad z \in \mathbb{C}_\pm. \tag{3.12}$$

*Proof.* We compute:

$$C_j^D := \sup_{\lambda \in \mathbb{R}} |m_j^D(i - \lambda)| < \infty, \quad \text{and} \quad \Lambda_j^D := \sup_{\lambda \in \mathbb{R}} \frac{1}{|m_j^D(i - \lambda)|} < \infty, \tag{3.13}$$

$j = 1, 2$ . This relies on the fact that  $\sup_{\lambda \in \mathbb{R}} |k_1(i - \lambda)| < \infty$  and  $\sup_{\lambda \in \mathbb{R}} \frac{1}{|k_1(i - \lambda)|} < \infty$ .

Let us rewrite  $L_n = D + n$ ,  $n \in \mathbb{N}_0$  which is a closed symmetric operator defined on  $\mathfrak{L}_n = \mathfrak{D} \otimes \mathfrak{X}_n$ . Notice that  $\mathfrak{L} = \bigoplus_{n \in \mathbb{Z}} \mathfrak{L}_n$  and  $L = \bigoplus_{n \in \mathbb{Z}} L_n$ . The triplet  $\Pi_{L_n} = \Pi_D \otimes I_{\mathfrak{X}_n} = \{\mathcal{H}^{L_n}, \Gamma_0^{L_n}, \Gamma_1^{L_n}\}$ ,

$$\mathcal{H}^{L_n} := \mathcal{H}^D \otimes I_{\mathfrak{X}_n}, \quad \Gamma_0^{L_n} = \Gamma_0^D \otimes I_{\mathfrak{X}_n}, \quad \Gamma_1^{L_n} = \Gamma_1^D \otimes I_{\mathfrak{X}_n}, \tag{3.14}$$

is a boundary triplet for  $L_n^*$ ,  $n \in \mathbb{Z}$ . The corresponding Weyl function  $M^{L_n}(\cdot)$  is given by:

$$M^{L_n}(z) = \begin{pmatrix} m_1^D(z - T_n) & 0 \\ 0 & m_2^D(z - T_n) \end{pmatrix}, \quad n \in \mathbb{Z}, \quad z \in \mathbb{C}_\pm. \quad (3.15)$$

Notice that:

$$C_{jn}^D := \|m_j^D(i - T_n)\| = \sup_{\lambda \in \Delta_n} |m_j^D(i - \lambda)| \leq C_j^D < \infty, \quad j = 1, 2, \quad (3.16)$$

which yields:

$$\|M^{L_n}(i)\| \leq \max\{C_{1n}^D, C_{2n}^D\} \leq \max\{C_1^D, C_2^D\} < \infty. \quad (3.17)$$

Similarly, we verify:

$$\|(M^{L_n}(i))^{-1}\| \leq \max\{\Lambda_{1n}^D, \Lambda_{2n}^D\} \leq \max\{\Lambda_1^D, \Lambda_2^D\} < \infty, \quad (3.18)$$

where:

$$\Lambda_{jn}^D := \|(m_j^D(i - T_n))^{-1}\| = \sup_{\lambda \in \Delta_n} \frac{1}{|m_j^D(i - \lambda)|} < \Lambda_j^D < \infty, \quad (3.19)$$

$j = 1, 2$ . By Theorem 2.5, we see that  $\Pi'_L = \bigoplus_{n \in \mathbb{Z}} \Pi_{L_n}$  is a boundary triplet for  $L$ . In particular, the Weyl function  $M^L(\cdot)$  is computed by:

$$M^L(z) = \begin{pmatrix} m_1^D(z - T) & 0 \\ 0 & m_2^D(z - T) \end{pmatrix}, \quad z \in \mathbb{C}_\pm. \quad (3.20)$$

□

The considerations remain true if we use the boundary triplet of [7, Section 3.1].

## Acknowledgments

This work was partially financially supported by the Government of the Russian Federation (grant 074-U01), by Ministry of Science and Education of the Russian Federation (GOSZADANIE 2014/190, Projects No 14.Z50.31.0031 and No. 1.754.2014/K), by grants MK-5001.2015.1 and MK-5161.2016.1 of the President of the Russian Federation, by grant 16-11-10330 of Russian Science Foundation. The first author acknowledge hospitality and financial support of WIAS Berlin. The second author thanks the European Research Council and the DFG supporting the preparation of the paper via ERC-2010-AdG no. 267802 (Analysis of Multiscale Systems Driven by Functionals) and Grant NE 1439/3-1 (Development of Methods in the Theory of Self-adjoint Extensions), respectively.

## References

- [1] Pan L., Fu X., Zhou G. Electron dwell time through a quantum wire under a electromagnetic field irradiation. *Phys. Lett. A*, 2007, **368**(1-2), P. 97–100.
- [2] Popov I.Y. Operator extensions theory model for electromagnetic field-electron interaction. *J. Math. Phys.*, 2012, **53**, P. 063505.
- [3] Neidhardt H., Wilhelm L., Zagrebnev V.A. A new model for quantum dot light emitting-absorbing devices. *J. Math. Phys., Anal., Geom.*, 2014, **10**(3), P. 350–385.
- [4] Neidhardt H., Wilhelm L., Zagrebnev V.A. A new model for quantum dot light emitting-absorbing devices: proofs and supplements. *Nanosystems: Phys. Chem. Math.*, 2015, **6**(1), P. 6–45.
- [5] Albeverio S., Brasche J.F., Malamud M.M., Neidhardt H. Inverse spectral theory for symmetric operators with several gaps: scalar-type Weyl functions. *J. Funct. Anal.*, 2005, **228**(1), P. 144–188.
- [6] Boitsev A.A., Neidhardt H., Popov I.Y. Weyl function for sum of operators tensor products. *Nanosystems: Phys. Chem. Math.*, 2013, **4**(6), P. 747–757.

- [7] Carlone R., Malamud M., Posilicano A. On the spectral theory of Gesztesy-Šeba realizations of 1-D Dirac operators with point interactions on a discrete set. *J. Differential Equations*, 2013, **254**(9), P. 3835–3902.
- [8] Derkach V.A., Malamud M.M. On the Weyl function and Hermite operators with lacunae. *Dokl. Akad. Nauk SSSR*, 1987, **293**(5), P. 1041–1046.
- [9] Derkach V.A., Malamud M.M. Generalized resolvents and the boundary value problems for Hermitian operators with gaps. *J. Funct. Anal.*, 1991, **95**(1), P. 1–95.
- [10] Derkach V.A., Malamud M.M. The extension theory of Hermitian operators and the moment problem. *J. Math. Sci.*, 1995, **73**(2), P. 141–242.
- [11] Gorbachuk V.I., Gorbachuk M.L. *Boundary value problems for operator differential equations*, volume 48 of *Mathematics and its Applications (Soviet Series)*. Kluwer Academic Publishers Group, Dordrecht, 1991.
- [12] Kočubei A. N. Extensions of symmetric operators and of symmetric binary relations. *Mat. Zametki*, 1975, **17**, P. 41–48.
- [13] Malamud M.M. Some classes of extensions of a Hermitian operator with lacunae. *Ukrain. Mat. Zh.*, 1992, **44**(2), P. 215–233.
- [14] Malamud M.M., Neidhardt H. Sturm-Liouville boundary value problems with operator potentials and unitary equivalence. *J. Differential Equations*, 2012, **252**(11), P. 5875–5922.
- [15] Schmüdgen K. *Unbounded self-adjoint operators on Hilbert space*, 2012, volume 265 of *Graduate Texts in Mathematics*. Springer, Dordrecht.

## An interpretation of the strongest X-ray diffraction peak for various carbon nanoclusters

A. V. Siklitskaya<sup>1</sup>, S. G. Yastrebov<sup>2</sup>, R. Smith<sup>3</sup>

<sup>1</sup>Institute of Theoretical Physics, University of Warsaw, Warsaw, Poland

<sup>2</sup>Ioffe Institute, St. Petersburg, Russia

<sup>3</sup>Loughborough University, Department of Mathematical Sciences,  
Loughborough, United Kingdom

Yastrebov@mail.ioffe.ru

PACS 61.05.C, 61.72.Dd, Ff

DOI 10.17586/2220-8054-2016-7-2-340-348

The most intensive X-ray diffraction peaks for three types of carbon allotropes are analyzed: i) temperature-annealed nanodiamond powder (carbon “onions”), ii) multi-walled carbon nanotubes, iii) layers of epitaxial graphene. A reconstruction of the X-ray diffraction pattern using an intershell distribution, obtained by high resolution transmission electron microscopy, was compared to the XRD data. For a qualitative analysis of the diffraction profiles, the method of convolution of Lorentzians (size broadening profile), together with a statistical consideration of interlayer spacings (lattice strain broadening profile) were used. For the case of iii) the statistical distribution reduces to a Gaussian and the method itself transforms to a best fit procedure of the classical Voigt function to the experimental data. For cases i) and ii) and the high-resolution electron microscopy-reconstructed data, the method fits the experiment better using either negatively or positively -skewed statistical distributions, correspondingly. A model of particles with a spiral internal structure and with radius-dependent spacings between the successive turns may explain experimental data for these cases. The data for epitaxial graphene allows different interpretations, including fluctuations of lattice spacings caused by distortions of the valence bands and angles in the graphene planes or by the formation of scrolls.

**Keywords:** graphene, carbon onions, carbon, multiwalled carbon nanotubes, X-ray diffraction.

*Received:* 23 January 2016

### 1. Introduction

A study of the internal structure of new allotropic forms of carbon is important for the progress of materials science. In particular, obtaining information about the structure of materials and, therefore, their degree of perfection, helps to outline the areas for their practical applications. Thus, the study of structures that break the symmetry of graphitic planes is important for better understanding the practical realization of “theoretic” graphene as a material with a zero band gap and high electron mobility. In this paper, we present results of a qualitative analysis of the most intensive diffraction peak for several types of carbon allotropes constructed with  $sp^2$ -bonded atoms [1–4].

Because of graphene’s unique geometry, there exists various possibilities for the modification of valence angles and bond lengths which change the structure; e.g. the Dienes (Stone-Wales) rearrangement [5]. Moreover, carbon polyhedra assembled with  $sp^2$  bonds play an important role in the construction of nanoclusters having different shapes (e.g. carbon spheroids and spiroids).

It is very well known that X-ray diffraction (XRD) is the standard method for crystal structure analysis. However, allotropes such as graphene cannot be characterized by XRD because there is only a single (002) plane. For formation of the most intensive XRD peak,

similar to that for graphite, at least three planes are required [4]. Another problem with new allotropes of carbon is a lack of symmetry of the XRD profiles for carbon “onions”, or, more strictly, for “temperature-annealed nanodiamond powder” [1], and for multi-walled carbon nanotubes (see, e.g. [2]). Here, we analyze the diffraction peaks for various carbon-based materials that belong to the region of XRD angles where peaks corresponding to those between (002) planes for crystalline graphite manifest themselves.

Usually line shape analysis of XRD peaks reduces to the realization of a best fit procedure for minimization of a functional, containing squares of sum of differences between experimental data and the convolution of a size- (commonly a Lorentzian (Cauchy) function) together with lattice strain broadening (commonly Gaussian) -profiles [6]. However, one may consider the lattice-strain profile as a statistical distribution different for the normal law without loss of generality. This statistical distribution can be asymmetric, e.g. negatively-skewed, as was shown by us for carbon onions obtained in the course of temperature annealing of nanodiamonds [1]. Here, we will also show that the negatively-skewed distribution will fit the XRD profile for multi-walled carbon nanotubes as well as for the carbon onions case. Moreover, we will demonstrate that for the case of a lattice-spacing distribution of a single carbon onion investigated by HRTEM [3], a statistical distribution with positive skewness will fit the experimental data. When a Gaussian distribution is used in the convolution, the resulting profile is termed Voigtian. Here, we will show that for the case of epitaxial graphite [4], a Voigt function fits the experimental diffraction profiles quite well.

## 2. Experimental and methodology

We accurately digitized data presented in papers [1–4]. The technological parameters of the manufactured samples are presented there. All XRD spectra were measured for CuK $\alpha$  radiation.

### 2.1. Formalism

The intensity of diffraction  $V$  as a function of double diffraction angle  $\theta$  may be written in the following way:

$$V(\theta) = \int_{-\infty}^{\infty} S(\theta)L(\theta - \theta' - \theta_0)d\theta'. \quad (1)$$

Where  $\theta_0$  is doubled Bragg’s angle,  $S(\theta)$  is a statistical distribution function,  $L(\theta)$  is Lorentzian (Cauchy function):

$$L(\theta) = \frac{2A}{\pi} \frac{w_L}{\theta^2 + w_L^2}. \quad (2)$$

Here,  $w_L$  is full width of the Lorentz’s contour measured at its half height, and  $A$  is a constant. The parameter  $w_L$  is linked to Scherrer’s equation:

$$D = \frac{K\lambda}{w_L \cos(\theta_0/2)}, \quad (3)$$

and  $K$  is dimensionless constant that approximately equals to unity,  $\theta_0/2$  is Bragg’s angle. The equation (1) transforms to a Voigtian (Voigt function) when the function  $S_s(\theta)$  follows the normal distribution (Gaussian) law:

$$S_s(\theta) = \sqrt{\frac{b}{\pi}} e^{-\theta^2 b}, \quad (4)$$

where  $b = 4 \ln(2)/w_G^2$  and  $w_G$  is full width of Gaussian contour measured at its half height. In this paper, we also modeled another statistical function, asymmetric,  $S_a$ . For its modeling we used a double sigmoidal law in the following form:

$$S_a(\theta) = \frac{1}{1 + \exp\left(-\frac{\theta + \frac{w_1}{2}}{w_2}\right)} \left(1 - \frac{1}{1 + \frac{\theta - \frac{w_1}{2}}{w_3}}\right), \quad (5)$$

where  $w_1$ ,  $w_2$  and  $w_3$  are parameters. For analysis of the intershell spacings in carbon onions obtained by analysis of HRTEM images, we used a probe function which was selected empirically:

$$\langle R(\delta r) \rangle = A_1 + \frac{A_1 - A_2}{1 + \exp\left(-\frac{\delta r - \delta r_0}{\beta}\right)}, \quad (6)$$

where  $A_1$ ,  $A_2$ ,  $\beta$ ,  $\delta r_0$  are parameters,  $\langle R(\delta r) \rangle$  is the mean radius of the shell:  $\langle R(\delta r) \rangle \leq R_{\max}$ ;  $\delta r$  is a distance between two adjacent shells;  $R_{\max}$  is the onion's outer radius.

One may introduce a function representing the distribution of intershell distances,  $g(\delta r)$ :

$$g(\delta r) = \frac{d \langle M(\delta r) \rangle}{d \delta r}, \quad (7)$$

where  $\langle M(\delta r) \rangle$  is the mean number of intershell distances  $\delta r$  appearing in the interval  $d \delta r$ . On other hand, the following equation is also valid:

$$\langle R(\delta r) \rangle = \langle M(\delta r) \rangle \langle \delta r \rangle, \quad (8)$$

where  $\delta r$  is a mean intershell distance. One may calculate moments of the above distribution function (equation (7)) in the following way:

$$\langle M(\delta r) \rangle = \int_{\delta r_{\min}}^{\delta r} g(\delta r) d \delta r, \quad (9)$$

and

$$\langle \delta r \rangle = \int_{\delta r_{\min}}^{\delta r} \delta r g(\delta r) d \delta r. \quad (10)$$

Exploiting equation (8) and the assumption  $g(\delta r) \sim \delta r g(\delta r)$ , it easy to obtain the equation:

$$\langle R(\delta r) \rangle \approx \left( \int_{\delta r_{\min}}^{\delta r} g(\delta r) d \delta r \right)^2. \quad (11)$$

Thus:

$$g(\delta r) \approx \frac{\partial \left( \langle R(\delta r) \rangle^{1/2} \right)}{\partial \delta r}. \quad (12)$$

## 2.2. Analysis of experimental data

2.2.1. *Annealed nanodiamonds and multiwalled carbon nanotubes.* Figure 1 presents the XRD pattern for temperature-annealed nanodiamonds [1]. It is negatively-skewed. We met a difficulty finding a unique selection of the symmetric component for the results presented in the Fig. 1 and so used equations (1), (2) and (5) for a single negatively-skewed profile. The result of the calculation is depicted by the continuous curve. Parameters were obtained by the least squares fitting technique. The asymmetry of the internal structure of the onion may result in the skewness. A sketch of the cross section of such an onion is presented in the inset. Such kind of spiral onions were termed as carbon spiroids [7]. In the particular case presented here, the radius of the spiral turn depends irregularly on the spacing between successive turns. The principal role of such spiroidal particles in the formation of the XRD profile may reflect their prevailing number in a comparison to ‘deal’ spheroids.

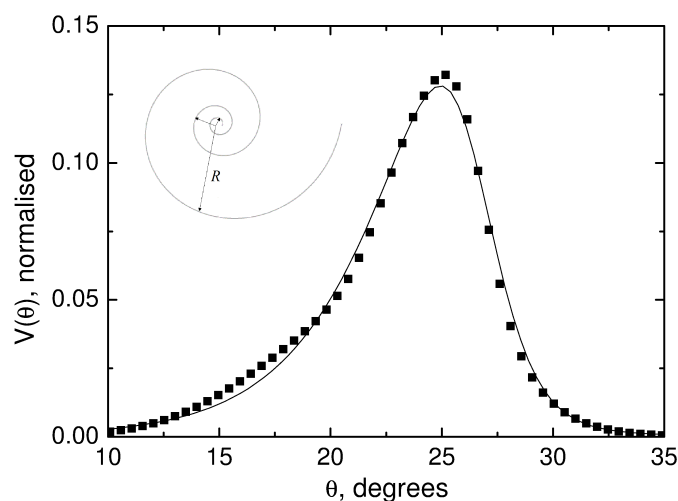


FIG. 1. The XRD profile for a powder of nanodiamonds transformed to onions by annealing. The black squares and solid contour show experimental data from [1] and the result of calculation with equations (1), (2) and (5), correspondingly for  $w_1 = 0^\circ$ ,  $w_2 = 3.11^\circ$ ,  $w_3 = 1.01^\circ$ ,  $w_L = 0.5^\circ$ . The insert shows a schematic of the equatorial section of a spiroidal particle (spiroid).

A slightly different situation occurs in the case of multi-walled carbon nanotubes. Fig. 2 shows XRD profile for the nanotubes. One may see the result of decomposition of the experimental data [2] on two contours. One is asymmetric ([equations (1), (2) and (5)]; the curve marked by number 1) and the second one is symmetric (Voigtian [equations (1),(2) and (4)]; curve 2). By analogy with carbon spiroids, we may term nanotubes contributing to contour (1) as spirocylindroids. A sketch of the cross-section of a spirocylindroid is presented in the insert to Fig. 2. In this case there is no principal role played by spiroidal particles to the XRD profile which may reflect a contribution from ‘ideal’ nanotubes that is comparable with the contribution of the spirocylindroids.

2.2.2. *Carbon onions.* Here, we interpret the experimental data from paper [1] where the dependence of the distances between successive shells of the carbon spheroids are presented as a function of the shell’s radius. The inverse function is portrayed in Fig. 3. For simplicity, we kept symbols marking experimental points similar to ones presented in [1]. The full line marked by number 1 represents data calculated with equation (6) and the triangles illustrate

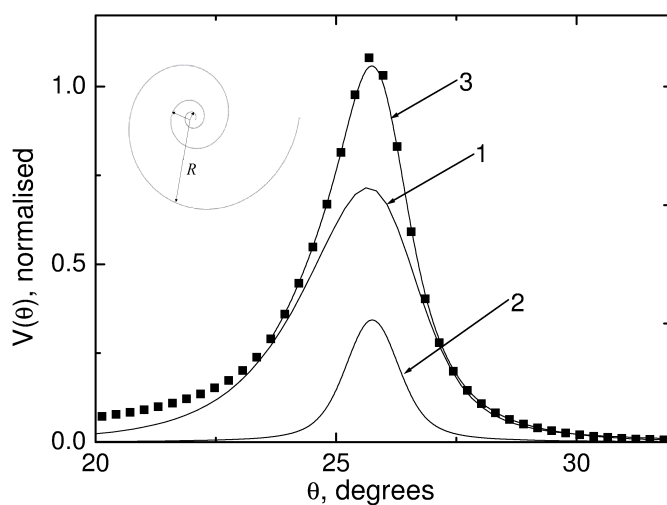


FIG. 2. The XRD profile for multi-walled carbon nanotubes. The black squares portray experimental data from [2]; the curve marked by number 1 presents results of calculation with equations (1), (2) and (5) with the following parameters:  $w_1 = 0^\circ$ ,  $w_2 = 2^\circ$ ,  $w_3 = 0.456^\circ$ ,  $w_L = 1^\circ$ ,  $A = 0.43$ . The line marked by number 2 shows the calculation with equations (1), (2) and (4) for  $\theta_0 = 25.75^\circ$ ,  $A = 0.178$ ,  $w_G = 0.87^\circ$ ,  $w_L = 0.633^\circ$  (“ideal” nanotube). Curve 3 is the sum of curves (1) and (2). The insert shows a schematic of the cross section of a spirocylinder.

equation (12). The full line connecting the triangles is the Gaussian approximation. Therefore, the obtained distribution is symmetric. However, it is easy to see in Fig. 4 that after conversion of the intershell distances to the double diffraction angles with the help of Bragg’s law, the resulting dependence is no longer symmetric and is positively-skewed. This characterizes the lattice strain function. To use the lattice strain function in equation (1), one has to shift the argument values to the left, starting the new argument zero point from the position of the maximum. The parameter  $w_L$  was calculated using equation (3) using data of the diameter of carbon onions from [3] and the  $\text{CuK}\alpha$  radiation wavelength. The resulting convolution of the lattice strain and Lorentzian profiles are presented in Fig. 4 by open circles. Such dependences characterize the internal structure of the carbon onion. Obviously, while the area of larger angles characterizes the central part of the onion, where some compression of the lattice spacings was observed [3], the region for smaller angles characterizes its peripheral region. It is natural to attribute such behavior to a spiroid with lattice spacings expanding from central to peripheral area. It seems obvious to draw similar conclusions about the behavior of lattice spacings for the cases considered above. However, the degrees of expansions are different. For cases of Figs. 1 and 2, the diffraction profiles are negatively skewed, meaning a faster drop of the function in the smaller intershell distances region and a slower drop in the larger intershell distances region.

An estimation of Scherrer’s size for thermally annealed nanodiamonds and multi-walled nanotubes (see captions to Fig. 1 and Fig. 2 and equation (3)), i.e.  $\sim 14$  nm, indicates the formation of relatively large clusters. These may appear for the case of thermally-annealed nanodiamonds because this size is sufficiently larger than the mean size of pristine nanodiamonds ( $\sim 4$  nm). The cluster enlargement may appear because of single cluster aggregation to bigger particles. However we cannot extend this result to nanotubes because of a lack of information about their origin. In this case of aggregation to the resulting “lattice strain” profile may transform to statistics of lattice spacings in larger clusters with more complex structures.

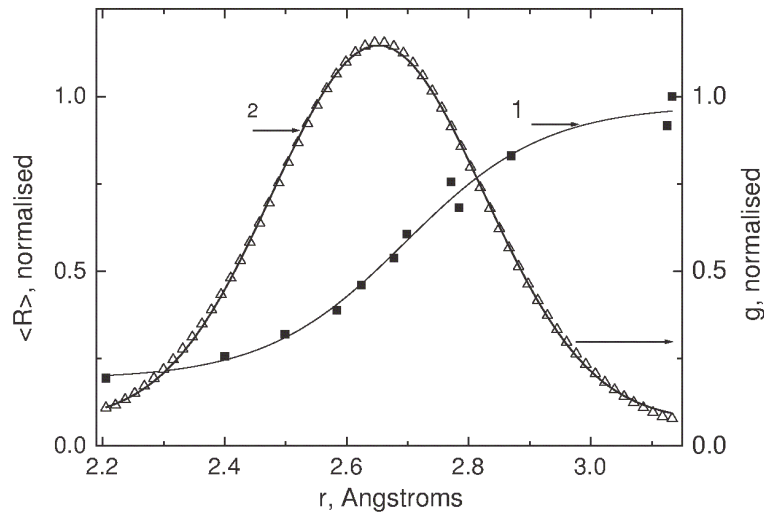


FIG. 3. The black squares give the experimental dependence of a shell's radius normalized to the external radius of a multishell carbon spheroid (carbon "onion") as a function of the intershell distances, as published in [3]. The continuous line 1 represents an approximation of the experimental data using equation (6) with the following set of parameters:  $A_1 = 0.19 \pm 0.03$ ,  $A_2 = 0.97 \pm 0.03$ ,  $\delta r_0 = 2.696 \pm 0.016 \text{ \AA}$ ,  $\beta = 0.11 \pm 0.02 \text{ \AA}$ . The triangles give results for the calculation of the distribution function using equation (12); the full line shows the Gaussian fit.

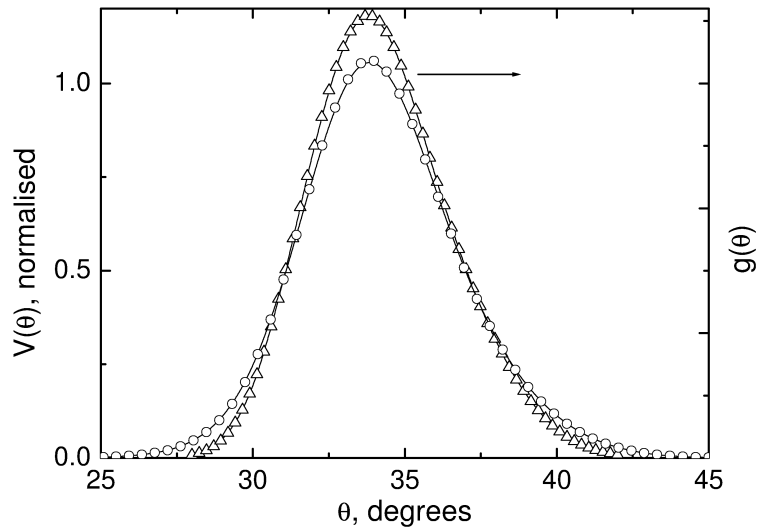


FIG. 4. The lattice strain function  $g(\theta)$  of intershell spacings for a carbon multishell particle plotted versus the diffraction angle is given by triangles after conversion of the spacings to double diffraction angles by Bragg's law. Circles depict results of the calculation with equation (1) with the diffraction profile from a shifted lattice strain function. Here, for calculation of the XRD profile, the following parameters were used:  $\theta_0 = 33.98^\circ$  is position of the maximum and the parameter  $w_L = 0.6^\circ$  is calculated with Scherrer's equation (3) for the actual cluster diameter (see paper [3]).

2.2.3. *Epitaxial graphite.* The experimental data for epitaxial graphite together with their fit by a Voigtian function are collected in Fig. 5 [4]. One may see a good agreement between the model and experimental data for all cases presented in Fig. 5. Two possible versions of graphene flaks deformation are presented in the insets- *sine* and *cosine* types of distortions (the left inset to Fig. 5) and formation of scrolls (spirocylindroids). A similar effect of transformation of material from graphene to scrolls has been presented in paper [8]. The distortion of the graphene planessymmetries results in the annihilation of their valuable properties such as zero effective mass and high mobility of charge carriers. Fig. 6 shows the width of the lattice strain profile vs substrate material and technology of deposition. One can clearly see that all grown layers are distorted. The lesser distorted sample is graphite obtained by the thermal decomposition of SiC. The parameter  $w_L \rightarrow 0$  is only for the profile marked in Fig. 5 by by triangles. It means that size of graphite fragment is large enough to be estimated by Scherrer's formula (equation 3) and the Voigtian transforms to a Gaussian. Only the lattice strain profile is available from the experiment. Fig. 7 presents Scherrer's diameter for a cluster of epitaxial graphite grown on different substrates, calculated using  $w_L$  from the caption to Fig. 5.

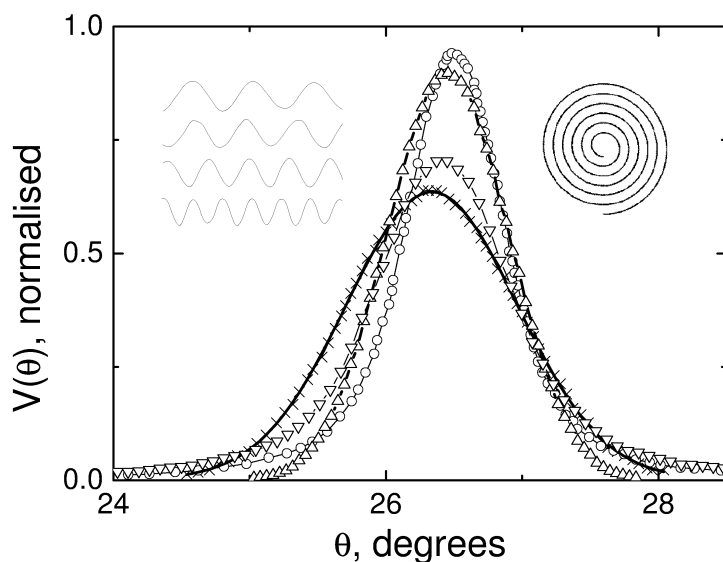


FIG. 5. A Voigtian fit of experimental diffraction profiles for epitaxial graphite [4]. Different symbols stand for different substrates. The continuous line presents results of the best fit. 1. The inverted triangles correspond to epitaxial graphite grown by CVD on the surface  $C$  6H-SiC:  $\theta_0 = 26.42^\circ \pm 0.002$ ,  $A = 1.09 \pm 0.003$ ,  $w_G = 0.81 \pm 0.01^\circ$ ,  $w_L = 0.601 \pm 0.01$ . 2. The inclining crosses give the thermal decomposition of the surface  $C$  4H-SiC:  $\theta_0 = 26.33 \pm 0.002^\circ$ ,  $A = 1.012 \pm 0.005$ ,  $w_G = 1.465 \pm 0.014^\circ$ ,  $w_L = 0.034 \pm 0.02$ . 3. The circles represent the thermal decomposition of the surface  $C$  6H-SiC:  $\theta_0 = 26.51 \pm 0.001^\circ$ ,  $A = 1.07 \pm 0.004$ ,  $w_G = 0.57 \pm 0.01^\circ$ ,  $w_L = 0.465 \pm 0.01^\circ$ . 4. Triangles – CVD grown epitaxial graphite grown by CVD on substrate Si-SiO<sub>2</sub>-Ni:  $\theta_0 = 26.45 \pm 0.001^\circ$ ,  $A = 1.000 \pm 0.0004$ ,  $w_G = 1.04 \pm 0.001^\circ$ ,  $w_L = 0$ . Insets show two modes of deformation for the graphene planes: left – sine (cosine) through formation of Dienes (Stone-Wales) defects and right – through formation of spirocylindroids.

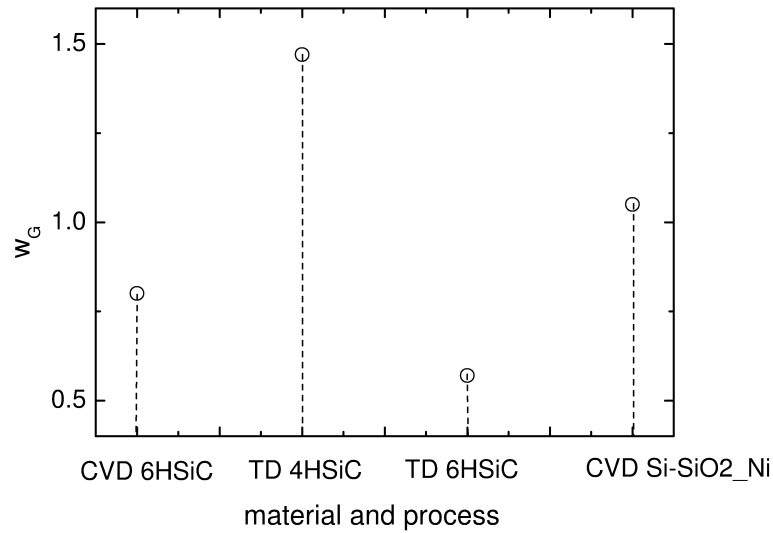


FIG. 6. The parameter  $w_G$  calculated by the best fit procedure from results presented in Fig. 5 for different materials

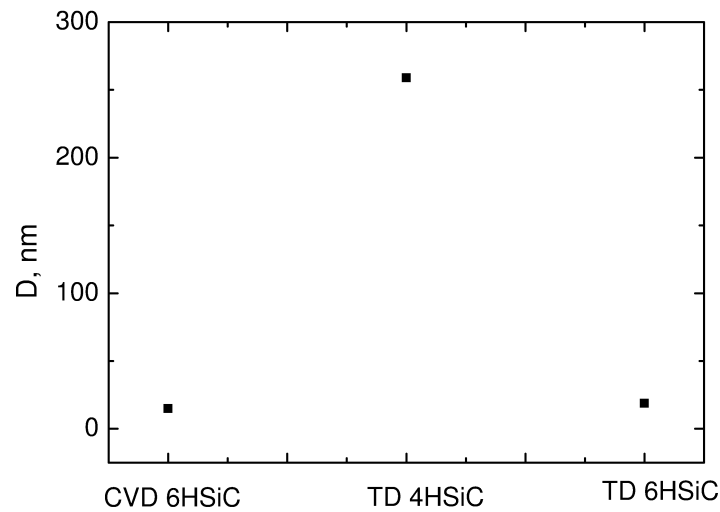


FIG. 7. Scherrer's diameter calculated from equation (3) and parameters  $w_L$  presented in the captions to Fig. 5 for different substrate materials and technologies

### 3. Conclusions

The estimations performed in this paper lead to two preliminary conclusions:

1. The spiroid-spirocyliindroid model of a particle with interturn distances expanding from center of the particle to its peripheral area fits experimental data for carbon onions and multi-walled carbon nanotubes quite well.
2. Spiroidal models might not be unique.
3. XRD study reveals a distortion of the symmetry of graphene planes for the epitaxial-grown graphite clusters.

4. The distortions break the symmetry of graphene planes and, therefore, may affect negatively charge transport properties.
5. A lack of profiles for a single graphene layer makes it difficult to standardize XRD for this material.

## References

- [1] Mykhaylyk O. O., Solonin Y. M., Batchelder D. N. et al. Transformation of nanodiamond into carbon onions: A comparative study by high-resolution transmission electron microscopy, electron energy-loss spectroscopy, x-ray diffraction, small-angle X-ray scattering, and ultraviolet Raman spectroscopy. *Appl. Phys.*, 2005, **97**, 074302, 16 pp.
- [2] Shah N. A., Abbas M., Amin M. et al. Design and analysis of functional multiwalled carbon nanotubes for infrared sensors. *Sensor Actuat A-Phys.*, 2013, **203**, P. 142–148.
- [3] Banhart F., Ajayan P. M. Carbon onions as nanoscopic pressure cells for diamond formation. *Nature*, 1996, **382**, P. 433–435.
- [4] Tokarczyk M., Kowalski G., Kepa H. et al. Multilayer graphene stacks grown by different methods-thickness measurements by X-ray diffraction, Raman spectroscopy and optical transmission. *Crystallogr. Reports*, 2013, **58**(7), P. 1053–1057.
- [5] Ma J. Stone-Wales defects in graphene and other planar  $sp^2$ -bonded materials. *Phys. Rev.B*, 2009, **80**, 033407, 4 pp.
- [6] Langford J. L., Delhez R., de Keijser Th., et al. Profile Analysis for Microcrystalline Properties by the Fourier and Other Methods. *Aust. J. Phys.*, 1988, **41**, P. 173–181.
- [7] Ozawa M., Goto H., Kusunoki M. Continuously Growing Spiral Carbon Nanoparticles as the Intermediates in the Formation of Fullerenes and Nanoonions. *Phys. Chem. B*, 2002, **106**, P. 7135–7138.
- [8] Zilong Liu Z., Qingzhong X., Tao Ye. Carbon nanoscroll from  $C_4H/C_4F$ -type graphene superlattice: MD and MM simulation insights. *Phys. Chem. Chem. Physics*, 2015, **17**(5), P. 3441–3450.

# Light scattering of Laguerre-Gaussian beams: near-field structures and symmetries

A. D. Kiselev<sup>1</sup>, D. O. Plutenko<sup>2,3</sup>

<sup>1</sup>ITMO University, Kronverkskiy, 49, St. Petersburg, 197101, Russia

<sup>2</sup>Institute of Physics of National Academy of Sciences of Ukraine, Kiev, Ukraine

<sup>3</sup>Physical Engineering Teaching Research Center of National Academy of Sciences of Ukraine, Kiev, Ukraine

alexei.d.kiselev@gmail.com, dmplutenko@gmail.com

PACS 42.25.Fx, 42.68.Mj, 42.25.Bs

DOI 10.17586/2220-8054-2016-7-2-349-370

We apply the method of far-field matching to remodel laser beams and study light scattering from spherical particles illuminated by a Laguerre-Gaussian (LG) light beam. The optical field in the near-field region is analyzed for purely azimuthal LG beams characterized by a nonzero azimuthal mode number  $m_{LG}$ . The morphology of photonic nanojets is shown to significantly vary, depending the mode number and the scatterer's characteristics. The cases of negative index metamaterial and metallic Mie scatterers are discussed. We also discuss the symmetry properties of laser beams and related results for the optical forces. The near-field structure of optical vortices associated with the components of the electric field, being highly sensitive to the mode number, is found to be determined by the twofold rotational symmetry.

**Keywords:** light scattering, Laguerre-Gaussian beams, photonic nanojets, optical vortices.

*Received: 22 January 2016*

## 1. Introduction

The scattering of light and other radiation by particles has long been known to be of crucial importance in a great variety of science and engineering disciplines. The problem of light scattering by spherically shaped particles dates back to the more than century-old classical exact solution due to Mie [1]. The analysis of a Mie-type theory uses a systematic expansion of the electromagnetic field over vector spherical harmonics [2–5]. The specific form of the expansions is also known as the  $T$ -matrix ansatz that has been widely used in the related problem of light scattering by nonspherical particles [4, 6, 7]. More recently, this strategy has been successfully applied to optically anisotropic particles [8–13].

The Mie solution, in its original form, applies to the scattering of plane electromagnetic waves by uniform optically isotropic spherical particles (the so-called Mie scatterers). For laser beams, it is generally necessary to go beyond the plane-wave approximation and light scattering from arbitrary shaped laser beams [14–18] has been the key subject of the Mie-type theory – the so-called generalized Lorenz–Mie theory (GLMT) – extended to the case of arbitrary incident-beam scattering [5, 19]. In such generalization of the Mie theory, the central and the most important task is to describe the illuminating beams in terms of expansions over a set of basis wavefunctions. In GLMT, a variety of methods were developed to evaluate the expansion coefficients that are referred to as the *beam shape coefficients* (for a recent review see Ref. [20] and references therein).

The central problem with laser beams is due to the fact that in their standard mathematical form, these beams are not radiation fields which are solutions to Maxwell's equations.

Typically, the analytical treatment of laser beams is performed using the paraxial approximation [21] and the beams are described as pseudo-fields which are only approximate solutions of the vector Helmholtz equation (higher order corrections can be used to improve the accuracy of the paraxial approximation [21, 22]).

Unfortunately, multipole expansions do not exist for such approximate pseudo-fields. Therefore, some remodelling procedure must be invoked to obtain a real radiation field which can be regarded as an approximation to the original paraxial beam.

The basic concept that might be called *matching the fields on a surface* lies at the heart of various traditional approaches to the laser beam remodelling and is based on the assumption that there is a surface where the actual incident field is equal to the paraxial field. Examples of physically reasonable and natural choice are scatterer-independent matching surfaces such as a far-field sphere [23], the focal plane (for beams with well-defined focal planes) [23, 24], and a Gaussian reference sphere representing a lens [25]. Given the paraxial field distribution on the matching surface, the beam shape coefficients can be evaluated using either numerical integration or the one-point matching method [23].

An alternative approach is to analytically describing the propagation of a laser beam, which is known in the paraxial limit, without recourse to the paraxial approximation. In Refs. [26–30] this strategy has been applied to the important case of Laguerre–Gaussian (LG) beams using different methods such as the vectorial Rayleigh–Sommerfeld formulas [27, 30], the vector angular spectrum method [29], approximating LG beams by nonparaxial beams with (near) cylindrical symmetry [26, 28].

The nonparaxial beams are solutions of Maxwell’s equations and the beam shape coefficients can be computed using the methods of GLMT. In recent studies of light scattering by spherical and spheroidal particles illuminated with LG beams [31, 32], the analytical results of Ref. [28] were used to calculate the beam shape coefficients.

In this paper, the problem of light scattering from LG beams that represent optical vortex laser beams exhibiting a helical phase front and carrying a phase singularity will be of our primary interest. The topological charge characterizing the phase singularity and associated orbital angular momentum gives rise to distinctive phenomena such as soliton generation [33], entanglement of photon quantum states, orbital angular momentum exchange with atoms and molecules (in addition to the collection of papers [34], see reviews in Ref. [35]), rotation and orbital motion of spherical particles illuminated with LG beams [36, 37].

In our calculations, we shall follow Refs. [10, 38] and use the  $T$ -matrix approach in which the far-field matching method is combined with the results for nonparaxial propagation of LG beams [29, 30]. Our goal is to examine the near-field structure of optical field depending on the parameters characterizing both the beam and the scatterer.

This structure has recently attracted considerable attention that was stimulated by an upsurge of interest in the so-called *photonic nanojets* and their applications (for a review see Ref. [39]). These nanojets were originally identified in finite-difference-time-domain simulations [40, 41] as narrow, high-intensity electromagnetic beams that propagate into background medium from the shadow-side surface of a plane-wave illuminated dielectric microcylinder [40] or microsphere [41] of diameter greater than the illuminating wavelength. There are several potentially important applications for the photonic nanojets to detect and manipulate nanoscale objects, subdiffraction-resolution nanopatterning and nanolithography, low-loss waveguiding, and ultra-density optical storage. These applications are reviewed in Ref. [39].

The layout of the paper is as follows: in Sec. 2, we outline our theoretical approach. The analytical results for the beam shape coefficients of LG beams and the fundamental properties of the far-field angular distributions are described in Sec. 3. The numerical procedure and the

results of numerical computations representing the near-field intensity distributions and phase maps of electric field components for purely azimuthal LG beams are presented in Sec. 4. Finally, in Sec. 5, we present our results and make some concluding remarks.

## 2. Lorenz–Mie theory: Wave functions and $T$ -matrix

In this section, we introduce all necessary notations and briefly discuss how the properties of Mie scattering can be described in terms of the  $T$ -matrix [2,4]. Our formulation closely follows to the line of our presentation given in Refs. [10,38].

We consider scattering by a spherical particle of radius  $R_p$  embedded in a uniform isotropic dielectric medium with dielectric constant  $\epsilon_{\text{med}}$  and magnetic permeability  $\mu_{\text{med}}$ . The dielectric constant and magnetic permittivity of the particle are  $\epsilon_p$  and  $\mu_p$ , respectively. For a harmonic electromagnetic wave (time-dependent factor is  $\exp\{-i\omega t\}$ ), the Maxwell equations can be written in the following form:

$$-ik_i^{-1} \nabla \times \mathbf{E} = \frac{\mu_i}{n_i} \mathbf{H}, \quad (1a)$$

$$ik_i^{-1} \nabla \times \mathbf{H} = \frac{n_i}{\mu_i} \mathbf{E}, \quad i = \begin{cases} \text{med}, & r > R_p \\ p, & r < R_p \end{cases} \quad (1b)$$

where  $n_{\text{med}} = \sqrt{\epsilon_{\text{med}}\mu_{\text{med}}}$  is the refractive index outside the scatterer (in the ambient medium), where  $r > R_p$  ( $i = \text{med}$ ) and  $k_i = k_{\text{med}} = n_{\text{med}}k_{\text{vac}}$  ( $k_{\text{vac}} = \omega/c = 2\pi/\lambda$  is the free-space wave number);  $n_p = \sqrt{\epsilon_p\mu_p}$  is the refractive index for the region inside the spherical particle (scatterer), where  $r < R_p$  ( $i = p$ ) and  $k_i = k_p = n_pk_{\text{vac}}$ .

The electromagnetic field can always be expanded using the vector spherical harmonic basis [42]. There are three cases of these expansions that are of particular interest. They correspond to the incident wave,  $\{\mathbf{E}_{\text{inc}}, \mathbf{H}_{\text{inc}}\}$ , the outgoing scattered wave,  $\{\mathbf{E}_{\text{sca}}, \mathbf{H}_{\text{sca}}\}$  and the electromagnetic field inside the scatterer,  $\{\mathbf{E}_p, \mathbf{H}_p\}$ :

$$\mathbf{E}_\alpha = \sum_{jm} [\alpha_{jm}^{(\alpha)} \mathbf{M}_{jm}^{(\alpha)}(\rho_i, \hat{\mathbf{r}}) + \beta_{jm}^{(\alpha)} \mathbf{N}_{jm}^{(\alpha)}(\rho_i, \hat{\mathbf{r}})], \quad \alpha \in \{\text{inc, sca, } p\} \quad (2a)$$

$$\mathbf{H}_\alpha = n_i/\mu_i \sum_{jm} [\alpha_{jm}^{(\alpha)} \mathbf{N}_{jm}^{(\alpha)}(\rho_i, \hat{\mathbf{r}}) - \beta_{jm}^{(\alpha)} \mathbf{M}_{jm}^{(\alpha)}(\rho_i, \hat{\mathbf{r}})], \quad (2b)$$

$$\mathbf{M}_{jm}^{(\alpha)}(\rho_i, \hat{\mathbf{r}}) = ik_i^{-1} \nabla \times \mathbf{N}_{jm}^{(\alpha)} = z_j^{(\alpha)}(\rho_i) \mathbf{Y}_{jm}^{(m)}(\hat{\mathbf{r}}), \quad (2c)$$

$$\mathbf{N}_{jm}^{(\alpha)}(\rho_i, \hat{\mathbf{r}}) = -ik_i^{-1} \nabla \times \mathbf{M}_{jm}^{(\alpha)} = \frac{\sqrt{j(j+1)}}{\rho_i} z_j^{(\alpha)}(\rho_i) \mathbf{Y}_{jm}^{(0)}(\hat{\mathbf{r}}) + Dz_j^{(\alpha)}(\rho_i) \mathbf{Y}_{jm}^{(e)}(\hat{\mathbf{r}}), \quad (2d)$$

$$i = \begin{cases} \text{med}, & \alpha \in \{\text{inc, sca}\} \\ p, & \alpha = p \end{cases}, \quad z_j^{(\alpha)}(\rho_i) = \begin{cases} j_j(\rho), & \alpha = \text{inc} \\ h_j^{(1)}(\rho), & \alpha = \text{sca}, \\ j_j(\rho_p), & \alpha = p \end{cases} \quad (2e)$$

where  $\rho \equiv \rho_{\text{med}} = k_{\text{med}}r$ ,  $\rho_p = k_p r \equiv n\rho$ , and  $n = n_p/n_{\text{med}}$  is the ratio of refractive indexes also known as the *optical contrast*;  $Df(x) \equiv x^{-1}\partial_x(xf(x))$ .

According to Ref. [10], the spherical harmonics can be conveniently expressed in terms of the Wigner  $D$ -functions [42, 43] as follows:

$$\mathbf{Y}_{jm}^{(m)}(\hat{\mathbf{r}}) = N_j/\sqrt{2} \{D_{m,-1}^{j*}(\hat{\mathbf{r}}) \mathbf{e}_{-1}(\hat{\mathbf{r}}) - D_{m,1}^{j*}(\hat{\mathbf{r}}) \mathbf{e}_{+1}(\hat{\mathbf{r}})\}, \quad (3a)$$

$$\mathbf{Y}_{jm}^{(e)}(\hat{\mathbf{r}}) = N_j/\sqrt{2} \{D_{m,-1}^{j*}(\hat{\mathbf{r}}) \mathbf{e}_{-1}(\hat{\mathbf{r}}) + D_{m,1}^{j*}(\hat{\mathbf{r}}) \mathbf{e}_{+1}(\hat{\mathbf{r}})\}, \quad (3b)$$

$$\mathbf{Y}_{jm}^{(0)}(\hat{\mathbf{r}}) = N_j D_{m,0}^{j*}(\hat{\mathbf{r}}) \mathbf{e}_0(\hat{\mathbf{r}}) = Y_{jm}(\hat{\mathbf{r}}) \hat{\mathbf{r}}, \quad N_j = [(2j+1)/4\pi]^{1/2}, \quad (3c)$$

where  $\mathbf{Y}_{jm}^{(m)}$ ,  $\mathbf{Y}_{jm}^{(e)}$  and  $\mathbf{Y}_{jm}^{(0)}$  are electric, magnetic and longitudinal harmonics, respectively;  $\mathbf{e}_{\pm 1}(\hat{\mathbf{r}}) = \mp(\mathbf{e}_x(\hat{\mathbf{r}}) \pm i\mathbf{e}_y(\hat{\mathbf{r}}))/\sqrt{2}$ ;  $\mathbf{e}_x(\hat{\mathbf{r}}) \equiv \hat{\boldsymbol{\theta}} = (\cos\theta \cos\phi, \cos\theta \sin\phi, -\sin\theta)$ ,  $\mathbf{e}_y(\hat{\mathbf{r}}) \equiv \hat{\boldsymbol{\varphi}} = (-\sin\phi, \cos\phi, 0)$  are the unit vectors tangential to the sphere;  $\phi$  ( $\theta$ ) is the azimuthal (polar) angle of the unit vector  $\hat{\mathbf{r}} = \mathbf{r}/r = (\sin\theta \cos\phi, \sin\theta \sin\phi, \cos\theta) \equiv \mathbf{e}_0(\hat{\mathbf{r}}) \equiv \mathbf{e}_z(\hat{\mathbf{r}})$ ;  $f(\hat{\mathbf{r}}) \equiv f(\phi, \theta)$ . (Hats will denote unit vectors and an asterisk will indicate complex conjugation).

Note that, for the irreducible representation of the rotation group with the angular number  $j$ , the  $D$ -functions,  $D_{m\nu}^j(\alpha, \beta, \gamma) = \exp(-im\alpha) d_{m\nu}^j(\beta) \exp(-i\nu\gamma)$ , give the elements of the rotation matrix parametrized by the three Euler angles [42, 43]:  $\alpha$ ,  $\beta$  and  $\gamma$ . In formulas (3) and throughout this paper, we assume that  $\gamma = 0$  and  $D_{m\nu}^j(\hat{\mathbf{r}}) \equiv D_{m\nu}^j(\phi, \theta, 0)$ . These  $D$ -functions meet the following orthogonality relations [42, 43]

$$\langle D_{m\nu}^{j*}(\hat{\mathbf{r}}) D_{m'\nu'}^j(\hat{\mathbf{r}}) \rangle_{\hat{\mathbf{r}}} = \frac{4\pi}{2j+1} \delta_{jj'} \delta_{mm'}, \quad (4)$$

where  $\langle f \rangle_{\hat{\mathbf{r}}} \equiv \int_0^{2\pi} d\phi \int_0^\pi \sin\theta d\theta f(\hat{\mathbf{r}})$ . The orthogonality condition (4) and Eqs. (3) show that a set of vector spherical harmonics is orthonormal:

$$\langle \mathbf{Y}_{jm}^{(\alpha)*}(\hat{\mathbf{r}}) \cdot \mathbf{Y}_{j'm'}^{(\beta)}(\hat{\mathbf{r}}) \rangle_{\hat{\mathbf{r}}} = \delta_{\alpha\beta} \delta_{jj'} \delta_{mm'}. \quad (5)$$

It can be shown [38] that the vector spherical harmonics (3) can also be recast into the well-known standard form [44]:

$$\mathbf{Y}_{jm}^{(m)}(\hat{\mathbf{r}}) = n_j \mathbf{L} Y_{jm} = -i\hat{\mathbf{r}} \times \mathbf{Y}_{jm}^{(e)}, \quad (6)$$

$$\mathbf{Y}_{jm}^{(e)}(\hat{\mathbf{r}}) = n_j r \nabla Y_{jm} = -i\hat{\mathbf{r}} \times \mathbf{Y}_{jm}^{(m)}, \quad n_j \equiv [j(j+1)]^{-1/2}, \quad (7)$$

where  $\partial_x$  stands for a derivative with respect to  $x$  and  $Y_{jm}(\hat{\mathbf{r}}) \equiv Y_{jm}(\phi, \theta)$  is the normalized spherical function;  $\mathbf{L}$  is the operator of angular momentum given by:

$$i\mathbf{L} = \mathbf{r} \times \nabla = \hat{\boldsymbol{\varphi}} \partial_\theta - \hat{\boldsymbol{\theta}} [\sin\theta]^{-1} \partial_\phi. \quad (8)$$

The vector wave functions,  $\mathbf{M}_{jm}^{(\alpha)}$  and  $\mathbf{N}_{jm}^{(\alpha)}$ , are the solenoidal solutions of the vector Helmholtz equation that can be derived (a discussion of the procedure can be found, e.g., in Ref. [45]) from solutions of the scalar Helmholtz equation,  $(\nabla^2 + k^2)\psi(\mathbf{r}) = 0$ , taken in the form:

$$\psi_{jm}^{(\alpha)} = n_j z_j^{(\alpha)}(kr) Y_{jm}(\hat{\mathbf{r}}), \quad n_j \equiv [j(j+1)]^{-1/2}, \quad (9)$$

where  $z_j^{(\alpha)}(x)$  is either a spherical Bessel function,  $j_j(x) = [\pi/(2x)]^{1/2} J_{j+1/2}(x)$ , or a spherical Hankel function [46],  $h_j^{(1,2)}(x) = [\pi/(2x)]^{1/2} H_{j+1/2}^{(1,2)}(x)$ .

In the far field region ( $\rho \gg 1$ ), the asymptotic behavior of the spherical Bessel and Hankel functions is known [46]:

$$i^{j+1}h_j^{(1)}(\rho), i^j Dh_j^{(1)}(\rho) \sim \exp(i\rho)/\rho, \quad (10)$$

$$(-i)^{j+1}h_j^{(2)}(\rho), (-i)^j Dh_j^{(2)}(\rho) \sim \exp(-i\rho)/\rho, \quad (11)$$

$$i^{j+1}j_j(\rho), i^{j+1}Dj_{j+1}(\rho) \sim [\exp(i\rho) - (-1)^j \exp(-i\rho)]/(2\rho). \quad (12)$$

So, the spherical Hankel functions of the first kind,  $h_j^{(1)}(\rho)$ , describe the outgoing waves, whereas those of the second kind,  $h_j^{(2)}(\rho)$ , represent the incoming waves.

Thus, outside the scatterer, the optical field is the sum of the incident wave field with  $z_j^{(\text{inc})}(\rho) = j_j(\rho)$  and the scattered waves with  $z_j^{(\text{sca})}(\rho) = h_j^{(1)}(\rho)$ , as required by the Sommerfeld radiation condition. The incident field is the field that would exist without a scatterer and therefore includes both incoming and outgoing parts (see Eq. (12)) because, without scattering, what comes in must go outwards again. As opposed to the spherical Hankel functions that are singular at the origin, the incident wave field should be finite everywhere, and thus, is described by the regular Bessel functions  $j_j(\rho)$ .

Now the incident wave is characterized by amplitudes  $\alpha_{jm}^{(\text{inc})}$ ,  $\beta_{jm}^{(\text{inc})}$  and the scattered outgoing waves are similarly characterized by amplitudes  $\alpha_{jm}^{(\text{sca})}$ ,  $\beta_{jm}^{(\text{sca})}$ . As long as the scattering problem is linear, the coefficients  $\alpha_{jm}^{(\text{sca})}$  and  $\beta_{jm}^{(\text{sca})}$  can be written as linear combinations of  $\alpha_{jm}^{(\text{inc})}$  and  $\beta_{jm}^{(\text{inc})}$ :

$$\begin{aligned} \alpha_{jm}^{(\text{sca})} &= \sum_{j',m'} \left[ T_{jm,j'm'}^{11} \alpha_{j'm'}^{(\text{inc})} + T_{jm,j'm'}^{12} \beta_{j'm'}^{(\text{inc})} \right], \\ \beta_{jm}^{(\text{sca})} &= \sum_{j',m'} \left[ T_{jm,j'm'}^{21} \alpha_{j'm'}^{(\text{inc})} + T_{jm,j'm'}^{22} \beta_{j'm'}^{(\text{inc})} \right]. \end{aligned} \quad (13)$$

These formulas define the elements of the  $T$ -matrix in the most general case.

In general, the scattering process mixes angular momenta [6]. The light scattering from uniformly anisotropic scatterers [10,11,47,48] provides an example of such a scattering process. By contrast, in simpler scattering processes, such angular momentum mixing does not take place. For example, radial anisotropy maintains the spherical symmetry of the scatterer [8,10,13]. The  $T$ -matrix of a spherically symmetric scatterer is diagonal over the angular momenta and the azimuthal numbers:  $T_{jj',mm'}^{nn'} = \delta_{jj'} \delta_{mm'} T_j^{nn'}$ .

In order to calculate the elements of  $T$ -matrix and the coefficients  $\alpha_{jm}^{(p)}$  and  $\beta_{jm}^{(p)}$ , we need to use the continuity for the tangential components of the electric and magnetic fields as boundary conditions at  $r = R_p$  ( $\rho = k_{\text{med}} R_p \equiv x$ ). Thus, the coefficients of the expansion for the wave field inside the scatterer,  $\alpha_{jm}^{(p)}$  and  $\beta_{jm}^{(p)}$ , are expressed in terms of the coefficients describing the incident light as follows:

$$i\alpha_{jm}^{(p)} = \frac{\alpha_{jm}^{(\text{inc})}}{\mu^{-1}v_j(x)u'_j(nx) - n^{-1}v'_j(x)u_j(nx)}, \quad \mu = \mu_p/\mu_{\text{med}}, \quad (14)$$

$$i\beta_{jm}^{(p)} = \frac{\beta_{jm}^{(\text{inc})}}{n^{-1}v_j(x)u'_j(nx) - \mu^{-1}v'_j(x)u_j(nx)}, \quad n = n_p/n_{\text{med}}, \quad (15)$$

where  $x = k_{\text{med}} R_p$ ,  $u_j(x) = x j_j(x)$  and  $v_j(x) = x h_j^{(1)}(x)$ . A similar result relates the scattered and incident waves:

$$\alpha_{jm}^{(\text{sca})} = T_j^{11} \alpha_{jm}^{(\text{inc})} = \frac{n^{-1} u_j'(x) u_j(nx) - \mu^{-1} u_j(x) u_j'(nx)}{\mu^{-1} v_j(x) u_j'(nx) - n^{-1} v_j'(x) u_j(nx)} \alpha_{jm}^{(\text{inc})}, \quad (16)$$

$$\beta_{jm}^{(\text{sca})} = T_j^{22} \beta_{jm}^{(\text{inc})} = \frac{\mu^{-1} u_j(x) u_j'(nx) - n^{-1} u_j'(x) u_j(nx)}{n^{-1} v_j(x) u_j'(nx) - \mu^{-1} v_j'(x) u_j(nx)} \beta_{jm}^{(\text{inc})}, \quad (17)$$

defining the  $T$ -matrix for the simplest case of a spherically symmetric scatterer. In addition, since the parity of electric and magnetic harmonics with respect to the spatial inversion  $\hat{\mathbf{r}} \rightarrow -\hat{\mathbf{r}}$  ( $\{\phi, \theta\} \rightarrow \{\phi + \pi, \pi - \theta\}$ ) is different:

$$\mathbf{Y}_{jm}^{(m)}(-\hat{\mathbf{r}}) = (-1)^j \mathbf{Y}_{jm}^{(m)}(\hat{\mathbf{r}}), \quad \mathbf{Y}_{jm}^{(e)}(-\hat{\mathbf{r}}) = (-1)^{j+1} \mathbf{Y}_{jm}^{(e)}(\hat{\mathbf{r}}), \quad (18)$$

where  $f(\hat{\mathbf{r}}) \equiv f(\phi, \theta)$  and  $f(-\hat{\mathbf{r}}) \equiv f(\phi + \pi, \pi - \theta)$ , they do not mix provided the mirror symmetry has not been broken. In this case the  $T$ -matrix is diagonal and  $T_j^{12} = T_j^{21} = 0$ . The diagonal elements  $T_j^{11} \equiv a_j$  and  $T_j^{22} \equiv b_j$  are also called the *Mie coefficients*.

### 3. Far-field matching

The formulas (14)–(17) are useful only if the expansion for the incident light beam is known. First we briefly review the most studied and fundamentally important case where the incident light is represented by a plane wave.

The electric field of a transverse plane wave propagating along the direction specified by a unit vector  $\hat{\mathbf{k}}_{\text{inc}}$  is:

$$\mathbf{E}_{\text{inc}} = \mathbf{E}^{(\text{inc})} \exp(i \mathbf{k}_{\text{inc}} \cdot \mathbf{r}), \quad \mathbf{E}^{(\text{inc})} = \sum_{\nu=\pm 1} E_\nu^{(\text{inc})} \mathbf{e}_\nu(\hat{\mathbf{k}}_{\text{inc}}), \quad \mathbf{k}_{\text{inc}} = k \hat{\mathbf{k}}_{\text{inc}}. \quad (19)$$

where the basis vectors  $\mathbf{e}_{\pm 1}(\hat{\mathbf{k}}_{\text{inc}})$  are perpendicular to  $\hat{\mathbf{k}}_{\text{inc}}$ . Then, the vector version of the well-known Rayleigh expansion (see, for example, [2, 10, 38]) immediately gives the expansion coefficients for the plane wave:

$$\alpha_{jm}^{(\text{inc})} = i \alpha_j \sum_{\nu=\pm 1} D_{m\nu}^j(\hat{\mathbf{k}}_{\text{inc}}) \nu E_\nu^{(\text{inc})}, \quad \beta_{jm}^{(\text{inc})} = -\alpha_j \sum_{\nu=\pm 1} D_{m\nu}^j(\hat{\mathbf{k}}_{\text{inc}}) E_\nu^{(\text{inc})}, \quad (20)$$

where  $\alpha_j = j^{j+1} [2\pi(2j+1)]^{1/2}$ .

Now, we consider a more general, case where an incident electromagnetic wave is written as a superposition of propagating plane waves:

$$\mathbf{E}_{\text{inc}}(\mathbf{r}) \equiv \mathbf{E}_{\text{inc}}(\rho, \hat{\mathbf{r}}) = \langle \exp(i\rho \hat{\mathbf{k}} \cdot \hat{\mathbf{r}}) \mathbf{E}_{\text{inc}}(\hat{\mathbf{k}}) \rangle_{\hat{\mathbf{k}}}, \quad \mathbf{E}_{\text{inc}}(\hat{\mathbf{k}}) = \sum_{\nu=\pm 1} E_\nu(\hat{\mathbf{k}}) \mathbf{e}_\nu(\hat{\mathbf{k}}), \quad (21a)$$

$$\mathbf{H}_{\text{inc}}(\mathbf{r}) \equiv \mathbf{H}_{\text{inc}}(\rho, \hat{\mathbf{r}}) = \frac{n}{\mu} \langle \exp(i\rho \hat{\mathbf{k}} \cdot \hat{\mathbf{r}}) [\hat{\mathbf{k}} \times \mathbf{E}_{\text{inc}}(\hat{\mathbf{k}})] \rangle_{\hat{\mathbf{k}}}, \quad (21b)$$

where  $\langle f \rangle_{\hat{\mathbf{k}}} \equiv \int_0^{2\pi} d\phi_k \int_0^\pi \sin \theta_k d\theta_k f$ .

Our first step is to examine asymptotic behavior of the wave field (21) in the far-field region,  $\rho \gg 1$ . The results can be easily obtained by using the asymptotic formula for a plane wave (see, e.g., [4])

$$\exp(i\rho \hat{\mathbf{k}} \cdot \hat{\mathbf{r}}) \sim \frac{-2\pi i}{\rho} [\exp(i\rho) \delta(\hat{\mathbf{k}} - \hat{\mathbf{r}}) - \exp(-i\rho) \delta(\hat{\mathbf{k}} + \hat{\mathbf{r}})] \quad \text{at } \rho \gg 1, \quad (22)$$

where  $\delta(\hat{\mathbf{k}} \mp \hat{\mathbf{r}})$  is the solid angle Dirac  $\delta$ -function symbolically defined through the expansion:

$$\delta(\hat{\mathbf{k}} \mp \hat{\mathbf{r}}) = \sum_{l=0}^{\infty} \sum_{m=-l}^l Y_{lm}(\pm \hat{\mathbf{r}}) Y_{lm}^*(\hat{\mathbf{k}}). \quad (23)$$

Applying relation (22) to the plane wave superposition (21a) gives the electric field of the incident wave in the far-field region:

$$\mathbf{E}_{\text{inc}}(\rho, \hat{\mathbf{r}}) \sim \mathbf{E}_{\text{inc}}^{(\infty)}(\rho, \hat{\mathbf{r}}) = \frac{1}{\rho} [\exp(i\rho) \mathbf{E}_{\text{out}}^{(\text{inc})}(\hat{\mathbf{r}}) + \exp(-i\rho) \mathbf{E}_{\text{in}}^{(\text{inc})}(\hat{\mathbf{r}})], \quad (24)$$

$$\mathbf{E}_{\text{in}}^{(\text{inc})}(\hat{\mathbf{r}}) = -\mathbf{E}_{\text{out}}^{(\text{inc})}(-\hat{\mathbf{r}}), \quad (25)$$

where  $\mathbf{E}_{\text{out}}(\hat{\mathbf{r}})$  is the far-field angular distribution for the outgoing part of the electric field of the incident wave:

$$\mathbf{E}_{\text{out}}^{(\text{inc})}(\hat{\mathbf{r}}) = -2\pi i \mathbf{E}_{\text{inc}}(\hat{\mathbf{r}}) = E_{\theta}^{(\text{out})}(\hat{\mathbf{r}}) \mathbf{e}_{\theta}(\hat{\mathbf{r}}) + E_{\phi}^{(\text{out})}(\hat{\mathbf{r}}) \mathbf{e}_{\phi}(\hat{\mathbf{r}}), \quad (26)$$

whereas the incoming part of the incident wave is described by the far-field angular distribution  $\mathbf{E}_{\text{in}}^{(\text{inc})}(\hat{\mathbf{r}})$ .

The result for the far-field distribution of the magnetic field (21b) can be written in the similar form:

$$\mathbf{H}_{\text{inc}}(\rho, \hat{\mathbf{r}}) \sim \mathbf{H}_{\text{inc}}^{(\infty)}(\rho, \hat{\mathbf{r}}) = \frac{1}{\rho} [\exp(i\rho) \mathbf{H}_{\text{out}}^{(\text{inc})}(\hat{\mathbf{r}}) + \exp(-i\rho) \mathbf{H}_{\text{in}}^{(\text{inc})}(\hat{\mathbf{r}})], \quad (27)$$

$$\mathbf{H}_{\text{in}}^{(\text{inc})}(\hat{\mathbf{r}}) = -\mathbf{H}_{\text{out}}^{(\text{inc})}(-\hat{\mathbf{r}}), \quad (28)$$

$$\mu/n \mathbf{H}_{\text{out}}^{(\text{inc})}(\hat{\mathbf{r}}) = \hat{\mathbf{r}} \times \mathbf{E}_{\text{out}}^{(\text{inc})}(\hat{\mathbf{r}}), \quad \mu/n \mathbf{H}_{\text{in}}^{(\text{inc})}(\hat{\mathbf{r}}) = \hat{\mathbf{r}} \times \mathbf{E}_{\text{out}}^{(\text{inc})}(-\hat{\mathbf{r}}). \quad (29)$$

Formulas (24)-(29) explicitly show that, in the far-field region, the incident wave field is defined by the angular distribution of the outgoing wave (26).

Alternatively, the far-field distribution of an incident light beam,  $\mathbf{E}_{\text{out}}^{(\text{inc})}(\hat{\mathbf{r}})$ , can be found from the expansion over the vector spherical harmonics (2a). The far-field asymptotics for the vector wave functions that enter the expansion for the incident wave (2):

$$\mathbf{M}_{jm}^{(\text{inc})}(\rho, \hat{\mathbf{r}}) \sim \frac{(-i)^{j+1}}{2\rho} [\exp(i\rho) \mathbf{Y}_{jm}^{(m)}(\hat{\mathbf{r}}) - \exp(-i\rho) \mathbf{Y}_{jm}^{(m)}(-\hat{\mathbf{r}})], \quad (30)$$

$$\mathbf{N}_{jm}^{(\text{inc})}(\rho, \hat{\mathbf{r}}) \sim \frac{(-i)^j}{2\rho} [\exp(i\rho) \mathbf{Y}_{jm}^{(e)}(\hat{\mathbf{r}}) - \exp(-i\rho) \mathbf{Y}_{jm}^{(e)}(-\hat{\mathbf{r}})], \quad (31)$$

can be derived from Eqs. (2c)-(2d) with the help of the far-field relation (12). Substituting Eqs. (30) and (31) into expansion (2a) gives the far-field distribution of the form (24) with:

$$\mathbf{E}_{\text{out}}^{(\text{inc})}(\hat{\mathbf{r}}) = 2^{-1} \sum_{jm} (-i)^{j+1} [\alpha_{jm}^{(\text{inc})} \mathbf{Y}_{jm}^{(m)}(\hat{\mathbf{r}}) + i\beta_{jm}^{(\text{inc})} \mathbf{Y}_{jm}^{(e)}(\hat{\mathbf{r}})]. \quad (32)$$

The coefficients of the incident wave can now easily be found as the Fourier coefficients of the far-field angular distribution,  $\mathbf{E}_{\text{out}}$ , expanded using the vector spherical harmonics basis (3). The final result reads:

$$\alpha_{jm}^{(\text{inc})} = 2 i^{j+1} \langle \mathbf{Y}_{jm}^{(m)*}(\hat{\mathbf{r}}) \cdot \mathbf{E}_{\text{out}}^{(\text{inc})}(\hat{\mathbf{r}}) \rangle_{\hat{\mathbf{r}}} = i\alpha_j \sum_{\nu=\pm 1} \nu \langle D_{m\nu}^j(\hat{\mathbf{k}}) E_{\nu}(\hat{\mathbf{k}}) \rangle_{\hat{\mathbf{k}}}, \quad (33a)$$

$$\beta_{jm}^{(\text{inc})} = 2 i^j \langle \mathbf{Y}_{jm}^{(e)*}(\hat{\mathbf{r}}) \cdot \mathbf{E}_{\text{out}}^{(\text{inc})}(\hat{\mathbf{r}}) \rangle_{\hat{\mathbf{r}}} = -\alpha_j \sum_{\nu=\pm 1} \langle D_{m\nu}^j(\hat{\mathbf{k}}) E_{\nu}(\hat{\mathbf{k}}) \rangle_{\hat{\mathbf{k}}}. \quad (33b)$$

A comparison between the expressions on the right hand side of Eq. (33) and those for the plane wave (20) shows that, in agreement with the representation (21a), the result for plane waves represents the limiting case where the angular distribution is singular:  $E_\nu(\hat{\mathbf{k}}) = E_\nu^{(\text{inc})} \delta(\hat{\mathbf{k}} - \hat{\mathbf{k}}_{\text{inc}})$ .

By using Eqs. (6) and (7) formulas (33) can conveniently be rewritten in the explicit form:

$$\begin{aligned} \alpha_{jm}^{(\text{inc})} &= 2n_j i^{j+1} \langle Y_{jm}^*(\hat{\mathbf{r}}) (\mathbf{L} \cdot \mathbf{E}_{\text{out}}^{(\text{inc})}(\hat{\mathbf{r}})) \rangle_{\hat{\mathbf{r}}} = \\ &2n_j i^j \int_0^{2\pi} d\phi \int_0^\pi d\theta Y_{jm}^*(\phi, \theta) \left[ \partial_\theta (\sin \theta E_\phi^{(\text{out})}) - \partial_\phi E_\theta^{(\text{out})} \right], \end{aligned} \quad (34a)$$

$$\begin{aligned} \beta_{jm}^{(\text{inc})} &= -2n_j i^j \langle Y_{jm}^*(\hat{\mathbf{r}}) (r \nabla \cdot \mathbf{E}_{\text{out}}^{(\text{inc})}(\hat{\mathbf{r}})) \rangle_{\hat{\mathbf{r}}} = \\ &-2n_j i^j \int_0^{2\pi} d\phi \int_0^\pi d\theta Y_{jm}^*(\phi, \theta) \left[ \partial_\theta (\sin \theta E_\theta^{(\text{out})}) + \partial_\phi E_\phi^{(\text{out})} \right], \end{aligned} \quad (34b)$$

which might be useful for computational purposes.

We conclude this section with the remark concerning the effect of translation:

$$\{\mathbf{E}_{\text{inc}}(\mathbf{r}), \mathbf{H}_{\text{inc}}(\mathbf{r})\} \rightarrow \{\mathbf{E}_{\text{inc}}(\mathbf{r} - \mathbf{r}_p), \mathbf{H}_{\text{inc}}(\mathbf{r} - \mathbf{r}_p)\} \quad (35)$$

on the far-field angular distribution (26). Note that, under the action of transformation (35), the focal plane is displaced from its initial position by the vector  $\mathbf{r}_p$ . From Eqs. (21) and (26), it follows that, for the far-field distribution (26), translation results in a phase shift:

$$\mathbf{E}_{\text{out}}^{(\text{inc})}(\hat{\mathbf{r}}) \rightarrow \mathbf{E}_{\text{out}}^{(\text{inc})}(\hat{\mathbf{r}}, \mathbf{r}_p) = \mathbf{E}_{\text{out}}^{(\text{inc})}(\hat{\mathbf{r}}) \exp[-ik(\mathbf{r}_p \cdot \hat{\mathbf{r}})]. \quad (36)$$

### 3.1. Poynting vector, Maxwell's stress tensor and optical force

From Eqs. (24)-(29), it is not difficult to obtain the far-field expression for the time-averaged Poynting vector of the incident wave  $\mathbf{S}_{\text{inc}} = c/(8\pi) \text{Re}(\mathbf{E}_{\text{inc}} \times \mathbf{H}_{\text{inc}}^*)$ :

$$\mathbf{S}_{\text{inc}}(\rho, \hat{\mathbf{r}}) \sim \mathbf{S}_{\text{inc}}^{(\infty)}(\rho, \hat{\mathbf{r}}) = \rho^{-2} \{ \mathbf{S}_{\text{in}}^{(\text{inc})}(\hat{\mathbf{r}}) + \mathbf{S}_{\text{out}}^{(\text{inc})}(\hat{\mathbf{r}}) \}, \quad (37)$$

$$\mathbf{S}_{\text{in}}^{(\text{inc})}(\hat{\mathbf{r}}) = -\mathbf{S}_{\text{out}}^{(\text{inc})}(-\hat{\mathbf{r}}), \quad \mu/n \mathbf{S}_{\text{out}}^{(\text{inc})}(\hat{\mathbf{r}}) = c/(8\pi) |\mathbf{E}_{\text{out}}^{(\text{inc})}(\hat{\mathbf{r}})|^2 \hat{\mathbf{r}}, \quad (38)$$

where  $|\mathbf{E}_{\text{out}}^{(\text{inc})}(\hat{\mathbf{r}})|^2 = (\mathbf{E}_{\text{out}}^{(\text{inc})}(\hat{\mathbf{r}}) \cdot [\mathbf{E}_{\text{out}}^{(\text{inc})}(\hat{\mathbf{r}})]^*)$ . From this expression, it immediately follows that the flux of the Poynting vector for the outgoing wave,  $\mathbf{S}_{\text{out}}^{(\text{inc})}(\hat{\mathbf{r}})$ , through a sphere  $S_f$  of sufficiently large radius,  $R_f$ , is exactly balanced by the flux of Poynting vector of the incoming wave,  $\mathbf{S}_{\text{in}}^{(\text{inc})}(\hat{\mathbf{r}})$ .

For the total optical field, which is a sum of the incident and scattered wavefields, the electric and magnetic fields in the far-field region can also be separated into incoming and the outgoing portions as follows:

$$\mathbf{E}_{\text{tot}} = \mathbf{E}_{\text{inc}} + \mathbf{E}_{\text{sca}} \sim \mathbf{E}_{\text{tot}}^{(\infty)} = \frac{1}{\rho} [\exp(i\rho) \mathbf{E}_{\text{out}}(\hat{\mathbf{r}}) + \exp(-i\rho) \mathbf{E}_{\text{in}}(\hat{\mathbf{r}})], \quad (39)$$

$$\mathbf{H}_{\text{tot}} = \mathbf{H}_{\text{inc}} + \mathbf{H}_{\text{sca}} \sim \mathbf{H}_{\text{tot}}^{(\infty)} = \frac{1}{\rho} [\exp(i\rho) \mathbf{H}_{\text{out}}(\hat{\mathbf{r}}) + \exp(-i\rho) \mathbf{H}_{\text{in}}(\hat{\mathbf{r}})], \quad (40)$$

$$\mu/n \mathbf{H}_{\text{out}}(\hat{\mathbf{r}}) = \hat{\mathbf{r}} \times \mathbf{E}_{\text{out}}(\hat{\mathbf{r}}), \quad \mu/n \mathbf{H}_{\text{in}}(\hat{\mathbf{r}}) = -\hat{\mathbf{r}} \times \mathbf{E}_{\text{in}}(\hat{\mathbf{r}}), \quad (41)$$

$$\mathbf{E}_{\text{out}}(\hat{\mathbf{r}}) = \mathbf{E}_{\text{out}}^{(\text{inc})}(\hat{\mathbf{r}}) + \mathbf{E}_{\text{out}}^{(\text{sca})}(\hat{\mathbf{r}}), \quad \mathbf{E}_{\text{in}}(\hat{\mathbf{r}}) = -\mathbf{E}_{\text{out}}^{(\text{inc})}(-\hat{\mathbf{r}}), \quad (42)$$

where, similar to the case of the incident wave (32), the far-field angular distribution of the scattered wave,  $\mathbf{E}_{\text{out}}^{(\text{sca})}(\hat{\mathbf{r}})$ , is determined by the expansion in vector spherical harmonics:

$$\mathbf{E}_{\text{out}}^{(\text{sca})}(\hat{\mathbf{r}}) = \sum_{jm} (-i)^{j+1} \left[ \alpha_{jm}^{(\text{sca})} \mathbf{Y}_{jm}^{(m)}(\hat{\mathbf{r}}) + i\beta_{jm}^{(\text{sca})} \mathbf{Y}_{jm}^{(e)}(\hat{\mathbf{r}}) \right]. \quad (43)$$

We can now generalize the Poynting vector expression (37) to the case of the total wavefield given in Eqs. (39)–(41):

$$\mu/n \mathbf{S}_{\text{tot}}^{(\infty)}(\rho, \hat{\mathbf{r}}) = \frac{c}{8\pi\rho^2} \left\{ |\mathbf{E}_{\text{out}}(\hat{\mathbf{r}})|^2 - |\mathbf{E}_{\text{in}}(\hat{\mathbf{r}})|^2 \right\} \hat{\mathbf{r}}, \quad (44)$$

and use the relations (42) to evaluate the flux of the Poynting vector (44) through the far-field sphere  $S_f$  of the radius  $R_f$ . The result can be written in the following well-known form:

$$\oiint_{S_f} (\mathbf{S}_{\text{tot}}^{(\infty)} \cdot d\mathbf{s}) = R_f^2 \langle (\mathbf{S}_{\text{tot}}^{(\infty)}(kR_f, \hat{\mathbf{r}}) \cdot \hat{\mathbf{r}}) \rangle_{\hat{\mathbf{r}}} \equiv -W_{\text{abs}} = W_{\text{sca}} - W_{\text{ext}}, \quad (45)$$

$$W_{\text{sca}} = \frac{cn}{8\pi\mu k^2} \langle |\mathbf{E}_{\text{out}}^{(\text{sca})}(\hat{\mathbf{r}})|^2 \rangle_{\hat{\mathbf{r}}}, \quad W_{\text{ext}} = -\frac{cn}{4\pi\mu k^2} \text{Re} \langle (\mathbf{E}_{\text{out}}^{(\text{sca})}(\hat{\mathbf{r}}) \cdot [\mathbf{E}_{\text{out}}^{(\text{inc})}(\hat{\mathbf{r}})]^*) \rangle_{\hat{\mathbf{r}}}, \quad (46)$$

where  $W_{\text{sca}}$  is the energy scattering rate (the rate at which the scattered energy crosses the sphere in an outward direction),  $W_{\text{abs}}$  is the energy absorption rate and  $W_{\text{ext}} = W_{\text{sca}} + W_{\text{abs}}$  is the extinction rate. When the scatterer and the surrounding medium are both non-absorbing, the energy absorption rate vanishes,  $W_{\text{abs}} = 0$ , and Eq. (45) yields unitarity relations for the  $T$ -matrix [4]. In our spherically symmetric case, these are:  $|2T_j^{11} + 1| = |2T_j^{22} + 1| = 1$ .

The far-field angular distributions,  $\mathbf{E}_{\text{out}}^{(\text{sca})}(\hat{\mathbf{r}})$  and  $\mathbf{E}_{\text{out}}^{(\text{inc})}(\hat{\mathbf{r}})$ , also determine the time-averaged optical force,  $\mathbf{F}$ , acting upon the particle. This force can be expressed in terms of the time-average of Maxwell's stress tensor  $\mathbf{T}_M$ :

$$\mathbf{T}_M = \frac{1}{8\pi} \text{Re} \{ \epsilon \mathbf{E} \otimes \mathbf{E}^* + \mu \mathbf{H} \otimes \mathbf{H}^* - \mathbf{I}_3 (\epsilon |\mathbf{E}|^2 + \mu |\mathbf{H}|^2) / 2 \}, \quad (47)$$

where  $\mathbf{I}_3$  is the  $3 \times 3$  identity matrix, as follows:

$$\mathbf{F} = \oiint_{S_f} (\mathbf{T}_M^{(\infty)} \cdot d\mathbf{s}), \quad (48)$$

where  $\mathbf{T}_M^{(\infty)}$  is the Maxwell stress tensor (47) in the far-field region. Substituting Eqs. (39)–(41) into the stress tensor (47) gives the following expression for the dot product:

$$(\mathbf{T}_M^{(\infty)} \cdot \hat{\mathbf{r}}) = -\frac{\epsilon}{8\pi\rho^2} \left\{ |\mathbf{E}_{\text{out}}(\hat{\mathbf{r}})|^2 + |\mathbf{E}_{\text{in}}(\hat{\mathbf{r}})|^2 \right\} \hat{\mathbf{r}}, \quad (49)$$

that enter the integrand on the right-hand side of Eq. (48). The final result for the optical force reads:

$$\mathbf{F}(\mathbf{r}_p) = -\frac{\epsilon}{8\pi k^2} \left\{ \langle \hat{\mathbf{r}} |\mathbf{E}_{\text{out}}^{(\text{sca})}(\hat{\mathbf{r}}, \mathbf{r}_p)|^2 \rangle_{\hat{\mathbf{r}}} + 2 \langle \hat{\mathbf{r}} \text{Re} (\mathbf{E}_{\text{out}}^{(\text{sca})}(\hat{\mathbf{r}}, \mathbf{r}_p) \cdot [\mathbf{E}_{\text{out}}^{(\text{inc})}(\hat{\mathbf{r}}, \mathbf{r}_p)]^*) \rangle_{\hat{\mathbf{r}}} \right\}, \quad (50)$$

where we have indicated that the net force exerted on the particle depends on the displacement vector  $\mathbf{r}_p$  describing position of the scatterer with respect to the focal plane.

### 3.2. Remodelled Laguerre–Gaussian beams

In the paraxial approximation, the beams are described in terms of scalar fields of the form:  $u(\mathbf{r}) \exp(ikz)$ , where  $u(\mathbf{r})$  is a solution of the paraxial Helmholtz equation:

$$[\nabla_{\perp}^2 + 2ik\partial_z]u = 0, \quad \nabla_{\perp}^2 = \partial_x^2 + \partial_y^2. \quad (51)$$

For LG beams, the solution can be conveniently written in the cylindrical coordinate system,  $(r_{\perp}, \phi, z)$ , as follows

$$u_{nm}(r_{\perp}, \phi, z) = |\sigma|^{-1} \psi_{nm}(\sqrt{2}r_{\perp}/w) \exp\{-r_{\perp}^2/(w_0^2\sigma) + im\phi - i\gamma_{nm}\}, \quad (52a)$$

$$\sigma \equiv \sigma(z) = 1 + iz/z_R, \quad w \equiv w(z) = w_0|\sigma|, \quad (52b)$$

$$\gamma_{nm} \equiv \gamma_{nm}(z) = (2n + m + 1) \arctan(z/z_R), \quad \psi_{nm}(x) = x^{|m|} L_n^{|m|}(x^2), \quad (52c)$$

where  $L_n^m$  is the generalized Laguerre polynomial given by [49]:

$$L_n^m(x) = (n!)^{-1} x^{-m} \exp(x) \partial_x^n [x^{n+m} \exp(-x)], \quad (53)$$

where  $n$  ( $m$ ) is the radial (azimuthal) mode number;  $w_0$  is the initial transverse Gaussian half-width (the beam diameter at waist)  $z_R = kw_0^2/2 = [2kf^2]^{-1}$  is the Rayleigh range and  $f = [kw_0]^{-1}$  is the *focusing parameter*.

The problem studied in Refs. [27, 29, 30] deals with the exact propagation of the optical field in the half-space,  $z > 0$ , when its transverse components at the initial (source) plane,  $z = 0$ , are known. In Ref. [29], the results describing asymptotic behavior of the linearly polarized field:

$$\mathbf{E}(r_{\perp}, \phi, 0) = u_{nm}(r_{\perp}, \phi, 0) \hat{\mathbf{x}} = \psi_{nm}(\sqrt{2}r_{\perp}/w_0) \exp\{-r_{\perp}^2/w_0^2 + im\phi\} \hat{\mathbf{x}}, \quad (54)$$

were derived using the angular spectrum representation (Debye integrals) and comply with both results of rigorous mathematical analysis performed in Ref. [50] and those obtained using the vectorial Rayleigh-Sommerfeld integrals [27, 30]. The resulting expression for the far-field angular distribution can be written in the following form:

$$\mathbf{E}_{\text{out}}^{(\text{LG})}(\phi, \theta) = E_{nm}(f^{-1} \sin \theta / \sqrt{2}) \exp(im\phi) \mathbf{e}_{\text{out}}, \quad (55a)$$

$$\mathbf{e}_{\text{out}} = \cos \phi \mathbf{e}_{\theta}(\hat{\mathbf{r}}) - \cos \theta \sin \phi \mathbf{e}_{\phi}(\hat{\mathbf{r}}) = \cos \theta \hat{\mathbf{x}} - \sin \theta \cos \phi \hat{\mathbf{z}}, \quad (55b)$$

$$E_{nm}(x) = \frac{x^m}{i^{2n+m+1} 2 f^2} L_n^m(x^2) \exp(-x^2/2). \quad (55c)$$

We can now combine relations (26) and (21) with the outgoing part of the far-field distribution (55a) to deduce the expression for the electric field of the remodelled LG beam:

$$\begin{aligned} \mathbf{E}_{\text{inc}}^{(\text{LG})}(\rho_{\perp}, \phi, \rho_z) &= E_x^{(\text{LG})}(\rho_{\perp}, \phi, \rho_z) \hat{\mathbf{x}} + E_z^{(\text{LG})}(\rho_{\perp}, \phi, \rho_z) \hat{\mathbf{z}} = \\ &= \frac{i}{2\pi} \langle \exp[i(\rho_{\perp} \sin \theta_k \cos(\phi - \phi_k) + \rho_z \cos \theta_k)] \mathbf{E}_{\text{out}}^{(\text{LG})}(\hat{\mathbf{k}}) \rangle_{\hat{\mathbf{k}}}, \end{aligned} \quad (56)$$

where  $\rho_{\perp} = kr_{\perp}$  and  $\rho_z = kz$ .

### 3.3. Laser beam symmetries

In Sec. 3.1, we have shown that the scattering characteristics such as the cross-sections and the radiation force can be expressed in terms of the far-field angular distributions that can be regarded as vector fields on a sphere. Under the action of the orthogonal transformation  $M$ :  $\hat{\mathbf{r}} \mapsto \hat{\mathbf{r}}' = M\hat{\mathbf{r}}$ , such fields transform as follows:

$$\mathbf{E}_{\text{out}}(\hat{\mathbf{r}}) \mapsto \mathbf{E}'_{\text{out}} = M\mathbf{E}_{\text{out}}(M^{-1}\hat{\mathbf{r}}). \quad (57)$$

From Eqs. (21a) and (50), we derive the following relations:

$$\mathbf{E}_{\text{inc}}(\mathbf{r}) \mapsto \mathbf{E}'_{\text{inc}} = M\mathbf{E}_{\text{inc}}(M^{-1}\mathbf{r}), \quad \mathbf{F}[\mathbf{E}_{\text{out}}] \mapsto \mathbf{F}[\mathbf{E}'_{\text{out}}] = M\mathbf{F}[\mathbf{E}_{\text{out}}], \quad (58)$$

which define transformations of the incident wave and the optical force.

The symmetry transformation  $M_s$  for the far-field angular distribution of the incident wave may generally be defined through the symmetry relation:

$$M_s \mathbf{E}_{\text{out}}^{(\text{inc})}(M_s^{-1}\hat{\mathbf{r}}) = U_s \mathbf{E}_{\text{out}}^{(\text{inc})}(\hat{\mathbf{r}}), \quad (59)$$

where  $U_s$  is the matrix of a unitary transformation. At  $|\mathbf{r}_p| \neq 0$ , we can use Eq. (36) combined with the orthogonality relation:  $(\hat{\mathbf{r}} \cdot \mathbf{r}_p) = (M_s^{-1}\hat{\mathbf{r}} \cdot M_s^{-1}\mathbf{r}_p)$  to recast the symmetry condition (59) in the form:

$$U_s \mathbf{E}_{\text{out}}^{(\text{inc})}(\hat{\mathbf{r}}, \mathbf{r}_p) = M_s \mathbf{E}_{\text{out}}^{(\text{inc})}(M_s^{-1}\hat{\mathbf{r}}, M_s^{-1}\mathbf{r}_p). \quad (60)$$

As a direct consequence of the generalized symmetry relation (60) for the optical force, we have:

$$\mathbf{F}(\mathbf{r}_p) = M_s \mathbf{F}(M_s^{-1}\mathbf{r}_p), \quad \mathbf{K}(\mathbf{r}_p) = M_s \mathbf{K}(M_s^{-1}\mathbf{r}_p) M_s^{-1}, \quad (61)$$

where the elements of the stiffness (force) matrix  $\mathbf{K}(\mathbf{r}_p)$  are given by:

$$K_{ij}(\mathbf{r}_p) = \partial_j F_i(\mathbf{r}_p). \quad (62)$$

At equilibria, the force vanishes ( $\mathbf{F}(\mathbf{r}_{\text{eq}}) = \mathbf{0}$ ) and the stiffness matrix,  $\mathbf{K}_{\text{eq}} = \mathbf{K}(\mathbf{r}_{\text{eq}})$ , is known to govern the regime of linearized particle dynamics [51].

For the LG beams with the angular distribution (55a), it can easily be verified if the direction of propagation (the  $z$  axis) is the axis of twofold rotational symmetry  $C_2$  with  $C_2 : \phi \mapsto \phi + \pi$  and  $C_2 = \text{diag}(-1, -1, 1)$ . From Eq. (55a), we have:

$$C_2 \mathbf{E}_{\text{out}}^{(\text{LG})}(C_2 \hat{\mathbf{r}}) = C_2 \mathbf{E}_{\text{out}}^{(\text{LG})}(\phi + \pi, \theta) = (-1)^{m+1} \mathbf{E}_{\text{out}}^{(\text{LG})}(\hat{\mathbf{r}}). \quad (63)$$

When  $\mathbf{r}_d \parallel \hat{\mathbf{z}}$  and  $C_2 \mathbf{r}_d = \mathbf{r}_d$ , equation (61) for the twofold symmetry implies that the optical force is directed along the symmetry axis,  $\mathbf{F} \parallel \hat{\mathbf{z}}$ , and the stiffness matrix is of the form:

$$\mathbf{K} = \begin{pmatrix} K_{xx} & K_{xy} & 0 \\ K_{yx} & K_{yy} & 0 \\ 0 & 0 & K_{zz} \end{pmatrix}. \quad (64)$$

Since  $C_2 \mathbf{Y}_{jm}^{(e,m)}(C_2 \hat{\mathbf{r}}) = (-1)^m \mathbf{Y}_{jm}^{(e,m)}(\hat{\mathbf{r}})$ , for  $C_2$  symmetric LG beams, the azimuthal numbers of nonvanishing beam shape coefficients are of the same parity (all  $m$  are either odd or even).

#### 4. Near-field nanostructures

In this section, we present the results of numerical computations for the light scattering problem for the case where the incident wave is represented by the remodelled LG beams (56) with the vanishing radial mode number  $n = 0$  and the nonzero azimuthal number,  $m = m_{\text{LG}} \geq 0$ . Such beams are also known as *purely azimuthal LG beams* [52].

In agreement with our symmetry analysis, substituting the far-field distribution (55) into Eq. (34) gives the beam shape coefficients of these beams in the following form:

$$\alpha_{jm}^{(\text{inc})} = \alpha_{j, m_{\text{LG}}}^{(+)} \delta_{m, m_{\text{LG}}+1} + \alpha_{j, m_{\text{LG}}}^{(-)} \delta_{m, m_{\text{LG}}-1}, \quad (65a)$$

$$\beta_{jm}^{(\text{inc})} = \beta_{j, m_{\text{LG}}}^{(+)} \delta_{m, m_{\text{LG}}+1} + \beta_{j, m_{\text{LG}}}^{(-)} \delta_{m, m_{\text{LG}}-1}. \quad (65b)$$

Then, the coefficients of expansions (2) describing scattered wave and electromagnetic field inside the scatterer can be evaluated from formulas (14)–(17).

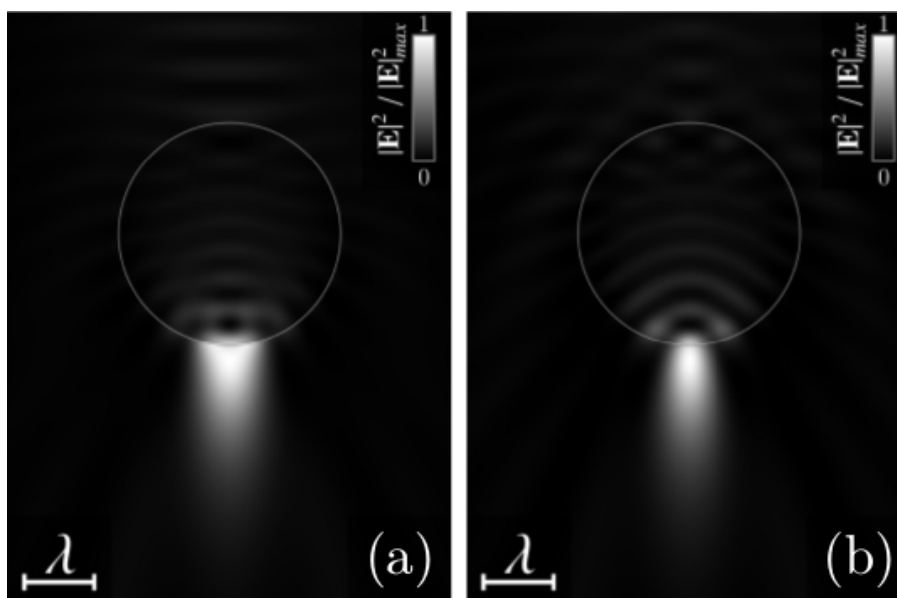


FIG. 1. Near-field intensity distributions of the total wavefield in (a) the  $x - z$  plane and (b) the  $y - z$  plane for the LG beam with  $m_{\text{LG}} = 0$ ,  $f = 0.05$  and  $|\mathbf{r}_p| = 0$ . The parameters are:  $R_p = 1.5\lambda$  is the scatterer radius and  $n_p = 1.3$  ( $n_{\text{med}} = 1.0$ ) is the refractive index inside (outside) the particle.

#### 4.1. Photonic nanojets

For spherical particles illuminated by plane waves, the formation of photonic nanojets and their structure was previously discussed in Refs. [53–55]. Plane waves can be regarded as Gaussian beams with  $n = m_{\text{LG}} = 0$  and sufficiently small focusing parameter,  $f \ll 1$ , which is defined after Eq. (53) through the ratio of wavelength,  $\lambda$ , and the beam diameter at waist,  $w_0$ ,  $f = (2\pi)^{-1}\lambda/w_0$ . This limiting case is illustrated in Fig. 1 which shows the near-field intensity distributions for the total light wavefield in both the  $x - z$  and the  $y - z$  planes computed at  $m_{\text{LG}} = 0$  and  $f = 0.05$  for the spherical particle of the radius  $R_p = 1.5\lambda$  with the refractive index  $n_p = 1.33$  (water) located in air ( $n_m = 1$ ).

It can be seen that the distributions are characterized by the presence of elongated focusing zones formed near the shadow surface of the scatterer. The transverse sizes of these zones are smaller than the wavelength of incident light, whereas their longitudinal size in the direction of incidence, which is along the  $z$  axis from top to bottom, is relatively large. Such a jetlike light structure is typical for the photonic nanojets. The characteristic length and width of nanojets along with the peak intensity are known to strongly depend on a number of factors, such as the scatterer size  $R_p$ , the particle absorption coefficient and the optical contrast ratio  $n_p/n_m$ . For microspheres, the results of a comprehensive numerical analysis including the case of shell particles are summarized in a recent paper [55].

The effects of non-plane incident waves, such as laser beams on the structure of photonic nanojets, are much less studied. Some theoretical results for tightly focused Gaussian beams are reported in Ref. [56] and the case of Bessel-Gauss beams was studied experimentally in [57].

For the LG beams, we begin with the effects of the azimuthal mode number and describe what happens to the near-field structure shown in Fig. 1 when the azimuthal number takes the smallest nonzero value,  $m_{\text{LG}} = 1$ . The latter represents the simplest case of an optical vortex beam in which, owing to the presence of phase singularity, the intensity of incident light at the beam axis (the  $z$  axis) vanishes (see Fig. 2(a)). From Fig. 2, it can be seen that, even though

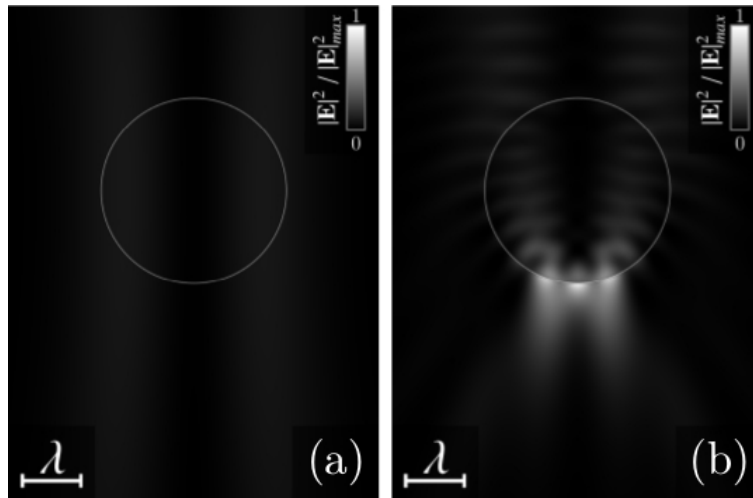


FIG. 2. Near-field intensity distribution in the  $x - z$  plane of (a) the incident wave beam and (b) the total wavefield for the LG beam with  $m_{\text{LG}} = 1$ ,  $f = 0.1$  and  $|\mathbf{r}_p| = 0$ . Other parameters are described in the caption of Fig. 1.

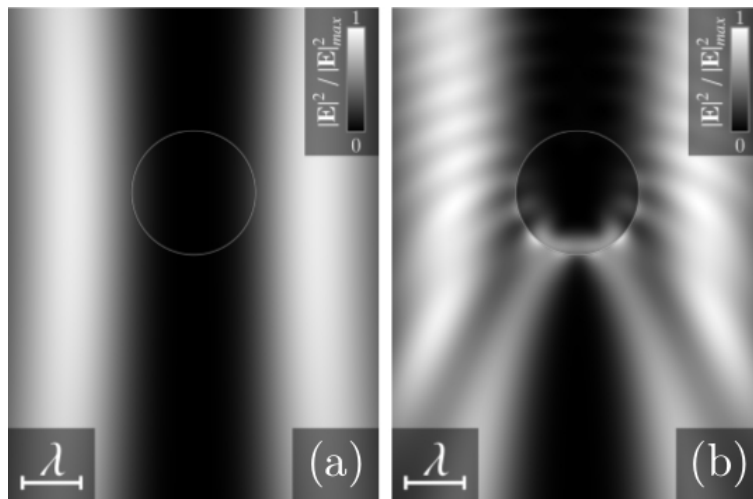


FIG. 3. Near-field intensity distribution in the  $x - z$  plane of (a) the incident wave beam and (b) the total wave field for the LG beam with  $m_{\text{LG}} = 2$ ,  $f = 0.08$  and  $|\mathbf{r}_p| = 0$ .

the bulk part of the scatterer is in the low intensity region surrounding the optical vortex, the scattering process is efficient enough to produce scattered waves that result in the formation of a pronounced jetlike photonic flux, emerging from the surface of the particle's shadow (see Fig. 2(b)).

A comparison between Fig. 2(b) and Fig. 1(a) shows that the three-peak structure of the photonic jet formed with Mie scattering of the optical vortex LG beam with  $m_{\text{LG}} = 1$  significantly differs from the well-known shape of the nanojet at  $m_{\text{LG}} = 0$ . Interestingly, similar to the case of Gaussian beams with  $m_{\text{LG}} = 0$ , the focusing zones at  $m_{\text{LG}} = 1$  involve the beam axis where one of the light intensity peaks is located.

From Fig. 2, it can be seen that, even though the bulk part of the scatterer is in the low intensity region surrounding the optical vortex, the scattering process is efficient enough to produce scattered waves that result in the formation of a pronounced jetlike photonic flux

emerging from the surface of the particle's shadow (see Fig. 2(b)). Figure 3 demonstrates that, for the weakly focused LG beam with  $f = 0.08$ , this effect can be even more pronounced at  $m_{\text{LG}} = 2$ .

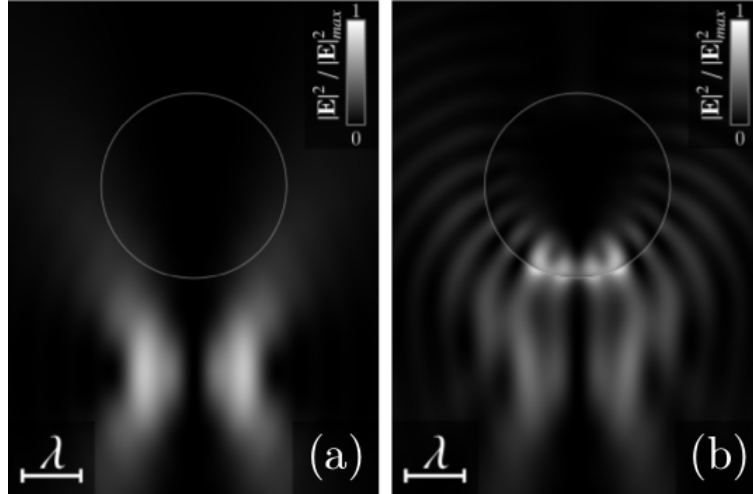


FIG. 4. Near-field intensity distribution in the  $x-z$  plane of (a) the incident wave beam and (b) the total wave field for the LG beam with  $m_{\text{LG}} = 2$ ,  $f = 0.25$  and  $\mathbf{r}_p = (0, 0, 3\lambda)$ .

The results for tightly focused LG beams with  $m_{\text{LG}} = 2$  and  $f = 0.25$  are shown in Fig. 4. When the displacement vector,  $\mathbf{r}_p$  defined in Eqs. (35) vanishes, the focal (waist) plane of the incident LG beam is  $z = 0$  and the bulk part of the four-peak structure of the focusing zones is localized inside of the particles. For  $\mathbf{r}_p = (0, 0, 3\lambda)$ , the focal plane,  $z = 3\lambda$ , is located behind the particle (see Fig. 4(a)). From Fig. 4(b), it is seen that four peaks of light intensity now develop in the immediate vicinity of the scatterer surface.

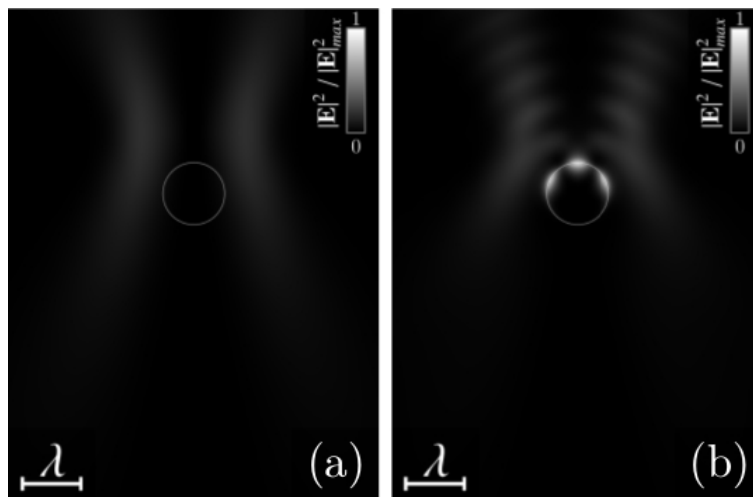


FIG. 5. Near-field intensity distribution in the  $x-z$  plane of (a) the incident wave beam and (b) the total wave field for the LG beam with  $m_{\text{LG}} = 2$ ,  $f = 0.2$  and  $\mathbf{r}_p = (0, 0, \lambda)$ . The small scatterer ( $R_p = 0.5\lambda$ ) is made of the negative index (left-handed) metamaterial with  $\epsilon_p = \mu_p = -1$ .

What all the wavefields depicted in Figs. 2(b)–4(b) have in common is that, in contrast to the incident optical vortex beams with  $m_{\text{LG}} = 1$  and  $m_{\text{LG}} = 2$ , the light intensity at the

incident beam axis (the  $z$  axis) clearly differs from zero. In other words, in the near-field region, the optical vortex with  $0 < |m_{\text{LG}}| \leq 2$  has been destroyed by Mie scattering. As it will be explained in the subsequent section this is no longer the case at  $m_{\text{LG}} \geq 3$ .

In the conclusion of this section, we briefly discuss the structure of the nanojets for scatterers made of the negative index (left-handed or double negative) metamaterial (such materials are reviewed in a number of books and papers [58–61]). This is case where  $\text{Re } \epsilon_p$  and  $\text{Re } \mu_p$  are both negative. For the limiting case of a nonabsorbing Veselago medium [62] with  $\epsilon_p = \mu_p = -1$ , Fig. 5 shows a rather unusual nanojet structure formed in the illuminated part of the small particle as opposed to the structures shown in Figs. 1–4. An important point is that, in real metamaterials, the effects of absorption cannot be neglected. In particular, these effects may prevent formation of jetlike structures near metallic particles and this is why, to the best of our knowledge, the current literature on photonic nanojets has been focused exclusively on the case of dielectric scattering. Figure 6 demonstrates that a jetlike structure may form near the shadow surface of a metallic particle illuminated by a vortex laser beam (the LG beam with  $m_{\text{LG}} = 1$ ). A comprehensive study of absorption effects in metallic and metamaterial scatterers is well beyond the scope of this paper and the corresponding results will be published elsewhere.

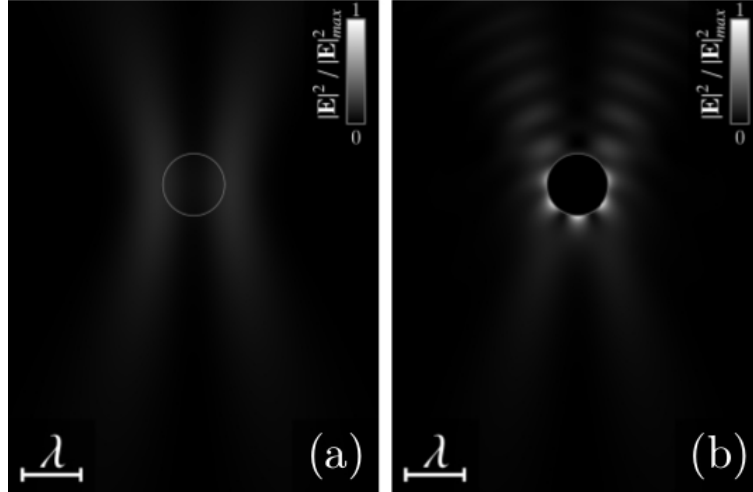


FIG. 6. Near-field intensity distribution in the  $x - z$  plane of (a) the incident wave beam and (b) the total wave field for the LG beam with  $m_{\text{LG}} = 1$ ,  $f = 0.2$  and  $\mathbf{r}_p = (0, 0, \lambda)$ . The metallic scatterer ( $R_p = 0.5\lambda$ ) is made of gold with  $\epsilon_p \approx -22 + 1.8i$  ( $\lambda \approx 800$  nm).

## 4.2. Optical vortices

In this section, we consider optical vortices and their near-field structure. The optical vortices are known to represent phase singularities of complex-valued scalar waves which are zeros of the wavefield  $\psi = |\psi| \exp(i\chi)$  where its phase  $\chi$  is undefined. A phase singularity is characterized by the topological vortex charge  $m_V$ , defined as the closed loop contour integral of the wave phase  $\chi$  modulo  $2\pi$ :

$$m_V = \frac{1}{2\pi} \oint_L d\chi, \quad (66)$$

where  $L$  is the closed path around the singularity.

Optical vortices associated with the individual components of electric field will be of our primary concern. More specifically, we shall examine the optical vortex structure of the

components  $E_z$  and  $E_x$  in the planes  $z = z_0$  parallel to the  $x - y$  plane. Since, in such planes, circles naturally play the role of closed loops, the starting point of our analysis is the electric field vector, expressed as a function of the azimuthal angle  $\phi$  in the following form:

$$\mathbf{E} = \sum_{\mu=-2}^2 \mathbf{E}_\mu \exp[i(m_{\text{LG}} + \mu)\phi], \quad (67)$$

$$\mathbf{E}_{\pm 2} \parallel \hat{\mathbf{x}} \mp i\hat{\mathbf{y}}, \quad \mathbf{E}_{\pm 1} \parallel \hat{\mathbf{z}}, \quad \mathbf{E}_0 \perp \hat{\mathbf{z}}. \quad (68)$$

This formula gives the  $\phi$  dependence of electric field expansion (2a), in which the coefficients are of the form given by Eq. (65). An immediate consequence of Eq. (67) is that  $\mathbf{E}_\mu$  can be different from zero on the  $z$  axis,  $\mathbf{E}_\mu(0, 0, z) \neq 0$ , only if  $m_{\text{LG}} + \mu = 0$ .

From Eq. (68), at  $|m_{\text{LG}}| = 1$ , the electric field non-vanishing at the beam axis is linearly polarized along the  $z$  axis, whereas it is circularly polarized at  $|m_{\text{LG}}| = 2$ . The intensity distributions shown in Figs 1–4 clearly indicate that the  $z$  axis is not entirely in the dark region provided that  $0 \leq m_{\text{LG}} < 3$ .

At  $|m_{\text{LG}}| \geq 3$  and  $|\mu| \leq 2$ , a sum  $m_{\text{LG}} + \mu$  cannot be equal to zero and the beam axis is always a nodal line for the components of electric field. For two-dimensional (2D) electric field distributions in planes normal to the  $z$  axis, it implies that there is an optical vortex located at the origin.

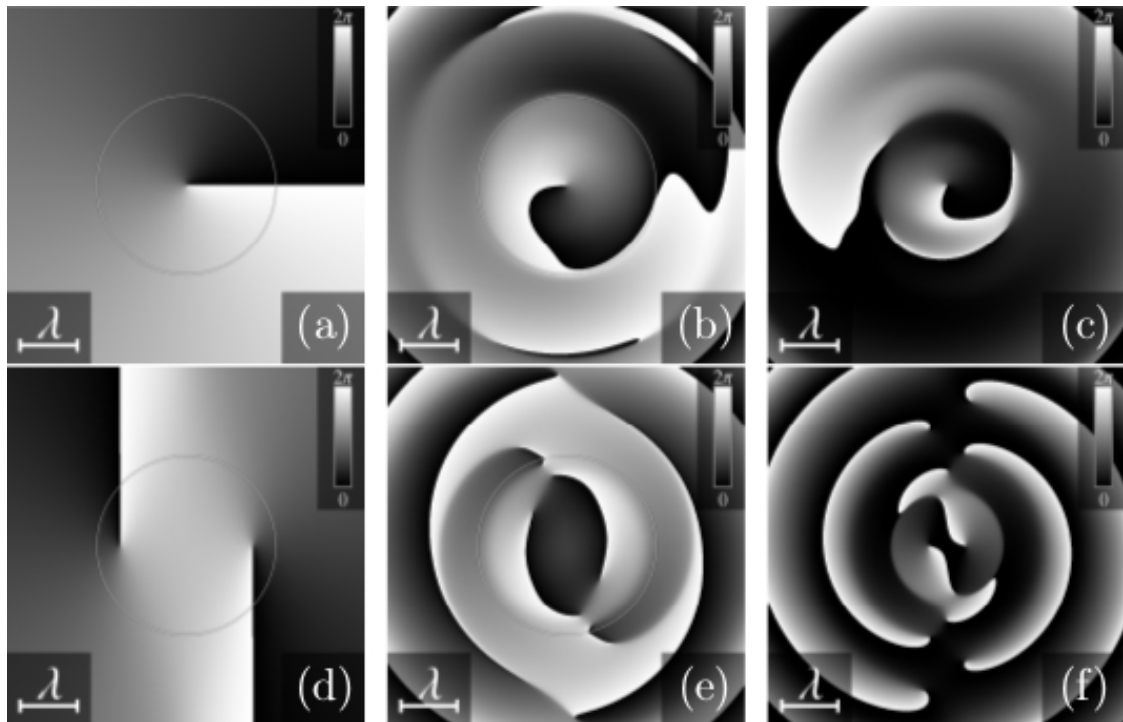


FIG. 7. Near-field phase maps of the electric field components  $E_x$  (a,b,c) and  $E_z$  (d,e,f) in the planes  $z = 0$  (a,b,d,e) and  $z = R_p = 1.5\lambda$  (c,f) for the LG beam with  $m_{\text{LG}} = 1$  and  $f = 0.1$ . (a) [(d)] Phase map of the electric field component  $E_x^{(\text{LG})}$  [ $E_z^{(\text{LG})}$ ] of the incident wave beam in the  $x - y$  plane ( $z = 0$ ). (b,c) [(e,f)] Phase maps for the electric field component  $E_x$  [ $E_z$ ] of the total light wavefield in the planes  $z = 0$  and  $z = R_p$ , respectively.

Now we return to the optical vortex structure for the components  $E_z$  and  $E_x$ . The  $\phi$  dependence of  $E_z$  can be written in the following form:

$$\exp[-im_{\text{LG}}\phi]E_z = \exp[-im_{\text{LG}}\phi + i\chi_z]|E_z| = E_{+1}^{(z)} \exp[i\phi] + E_{-1}^{(z)} \exp[-i\phi] = \exp[i\psi_+^{(z)}] \left\{ |E_{+1}^{(z)}| \exp[i(\phi + \psi_-^{(z)})] + |E_{-1}^{(z)}| \exp[-i(\phi + \psi_-^{(z)})] \right\}, \quad (69)$$

where  $E_{\pm 1}^{(z)} = (\mathbf{E}_{\pm 1} \cdot \hat{\mathbf{z}})$ ,  $2\psi_{\pm}^{(z)} = \arg(E_{+1}^{(z)}) \pm \arg(E_{-1}^{(z)})$  and  $\chi_z$  is the phase of  $E_z$ .

The complex plane formula (69) describes an ellipse parametrized by the azimuthal angle  $\phi$ . It is centered at the origin with the major (minor) semiaxis of the length  $E_{+}^{(z)}(R)$  ( $|E_{-}^{(z)}(R)|$ ), where  $E_{\pm}^{(z)}(R) = |E_{+1}^{(z)}(R)| \pm |E_{-1}^{(z)}(R)|$   $R$  is the radius of circle  $C_R$  in the plane of observation,  $z = z_0$ . Then the closed loop contour integral of the wave phase  $\chi_z$  is:

$$m_z = \frac{1}{2\pi} \oint_{C_R} d\chi_z = m_{\text{LG}} + \mu_z(R), \quad (70a)$$

$$\mu_z(R) = \text{sign}(E_-^{(z)}(R)) = \text{sign}(|E_{+1}^{(z)}(R)| - |E_{-1}^{(z)}(R)|). \quad (70b)$$

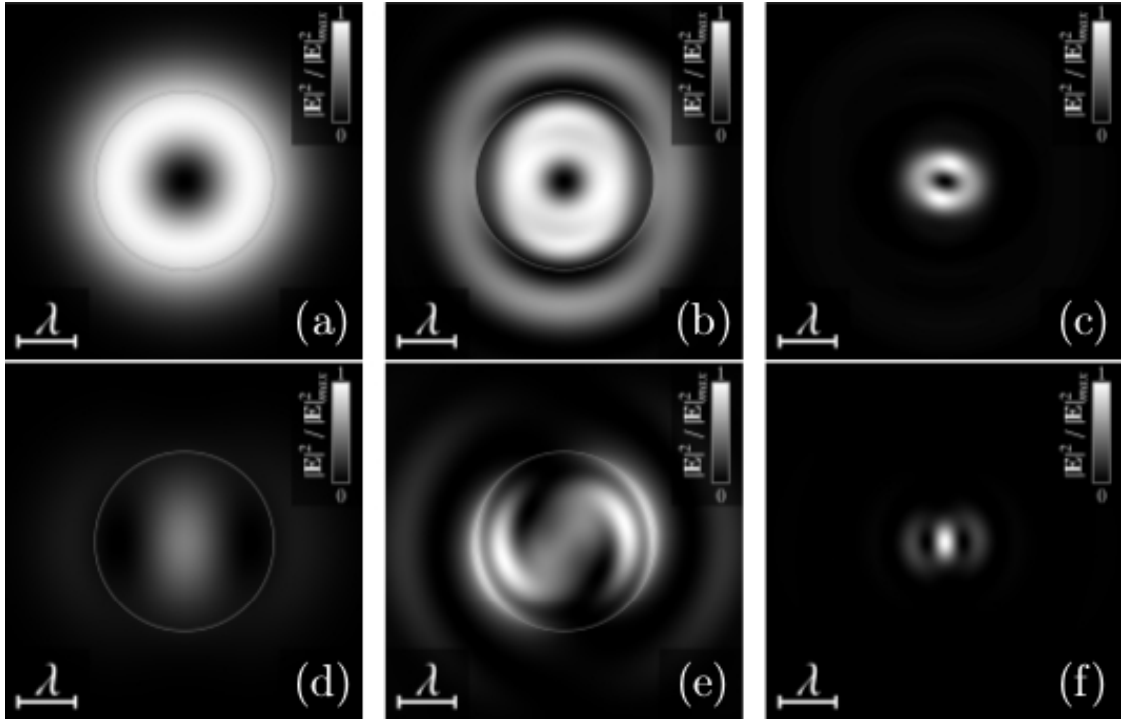


FIG. 8. Near-field intensity maps of the electric field components  $|E_x|^2$  (a,b,c) and  $|E_z|^2$  (d,e,f) in the planes  $z = 0$  (a,b,d,e) and  $z = R_p = 1.5\lambda$  (c,f) for the LG beam with  $m_{\text{LG}} = 1$  and  $f = 0.1$ . (a) [(d)] Intensity distribution for the  $x$  [ $z$ ] component,  $|E_x^{(\text{LG})}|^2$  [ $|E_z^{(\text{LG})}|^2$ ], of the incident wave beam in the  $x - y$  plane ( $z = 0$ ). (b,c) [(e,f)] Intensity distributions for the  $x$  [ $z$ ] component of electric field of the total light wavefield in the planes  $z = 0$  and  $z = R_p$ , respectively.

From Eq. (70), the net topological charge of vortices encircled by  $C_R$  can be either  $m_{\text{LG}} + 1$  or  $m_{\text{LG}} - 1$ . At  $|E_{+1}^{(z)}(R)| = |E_{-1}^{(z)}(R)|$ ,  $\mu_z(R)$  is undefined. This is the special case when  $|E_z| = 0$  at  $\cos(\phi + \psi_-^{(z)}) = 0$  and the circle contains a pair of symmetrically located vortices. Each of these vortices carries a charge of the magnitude equal to unity. Generally,

the vortices are of the same sign, which is determined by the change of  $\mu_z(R)$  as the radius  $R$  passes a critical value. When  $\mu_z(R)$  changes from  $+1$  ( $-1$ ) to  $-1$  ( $+1$ ) two vortices of the charge  $-1$  ( $+1$ ) intersect the boundary and move into the interior part of the circle.

The case of the  $x$  component of the electric field,  $E_x$ , can be analyzed along similar lines. From Eq. (67), we deduce the  $\phi$  dependence of  $E_x$  in the form:

$$\begin{aligned} \exp[-im_{\text{LG}}\phi + i\chi_x]|E_x| - E_0^{(x)} &= E_{+2}^{(x)} \exp[2i\phi] + E_{-2}^{(x)} \exp[-2i\phi] = \\ \exp[i\psi_+^{(x)}] \left\{ |E_{+2}^{(x)}| \exp[i(2\phi + \psi_-^{(x)})] + |E_{-2}^{(x)}| \exp[-i(2\phi + \psi_-^{(x)})] \right\}, \end{aligned} \quad (71)$$

where  $E_{\pm 2,0}^{(x)} = (\mathbf{E}_{\pm 2,0} \cdot \hat{\mathbf{x}})$ ,  $2\psi_{\pm}^{(x)} = \arg(E_{+2}^{(x)}) \pm \arg(E_{-2}^{(x)})$  and  $\chi_x$  is the phase of  $E_x$ . The center of the ellipse described by Eq. (71) is generally displaced from the origin and is determined by  $E_0^{(x)}$ . The length of its major (minor) semiaxis is  $E_+^{(x)}(R)$  ( $|E_-^{(x)}(R)|$ ), where  $E_{\pm}^{(x)}(R) = |E_{+2}^{(x)}(R)| \pm |E_{-2}^{(x)}(R)|$ .

The closed loop contour integral of the wave phase  $\chi_x$  is:

$$m_x = \frac{1}{2\pi} \oint_{C_R} d\chi_x = m_{\text{LG}} + \mu_x(R), \quad \mu_x(R) \in \{-2, 0, 2\}. \quad (72)$$

When the origin is enclosed by the ellipse (71), similar to Eq. (70b), we have the relation:

$$\mu_x(R) = 2 \text{sign}(E_-^{(x)}(R)) = 2 \text{sign}(|E_{+2}^{(x)}(R)| - |E_{-2}^{(x)}(R)|). \quad (73)$$

In the opposite case, when the origin is outside the area encircled by the ellipse,  $\mu_x(R)$  is zero. The latter is the case for the near-field phase maps shown in Figs. 7(a)–(c) that represent the 2D distributions of  $\chi_x$  in the  $x - y$  plane for the LG beam with  $m_{\text{LG}} = 1$  (see Fig. 2).

As is evident from Figs. 7(a)–(c) (see also the intensity maps in Figs. 8(a)–(c)), in these distributions, the only vortex is positioned at the center and possesses the charge  $m_x = m_{\text{LG}} = +1$ . As opposed to the case with  $m_{\text{LG}} = 2$  discussed in Ref. [38], at  $m_{\text{LG}} = 1$ , the central vortex of the  $x$  component,  $E_x$ , is structurally stable and cannot be destroyed.

The near-field phase maps for  $\chi_z$  are presented in Figs. 7(d)–(f). Figure 7(d) shows the 2D map for the incident optical vortex LG beam with  $m_{\text{LG}} = 1$  in the focal plane  $z = 0$ . The corresponding intensity map is depicted in Fig. 8(d). It is seen that there are no vortices at the center, so that, at sufficiently small  $R$ ,  $m_z = 0$  and  $\mu_z = -1$ . In addition, there is a pair of the symmetrically-arranged vortices of the charge  $+1$  inside the particle. So, when the radius  $R$  is large enough for the circle to enclose the vortices, the total charge is  $m_z = m_{\text{LG}} + 1 = 2$  and  $\mu_z = 1$ .

For the total wavefield at  $z = 0$ , the phase and intensity maps are given in Fig. 7(e) and Fig. 8(e), respectively. It can be seen that the vortex pattern is complicated by interference between the incident and the scattered waves. Referring to Fig. 7(e), there are two additional pairs of vortices whose charges are opposite in sign. The negatively charged vortices (the charge is  $-1$ ) are located inside the particle, whereas the positively charged ones (the charge is  $+1$ ) are formed on the surface of the particle. A similar structure is discernible from Figs. 7(f) and 8(f), representing the results for the plane tangent to the particle surface  $z = R_p$ .

## 5. Conclusions

In this paper, we have used a  $T$ -matrix approach in the form described in Refs. [10,38] to study the light scattering problem for optically isotropic spherical scatterers illuminated with LG beams that represent optical vortex laser beams. Our approach uses the remodelling procedure

in which the far-field matching method is combined with the results for nonparaxial propagation of LG beams. Scattering of such beams is thus described in terms of the far-field angular distributions,  $\mathbf{E}_{\text{out}}^{(\text{inc})}$  and  $\mathbf{E}_{\text{out}}^{(\text{sca})}$ , that determine the outgoing parts of the incident and scattered waves. The far-field distributions play a central role in the method giving, in particular, the differential cross-sections and the optical (radiation) force acting upon the Mie scatterer.

The analytical results are employed to perform numerical analysis of the optical field in the near-field region. In order to examine the effects of incident beam spatial structure on the light wavefield near the scatterer, we have computed a number of the 2D near-field intensity and phase distributions for purely azimuthal LG beams. In this case, a LG beam possesses the vanishing radial mode number and carries the optical vortex with the topological charge characterized by the azimuthal number  $m_{\text{LG}}$ .

The 2D near-field intensity distributions computed for the plane-wave limiting case in which the incident wave is a Gaussian beam ( $m_{\text{LG}} = 0$ ) with small focusing parameter  $f$  ( $2\pi f = \lambda/w_0 < 1$ ) reveal the well-known structure of photonic nanojets (see Fig. 1). Figures 2–4 represent the results for the LG beams with  $1 \leq m_{\text{LG}} \leq 2$  and show that the morphology of photonic jets formed at  $m_{\text{LG}} \neq 0$  significantly differs from the well-known shape of nanojet at  $m_{\text{LG}} = 0$ . The effect that a jetlike photonic flux emerging from the particle shadow surface can be formed even if the bulk part of the scatterer is in the low intensity region is illustrated in Figs. 2(b)–3(b)). In contrast, as can be seen from Fig. 5, the jetlike flux near negative index metamaterial Mie scatterers may emerge from the illuminated part of the particle surface.

The form of the beam shape coefficients (65) is dictated by the twofold rotational symmetry of the LG beam (see Sec. 3.3) and underlies general formula (67) giving the electric field vector expressed as a function of the azimuthal angle  $\phi$ . The latter is at the heart of our analysis of optical vortices associated with the electric field components.

An important consequence of Eq. (67) is that, at sufficiently large azimuthal numbers,  $|m_{\text{LG}}| \geq 3$ , light scattering of LG beams takes place without destroying the optical vortex located on the beam axis. By contrast, at  $|m_{\text{LG}}| < 3$ , the intensity of scattered wavefield does not vanish on the beam axis so that, in the near-field region, light scattering has a destructive effect on the optical vortex (see Figs. 2–4).

Using analytical expressions (69) and (71), we have described the geometry of optical vortices for the components  $E_z$  and  $E_x$  in the planes  $z = z_0$  normal to the beam axis (the  $z$  axis). It was found that, except for the central vortex, the topological charge of off-center vortices generally equals unity in magnitude. They are organized into pairs of symmetrically-arranged and equally-charged vortices. These pairs lie on concentric circles and their vortex charge alternate in sign with the circle radius (see, e.g., Fig. 7(f)).

The phase maps of  $E_x$  shown in Figs. 7(a)–(e) (the corresponding square amplitude distributions are presented in Figs. 8(a)–(e)) are computed for the LG beam with  $m_{\text{LG}} = 1$ . The central vortex having azimuthal number  $m_{\text{LG}} = 1$  was found to be the only vortex for both the incident beam and the total wavefield. Formula (69) implies that the  $z$  axis is a nodal line for the  $x$  component of the electric field,  $E_x$ , and the central vortex is structurally stable at  $m_{\text{LG}} = 1$ . When  $m_{\text{LG}} = 2$ , a similar result applies to the  $z$  component [38].

In the phase maps for  $E_z$ , depicted in Fig. 7(d)–(f), there are no vortices at the origin. For the incident wave, there is a pair of equally charged vortices (see Fig. 7(d)). As is seen from Figs. 7(e)–(f), interference between the incident and the scattered waves produces additional pairs of symmetrically arranged vortices.

## Acknowledgments

A.D.K. acknowledges partial financial support from the Government of the Russian Federation (Grant No. 074-U01), from the Ministry of Education and Science of the Russian Federation (Grant No. GOSZADANIE 2014/190, Project No. 14.Z50.31.0031, and ZADANIE Grant No. 1.754.2014/K), through a grant from the Russian Foundation for Basic Research, and through a grant from the President of Russia (Grant No. MK-2736.2015.2).

## References

- [1] Mie G. Beiträge zur Optik trüber Medien, speziell kolloidaler Metallösungen. *Ann. Phys.*, Leipzig, 1908, **25**, P. 377–445.
- [2] Newton R. G. *Scattering Theory of Waves and Particles*. 2 edition. Heidelberg, Springer, 1982, 745 p.
- [3] Tsang L., Kong J. A., Ding K.-H. *Scattering of Electromagnetic Waves. Theories and Applications*. NY : Wiley-Interscience Pub, 2000. Vol. 1 of Wiley Series in Remote Sensing. 426 p.
- [4] Mishchenko M. I., Travis L. D., Lacis A. A. *Scattering, Absorption and Emission of Light by Small Particles*. NY : Cambridge University Press, 2004, 448 p.
- [5] Gouesbet G., Gréhan G. *Generalized Lorenz–Mie theories*. Berlin, Springer, 2011, 310 p.
- [6] Mishchenko M. I., Travis L. D., Mackowski D. W. *T*-matrix computations of light scattering by nonspherical particles: a review. *J. of Quant. Spectr., & Radiat. Transf.*, 1996, **55**, P. 535–575.
- [7] *Light Scattering by Nonspherical Particles: Theory, Measurements and Applications* / Ed. by M. I. Mishchenko, J. W. Hovenier, L. D. Travis. New York, Academic Press, 2000.
- [8] Roth J., Digman M. J. Scattering and extinction cross sections for a spherical particle coated with an oriented molecular layer. *J. Opt. Soc. Am.*, 1973, **63**, P. 308–311.
- [9] Kiselev A. D., Reshetnyak V. Y., Sluckin T. J. Influence of the optical axis distribution in the anisotropic layer surrounding a spherical particle on the scattering of light. *Opt. Spectrosc.*, 2000, **89**(6), P. 907–913.
- [10] Kiselev A. D., Reshetnyak V. Y., Sluckin T. J. Light scattering by optically anisotropic scatterers: *T*-matrix theory for radial and uniform anisotropies. *Phys. Rev. E*, 2002, **65**(5), P. 056609.
- [11] Geng Y.-L., Wu X.-B., Li L.-W., Guan B.-R. Mie scattering by a uniaxial anisotropic sphere. *Phys. Rev. E*, 2004, **70**, P. 056609.
- [12] Novitsky A., Barkovsky L. Matrix approach for light scattering from a multilayered rotationally symmetric bianisotropic sphere. *Phys. Rev. A*, 2008, **77**, P. 033849.
- [13] Chengwei Qiu, Lei Gao, John D. Joannopoulos, Marin Soljačić. Light scattering from anisotropic particles: propagation, localization and nonlinearity. *Laser & Photon. Rev.*, 2010, **4**(2), P. 268–282.
- [14] Gréhan G., Maheu B., Gouesbet G. Scattering of laser beams by Mie scatter centers: numerical results using a localized approximation. *Appl. Opt.*, 1986, **25**(19), P. 3539–3548.
- [15] Gouesbet G., Maheu B., Gréhan G. Light scattering from a sphere arbitrarily located in a Gaussian beam, using a Bromwich formulation. *J. Opt. Soc. Am. A*, 1988, **5**(9), P. 1427–1443.
- [16] Barton J. P., Alexander D. R., Schaub S. A. Internal and near-surface electromagnetic fields for a spherical particle irradiated by a focused laser beam. *J. Appl. Phys.*, 1988, **64**(4), P. 1632–1639.
- [17] Barton J. P., Alexander D. R., Schaub S. A. Theoretical determination of net radiation force and torque for a spherical particle illuminated by a focused laser beam. *J. Appl. Phys.*, 1989, **66**(10), P. 4594–4602.
- [18] Schaub S. A., Alexander D. R., Barton J. P. Glare spot image calculations for a spherical particle illuminated by a tightly focused beam. *J. Opt. Soc. Am. A*, 1992, **9**(2), P. 316–330.
- [19] Lock J. A., Gouesbet G. Generalized Lorenz–Mie theory and applications. *J. of Quant. Spectr. & Radiat. Transf.*, 2009, **110**, P. 800–807.
- [20] Gouesbet G., Lock J. A., Gréhan G. Generalized Lorenz–Mie theories and description of electromagnetic arbitrary shaped beams: Localized approximations and localized beam models, a review. *J. of Quant. Spectr. & Radiat. Transf.*, 2011, **112**, P. 1–27.
- [21] Lax M., Louisell W. H., McKnight W. B. From Maxwell to paraxial wave optics. *Phys. Rev. A*, 1975, **11**(4), P. 1365–1370.
- [22] Davis L. W. Theory of electromagnetic waves. *Phys. Rev. A*, 1979, **19**, P. 1177–1179.
- [23] Nieminen T. A., Rubinsztein-Dunlop H., Heckenberg N. R. Multipole expansion of strongly focussed laser beams. *J. of Quant. Spectr. & Radiat. Transf.*, 2003, **79–80**, P. 1005–1017.
- [24] Bareil P. B., Sheng Y. Modeling highly focused laser beam in optical tweezers with the vector Gaussian beam in the *T*-matrix method. *J. Opt. Soc. Am. A*, 2013, **30**(1), P. 1–6.

- [25] Hoang T. X., Chen X., Sheppard C. J. R. Multipole theory for tight focusing of polarized light, including radially polarized and other special cases. *J. Opt. Soc. Am. A*, 2012, **29**(1), P. 32–43.
- [26] Barnett S. M., Allen L. Orbital angular momentum and nonparaxial light beams. *Opt. Commun.*, 1994, **110**(5-6), P. 670–678.
- [27] Duan K., Wang B., Lü B. Propagation of Hermite-Gaussian and Laguerre-Gaussian beams beyond the paraxial approximation. *J. Opt. Soc. Am. A*, 2005, **22**(9), P. 1976–1980.
- [28] Van De Nes A. S., Pereira S. F., Braat J. J. M. On the conservation of fundamental optical quantities in non-paraxial imaging systems. *Journal of Modern Optics*, 2006, **53**(5-6), P. 677–687.
- [29] Zhou G. Analytical vectorial structure of Laguerre–Gaussian beam in the far field. *Opt. Lett.*, 2006, **31**(17), P. 2616.
- [30] Zhou G. Propagation of a vectorial Laguerre-Gaussian beam beyond the paraxial approximation. *Optics & Laser Technology*, 2008, **40**(7), P. 930–935.
- [31] van de Nes A. S., Török P. Rigorous analysis of spheres in Gauss-Laguerre beams. *Opt. Express*, 2007, **15**(20), P. 13360–13374.
- [32] Yuesong Jiang, Yuwei Shao, Xiaosheng Qu et al. Scattering of a focused Laguerre–Gaussian beam by a spheroidal particle. *J. Opt.*, 2012, **14**(12), P. 125709.
- [33] Desyatnikov A. S., Kivshar Y. S., Torner L. Optical vortices and vortex solitons. *Progress in Optics* / Ed. by E. Wolf. Amsterdam, North-Holland, 2005. Vol. 47. P. 291–391.
- [34] *Optical Angular Momentum* / Ed. by L. Allen, S. M. Barnett, M. J. Padgett. London, Taylor & Francis, 2003.
- [35] *Structured Light and Its Applications: An Introduction to Phase-Structured Beams and Nanoscale Optical Forces* / Ed. by David L. Andrews. Amsterdam, Academic Press, 2008. 342 p.
- [36] Simpson S. H., Hanna S. Rotation of absorbing spheres in Laguerre–Gaussian beams. *J. Opt. Soc. Am. A*, 2009, **26**(1), P. 173–183.
- [37] Simpson S. H., Hanna S. Orbital motion of optically trapped particles in Laguerre–Gaussian beams. *J. Opt. Soc. Am. A*, 2010, **27**(9), P. 2061–2071.
- [38] Kiselev A. D., Plutenko D. O. Mie scattering of Laguerre-Gaussian beams: Photonic nanojets and near-field optical vortices. *Phys. Rev. A*, 2014, **89**, P. 043803. <http://dx.doi.org/10.1103/PhysRevA.89.04380>
- [39] A. Heifetz, Soon-Cheol Kong, A. V. Sahakian et al. Photonic Nanojets. *J. Comput. Theor. Nanosci.*, 2009, **12**(7), P. 1214–1220.
- [40] Chen Z., Taflove A., Backman V. Photonic nanojet enhancement of backscattering of light by nanoparticles: a potential novel visible light ultramicroscopy technique. *Opt. Express*, 2004, **12**(7), P. 1214–1220.
- [41] Xu Li, Zhigang Chen, Allen Taflove, Vadim Backman. Optical analysis of nanoparticles via enhanced backscattering facilitated by 3-D photonic nanojets. *Opt. Express*, 2005, **13**(2), P. 526–533.
- [42] Biedenharn L. C., Louck J. D. *Angular Momentum in Quantum Physics: Theory and Application*. Reading, Massachusetts, Addison–Wesley, 1981. Vol. 8 of Encyclopedia of Mathematics and its Applications. 717 p.
- [43] Varshalovich D. A., Moskalev A. N., Khersonskii V. K. Quantum theory of angular momentum: Irreducible tensors, spherical harmonics, vector coupling coefficients, 3nj symbols. Singapore, World Scientific Publishing Co., 1988. 514 p.
- [44] Jackson J. D. *Classical Electrodynamics*, 3rd edition. New York, Wiley, 1999.
- [45] Sarkar D., Halas N. J. General vector basis function solution of Maxwells equations. *Phys. Rev. E*, 1997, **56**(1), P. 1102–1112.
- [46] *Handbook of Mathematical Functions* / Ed. by M. Abramowitz, I. A. Stegun. New York, Dover, 1972.
- [47] Kiselev A. D., Reshetnyak V. Y., Sluckin T. J. T-matrix theory of light scattering by uniformly anisotropic scatterers. *Mol. Cryst. Liq. Cryst.*, 2002, **375**, P. 373–386.
- [48] Stout B., Nevière M., Popov E. Mie scattering by an anisotropic object. Part I. Homogeneous sphere. *J. Opt. Soc. Am. A*, 2006, **23** (5), P. 1111–1123.
- [49] Gradshteyn I. S., Ryzhik I. M. Table of Integrals, Series, and Products. New York, Academic, 1980.
- [50] Sherman G. C., Stamnes J. J., Lalor E. Asymptotic approximations to angular–spectrum representations. *J. Math. Phys.*, 1976, **17**(5), P. 760–776.
- [51] Simpson S. H., Hanna S. First-order nonconservative motion of optically trapped nonspherical particles. *Phys. Rev. E*, 2010, **82**, P. 031141.
- [52] Rury A. S., Freeling R. Mie scattering of purely azimuthal Laguerre-Gauss beams: Angular-momentum-induced transparency. *Phys. Rev. A*, 2012, **86**, P. 053830.
- [53] Lecler S., Takakura Y., Meyrueis P. Properties of a three-dimensional photonic jet. *Opt. Lett.*, 2005, **30**(19), P. 2641–2643.

- [54] Devilez A., Stout B., Bonod N., Popov E. Spectral analysis of three-dimensional photonic jets. *Opt. Express*, 2008, 16(18), P. 14200–14212.
- [55] Geints Y. E., Zemlyanov A. A., Panina E. K. Control over parameters of photonic nanojets of dielectric microspheres. *Opt. Commun.*, 2010, **283**(23), P. 4775–4781.
- [56] Devilez A., Bonod N., Wegner J., et al. Three-dimensional subwavelength confinement of light with dielectric microspheres. *Opt. Express*, 2009, **17**(4), P. 2089–2094.
- [57] Myun-Sik Kim, Toralf Scharf, Stefan Mühlig et al. Engineering photonic nanojets. *Opt. Express*, 2011, **19**(11), P. 10206–10220.
- [58] Solymar L., Shamonina E. *Waves in Metamaterials*. NY, Oxford University Press, 2009. 385 p.
- [59] Cai W., Shalaev V. *Optical Metamaterials. Fundamentals and Applications*, NY, Springer, 2010. 200 p.
- [60] Kivshar Y. S. From metamaterials to metasurfaces and metadevices. *Nanosystems: Physics, Chemistry, Mathematics*, 2015, **6**(3), P. 346–352.
- [61] Pravdin K. V., Popov I. Y. Photonic crystal with negative index material layers. *Nanosystems: Physics, Chemistry, Mathematics*, 2014, **5**(5), P. 626–643.
- [62] Veselago V. G. The electrodynamics of substances with simultaneously negative values of  $\epsilon$  and  $\mu$ . *Soviet Physics Uspekhi*, 1968, **10**(4), P. 509–514.

# Temperature dependence of the optical fiber cable parameters in subcarrier wave quantum communication systems

V. D. Dubrovskaya, S. A. Chivilikhin

ITMO University, St. Petersburg, Russia

vddubrovskaya@gmail.com

PACS 03.67.-a, 41.20.Jb

DOI 10.17586/2220-8054-2016-7-2-371-377

A common approach to establishing long-distance synchronization links in quantum communication (QC) systems is based on using optical signals transmitted in cables, where they decay and are distorted. It is necessary to evaluate the transformation of the signal parameters during propagation and their influence on the QC systems. We investigate the temperature dependence of the synchronization signal phase of a subcarrier wave quantum communication system (SCWQC) in optical fiber cables. A temperature model was created in order to determine the signal phase delay in the cable. We estimate the influence of daily temperature fluctuations on the phase delay in ground- and air-based cables. For systems operating with ground-based cables, they do not have any significant impact on the synchronization of the signal phase. However, for systems operating through air-based cables, phase adjustment is required every 158 ms for stable operation. This allowed us to optimize the parameters for a calibration procedure of a previously-developed SCWQC system, increasing the overall sifted key generation rate.

**Keywords:** quantum communications, clock synchronization, temperature dependence of the signal.

*Received: 23 January 2016*

## 1. Introduction

During the last two decades, significant progress has been made in the development of experimental quantum communication systems (QC) [1, 2] which could have potential future use in protecting confidential data by quantum key distribution technique (QKD) [1]. This has led to increased interest in their integration into telecommunication infrastructure [1, 2]. One of the promising approaches to QC in optical fibers is subcarrier wave quantum communication system (SCWQC) [1].

In practical QC, systems several technological challenges still remain, including synchronization of their receiver and transmitter devices by precisely controlling the phase of high-frequency electrical modulating signals. A common approach to establishing long-distance synchronization links in QC is based on using optical signals transmitted in a separate channel [3, 4]. However, these synchronization signals decay and are distorted during transmission through the fibers, therefore it is necessary to evaluate transformation of their parameters, its influence on the QC system operation, and to develop methods of compensating for the negative effects.

This paper investigates the temperature dependence of the synchronization signal in optical fiber in ground- and air-based cables. A temperature model is created in order to determine the signal phase delay in the cable. We estimate the influence of daily temperature fluctuations on the phase delay in ground- and air-based cables. Finally, we apply the calculation

results to a synchronization system of a previously developed experimental SCWQC device [5–8] in order to optimize its sifted key [1] generation rate.

## 2. Synchronization system

### 2.1. Subcarrier wave quantum communication system clock synchronization problem

The main parameter that determines the characteristics of QC and QKD systems is QBER. It is defined as the ratio between the erroneous bits and the total number of received bits. QBER is the main factor that limits the maximal possible distance of secure quantum key distribution [1]. For the widely-used BB84 protocol family, the limiting QBER value is about 11 % [1].

Two main factors contribute to the QBER value: the signal visibility in the quantum channel and the dark count of the detector:

$$\text{QBER} = \frac{1 - V}{2} + \frac{p}{4\mu\eta \cdot 10^{(-\alpha L - \beta)/10}},$$

where  $V$  is interference pattern visibility,  $\beta$  represents the losses in the receiver module,  $p$  is the dark count probability per bit,  $\alpha$  is the optical fiber attenuation coefficient at the central wavelength of the photon source,  $L$  is the optical fiber length and  $\eta$  is the detection efficiency. Visibility value represents the probability of photon out-of-phase detection and therefore depends on the quality of optical phase matching of the transmitter and receiver phase modulators used for encoding qubits. Clearly, it is always beneficial to maximize the quantum channel visibility. In modern practical QC systems [3, 4, 6–8] the achieved visibility value is usually around 98 – 99 %. As is shown on Fig. 1, such visibility values in SCWQC system are correspond to maximum modulating signal phase mismatch  $\Delta\varphi = 0.043$ .

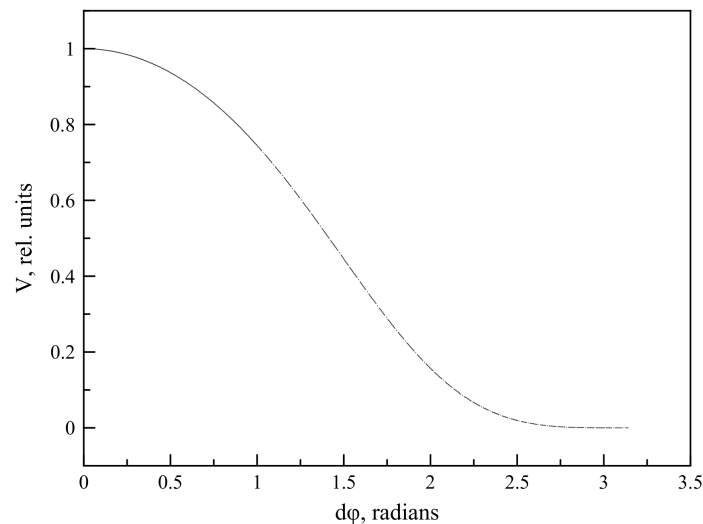


FIG. 1. Signal phase mismatch dependence of visibility

### 2.2. Subcarrier wave quantum communication system clock synchronization

Since phase matching between the transmitter (Alice) and receiver (Bob) is defined by clock signals from respective voltage controlled oscillators (VCO), preservation of the optical synchronization signal phase appears crucial to achieving high quantum signal visibility. The uncontrollable synchronization signal phase shift appears under influence of different external

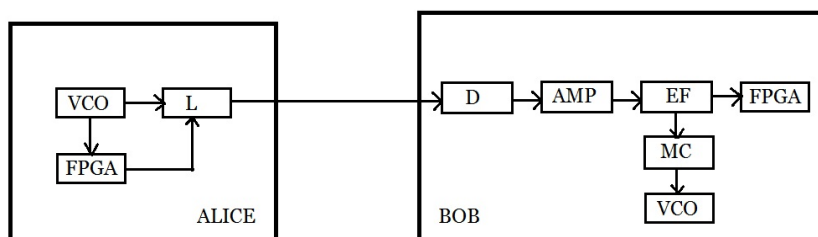


FIG. 2. Block diagram of the synchronization subsystem in SCWQC system

effects. One of them is daily temperature fluctuation that affects the refractive index of the fiber, thus inducing optical delays. For the SCWQC system described in [4,5], this problem is solved by the calibration procedure described below.

The synchronization pulse is sent through a separate optical fiber to avoid its influence on QBER [3,4]. Synchronization channel laser  $L$  generates a sinusoidal signal with a frequency defined by the VCO that acts as a generator (Fig. 2). This signal is also modulated by the transmitter logic board (FPGA). After passing through the communication channel optical signal is recorded at the photodetector (D) in receiver block, where it is amplified (AMP) and filtered in the electric filter (EF). The sinusoidal component flows through the microcontroller (MC) to the receiver VCO and is used to adjust the oscillator frequency. The component inserted by the transmitter logic is used as the start and reset signal. A subsystem composed of the VCO and a phase-locked loop device then generates the driving signal of the optical modulator with frequency  $\Omega$ . A more detailed description of phase modulation in the system is provided in [6].

As the synchronization subsystem performs two functions, synchronization of transmitter and receiver generators and transmitting a start/reset signal, two main problems caused by signal phase difference appear. First, the generators in the transmitter and receiver modules have to be precisely phase-locked, so that the phase delay of the synchronization signal should not exceed  $\Delta\varphi$ . Second, the delay between the synchronization and quantum signals in different fibers should not exceed 10 % of the gate interval for correct system operation. Thus, for the described system with 100 MHz clock rate, the limiting delay value is 1 ns.

In order to solve these problems in the SCWQC system, a novel calibration procedure was developed. After a certain time interval of quantum bit transmission ( $t_{qc}$ ), the procedure switches the system into calibration mode (time interval  $t_{cal}$ ), during the course of which it resets the gate starting time and redefines the optical phase values induced by different modulator driving voltages (“modulation tables”) in Alice and Bob units. During SCWQC experiments in optical fibers, the values of  $t_{qc}$  and  $t_{cal}$  were chosen to be 50 ms and 10 ms, respectively. Therefore, the effective sifted key generation rate is reduced by approximately 15 %.

In the following sections, we find the temperature dependence of synchronization signal phase. Then, we develop a temperature model of optical fiber cables, which will be employed during the scheduled SCWQC experiments, and calculate the temperature-induced phase delay. This allows us to optimize the value of  $t_{cal}$  and therefore the sifted key rate in practical SCWQC systems.

### 2.3. Phase temperature dependence

To determine the maximum interval between two following calibration procedures, we need to know the temporal delay  $\Delta t$  of the signal, which corresponds to the maximum tolerated phase delay,  $\Delta\varphi$ . The  $\Delta t$  value depends on the cable length  $L$  and refractive index changes in

the fiber  $\Delta n$ :

$$\Delta t = \frac{L\Delta n}{c}. \quad (1)$$

In turn, the fiber's refractive index is linearly dependent upon the temperature  $T$  and two constants, representing the change of  $n$  due to temperature (T-component) and bending (R-component) [9]:

$$\Delta n = \left[ \left( \frac{dn}{dT} \right)_T + \left( \frac{dn}{dT} \right)_R \right] \Delta T.$$

As shown in [9], for the Corning SMF-28 fiber widely used in telecommunication cables, these coefficients are:

$$\begin{aligned} \left( \frac{dn}{dT} \right)_T &= 6.8 \cdot 10^{-5} \text{ }^\circ\text{C}^{-1}, \\ \left( \frac{dn}{dT} \right)_R &= 0.8 \cdot 10^{-5} \text{ }^\circ\text{C}^{-1}. \end{aligned}$$

We chose the optical cable length  $L = 100$  km, since it is a typical distance for metropolitan area local networks. For this  $L$  value, the signal delay is:

$$\Delta t = 2.53 \cdot 10^{-8} \Delta T \text{ [s]}.$$

The relation between the phase and time delays of a signal with frequency  $\Omega$  is given by:

$$\Delta t = \Delta\varphi/\Omega.$$

The  $\Omega$  value is typically several gigahertz for SCWQC systems [4, 5]; we used a value of 4 GHz in our calculations.

It can be seen that the phase delay is in direct ratio with the temperature  $T$  of the fiber core. A temperature model of the cable was therefore created in order to determine it.

### 3. Process modeling

#### 3.1. Cable temperature model

To estimate the temperature fluctuations of the fiber optical cable core we have developed the following temperature model. We solve the heat equation and choose appropriate boundary conditions for the two cases: the air- and ground-based cables.

The two-dimensional heat equation for the cable is:

$$c\rho \frac{\partial T}{\partial t} = \frac{\partial}{\partial x} \left( \lambda \frac{\partial T}{\partial x} \right) + \frac{\partial}{\partial y} \left( \lambda \frac{\partial T}{\partial y} \right), \quad (2)$$

where  $\lambda$  is thermal conductivity,  $\rho$  represents density and  $c$  is heat capacity. We write the air temperature in the form  $T_a(t) = \bar{T}_a + \delta T_a \cos(\omega t)$ , where  $\bar{T}_a$  is the average daily temperature,  $\delta T_a$  is the temperature amplitude.

The first boundary condition corresponds to the cable in the air:

$$\lambda \left. \frac{\partial T}{\partial r} \right|_{r=R} = \alpha(T_a(t) - T|_{r=R}), \quad (3)$$

where  $\alpha$  is the coefficient of convective heat exchange,  $r$  and  $R$  are the radial coordinate and radius of the cable.

The temperature  $T_g(t)$  in the ground at depth  $z$  has reduced amplitude and phase shift [10]. The second boundary condition corresponds to the cable located in the ground:

TABLE 1. Cable element parameters

Element	$R$ , mm	Thermal diffusivity, $m^2/s, \cdot 10^{-6}$
Outer jacket	3	0.11
Strength member	2.3	13.3/0.09*
Coating	2	0.11
Water blocking material	1.35	0.174
Optical fiber	0.45	1.1
Central member	0.45	0.15

\*for the air /ground cables

$$T|_{r=R} = T_g(t) \equiv \bar{T}_a + \delta T_a \exp\left(-z\sqrt{\frac{\omega}{2a}}\right) \cos\left(\omega t - z\sqrt{\frac{\omega}{2a}}\right), \quad (4)$$

where  $a$  is the thermal diffusivity of ground.

Figure 3a shows the model of the cable with chosen configuration. The cable consists of an outer jacket, a strength member, a coating, water blocking material, optical fibers and a central member.

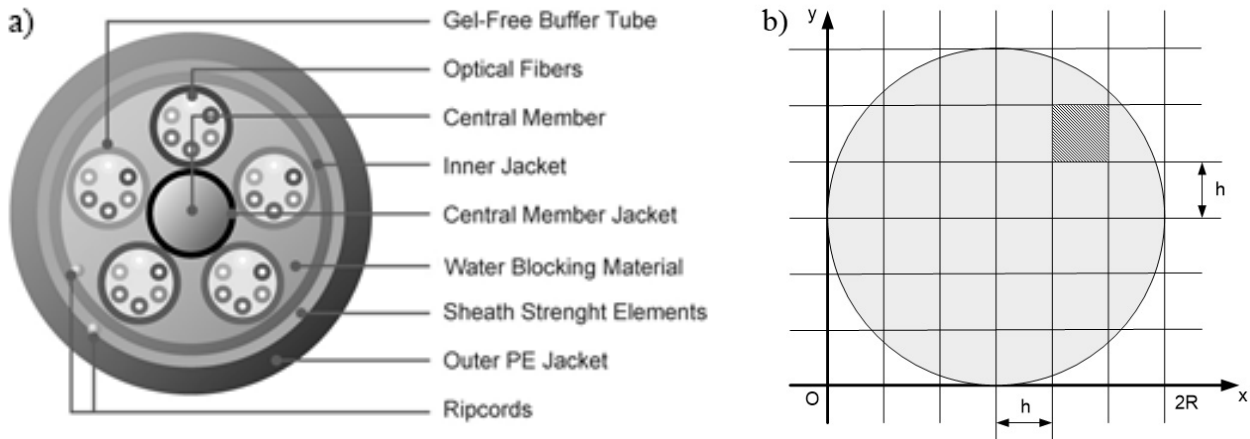


FIG. 3. a) Cable model with chosen configuration; b) The computational domain model

Let the radius of the cable be  $R$ . We then divide the area using a uniform grid consisting of  $n + 1$  knot (Fig. 3b). We solve the eq. (2) using a difference Crank–Nicolson scheme with boundary conditions (3–4) with Thomas algorithm for  $n = 1000$ . Different elements of the cable have different thermal diffusivity coefficients, as indicated in Table 1.

### 3.2. Modeling results and discussion

The main difference between an air-based cable and one lying in the ground is the lack of steel armor, optional for this type of operation, which is replaced by an aramid yarn. Therefore in the case of air-based cable, the thermal diffusivity of the strength member will be lower. In the cable lying underground, the temperature is distributed in the form of a wave, depending on the depth. In our model, we have chosen a typical ground depth of 1 meter. With a small-sized cable, even after a while, the temperature and the difference between the coefficients of thermal diffusivity for different elements were insignificantly affected.

The initial temperature  $T_a$  of the cable is 15 degrees; the initial (mean) environmental temperature  $\bar{T}_a$  is 15 degrees, with  $\delta T_a = 10$  degrees oscillation amplitude over a period of 24 hours. Temperature fluctuations for the chosen fiber in the cable over 12 hours are shown on Fig. 4.

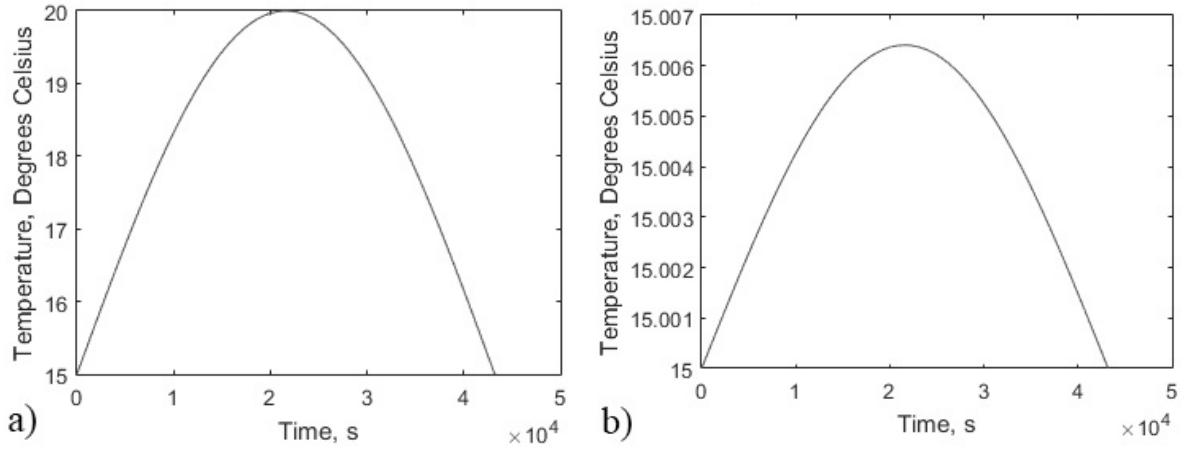


FIG. 4. Change of cable temperature during daytime in air (a) and in the ground (b)

As discussed previously, the signal phase delay in the system is in direct ratio with the temperature of the fiber optic core.

Figure 5 shows the dependence of the synchronization signal temporal delay induced by cable heating. Eq. (1) allows us to calculate the delay  $\Delta t$ , which leads to maximum tolerated phase difference  $\Delta\varphi = 0.043$ , as 0.0017 ns. According to our model (Fig. 5) for air-based cables, such  $\Delta t$  accumulates every 158 ms. Therefore, for SCWQC systems operating in air, the modulation signal adjustment may be performed every 158 ms instead of every 50 ms, as was previously implemented. This would allow for longer  $t_{qc}$  and about 15 % higher effective sifted bitrate.

At the same time, for ground-based cables, the temperature-induced signal delay never reaches the critical value due to the small daily temperature fluctuations at 1 meter depth underground (Fig. 6). Therefore, the temperature (under normal conditions) does not affect the course of SCWQC system operation.

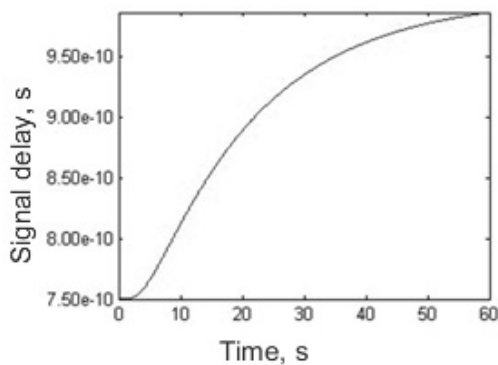


FIG. 5. Dependence of the signal delay time upon cable heating

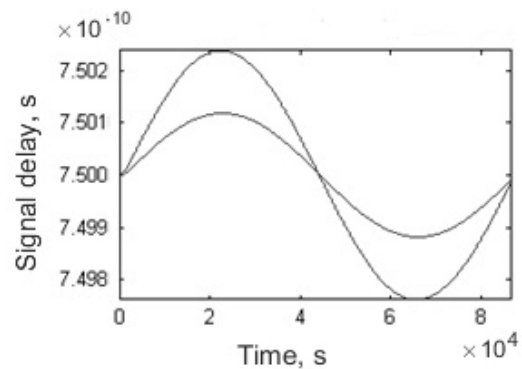


FIG. 6. The dependence of the signal delay time upon the heating cable at different points in a 24 hour period

#### 4. Conclusion

Optical signals transmitted in cables for quantum communication systems are transformed during their propagation. In this paper, the temperature dependencies of the synchronization signals in optical fiber cables in the ground and in air were investigated. In order to determine the signal delay in the cable, a temperature model was created. The influence of daily temperature fluctuations on the phase delay was estimated for the air- and ground-based cables. The calculated results can be used to optimize calibration procedures in SCWQC systems.

For systems operating in ground-based cables, daily temperature fluctuations do not significantly impact the synchronization of the signal phase. However, it has been shown that for systems operating through air-based cables, phase adjustment is required every 158 ms for stable operation. This allowed us to optimize the parameters for the calibration procedure of a previously developed SCWQC system. Therefore, this allowed an increase in the overall sifted key generation rate.

#### Acknowledgements

This work was partially financially supported by the Government of the Russian Federation (grant 074-U01).

#### References

- [1] Scarani V., Bechmann-Pasquinucci H., et al. The security of practical quantum key distribution. *Reviews of modern physics*, 2009, **81**, P. 1302–1345.
- [2] Bennett C., Brassard G. Quantum cryptography: Public key distribution and coin tossing. *Proceedings of IEEE International Conference on Computers. Systems and Signal Processing*, 1984, P. 175–179.
- [3] Korzh B., Wen Lim C.C., et al. Provably secure and practical quantum key distribution over 307 km of optical fibre. *Nature Photonics*, 2015, **9**, P. 163–168.
- [4] Wang S., Chen W., et al. 2 GHz clock quantum key distribution over 260 km of standard telecom fiber. *Optics letters*, 2012, **37**(6), P. 1008–1010.
- [5] Merolla J.-M., Mazurenko Y., et al. Phase-modulation transmission system for quantum cryptography. *Optics letters*, 1999, **24**(2), P. 104–106.
- [6] Egorov V.I., Vavulin D.N., et al. Analysis of a sidebands-based quantum cryptography system with different detector types. *Nanosystems: physics, chemistry, mathematics*, 2013, **4**(2), P. 190–195.
- [7] Gleim A.V., Anisimov A.A., et al. Quantum key distribution in an optical fiber at distances of up to 200 km and a bit rate of 180 bit/s. *Bulletin of the Russian Academy of Sciences: Physics*, 2014, **78**(3), P. 171–175.
- [8] Gleim A.V., Egorov V.I., et al. Polarization Insensitive 100 MHz Clock Subcarrier Quantum Key Distribution over a 45 dB Loss Optical Fiber Channel. *Proceeding of “CLEO: 2015 – Laser Science to Photonic Applications”*, OSA, 2015.
- [9] Rezak E., Prokopovich M. Errors accounting of optical fiber length measurement. *Vestn. TOGU*, 2008, **4**, P. 167–171.
- [10] Carslaw H.S., Jaeger J.C. *Conduction of heat in solids*. Clarendon Press, Oxford, 1959, 510 p.

# The use of beam and fiber splitters in quantum random number generators based on vacuum fluctuations

A. E. Ivanova, S. A. Chivilikhin, A. V. Gleim

ITMO University, Kronverkskiy, 49, St. Petersburg, 197101, Russia  
 newiva@mail.ru, sergey.chivilikhin@gmail.com, aglejm@yandex.ru

PACS 03.67.-a

DOI 10.17586/2220-8054-2016-7-2-378-383

Quantum random number generators based on vacuum fluctuations produce truly random numbers that can be used for applications requiring a high degree of randomness. A beam splitter with two inputs and two outputs is normally used in these systems. In this paper, mathematical descriptions were obtained for the use of such beam splitter and fiber Y-splitter in quantum random number generation systems with homodyne detection. We derived equations which allowed us to estimate the impact of the scheme parameters' imperfection upon measurement results. We also obtained mathematical expressions, demonstrating the equivalence of quantum descriptions for a Y-splitter and a beam splitter with two inputs.

**Keywords:** quantum random number generation, beam splitter, Y-splitter, vacuum fluctuations.

*Received:* 22 January 2016

## 1. Introduction

Random numbers can be generated algorithmically, but resulting sequences are pseudorandom and not suitable for applications in which a high degree of randomness is needed, such as quantum cryptography [1]. These applications necessitate true random number generation obtained by indeterminate physical processes, including quantum processes. Existing approaches to quantum random number generation include the use of radiation separation [2], entangled photon states [3], quantum noise of a laser [4], processes of photon emission and detection [5]. An alternative approach is quantum random number generators based on quantum vacuum fluctuations (Fig. 1) [6, 7].

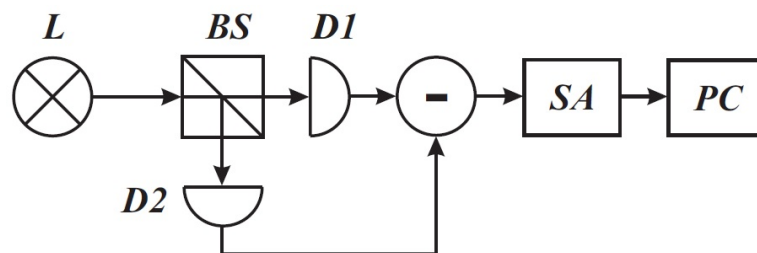


FIG. 1. Quantum random number generation scheme based on vacuum fluctuations: L – laser, BS – beam splitter, D1, D2 – detectors, SA – spectrum analyzer, PC – computer

This type of quantum random number generator extracts randomness from quantum noise obtained when balanced detector subtracts signals received from beam splitter outputs. In these schemes, beam splitters with two inputs and two outputs (Fig. 2a) are normally used. To the first splitter input, a coherent state is sent from a laser, and to the other input – a vacuum

state. These two signals are mixed via a beam splitter, then, signals are sent from the beam splitter outputs to the balanced detector. The subtracted signal is quantum noise, which can be processed on a PC. Random numbers are obtained as a result of received differential signal processing. The purpose of this research was the comparison of quantum descriptions of optical beam splitter and a fiber splitter with one input and two outputs (Fig. 2b). If these quantum descriptions are equal, it will allow us to use a Y-splitter to implement a quantum random number generation system based on quantum vacuum fluctuations.

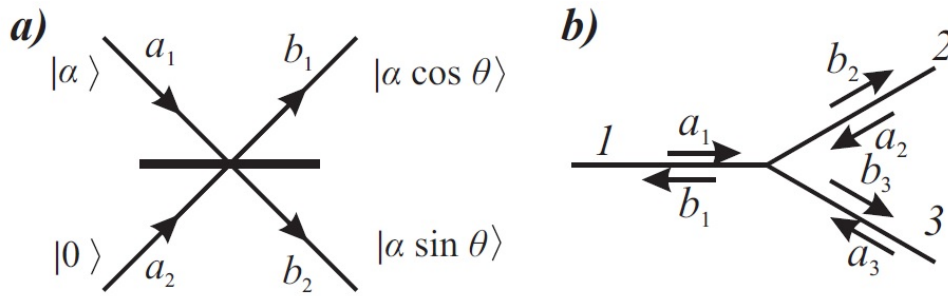


FIG. 2. a) Scheme of a beam splitter with angle  $\theta$ , where a coherent state is sent to the 1st splitter input, and to the other input – a vacuum state. b) Optical Y-splitter.  $a_1, a_2, a_3$  – input signals of the 1st, 2nd and 3rd ports, respectively,  $b_1, b_2, b_3$  – output signals from the splitter

## 2. Beam splitter

Beam splitter is a key element for quantum random number generation schemes based on vacuum fluctuations [6,7]. We consider its impact upon the signal. Mathematical description of a beam splitter, when a strong laser signal, described by the Poisson distribution, arrives at one of its inputs and vacuum state arrives at the other, has been derived in the operator form. In this description, the mean photon number of laser signal  $\alpha$ , the angle of beam splitter  $\theta$  and quantum efficiencies of detectors  $\gamma_1$  and  $\gamma_2$  were taken into account.

If signals  $a_1$  and  $a_2$  come to beam splitter inputs, as shown on Fig. 2a, then signals at outputs,  $b_1$  and  $b_2$  can be described by formula (1):

$$\begin{cases} b_1 = a_1 \cos \theta - a_2 \sin \theta, \\ b_2 = a_1 \sin \theta + a_2 \cos \theta. \end{cases} \quad (1)$$

Laser radiation at the first input is characterized by a Poisson distribution with parameter  $\alpha$  (describing mean photon number), which in operator form is expressed as follows:

$$|\alpha\rangle = e^{\alpha a_1^+ - \alpha^* a_1} |0\rangle, \quad (2)$$

where  $a_1^+$  and  $a_1$  – photon creation and annihilation operators at first input of beam splitter,  $|\alpha\rangle$  – coherent state,  $|0\rangle$  – vacuum state.

When a coherent state is sent to first splitter input and a vacuum state is sent to the second splitter input, then the input signal on the beam splitter is expressed as a tensor product:

$$|\alpha\rangle|0\rangle = e^{\alpha a_1^+ - \alpha^* a_1} |0\rangle_1 |0\rangle_2. \quad (3)$$

If the radiation is characterized by a Poisson distribution with parameter  $|\alpha\rangle$  that passes through a beam splitter with angle  $\theta$  (Fig. 2a), then one of beam splitter outputs is characterized by a

Poisson distribution with parameter  $|a \cos \theta\rangle$ , and second is characterized by Poisson distribution with parameter  $|a \sin \theta\rangle$ .

In the case of the symmetric beam splitter, we obtain expression, describing signals at both outputs:

$$b_1^+ = b_2^+ = \frac{1}{\sqrt{2}}a_1^+. \quad (4)$$

The differential current after detection can be defined as follows:

$$\Delta i = i_2 - i_1 = \gamma_2 b_2^+ b_2 - \gamma_1 b_1^+ b_1, \quad (5)$$

where  $i_1, i_2$  are photocurrents at first and second detectors,  $\gamma_1, \gamma_2$  are quantum efficiencies of detectors.

For a symmetric beam splitter and detectors with equal quantum efficiencies, the mean value of the differential current is determined to be zero, and amplitude of the differential current deviation is directly proportional to the intensity of incident radiation.

In the case of using an asymmetric beam splitter and detectors with different quantum efficiencies, the mean value of the differential current is characterized by the following equation:

$$\langle \Delta i \rangle = \alpha^2 (\gamma_2 \sin^2 \theta - \gamma_1 \cos^2 \theta). \quad (6)$$

In this case, the amplitude of differential current deviation can be estimated by the following formula (7):

$$\delta i = \alpha \sqrt{\gamma_2^2 \sin^2 \theta + \gamma_1^2 \cos^2 \theta}. \quad (7)$$

### 3. Y-splitter

Using a Y-splitter as a basic element for homodyne detection allows one to obtain the lower level of determined ambient noise and reduce the size of the device without compromising the generation rate or degree of randomness for the generated sequences. We consider the Y-splitter (Fig. 2b) as a system with three inputs and three outputs [8], because input and output signals can pass through one channel.

The relationship between the input and output signals in a Y-splitter which allows showing the correlation between each pair of signals, can be described by the following expression:

$$\begin{pmatrix} b_1 \\ b_2 \\ b_3 \end{pmatrix} = \begin{pmatrix} -\sqrt{1-2\lambda^2} & \beta & \beta \\ \lambda & -\gamma & \sqrt{1-\beta^2-\gamma^2} \\ \lambda & \sqrt{1-\beta^2-\gamma^2} & -\gamma \end{pmatrix} \begin{pmatrix} a_1 \\ a_2 \\ a_3 \end{pmatrix}, \quad (8)$$

where  $\lambda$  is the proportionality factor connecting the input signal at the 1st port and output signals at 2nd and 3rd ports;  $\beta$  is the proportionality factor connecting the input signals at the 2nd or 3rd ports and the output signal at the 1st port;  $\gamma$  is the proportionality factor connecting the input and output signals of the 2nd port or input and output signals of the 3rd port.

These coefficients are selected in accordance with requirements of the unitary property for the matrix. The next expressions also arise from unitarity conditions:

$$\begin{cases} -\sqrt{1-2\lambda^2}\beta - \lambda\gamma + \lambda\sqrt{1-\beta^2-\gamma^2} = 0, \\ -\sqrt{1-2\lambda^2}\beta + \lambda\sqrt{1-\beta^2-\gamma^2} - \lambda\gamma = 0, \\ \beta^2 - 2\gamma\sqrt{1-\beta^2-\gamma^2} = 0. \end{cases} \quad (9)$$

After selection of matrix proportionality factors, it is possible to simplify the matrix form using the fact that the parameters  $\lambda$  and  $\beta$  can be expressed for this system through the  $\gamma$ :

$$\lambda = \beta = \sqrt{2\gamma(1-\gamma)}. \quad (10)$$

Then, the original matrix takes form:

$$\begin{pmatrix} 1-2\gamma & \sqrt{2\gamma(1-\gamma)} & \sqrt{2\gamma(1-\gamma)} \\ \sqrt{2\gamma(1-\gamma)} & -\gamma & 1-\gamma \\ \sqrt{2\gamma(1-\gamma)} & 1-\gamma & -\gamma \end{pmatrix}. \quad (11)$$

We consider the special case when a signal from 1st input port is distributed only between ports 2 and 3 without reflection on the 1st port. In this case  $\sqrt{1-2\lambda^2} = 0$ , and  $\lambda = \frac{1}{\sqrt{2}}$ , then by using expressions were obtained above, we can derive the values  $\beta = \frac{1}{\sqrt{2}}$  and  $\gamma = \frac{1}{2}$ .

If signal  $a_1$  is sent to 1st port of Y-splitter, then signals from outputs 2 and 3 can be described by using matrix with these proportionality factors:

$$\begin{pmatrix} b_1 \\ b_2 \\ b_3 \end{pmatrix} = \begin{pmatrix} 0 & \frac{1}{\sqrt{2}} & \frac{1}{\sqrt{2}} \\ \frac{1}{\sqrt{2}} & -\frac{1}{2} & \frac{1}{2} \\ \frac{1}{\sqrt{2}} & \frac{1}{2} & -\frac{1}{2} \end{pmatrix} \begin{pmatrix} a_1 \\ 0 \\ 0 \end{pmatrix} = \begin{pmatrix} 0 \\ \frac{1}{\sqrt{2}}a_1 \\ \frac{1}{\sqrt{2}}a_1 \end{pmatrix}. \quad (12)$$

Thus,

$$b_2^+ = b_3^+ = \frac{1}{\sqrt{2}}a_1^+. \quad (13)$$

Then, we can consider the matrix elements describing the interconnection between signal at 1st input port of Y-splitter and signals, emanating from 2nd and 3rd ports, thus:

$$b_2^+ = b_3^+ = \frac{1}{\sqrt{2}}a_1^+. \quad (14)$$

This expression coincides with signals that were obtained at output ports of symmetric beam splitter, when the coherent state  $a_1$  was sent to the first splitter input, and a vacuum state – to the other. Thus, as the description for the beam splitter and Y-splitter are equal, we can use results for beam splitter, obtained earlier, to evaluate work of quantum random generation systems, based on vacuum fluctuations using the Y-splitter.

#### 4. Y-splitter with complex parameters

When we use complex parameters to mathematically describe the Y-splitter, then original system (8) is changing. Relationship between signals at inputs and outputs of Y-splitter is shown in the following expression:

$$\begin{pmatrix} b_1 \\ b_2 \\ b_3 \end{pmatrix} = \begin{pmatrix} -\sqrt{1-2|\lambda|^2} & \beta & \beta \\ \lambda & -\gamma & \sqrt{1-|\beta|^2-|\gamma|^2} \\ \lambda & \sqrt{1-|\beta|^2-|\gamma|^2} & -\gamma \end{pmatrix} \begin{pmatrix} a_1 \\ a_2 \\ a_3 \end{pmatrix}. \quad (15)$$

In the next matrix parameters,  $\lambda$  and  $\beta$  were derived from the original matrix through the parameter  $\gamma = \gamma_r + i\gamma_i$ :

$$\begin{pmatrix} 2\gamma_r - 1 & \sqrt{2\gamma_r(1-\gamma_r)} + i\gamma_i\sqrt{\frac{1-\gamma_r}{2\gamma_r}} & \sqrt{2\gamma_r(1-\gamma_r)} + i\gamma_i\sqrt{\frac{1-\gamma_r}{2\gamma_r}} \\ \sqrt{2\gamma_r(1-\gamma_r)} + i\frac{\gamma_i\sqrt{1-\gamma_r}}{\sqrt{2\gamma_r(2\gamma_r-1)}} & -\gamma_r - i\gamma_i & 1 - \gamma_r \\ \sqrt{2\gamma_r(1-\gamma_r)} + i\frac{\gamma_i\sqrt{1-\gamma_r}}{\sqrt{2\gamma_r(2\gamma_r-1)}} & 1 - \gamma_r & -\gamma_r - i\gamma_i \end{pmatrix} \quad (16)$$

We can see, that coefficient  $\gamma$  shows reflection at port 2, when signal  $a_2$  is sent to the 2st port of Y-splitter, and there are no input signals at other ports. Then, we consider when signal  $a_1$  is sent to the 1st port of Y-splitter, and there are no input signals at other ports, then signal is distributed only between output ports 2 and 3, and we can estimate signals for the 2nd and 3rd ports:

$$b_2^+ = b_3^+ = \sqrt{2(1-\gamma_r)} \exp\left(i\frac{\gamma_i}{2\gamma_r(2\gamma_r-1)}\right) a_1^+. \quad (17)$$

These result, with the exception of phase shift, coincides with signals that were obtained at output ports of symmetric beam splitter, when coherent state  $a_1$  was sent to the first splitter input, and a vacuum state - to the other.

#### 5. Conclusion

In this research, we obtained expressions describing the relationship between beam splitter input radiation and differential current. For a symmetric beam splitter and detectors with equal quantum efficiencies, the mean value of differential current is determined to be zero, and the amplitude of the differential current deviation is directly proportional to the intensity of the incident radiation. We also derived equations for an asymmetric beam splitter, allowing estimation of how the scheme parameters imperfection affect the measurement results.

We obtained mathematical expressions, demonstrating the equivalence for the quantum description of beam splitter with two inputs and Y-splitter, when we didn't use complex parameters in equations. When we use complex parameters in equations, then the results, with the exception of the phase shift, coincide with the signals obtained for output ports of symmetric beam splitter with two inputs and two outputs, when coherent state is sent to the first splitter

input, and a vacuum state – to the other. That allows us to use a Y-splitter for the implementation of a quantum random number generation system based on quantum vacuum fluctuations, and to apply formulas previously-obtained for the calculations of systems consisting of a beam splitter with two inputs and two outputs.

### Acknowledgements

This work was partially financially supported by the Government of the Russian Federation (grant 074-U01).

### References

- [1] Scarany V., Bechmann-Pasquinucci H., et. al. The security of practical quantum key distribution. *Rev. Mod. Phys.*, 2009, **81**, P. 1301–1350.
- [2] Jennewein T., Achleitner U., et. al. A fast and compact quantum random number generator. *Rev. Sci. Instrum.*, 2000, **71**(4), P. 1675–1680.
- [3] Kwon O., Cho Y.-W., Kim Y.-H. Quantum random number generator using photon-number path entanglement. *Appl. Opt.*, 2009, **48**, P. 1774–1778.
- [4] Qi B., Chi Y.-M., et. al. High-speed quantum random number generation by measuring phase noise of a single-mode laser. *Optics Letters*, 2010, **35**, P. 312–314.
- [5] Dynes J.F., Yuan Z.L., et al. A high speed, post-processing free, quantum random number generator. *Appl. Phys. Lett.*, 2008, **93**, P. 031109.
- [6] Shen Y., Tian L., Zou H. Practical quantum random number generator based on measuring the shot noise of vacuum states. *Phys. Rev. A.*, 2010, **81**, P. 063814.
- [7] Gabriel C., Wittmann C., et. al. A generator for unique quantum random numbers based on vacuum states. *Nature Phot.*, 2010, **4**, P. 711–715.
- [8] Ivanova A.E., Chivilikhin S.A., Popov I.Yu., Gleim A.V. On the possibility of using optical Y-splitter in quantum random number generation systems based on fluctuations of vacuum. *Nanosyst.: Phys., Chem., Math.*, 2015, **6**(1), P. 95–99.

# Laser generation without inversion on the fine levels of the helium atom

A. G. Petrashen, N. V. Sytenko

ITMO University, 197101, Saint Petersburg, Russia

apetrashen@mail.ru

PACS 32.80.Qk

DOI 10.17586/2220-8054-2016-7-2-384-393

By using the example of transfer between fine structure levels in the helium atom, the possibility of laser generation without inversion has been studied.

**Keywords:** coherent excitation, density matrix evolution, dark states.

*Received: 20 November 2015*

## 1. Introduction

The possibility of lasing without inversion (LWI) was first postulated by Kocharovskaya and Harris [1,2]. In the latter of these works, the assumption of LWI viability had been based on a comparison of the absorption and transmission coefficients of a three-level system, which is excited according to  $V$ -scheme, whereas in previous works, it was shown that, for certain parameter values for a system which is excited according to  $\Lambda$ -scheme, the laser generation without inversion is possible. Furthermore, in our opinion, the work of Imamoglu and Harris [3], must be highlighted. In this work, issued shortly after those two mentioned above, the opinion was first expressed that LWI could be produced using the absorption that disappeared within one of the  $\Lambda$ -scheme arms, whereas within another arm, excitation is performed by means of a strong EM-field (phenomenon of electromagnetic induced transparency (EIT)) [4]. In the subsequent works, the possibility for LWI, in principle, has been widely discussed (see, e.g. [4–9]).

However, Zibrov et al. [11] were the first to experimentally observe the LWI phenomenon, where a set of four levels for the hyperfine atomic structure of  $^{87}\text{Rb}$  was considered: two hyperfine levels for the ground  $^2\text{S}_{1/2}$  state, as well as two analogous levels for the first excited  $^2\text{P}_{1/2}$  state. The strong-coupled and weak probe fields were bound according to the  $V$ -scheme one superfine level of the ground state with two superfine levels of the first excited state. In the article, the frequency range at which the absorption coefficient becomes negative, i.e. lasing generation occurs, was determined both theoretically (by means of numerical solution of the Liouville equation for the density matrix) and experimentally.

Work [12] is similar to one just mentioned, with the difference being that LWI was experimentally implemented using sodium atoms in the framework of the  $\Lambda$ -scheme, formed by two hyperfine levels of the ground state  $^2\text{S}_{1/2}$  and level  $F = 1$  of the first excited state  $^2\text{P}_{1/2}$  of this atom. In this work, the strong coupling field acts between the  $F = 2$  levels of the  $^2\text{S}_{1/2}$  state and the  $F = 1$  level of the  $^2\text{P}_{1/2}$  state. This field, in combination with very weak probe field, connecting levels of the hyperfine structure with  $F = 1$  of the  $^2\text{S}_{1/2}$  and  $^2\text{P}_{1/2}$  states leads to the appearance of EIT resonance. Additionally, it was experimentally shown that at a frequency close to where EIT occurs, amplification of the probe signal is observed. Subsequently, the system has been positioned inside an annular resonator, and laser oscillation was observed within the system, being provided by vacuum fluctuations.

In this work, the possibility of laser generation without inversion (LWI) within a multi-level system that is positioned inside a high- $Q$  annular resonator will be considered. The subject being dealt with here is closely allied with work [13], where a non-inversion superreliance impulse was observed for fine levels of the helium atom.

## 2. The statement of the problem

In this work, radiation emitted from  $3^3S_1$  state (level “b”) of isotope  $^4\text{He}$ , whose coherent excitation is performed according to the  $\Lambda$ -scheme from levels  $2^3P_2$  and  $2^3P_1$  (hereafter referred to as, levels “a” and “c”) of this atom (see Fig. 1), will be considered. It should be noted that the first of those two lower states could be referred to as metastable ones [16], and hereupon a considerable population could be created at this level, for example, by means of an impact from the ground state. In the framework of such an excitation, the fine bond is broken, and the efficiency of population induction for the  $2^3P$  state could be described as follows:

$$\sigma_{j,m;j',m'} = \frac{1}{2j+1} A^{(0)}(j, j', s) + \alpha \sum_q (-1)^{j'+m'} \begin{bmatrix} j & j' & 2 \\ m & -m' & q \end{bmatrix} D_{0,q}^{(2)}(\theta) A^{(2)}(j, j', l, s), \quad (1)$$

where  $j$  and  $s$  depict total electron and spin moments, parameter  $\alpha$  characterizes an anisotropy of impact excitation. As an example, this value may be set as a ratio of induced orbital alignment to a population [14]:  $\alpha = T_0^2/T_0^0$ , and, finally,  $D_{m,m'}^{(2)}(\theta)$  – elements of three-dimensional rotational matrix [15]. The quantities  $A^{(k)}$  in this expression depend only on the kinematics of momentum vectorial addition:

$$A^{(k)}(j, j', l, s) = (-1)^{j'+s+k+l} \sqrt{(2j+1)(2j'+1)} \begin{Bmatrix} l & l & k \\ j & j' & s \end{Bmatrix}. \quad (2)$$

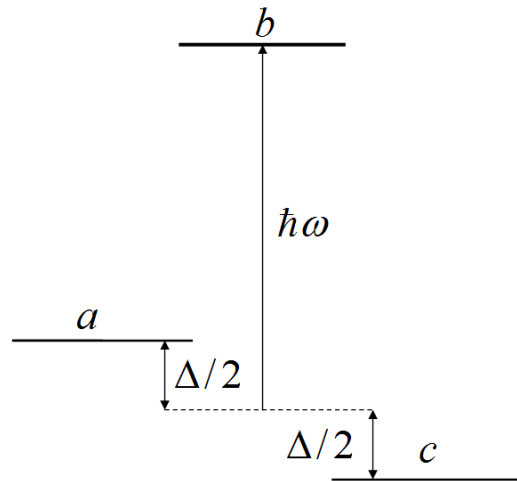


FIG. 1. The excitation scheme

In this work, we will assume, that the Hamilton operator of the atomic system takes the form:

$$\hat{H} = \hat{H}_0 + \hat{V}, \quad (3)$$

where  $H_0$  is the Hamiltonian operator of a free helium atom, while operator  $\hat{V}$  describes the excitation process of level  $j = 1$  (hereafter, of the level “b”) of  $3^3S_1$  state of the aforementioned atom. In regard to the excitation process, we will assume that in both arms,  $ab$  and  $cb$ , excitation is initiated by means of light polarized linearly along the  $OZ$ -axis laboratory frame of reference

(this axis coincides with the direction of propagation for the exiting radiation), at frequencies  $\omega - \delta_a/\hbar$  and  $\omega + \delta_c/\hbar$ , respectively. The wave functions of all states have been constructed according to general addition rules for angular momenta, whereas energy parameters of those functions have been chosen according to the quantum defect method:

$$\begin{aligned} (W_{ab})_{MM_1} &= \sum_{m,q} \begin{bmatrix} 1 & 1 & 1 \\ m & M_1 & M \end{bmatrix} \begin{bmatrix} 0 & 1 & 1 \\ 0 & q & m \end{bmatrix} (e_{ab})_q \cos(\omega + \delta_a/\hbar), \\ (W_{cb})_{MM_1} &= \sum_{m,q} \begin{bmatrix} 1 & 1 & 2 \\ m & M_1 & M \end{bmatrix} \begin{bmatrix} 0 & 1 & 1 \\ 0 & q & m \end{bmatrix} (e_{cb})_q \cos(\omega + \delta_c/\hbar), \end{aligned} \quad (4)$$

where  $e_q$  is the path of the light polarization in some arm of the  $\Lambda$ -scheme.

Exciting electric field  $\vec{E}(t)$  causes medium polarization that is characterized by the polarization vector  $\vec{P}$ , whose quantity is proportional to the density of the atoms  $n_0$  and mean value of the dipole moment operator  $\hat{d}$ , calculated with the density correlation matrix:

$$\vec{P} = -n_0 \Im \left( \left[ \text{Sp} \left( \rho_{ab} \vec{d}_{ab} \right) \right] + \left[ \text{Sp} \left( \rho_{cb} \vec{d}_{cb} \right) \right] \right). \quad (5)$$

From the last expression, one can see that the medium polarization, as a result of excitation, is defined by the density correlation matrix, and, therefore, depends on its variation. In turn, the right side of Liouville equation that describes the density matrix evolution, depends on Rabi frequency, which is proportional to the electric field value. Therefore, mutual variation of the density matrix and of the induced electric field could be described by the following system of self-consistent equations:

$$\begin{aligned} \frac{d}{dt} \tilde{\rho}_{aa}(t) &= \Gamma \tilde{\rho}_{bb}(t) - \frac{i}{\hbar} (V_{ab}(t) \tilde{\rho}_{ba}(t) - \tilde{\rho}_{ab}(t) V_{ba}(t)), \\ \frac{d}{dt} \tilde{\rho}_{bb}(t) &= -\Gamma \tilde{\rho}_{bb}(t) - \frac{i}{\hbar} (V_{ba}(t) \tilde{\rho}_{ab}(t) - \tilde{\rho}_{ba}(t) V_{ab}(t)) - \frac{i}{\hbar} (V_{bc}(t) \tilde{\rho}_{cb}(t) - \tilde{\rho}_{bc}(t) V_{cb}(t)), \\ \frac{d}{dt} \tilde{\rho}_{cc}(t) &= \Gamma \tilde{\rho}_{bb}(t) - \frac{i}{\hbar} (V_{cb}(t) \tilde{\rho}_{bc}(t) - \tilde{\rho}_{cb}(t) V_{bc}(t)), \\ \frac{d}{dt} \tilde{\rho}_{ab}(t) &= -\frac{\Gamma}{2} \tilde{\rho}_{ab}(t) - \frac{i}{\hbar} (E_a - E_b) \tilde{\rho}_{ab}(t) - \frac{i}{\hbar} (V_{ab}(t) \tilde{\rho}_{bb}(t) - \tilde{\rho}_{aa}(t) V_{ab}(t)), \\ \frac{d}{dt} \tilde{\rho}_{cb}(t) &= -\frac{\Gamma}{2} \tilde{\rho}_{cb}(t) - \frac{i}{\hbar} (E_c - E_b) \tilde{\rho}_{cb}(t) - \frac{i}{\hbar} (V_{cb}(t) \tilde{\rho}_{bb}(t) - \tilde{\rho}_{cc}(t) V_{cb}(t)), \\ \tilde{\rho}_{ba}(t) &= \tilde{\rho}_{ab}^\dagger(t); \quad \tilde{\rho}_{bc}(t) = \tilde{\rho}_{cb}^\dagger(t), \\ \nabla^2 \vec{E} - \frac{1}{c^2} \frac{\partial^2}{\partial t^2} \vec{E} &= \frac{4\pi}{c^2} \frac{\partial^2}{\partial t^2} \vec{P}, \end{aligned} \quad (6)$$

where the matrix  $\Gamma$  describes the relaxation process,  $E_a$  and  $E_c$  are the energies for the lower levels "a" and "c" respectively,  $E_b$  is the energy of the upper  $3^3S_1$  state. Solution of such systems is usually attempted using the rotating wave approximation, which means, that in system (6), all terms that oscillate with the frequency  $\omega$  of the exciting field should be neglected. The higher order derivatives of slowly-varying summands should also be neglected. To separate such terms in the system, it is convenient to introduce density matrices  $\rho_{i,j}(t)$  ( $i, j = a, b, c$ ) connected with previously used similar matrices, by means of the relations:  $\rho_{ii}(t) = \tilde{\rho}_{ii}(t)$  ( $i = a, b, c$ ),  $\rho_{b,i}(t) = \tilde{\rho}_{b,i}(t) \exp(-i(E_b - E_i)t)$ ,  $i = a, c$ ,  $\rho_{j,i}(t) = \rho_{j,i}(t)^\dagger$ . In regard to the last equation, to separate rapidly oscillating summands, field strength and field polarization vectors should be solved in the following manner:  $E = \mathcal{E}(x, t) e^{i(\omega t + kx)} + \mathcal{E}^*(x, t) e^{-i(\omega t + kx)}$  and

$P = \mathcal{P}(x, t)e^{i(\omega t + kx)} + \mathcal{P}^*(x, t)e^{-i(\omega t + kx)}$ , where  $\mathcal{E}(x, t) = \Re\mathcal{E}(x, t) + i\Im\mathcal{E}(x, t)$  and  $\mathcal{P}(x, t) = \Re\mathcal{P}(x, t) + i\Im\mathcal{P}(x, t)$ . As a result of such substitutions, the last equation of system (6) will be reduced to a pair of first-order equations that links the real and imaginary parts of field strength and polarization vectors:

$$\begin{aligned}
 \frac{d}{dt}(\Im\mathcal{E}(x, t)) + c\frac{d}{dx}(\Im\mathcal{E}(x, t)) &= -2\pi\omega\Re(\mathcal{P}(x, t)), \\
 \frac{d}{dt}(\Re\mathcal{E}(x, t)) + c\frac{d}{dx}(\Re\mathcal{E}(x, t)) &= 2\pi\omega\Im(\mathcal{P}(x, t)).
 \end{aligned} \tag{7}$$

Hereafter, we will assume the polarization field to be independent from the spatial coordinates. Next, we introduce the dimensionless Rabi frequency  $\Omega_R(t)$ , which is linked to the polarization vector by the relation  $\Omega_R(t) = \mathcal{E}(t)\tau_0 ea_0/\hbar$ , where  $\tau_0 = 36 \cdot 10^{-9}$  s [16] is the time of life of excited state  $3^3S_1$ , and introduce dimensionless time  $\tau = t/\tau_0$ , and, additionally, assuming that functions  $\mathcal{P}$  and  $\mathcal{E}$  vary slowly with time, and that the system is positioned inside an annular resonator, such that one of the eigenfrequencies coincides with the transition frequency between the ‘‘centers of gravity’’ for the upper and lower multiples, then, for system (8), one can write:

$$\begin{aligned}
 \frac{d}{d\tau}\rho_{aa}(\tau) &= \Gamma_a\rho_{bb}(\tau) + \frac{i\Omega_R}{2}[\rho_{ab}(\tau)W_{ba}(\tau)/z_a - W_{ab}(\tau)\rho_{ba}(\tau)z_a], \\
 \frac{d}{d\tau}\rho_{cc}(\tau) &= \Gamma_c\rho_{bb}(\tau) + \frac{i\Omega_R}{2}[\rho_{cb}(\tau)W_{bc}(\tau)z_c - W_{cb}(\tau)\rho_{bc}(\tau)/z_c], \\
 \frac{d}{d\tau}\rho_{bb}(\tau) &= -\Gamma\rho_{bb}(\tau) - \frac{i\Omega_R}{2}\left[W_{ba}\rho_{ab}(\tau)/z_a - \frac{i}{2\hbar}\rho_{ba}(\tau)W_{ab}z_a\right] - \\
 &\quad \frac{i\Omega_R}{2}\left[W_{bc}\rho_{cb}(\tau)z_c - \frac{i}{2\hbar}\rho_{bc}(\tau)W_{cb}/z_c\right], \\
 \frac{d}{d\tau}\rho_{ab}(\tau) &= -\frac{\Gamma}{2}\rho_{ab}(\tau) + \frac{i\Omega_R}{2}\left[\rho_{aa}(\tau)W_{ab}z_a - \frac{i}{2\hbar}W_{ab}\rho_{bb}(\tau)z_a\right] + \frac{i\Omega_R}{2}\rho_{ac}(\tau)W_{cb}/z_a, \\
 \frac{d}{d\tau}\rho_{cb}(\tau) &= -\frac{\Gamma}{2}\rho_{cb}(\tau) - \frac{i\Omega_R}{2}\left[W_{cb}\rho_{bb}(\tau)/z_c + \rho_{cc}(\tau)W_{cb}/z_c\right] + \frac{i\Omega_R}{2}\rho_{ca}(\tau)W_{ab}z_a, \\
 \frac{d}{d\tau}\Omega_R &= -\Omega_M^2 i(\text{Sp}(\rho_{ab}d_z) + \text{Sp}(\rho_{bc}d_z)), \\
 \rho_{ba}(t) &= \rho_{ab}^\dagger(t); \quad \rho_{bc}(t) = \rho_{cb}^\dagger(t),
 \end{aligned} \tag{8}$$

where  $z_a = \exp(i\tau(\frac{\Delta}{2\hbar} + \delta_a))$  and  $z_c = \exp(i\tau(\frac{\Delta}{2\hbar} - \delta_c))$ , and  $\Omega_M$  is the dimensionless frequency of the field oscillation amplitude  $\Omega_M = \sqrt{4\pi n_0 \left(\frac{ea_0}{\hbar}\right)^2 \hbar\omega \frac{\langle r \rangle}{a_0}}$ , which depends on  $\langle r \rangle$  – dimensionless main value of operator  $\hat{r}$  for the  $3^3S_1$  state. The substitution of values for the fundamental constants in the last relation leads to the relation  $\Omega_M = 5.1610^{-4}\sqrt{n_0}$ , where  $n_0$  – density of the particulars.

### 3. The approximate solution of the Liouville equation

According to the fact, that the coupling field, which is acting in the ‘‘bc’’ arm of  $\Lambda$ -scheme, is considered strong relative to the field acting in the ‘‘ba’’ arm, a solution for system (9) could be found by means of perturbation theory, in the framework of initial conditions

$\rho_{aa}(0) = \rho_{aa}^{(0)}$ ,  $\rho_{cc}(0) = \rho_{cc}^{(0)}$  and  $\rho_{bb}(0) = 0$ , where  $\rho_{cc}(0)$  and  $\rho_{bb}(0)$  are determined by relation (1). Large values for the coupling field lead to the segmentation of them considered systems splitting into blocks, the first of which associates the density correlation matrices  $\rho_{ab}(t)$  and  $\rho_{ac}(t)$ :

$$\begin{aligned} \frac{d}{dt}\rho_{ab}(t) &= -\frac{\gamma_{ab}}{2}\rho_{ab}(t) + \frac{i}{2}\rho_{aa}^{(0)}W_{ab}e^{it(\delta_a+\Delta/2\hbar)} + \frac{i}{2}\rho_{ac}(t)W_{cb}e^{-it(-\delta_c+\Delta/2\hbar)}, \\ \frac{d}{dt}\rho_{ac}(t) &= -\frac{\gamma_{ac}}{2}\rho_{ac}(t) + \frac{i}{2}\rho_{ab}(t)W_{bc}e^{it(-\delta_c+\Delta/2\hbar)}. \end{aligned} \quad (9)$$

Now, it is pertinent to introduce matrix  $x_{ac}(t)$  and  $x_{ab}(t)$  according to expression:

$$\rho_{ac}(t) = x_{ac}(t)e^{-\gamma_{ac}t/2}; \quad \rho_{ab}(t) = x_{ab}(t)e^{-\gamma_{ab}t/2}, \quad (10)$$

then, according to the second equation of system (9), for matrix  $x_{ac}(t)$ , one can obtain that:

$$\frac{d}{dt}x_{ac}(t)W_{cb} = \frac{1}{2}i \exp\left(\frac{i\Delta + (\gamma_{ac} - \gamma_{ab} - 2i\delta_c)\hbar}{2\hbar}t\right)x_{ab}(t)W_{bc}W_{cb}. \quad (11)$$

Then, having differentiated the first of equations (9) and substituting it into expression (11), the equation for the  $x_{ac}(t)$  matrix may be obtained:

$$\begin{aligned} \frac{d^2}{dt^2}x_{ab}(t) + \frac{(i\Delta) + (\gamma_{ac} - \gamma_{ab} - 2i\delta_c)\hbar}{2\hbar} \frac{d}{dt}x_{ab}(t) + \\ \left[ x_{ab} \frac{W_{bc}W_{cb}}{4} + \frac{2\Delta + [(-i\gamma_{ac} + 2\delta_a - 2\delta_c)\hbar]}{4\hbar} \rho_{aa}^{(0)}W_{ab} \right] e^{\frac{t}{2}(\gamma_{ab} + i[\Delta + 2\delta_a\hbar]/\hbar)} = 0. \end{aligned} \quad (12)$$

Partial solution of this equation makes it possible to write a similar solution for  $\rho_{ab}(t)$  matrix:

$$\rho_{ab}(t) = e^{it[\Delta + 2\delta_a\hbar]/2\hbar} \frac{(2\Delta + (-i\gamma_{ac} + 2\delta_a - 2\delta_c)\hbar)}{2\hbar} \rho_{aa}^{(0)}W_{ab}U, \quad (13)$$

where  $U$  is a square matrix having the same order as the density matrix of the upper level ( $\rho_{bb}(t)$ , in the case under consideration), that contains  $I_b$  – the identity matrix of the same order as  $\rho_{bb}(t)$ :

$$U = \left[ \frac{1}{4}W_{bc}W_{cb} - I_b \frac{(\Delta - i\gamma_{ab}\hbar + 2\delta_a\hbar)(2\Delta + (-i\gamma_{ac} + 2\delta_a - 2\delta_c)\hbar)}{4\hbar^2} \right]^{-1}. \quad (14)$$

From expression (13), it is apparent that in the absence of relaxation processes, the difference of the frequency mismatches in each arm of the  $\Lambda$ -scheme is equal to the lower levels splitting of  $\delta_c - \delta_a = \Delta$ , and the absorption of the probe field in the  $bc$  arm vanishing. This effect is known as electromagnetically induced transparency (EIT).

Based on formula (13), the expression for density matrix that defines the “low-frequency coherence” can be obtained:

$$\rho_{ac}(t) = \frac{1}{4} \left( -e^{t\gamma_{ac}/2} + e^{it[\Delta + (\delta_a - \delta_c)\hbar]/\hbar} \right) \rho_{aa}^{(0)}W_{ab}UW_{bc} \left( 1 - e^{it[\Delta + (\delta_a - \delta_c)\hbar]/\hbar} \right), \quad (15)$$

as well as elements of the density matrix  $\rho_{bc}(t)$ , that determines coherence in  $bc$  arm:

$$\begin{aligned} \rho_{bc}(t) = \left\{ \frac{\hbar}{4} \left[ \frac{(e^{-\gamma_{bc}t/2} - e^{t(i\Delta + (\gamma_{ac} + 2i\delta_a)\hbar)/2\hbar})}{\Delta + (-i\gamma_{ac} + i\gamma_{bc} + 2\delta_a)\hbar} + \right. \right. \\ \left. \left. \frac{(e^{-t\gamma_{bc}/2} - e^{it(\Delta - 2\delta_c\hbar)/2\hbar})}{4(\Delta - i\gamma_{bc}\hbar + 2\delta_c\hbar)} \right] W_{ba}\rho_{aa}^{(0)}W_{ab}UW_{bc} \right\} - \frac{i}{2}e^{it(\Delta - 2\delta_c\hbar)/2\hbar}W_{bc}\rho_{cc}^{(0)}. \end{aligned} \quad (16)$$

#### 4. Discussion on the subject of numerical calculation results.

Before considering the items related to the solution of the system (9), some principal problems connecting to the possibility of laser generation should be discussed.

First of all, it should be noted that, as numerical calculation has demonstrated, the low-frequency coherence does not have a significant influence on the generation process. Much more significant impediments to the generation process are resonance collisions of excited atoms with atoms in ground state, that exhibit a destructive behavior, resulting in decay of generation.

From the theory of collisional depolarization [14], it is well-known that within the limits of the impact-parameter method, the relaxation constant of collisional process of two heavy particles, being described by the mutual interaction law  $W \sim 1/R^n$  (here  $R$  is an internuclear distance), is described by the relaxation constant:

$$\gamma = n_0 v \left( \frac{Q}{\hbar v} \right)^{\frac{2}{n-1}} F(n), \quad (17)$$

where  $n_0$  is a projectile density (the density of the of buffer gas particles),  $v$  – relative velocity of colliding particles, while  $Q$  is a constant that depends on angular moments and interaction law,  $F(n)$  is an expression that appears due to averaging of variation of the products of the density matrix over the impact parameter. Concerning the  $Q$  quantity, it should be noted that this value is equal to the Van der Waals constants difference in the case of interaction by law  $W \sim 1/R^6$ , and to the quadrupole moment in the case of interaction by law  $W \sim 1/R^3$ . The first of these laws is implemented at interaction of two different atoms, whereas the second is utilized for the interaction of identical atoms. Owing to the fact that in coherent excitation experiments, the hyperfine sublevels of the ground state are usually used as the lower levels, then the influence of the collisions on those atoms is described by the law  $W \sim 1/R^3$ , whereas influence of buffer gas on the excited state is described by law  $W \sim 1/R^6$ . It follows from what was said, that the resonance collisions (collisions of two identical particles) leads to significant broadening of the lower hyperfine levels, and even to their overlapping.

Within the work under consideration, when lower levels, having a fine structure for the excited state with splitting of about  $0.1 \text{ cm}^{-1}$  are used [16], as a consequence, the influence of collisions with particles of buffer gas is fairly insignificant. In support of this statement, the following could be noted. On the one hand, for successful laser emission recording, it is necessary to induce significant impact population of the  $2^3\text{P}$  state of helium atoms ensemble. Without going into technical difficulties, it should be noted that as soon as such an ensemble has been created, atoms engaged in  $2^3\text{P}$  state would interact with each other by law  $1/R^3$ , while with atoms of buffer gas by law  $1/R^6$ . But it is clear that at given general density of helium atoms, the density of impact-excited atoms would be significantly less than the density of non-excited particles, and therefore  $2^3\text{P}$  state of helium atom would be broadened to a significantly weaker extent. It should be noted as well that, in the case under consideration, one of the lower states  $2^3\text{P}_2$  is metastable [16], whereas the influence of finiteness of the lifetime of the second lower state  $2^3\text{P}_1$  can be taken into account by means of introducing the appropriate relaxation constants.

System (9) was integrated numerically, using method that has been described, in some detail, in our previous work [17]. On the system integration, we assumed that, at the initial point of time, the upper level is not populated  $\rho_{i,b}(0) = 0$  ( $i = a, b, c$ ), whereas a numerical vales of the rest blocks of the density matrix are defined by formula (1). As for the fields that are active in the arms of  $\Lambda$ -scheme, in each arm, they are equal to the vector sum of the two fields: the stationary pumping field and the polarization one. With regard to the stationary

pumping fields, we will assume that they are equal to zero at  $t \leq 0$ , and reach their preset values in a stepwise manner at  $t > 0$ . Additionally, we will assume that at the initial point of time, the system undergoes a short “start-up” impulse, and later, at  $t > 0$ , the field active in the system is defined by system (9). Numerical calculation results are represented in Figs. 2 – 6.

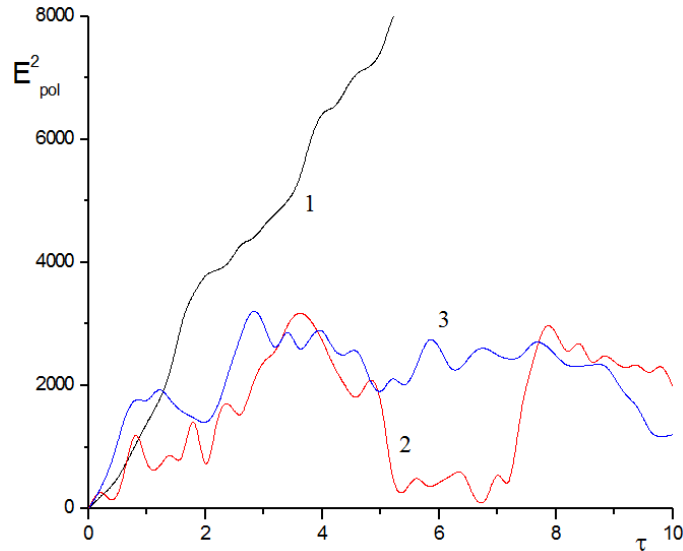


FIG. 2. The dependence of intensity of polarization field on dimensionless time. Curves 1–3 coincide the mismatches in  $bc$  arm of  $\Lambda$ -scheme equal to  $\delta_c = 0, \Delta/2, \Delta$  whereas mismatch in  $ba$  arm is equal to zero

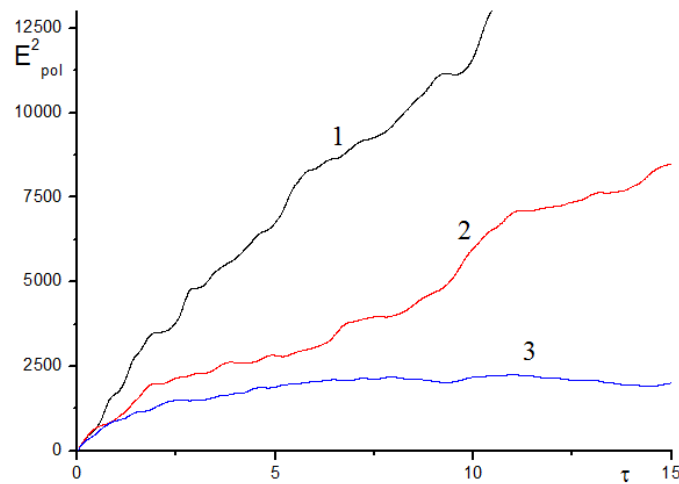


FIG. 3. The dependence of intensity of polarization field on the efficiency of excitation. Curves 1–3 coincide to values of angle  $\Theta = 0, \pi/4, \pi/2$

In Fig. 2, the intensity of the polarization field for dimensionless time is represented for several mismatched dimensionless laser frequency values in the  $bc$  arm:  $\delta_c = 0, \Delta/2, \Delta$  - whereas in another arm, the mismatch is constant:  $\delta_a = 0$ . To that end, relaxation constants in the arms have been taken into account, according to the tabular values of transition probability  $3^3S_1 \rightarrow 2^3P$  [16], with weights proportional to multiplicity of the above-mentioned states. It should be noted that the relaxation constants for the  $2^3P_j$  states, both in this figure and

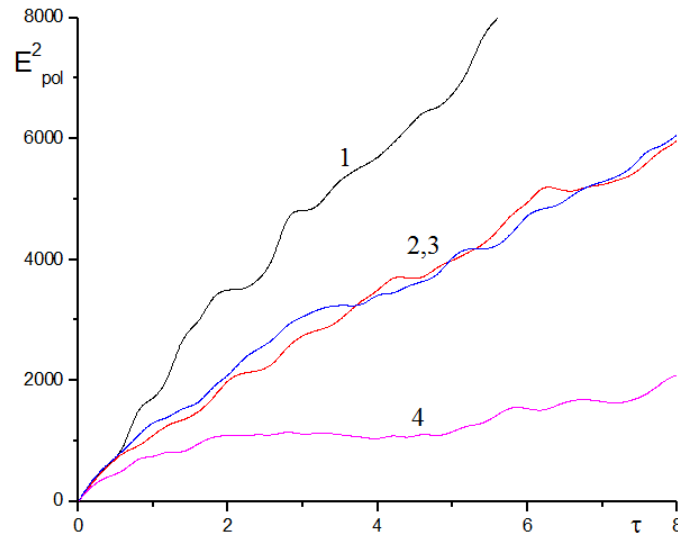


FIG. 4. The influence of relaxation on the generated field. Curve 1 is the curve 1 from the Fig. 1 (lower levels dose not relax); curve 2: each of levels “a” and “c” relaxed with the relaxation constant equal to the half of the spectroscopic value; curve 3: levels  $2^3P_2$  did not relax and  $2^3P_1$  relaxes with the constant equal to the spectroscopic value; curve 4: both lower levels relaxes with the rate constant equal to one-and-a-half time exceeding the spectroscopic value

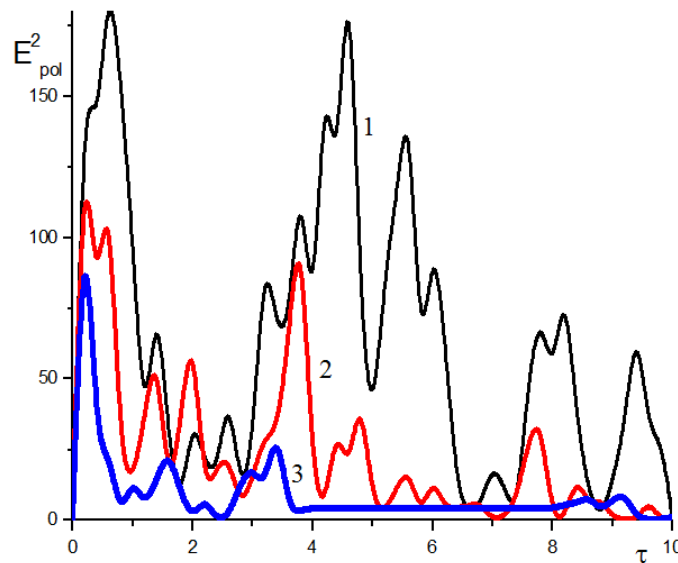


FIG. 5. All of the three levels,  $3^3S_1$ ,  $2^2P_1$  and  $2^2P_2$ , are relaxing, with equally large relaxation constants  $\gamma = 4, 6, 8$  (curves 1–3 consequently)

in subsequent ones, were assumed to be zero. It is apparent from this figure that emission represents a pulse train, with a magnitude that decreases as  $\delta_c$  increases.

Figure 3 illustrates the dependance of the polarization field intensity on the efficiency of the lower levels population, that is characterized by angle  $\Theta$  (see formula (1)). The calculation results show that the polarization field values are practically symmetrical with respect to the angle value  $\Theta = \pi/2$ . Therefore, this figure depicts the field-angle dependence, for  $\Theta = 0$ ,

$\pi/4$ ,  $\pi/2$ . It is apparent from the figure that for decreasing angle  $\Theta$  within the preset limits, the polarization field intensity also decreases.

Subsequent figures illustrate the influence of relaxation on the generated field. It is worth noting that, in the case under consideration, the  $2^2P$  state consists of two levels,  $2^2P_1$  and  $2^2P_2$ , the latter of which is the metastable one.

In Fig. 4, four curves are presented that illustrate the dependence of the polarization field intensity on dimensionless time. The first of these curves takes into account the radiative decay of the upper level  $3^3S_1$  on the lower levels  $2^2P_1$  and  $2^2P_2$ , with the constants that correspond to the spectroscopic values [16] (curve (1) from the previous figure). Curves 2 and 3, in addition to the relaxation process of the upper state, take into account the radiative decay from the lower states, and at that, when plotting curve 2, it has been assumed that each of  $2^2P$  levels decay at a rate equal to half that of the spectroscopic value, whereas curve 3 illustrates the case when level  $2^2P_1$  decays at a rate equal to the spectroscopic value, whereas the metastable level does not relax. Curve 4 describes the case when both of  $2P$  levels relax at a rate 1.5 times that of the spectroscopic value. It is apparent from this figure that curves 2 and 3 practically identical, while further increase of the relaxation rate results in a decrease in the polarization field intensity.

In Fig. 5, the case was illustrated when all three levels,  $3^3S_1$ ,  $2^2P_1$  and  $2^2P_2$ , are radiatively relaxing, with equally sized relaxation constants  $\gamma = 4, 6, 8$ . It is apparent from the Fig. 4 that, for the last two relaxation constant values, emission consists practically of one pulse, and this is in agreement with the results of previous work [13].

In the conclusion of this paragraph, we will provide some approximate formulas that explain the appearance of the generated signal, and, particularly, the fact that the strongest generation corresponds to the mismatch  $\delta_c = 0$ , provided that in another arm of the  $\Lambda$ -scheme there is no mismatch  $\delta_a = 0$  (see Fig. 2). To obtain these results, we used the software package Mathematica, deriving density matrixes values  $\rho_{aa}(0)$ ,  $\rho_{cc}(0)$  (formula (1)), at the angle value  $\Theta = 0$ , and after that, correlation matrixes elements  $\rho_{ab}$  and  $\rho_{cb}$  were calculated analytically with help of (13) and (16) formulas. Based on those matrixes, spurs of matrixes  $\text{Sp}(r_{ab}\rho_{aa}(0)r_{ab}U)$ ,  $\text{Sp}(r_{ba}\rho_{aa}(0)r_{ab}Ur_{bc}r_{cb})$  and  $\text{Sp}(\rho_{cc}(0)r_{cb})$ , were calculated analytically, making it possible to obtain the right side of equation defining the polarization field:

$$\frac{d}{dt}E_{pol} = kE_{pol} \text{Sp}(\rho_{bc}r_{cb} + \rho_{ba}r_{ba}). \quad (18)$$

Then, the variable  $x$  being imposed according to the relationship  $\delta_c = x\Delta$  and assuming  $\Delta$  to be large, in first order perturbation theory, the expression for the polarization field can be obtained :

$$\ln(E_{pol}) \sim \frac{(200 - 7\sqrt{70})e^{\frac{1}{2}it(1-2x)\Delta}}{4500(-1 + 2x)\Delta}. \quad (19)$$

From this formula, it is apparent that the maximum of polarization field is achievable at  $x = 0$  i.e.  $\delta_c = 0$ , which coincides with the data in Fig. 2.

## 5. Conclusion

In this work, the possibility of laser generation without inversion of the fine levels of helium atom is considered. It should be mentioned that considerations of the problem in this work and in articles quoted above [11, 12] differ in principle. In the first part of this article, the positiveness of the reinforcement coefficient is achieved via radiation transitions from a specially-populated additional level, whereas in the second part of the paper, generation occurs

in that arm of the  $\Lambda$ -scheme where the absorption is absent, due to the system achieving an EIT state.

A peculiar feature of this work consists in that for lower levels, used for the coherent excitation according to  $\Lambda$ -scheme, the excited states  $2^3P_1$  and  $2^3P_2$  of the He atom were used. The latter circumstances have permitted us to avoid significant broadening of the lower levels, by means of their interaction with buffer gas. At the same time, the creation and maintenance of a sufficient population at those levels is most probably caused by a strain to the system.

### Acknowledgments

This work was partially financially supported by the Government of the Russian Federation (grant 074U01), by Ministry of Science and Education of the Russian Federation (GOSZADANIE 2014/190, Projects No. 4.Z50.31.0031 and No. 1.754.2014/K), by grant 16-11-10330 of Russian Science Foundation.

### References

- [1] Kocharovskaya O., Hanin Ia.I. Coherent amplification of the ultra short impuls in the three level madium without the population iunversion. *Letters to JETP*, 1988, **48**, P. 581–583.
- [2] Harris S.E. Lasers without inversion: Interference of lifetime-broadening resonsnce. *Phys. Rev. Lett.*, 1989, **62**(9), P. 1033–1036.
- [3] Imamoglu A., Harris S. Lasers without inversion: interference of thr dressed lifetime-broadened states. *Opt. Lett.*, 1989, **14**(24), P. 1033–1036.
- [4] Scully M.O., Zubairy M.S. *Quantum Optics*, Cambridge University Press, 1997.
- [5] Kocharovskaya O., Mandel P. Amplidication without inversion: The double  $\Lambda$ -shime. *Phys. Rev. A*, 1990, **42**(1), P. 523–535.
- [6] Harris S.E., Field J.E., Imamoglu A. Nonlinear optical processes using electromagnetically induced transparency. *Phys. Rev. Lett.*, 1990, **64**(10), P. 1107–1110.
- [7] Scully M. Phys. Reports. From lasers and masers to phaseonium and phasers. 1992, **219**, P. 191–202.
- [8] Kocharovsaya O.A. From lasers without inversion to grasers? *Laser Phys.*, 1995, **5**(2), P. 284–291.
- [9] Kocharovsaya O.A. Amplification and lasing without inversion. *Phys. Reports*, 1992, **219**, P. 175–190.
- [10] Kocharovsaya O.A., Kolesov R., Rostovtsev Yu. Lasing without inversion: a new path to gamma-ray laser. *Laser Phys.*, 1999, **9**(4), P. 745–753.
- [11] Zibrov A.S., Lukin M.D., et al. Experimental demonstration of laser oscillation without population inversion via quantum interference in Rb. *Phys. Rev. Lett.*, 1995, **75**(8), P. 1499–1501.
- [12] Pandanabandu G.G., Welch G.R., et al. Laser oscillation without population inversion in sodiul laser beam. *Phys. Rev. Lett.*, **76**(12), P. 2053–2056.
- [13] Ni Cui, Christof C.H., Macovei M. Interference-induced peak splitting in extreme ultraviolet superfluorescence. *Optics Lett.*, 2013, **38**(4), P. 570–572.
- [14] Kazantsev S.A., Petrashen A.G., Firstova N.M. *Impact spectropolarimetric sensing*, Kiuwer Academic/Plenum Publishes, 1999.
- [15] Jucys A., Bandzaitis A.A. *Theory of the momentum in quantum mechsics*, Vilnius 1965, 462 p.
- [16] Radzig A.A., Smirnov B.M. *Reference data on atoms, molecules and ions*, Springer Series in Chemical Physics, Berlin, 1985.
- [17] Petrashen A.G., Sytenko N.V. Polarization characteristics of radiation of atomic ensamble under coherent exitation in the presnrce of the strong magnetic field. *Nanosist.: Phys., Chem., Math.*, 2015, **6**(1), P. 122–132.



# ***NANOSYSTEMS:***

## ***PHYSICS, CHEMISTRY, MATHEMATICS***

### **INFORMATION FOR AUTHORS**

The journal publishes research articles and reviews, and also short scientific papers (letters) which are unpublished and have not been accepted for publication in other magazines. Articles should be submitted in English. All articles are reviewed, then if necessary come back to the author to completion.

The journal is indexed in Chemical Abstract Service of the American Chemical Society and in Russian Scientific Citation Index.

#### **Author should submit the following materials:**

1. Article file in English, containing article title, the initials and the surname of the authors, Institute (University), postal address, the electronic address, the summary, keywords, MSC or PACS index, article text, the list of references.
2. Files with illustrations, files with tables.
3. The covering letter in English containing the article information (article name, MSC or PACS index, keywords, the summary, the literature) and about all authors (the surname, names, the full name of places of work, the mailing address with the postal code, contact phone number with a city code, the electronic address).
4. The expert judgement on possibility of publication of the article in open press (for authors from Russia).

Authors can submit a paper and the corresponding files to the following addresses: nanojournal.ifmo@gmail.com, popov1955@gmail.com.

#### **Text requirements**

Articles should be prepared with using of text editors MS Word or LaTeX (preferable). It is necessary to submit a pdf copy. In the name of files the English alphabet is used. The recommended size of short communications (letters) is 4-6 pages, research articles – 6-15 pages, reviews – 30 pages.

##### Recommendations for text in MS Word:

Formulas should be written using Math Type. Figures and tables with captions should be inserted in the text. Additionally, authors present separate files for all figures and Word files of tables.

### Recommendations for text in LaTeX:

Please, use standard LaTeX without macros and additional style files. The list of references should be included in the main LaTeX file. Single LaTeX file of the paper with the corresponding pdf file should be submitted.

References in the article text are given in square brackets. The list of references should be prepared in accordance with the following samples:

- [1] Surname N. *Book Title*. Nauka Publishing House, Saint Petersburg, 2000, 281 pp.
- [2] Surname N., Surname N. Paper title. *Journal Name*, 2000, 1(5), P. 17-23.
- [3] Surname N., Surname N. Lecture title. In: Abstracts/Proceedings of the Conference, Place and Date, P. 17-23, 2000.
- [4] Surname N., Surname N. Paper title, 2010. URL: <http://books.ifmo.ru/ntv>.
- [5] Surname N., Surname N. Patent Name. Patent No. 11111, Bul. No. 33, 5 pp., 2010.
- [6] Surname N., Surname N. Thesis Title. Thesis for full doctor degree in math. and physics, Saint Petersburg, 105 pp., 2000.

### **Requirements to illustrations**

Illustrations should be submitted as separate black-and-white files. Formats of files – jpeg, eps, tiff.



**B. S. Pavlov (27.07.1936 – 29.01.2016)**

The Editorial Board is very sad to inform readers that a member of our Editorial Board professor Boris Pavlov has suddenly passed away. It is a great loss and shock for all of us!